EXPLORING THE ROLE OF THE PULVINAR-CORTICAL INTERACTIONS IN VISION: A TALE OF MAPS, LOOPS AND GATES

By

Roan Trivette Marion

Dissertation

Submitted to the Faculty of the

Graduate School of Vanderbilt University

in partial fulfillment of the requirements

for the degree of

DOCTOR OF PHILOSOPHY

in

Neuroscience

December, 2013

Nashville, Tennessee

Approved:

Vivien A. Casagrande, Ph.D.

Mark T. Wallace, Ph.D.

Troy A. Hackett, Ph.D.

Ford F. Ebner, Ph.D.

Malcolm J. Avison, Ph.D.

ACKNOWLEDGMENTS

This work does not represent a solitary effort on my part. I have relied a great deal on others for aid and guidance in my academic endeavors. The intensity of my gratitude and fondness for many of the individuals below exceeds my abilities as a writer. So, instead of florid prose I offer a simple but heartfelt thank you to those that have helped me.

Thanks to the institutions and grants that have supported my research: The Vanderbilt Vision Research Center, The Vanderbilt Brain Institute, The Vanderbilt Neuroscience Graduate Program, The VUMC Cell Imaging Shared Resource, The Vanderbilt Kennedy Center, R01 EY01778, P30 EY008126, T32 EY07135, T32 MH64913 and P30 HD15052.

Thanks to my mentor, Vivien Casagrande, for the support, for the laughs, for having my back and most of all for teaching me to be a scientist. It has been an honor to be your student.

Thanks to my committee: Mark Wallace, Troy Hackett, Ford Ebner, and Calum Avison for the frank critiques of my work and wise counsel on how to improve.

Thanks to my past mentors, Terry Bunde and Yuri Razskazovskiy for giving me my first taste of research science.

Thanks to my lab manager, Julie Mavity-Hudson, for help with… well almost everything including but not limited to figures, spelling, sections and humor.

Thanks to more senior lab members: Walter Jermakowicz, Ilya Khaytin, Gyula Sáry and Gopathy Purushothaman for advice given and techniques taught.

Thanks to more junior lab members: Dmitry Yampolsky, Keji Li and Yao Jiang for nights worked, papers discussed and for making lab life much more fun.

Thanks to the undergrads who worked and studied with me: Sam Budoff, Phylicia Willis, Weston Eberbach, Tara Welytok, and especially Maria Tamborski for experiments worked, slides mounted and a chance to try my hand at mentoring.

Thanks to staff members past and present: Marie Rodriguez, Mary Feurtado, Carol Ann Bonner, Bob Matthews, Sean Schaffer, Shirin Pulous, Mary Early-Zald, and Roz Johnson for many many questions answered and for generally being great at your jobs.

Thanks to friends: Josh Buckholtz, Corrie Camalier, Liz Stringer, David Rinker, Josh Corlew, Mandy Cook, Bikebum Tim and Jen Cartwright for comradeship and good times, for intellectual discussions and discussions about intellectuals, for pretending to be a priest, for pretending to be a duck, for yard care in times of need, for listening to me bitch, and for occasionally reminding me that really I'm pretty lucky.

Thanks to my family: Janese Trivette, Ken Marion, Parks Marion and Minta Trivette for inspiring and sharing my fascination with the natural world and for your continuous, unwavering love and support these many years.

Finally and most importantly thanks to my wife, Shawna Marion, for your sacrifice, for your support and for loving me for who I am.

#

TAPLE OF CONTENS

LIST OF TABLES

CHAPTER II

CHAPTER III

CHAPTER VI

LIST OF FIGURES

CHAPTER II

CHAPTER III

CHAPTER IV

CHAPTER V

CHAPTER VI

CHAPTER I

INTRODUCTION

Pulvinar is the latinization of a German term for pillow originally used to describe a small mound protruding from the back of the brain above the colliculi (Jones, 2007). The term is now used to refer to the mass of cells that underlie that pillow shaped lump. As a whole, the pulvinar is a mysterious entity as frustrating as it is attractive to study. Lesions of the nucleus can cause massive hemineglect in some cases while in other cases lesions cause no noticeable deficits (Bender and Baizer, 1990; Bender and Butter, 1987; Leiby et al., 1982; Petersen et al., 1987; Wilke et al., 2010). The pulvinar has neurons with visual receptive fields like those of cortical neurons and receptive fields like those of subcortical neurons, e.g., the superior colliculus (Bender, 1982; Berman and Wurtz, 2011). It projects to areas as diverse as the primary visual cortex (V1) and the amygdala (Lund et al., 1975; Romanski et al., 1997). It has been proposed to have as few as 4 sub-divisions or as many as 10 subdivisions (Gray et al., 1999; Gutierrez et al., 2000; Kaas and Lyon, 2007; Lyon et al., 2010). The pulvinar may be named for a soft place to lay one's head but in modern neuroanatomy it more resembles a hard place to beat one's head.

It is unsurprising that the pulvinar has not found a place in the visual hierarchy, considering the ambiguity that surrounds both the structure and function of the nucleus. The concept of visual hierarchy in its most basic form has been around for more than a century

(Ferrier, 1886). Based on the effects of lesions, early neurologists deduced the basic concept that the eye, the lateral geniculate nucleus and V1 were necessary for sight and that there was a dependency between the areas such that V1 function depended on the LGN which depended on the eye (Ferrier, 1886; Glickstein, 1988). The visual hierarchy stopped at V1 for many years while other visual areas were being characterized. One difficulty facing researchers was that lesions outside of V1 have more varied and subtle effects when compared to lesions of V1 and the LGN (Goodale and Milner, 1992; Merigan et al., 1993), hence a new metric was needed to establish the hierarchal flow of information.

Felleman and Van Essen are the originators of the most well known hierarchy for the extrastriate visual areas. In their seminal 1991 paper they championed the idea of information moving up and down a hierarchy using feed forward or feedback projections that could be differentiated by the layer in which they terminated (Felleman and Van Essen, 1991). They did not include the pulvinar in the visual hierarchy because the anatomical divisions of the pulvinar and the way that these divisions relate to the cortex was not (and is not) well understood (Felleman and Van Essen, 1991).

A few years after Felleman and Van Essen's work, Sherman and Guillery (1996) began to promote the idea of using variables that are indicative of fast acting excitatory synapses to trace the main message (which they called Drive) through the brain building a hierarchy that would include the pulvinar and other thalamic nuclei (Sherman and Guillery, 1996). Along with the idea of driving, Sherman and Guillery (1996) also developed the concept of modulation, which in this case is the somewhat ill-defined alternative to passing the main message. In their initial review as well as in numerous subsequent publications, Sherman and Guillery have built a list of parameters that have been shown to correlate with driving or modulating inputs and may

be used to extend hierarchy when layer of termination is not applicable (Sherman, 2007; Sherman and Guillery, 1996; Sherman and Guillery, 1998; Sherman and Guillery, 2002; Sherman and Guillery, 2006; Sherman and Guillery, 2011; Sherman and Guillery, 2013).

Despite the tools provided by Sherman and Guillery, the pulvinar has still not found its place in the visual hierarchy and its role in visual function remains unclear. This thesis aimed to explore the role of the pulvinar in the contexts of the visual hierarchy using the concepts of driving and modulation. The second chapter provides the background for the chapters to follow. The background combined with altered versions of the introduction and the conclusion is intended to be a work that may stand on its own separate from the overall thesis, hence the background necessarily references the subsequent chapters in order to provide a current portrait of pulvinar research. The third chapter explores the divisions of the prosimian's pulvinar in an attempt to better understand the pulvinar of new and old world monkeys. Finding common divisions in the different branches of the primate lineage can help us understand how the pulvinar relates to the cortical visual hierarchy. Chapters four and five both attempt to better understand putative modulatory projections that originate in the pulvinar. These chapters aim to give better definition to modulators as a class, providing data on both form and function. Chapter six seeks to use Sherman and Guillery's proposals to classify V1 and pulvinar input to the second visual area (V2) in an attempt to see if part of the pulvinar might lie in an interim level of hierarchy between V1 and V2. The goal of this body of work was to add new data on the role of the pulvinar in vision and to help promote further dialogue about the position of the pulvinar within the visual hierarchy.

Reference List

Bender DB. 1982. Receptive-field properties of neurons in the macaque inferior pulvinar. J Neurophysiol 48(1):1-17.

Bender DB, Baizer JS. 1990. Saccadic eye movements following kainic acid lesions of the pulvinar in monkeys. Exp Brain Res 79(3):467-478.

Bender DB, Butter CM. 1987. Comparison of the effects of superior colliculus and pulvinar lesions on visual search and tachistoscopic pattern discrimination in monkeys. Exp Brain Res 69(1):140-154.

Berman RA, Wurtz RH. 2011. Signals conveyed in the pulvinar pathway from superior colliculus to cortical area MT. J Neurosci 31(2):373-384.

Felleman DJ, Van Essen DC. 1991. Distributed hierarchical processing in the primate cerebral cortex. Cereb Cortex 1(1):1-47.

Ferrier D. 1886. The functions of the brain. New York: G. P. Putnam's Sons.

Glickstein M. 1988 September, 1, 1988. The Discovery of the Visual Cortex. Scientific American:118-127.

Goodale MA, Milner AD. 1992. Separate visual pathways for perception and action. Trends Neurosci 15(1):20-25.

Gray D, Gutierrez C, Cusick CG. 1999. Neurochemical organization of inferior pulvinar complex in squirrel monkeys and macaques revealed by acetylcholinesterase histochemistry, calbindin and Cat-301 immunostaining, and Wisteria floribunda agglutinin binding. JComp Neurol 409(3):452-468.

Gutierrez C, Cola MG, Seltzer B, Cusick C. 2000. Neurochemical and connectional organization of the dorsal pulvinar complex in monkeys. J Comp Neurol 419(1):61-86.

Jones EG. 2007. The Thalmus Cambridge: Cambridge University Press.

Kaas JH, Lyon DC. 2007. Pulvinar contributions to the dorsal and ventral streams of visual processing in primates. Brain Res Rev 55(2):285-296.

Leiby CC, 3rd, Bender DB, Butter CM. 1982. Localization and detection of visual stimuli in monkeys with pulvinar lesions. Exp Brain Res 48(3):449-454.

Lund JS, Lund RD, Hendrickson AE, Bunt AH, Fuchs AF. 1975. The origin of efferent pathways from the primary visual cortex, area 17, of the macaque monkey as shown by retrograde transport of horseradish peroxidase. J Comp Neurol 164(3):287-303.

Lyon DC, Nassi JJ, Callaway EM. 2010. A disynaptic relay from superior colliculus to dorsal stream visual cortex in macaque monkey. Neuron 65(2):270-279.

Merigan WH, Nealey TA, Maunsell JH. 1993. Visual effects of lesions of cortical area V2 in macaques. J Neurosci 13(7):3180-3191.

Petersen SE, Robinson DL, Morris JD. 1987. Contributions of the pulvinar to visual spatial attention. Neuropsychologia 25(1A):97-105.

Romanski LM, Giguere M, Bates JF, GoldmanRakic PS. 1997. Topographic organization of medial pulvinar connections with the prefrontal cortex in the rhesus monkey. Journal of Comparative Neurology 379(3):313-332.

Sherman SM. 2007. The thalamus is more than just a relay. Curr Opin Neurobiol 17(4):417-422.

Sherman SM, Guillery RW. 1996. Functional organization of thalamocortical relays. J Neurophysiol 76(3):1367-1395.

Sherman SM, Guillery RW. 1998. On the actions that one nerve cell can have on another: distinguishing "drivers" from "modulators". Proc Natl Acad Sci U S A 95(12):7121-7126.

Sherman SM, Guillery RW. 2002. The role of the thalamus in the flow of information to the cortex. Philos Trans R Soc Lond B Biol Sci 357(1428):1695-1708.

Sherman SM, Guillery RW. 2011. Distinct functions for direct and transthalamic corticocortical connections. J Neurophysiol 106(3):1068-1077.

Sherman SM, Guillery RW. 2013. Functional Connections of Cortical Areas. Cambridge, Massachusetts: MIT press.

Wilke M, Turchi J, Smith K, Mishkin M, Leopold DA. 2010. Pulvinar inactivation disrupts selection of movement plans. J Neurosci 30(25):8650-8659.

CHAPTER II

BACKGROUND

This chapter provides a review of the anatomy and physiology of the primate pulvinar with emphasis on work done in non-human primates. It is broken into four sections, each having multiple subsections. The first section concentrates on the efforts to divide the pulvinar. The second section centers on the connections of the pulvinar. The third section focuses on the physiology of the pulvinar. Lastly, the fourth section discusses how the pulvinar relates to the visual hierarchy. Overarching conclusions are withheld for the final chapter of this thesis; hence, a conclusion section is not presented.

Divisions of the Pulvinar

In the following sections I will first discuss a traditional way of dividing the pulvinar into 4 parts based on cyto and myelo architecture. I will subsequently examine the modern views on the divisions of the pulvinar using the traditional divisions as a frame work. Next, I will compare the organization of the pulvinar in prosimians to that of simains. Finally, I will propose a schema for dividing the pulvinar that will be used during the rest of the background. This section will touch on the connections of the pulvinar only to the extent that the patterns of

connections pertain to the arguments used to defend subdivisions of the pulvinar. The connections of the pulvinar will be covered in detail in the next section.

Traditional divisions

There are a number of ways to subdivide the pulvinar based only on nissl and myelin stains; the most influential of these are the divisions of Jerzy Olszewski(1952). Building on the work of Walker (1938), Olszewski recognized 4 subdivisions of the macaque pulvinar: The lateral, medial, inferior and oral. The oral subdivision is now commonly referred to as the anterior subdivision (Jones, 2007b). These 4 subdivisions can be found in most simians, though they are less obvious or even absent in owl monkeys and prosimians (Jones, 2007b). In owl monkeys and prosimians the pulvinar is typically separated into only 2 divisions, the superior and the inferior, with the brachium of the superior colliculus (BrSC) acting as the border between these two areas (Allman et al., 1972; Raczkowski and Diamond, 1980). In the time since his monograph was published, Olszewski's divisions have been refined and subdivided but they are still used in many papers and serve as a starting point for most subsequent efforts. I will, therefore, describe the four divisions as originally proposed for the macaque.

In coronal sections moving from rostral to caudal the oral nucleus (also known as the anterior nucleus) is the first to appear then the inferior division and finally the lateral and medial divisions are the last to appear, filling the entire extent of the thalamus at its most posterior point. The pulvinar is described in a Nissl stain as generally having cells that are "lightly-stained…, medium sized, multipolar, and plump" (Olszewski, 1952, p24). With this description as a baseline some differences are noted between the nuclei. The oral division has loose irregular cell packing. The ventral division has tight cell packing and a subpopulation of large dark staining

cells. The lateral nucleus has small cells that are broken into bands by horizontally running fibers. Lastly, the cells of the medial nucleus are evenly distributed (Olszewski, 1952). Many researchers coming after Olszewski have used the descriptions above to define the border between PI and PL to be somewhat more ventral. These borders are shown in Figure 1 and will be used through the rest of this work when referencing PI, PL, PM and PA (Adams et al., 2000; Bender, 1981; Kaas and Lyon, 2007; Stepniewska et al., 2000).

Perhaps the most distinctive feature of the pulvinar is not its cells but the powerful fibers of the BrSC that demark the boundary between the inferior and medial nucleus and cause the characteristic banding of the lateral nucleus. It seems likely that the prominence of the BrSC is the central reason why the pulvinar has resisted many modern attempts at division, for though the observer is naturally drawn to incorporate its fiber structure into their organizational schemas much data suggests that the BrSC has little bearing on the actual functional divisions of the pulvinar.

The oral (anterior) division, which is unbroken by the BrSC, may be Olszewski's (1952) most important contribution. The oral division stands apart from the other divisions in two respects. First and foremost, it is differentiable because of its connections. The oral division receives the predominance of its inputs from somatosensory areas whereas the other 3 divisions receive inputs (at least in part) from visual areas (Jones, 2007b for review). Also as opposed to the other 3 divisions that have been re-arranged and re-divided, the oral division has stayed as a single entity. The absence of subdivisions within oral division may be due to prescience on Olszewski's part or simply a lack of interest on the part of others, but is none the less notable. This review will leave aside the oral pulvinar choosing instead to focus on the lateral, inferior and medial divisions.

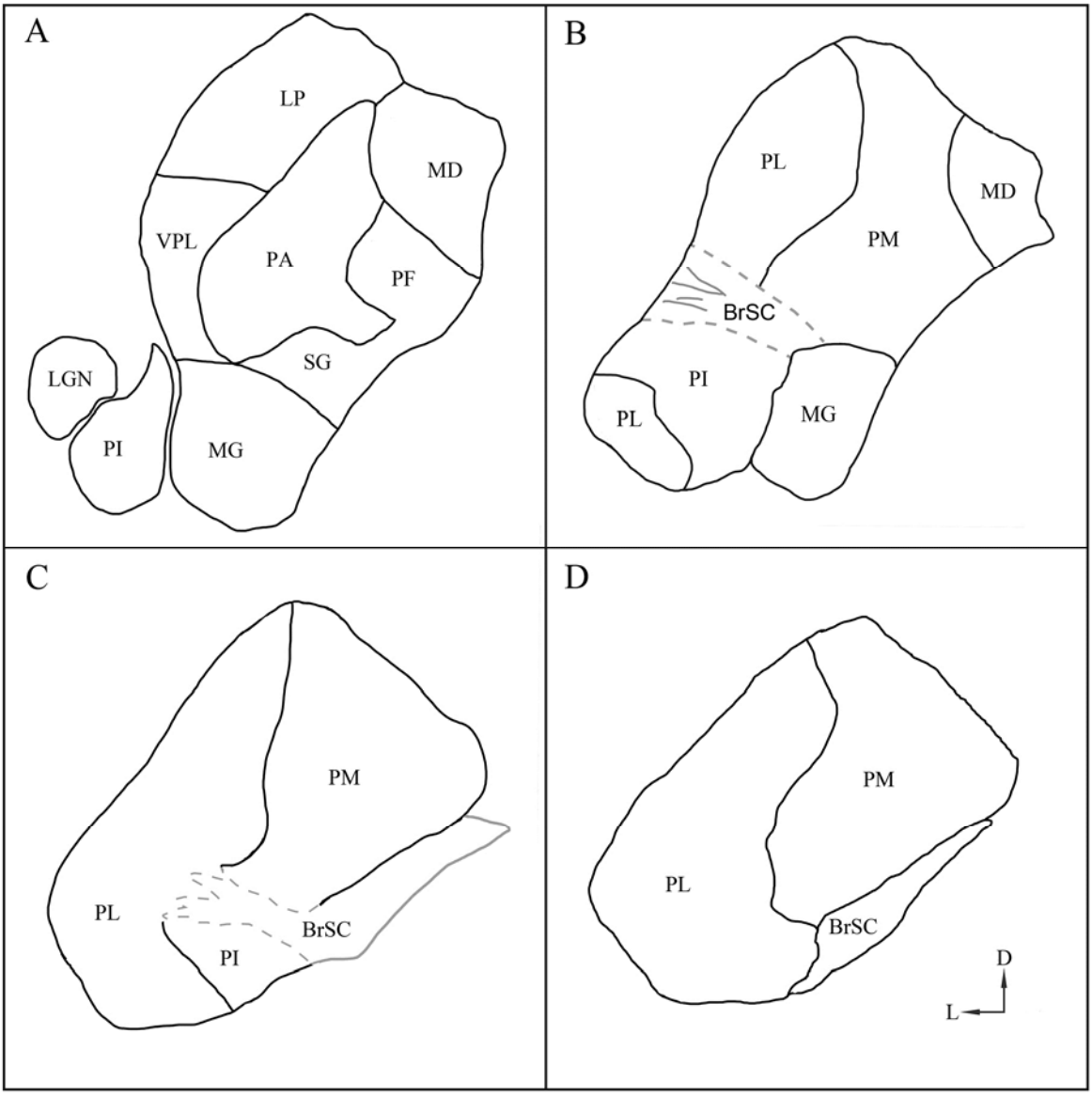

Figure 1.

The traditional divisions of the macaque pulvinar. Schematics of coronal sections of the thalamus depicting the traditional divisions of the Macaque pulvinar based on Olszewski (1952) descriptions of the pulvinar nuclei as re-interoperated by subsequent researchers (Adams et al., 2000; Bender, 1981; Stepniewska et al., 2000). Panel A is most anterior while panel D is most posterior. PA = anterior pulvinar, PI = inferior pulvinar, PM = medial pulvinar, PL = lateral pulvinar, BrSC = brachium superior colliculus, LGN = lateral geniculate nucleus, MG =medial geniculate nucleus, VPL = ventral posterolateral nucleus, LP = lateral posterior nucleus, MD = medial dorsal nucleus, SG = supragenicular nucleus, PF = parafascicular nucleus, D = dorsal, L = lateral

As a group these divisions are better researched and share the unifying feature of being connected with the visual cortex (Kaas and Lyon, 2007).

Modern views on dividing the pulvinar: The inferior and lateral pulvinar

Much of the organization of the inferior and lateral pulvinar in simians hangs on the strength of two compelling and reproducible findings; the lateral and inferior pulvinar possess one or more retinotopic maps and the inferior pulvinar can be divided into several architectonic subdivisions. I will cover each of these findings in turn, then discuss their intersection, and finally talk about two additional divisions that have been suggested based on neither chemoarchitecture nor retinotopy.

The strongest evidence for retinotopically organized maps in the simian pulvinar comes from work in macaques. In 1981 Bender used single and multiunit electrophysiological mapping to show evidence of two visuotopic maps located in the inferior and lateral pulvinar (Figure 2). The first of these maps lies along the lateral border of the inferior pulvinar with the bulk of the map in the inferior pulvinar but a significant portion extending into the lateral pulvinar. Bender referred to this first map as the inferior map. The inferior map is a first order map meaning that all adjacent points in visual space are represented by adjacent points within the map. The second map is encompassed entirely within the lateral pulvinar, wrapping around the first map on its posterior, dorsal, lateral, and ventral aspects. Bender referred to the second map as the lateral map. It has a split representation of the horizontal meridian along its lateral most aspects. This split representation makes the lateral map a second order map meaning that it has some adjacent points in visual space represented by non-adjacent points within the map. The two maps border each other along their representation of the vertical meridian with the lower field laying in the

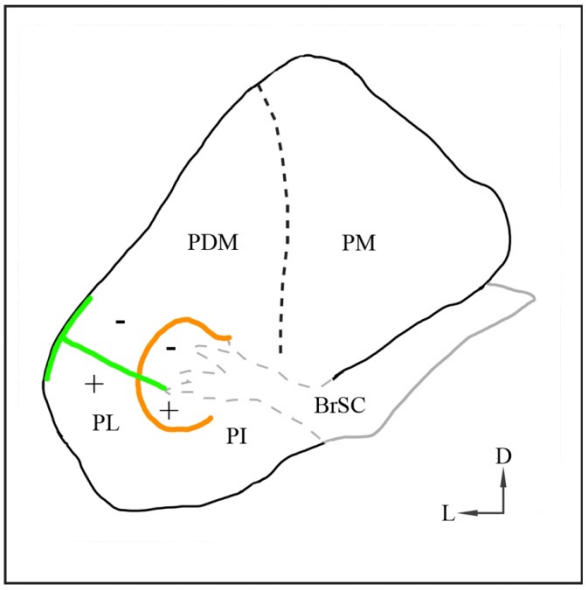

Figure 2.
The electrophysiologically defined divisions of the macaque pulvinar. Schematic of a coronal section depicting the electrophysiologically defined divisions of the macaque pulvinar. Axes of the two retinotopic maps in lateral and inferior pulvinar are represented in color. The green line represents the horizontal meridian. The orange line represents the vertical meridian. Minus signs represent position of the lower field while plus signs represent the position of the upper field in each of the maps. Dashed line represents the approximate border between PM and PDM. Based on: Bender, 1981; Petersen et al., 1985, PDM = dorsomedial lateral pulvinar

dorsal part of the mapped region and the upper field laying in the ventral part (Bender, 1981). These maps differ from cortical maps in that they represent both the vertical and horizontal meridians as two dimensional sheets meaning that the fovea is represented by a line. This arrangement means that the maps as purposed by Bender (1981) have a third dimension (besides the two dimension needed to represent the retina) which could be used to map or organize an additional feature (see *The pattern of pulvinar connection* section for more information).

The general arrangement of the maps in macaque pulvinar was electrophysiologically confirmed by Petersen and colleagues (1985). Further, Ungerleider and colleagues (1983) confirmed these results by demonstrating that injections of anterograde tracers into defined retinotopic regions of the primary visual cortex (V1) resulted in an arrangement of projections to the pulvinar consistent with two retinotopic divisions. The latter authors also suggested that the mapped region of the pulvinar is the only region to which V1 projects. In a second paper the same group (Ungerleider et al., 1984) extended their results by making anterograde tracer injections into the middle temporal area (MT) and then examining the pulvinar. Considering the MT projections to the pulvinar in the context of the two maps proposed by Bender (1981), the authors suggested a tripartite division of the pulvinar. In this scheme the three divisions are known as P1, P2 and P3. P1 and P2 correspond to Bender's inferior and lateral maps respectively. P3 takes up the rest of the inferior pulvinar and extends slightly into the medial pulvinar. P3 is the only part of the tripartite divisions that does not receive V1 projections and has no clear retinotopy (Ungerleider et al., 1984).

Retinotopic maps in the pulvinar have been demonstrated in two other primate species, both New World simians. In owl monkeys Allman and colleagues (Allman et al., 1972) mapped the inferior pulvinar exclusively (recall that in owl monkey the inferior pulvinar is effectively the

ventral half of the nucleus) and argued for the existence of a single map occupying the entire subnucleus. In this map central vision is located in the dorsal anterior portion of the subnucleus with the upper field on the lateral side and the lower field represented medially.

Two maps, occupying parts of the lateral and inferior nuclei, have been suggested in the cebus monkey (Gattass et al., 1978; Soares et al., 2001). Despite the similarities of number and position, these maps are not analogous to those found in macaque. In the latter arrangement there is a small dorsal map capping a much larger ventral map. Both maps are first order. In the dorsal maps the lower and upper field representations shift somewhat through their rostral-caudal extents. In the ventral map the lower field is represented dorsally, the upper field represented ventrally, and central vision is represented laterally. There has yet to be independent confirmation of the maps proposed in either the owl monkey or cebus monkey.

The roots of the modern chemoarchetectonic divisions of the inferior pulvinar originate in the work of Lin and Kaas (1979) who used myelin and cytoarchitecture to divide the inferior pulvinar of the owl monkey. They found a part of the inferior pulvinar was outlined by a myelin circle and observed that it naturally divided the inferior pulvinar into three parts. From rostral-lateral to medial -caudal, the three parts are the inferior pulvinar central division (PIc), inferior pulvinar medial division (PIm) and the inferior pulvinar posterior division (PIp). These parts are of uneven size taking up approximately 70%, 20%, and 10% respectively. These researchers also note that the dorsal extent of PIm appears to reach above the BrSC and that this area receives heavy projections from MT while the other two areas receive projections from the superior colliculus (SC). This nomenclature stayed dormant until the 1990's when the availability of new staining protocols led to a renewed interest in subdividing the pulvinar. Starting in 1993 and continuing for the next decade several groups divided and re-divided the

inferior pulvinar and inferior part of the lateral pulvinar in simian primates (or simply the inferior pulvinar in owl monkeys). Through this work consensus emerged on 3 divisions of the inferior pulvinar. These divisions occupy most of the caudo-medial half of the area under the BrSC leaving the lateral part still in contention. Below I will review the chemoarchitecture and location of the 3 consensus divisions and the possible ways of dividing the lateral aspect before moving on to how these parts interact with the maps in the inferior and lateral pulvinar.

The three divisions of the inferior pulvinar that have been recognized by the vast majority of researchers working in the field after 1979 are: PIp, PIm, and the inferior pulvinar central medial division (PIcm as it is referred to by the Kaas Lab see Kaas and Lyon, 2007 for review). PIm is the most recognizable and consistent of the divisions of the inferior pulvinar (Figure 3). After its initial discovery by Lin and Kaas (1979), an area of the squirrel monkey pulvinar was shown to receive heavy MT projections by Cusick and colleagues (Cusick et al., 1993). The concept of PIm had already been suggested for the squirrel monkey based on cytoarchitecture (Steele and Weller, 1993) and given that the MT projections to pulvinar lay in a similar place in both the owl and squirrel monkeys, PIm was generalized to the squirrel monkey. Cusick and colleagues (1993) also showed that PIm appeared to extend above the BrSC, staining heavily for the calcium binding protein, parvalbumin (Pv), lightly for the calcium binding protein, calbindin (CB) and heavily for cytochrome oxidase (CO). PIm's light staining for CB and dark staining for CO (as compared to PIcm and PIp Figure 3) have been used as anchoring markers to confirm PIm's existence in other species most notably in the macaque but also owl and cebus monkeys (Gray et al., 1999; Soares et al., 2001; Stepniewska et al., 1999). The myelin circle that was originally the marker of PIm in owl monkeys has also been found in marmoset and squirrel monkey but is not reported for macaque monkey (Stepniewska et al., 2000). A variety of other

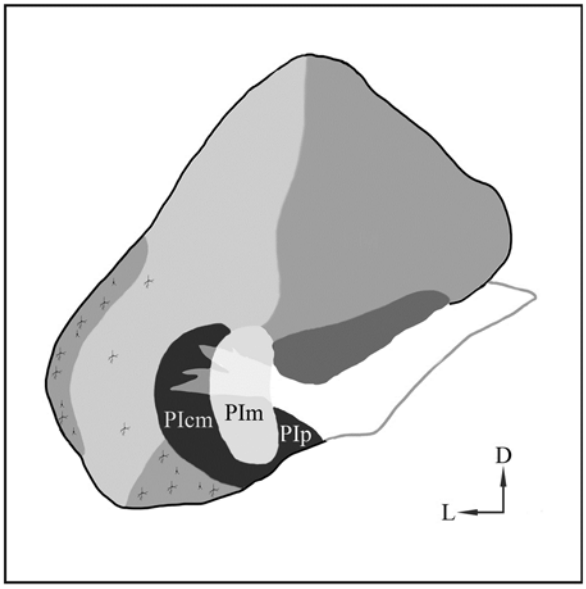

Figure 3.

Consensus architectonic divisions of the inferior pulvinar.Three most recognized architectonic divisions of the pulvinar shown in a schematic of a macaque coronal section stained for calbindin. Note how the dark staining of the inferior pulvinar posterior division (PIp) and the inferior pulvinar central medial division (PIcm) allow the differentiation of the Inferior pulvinar medial division (PIm). Also note the dark staining cells and differential staining lateral to PIcm. This lateral area is divided in different ways partly based on its calbinden staining (see text for more details). Staining pattern based on data from: Adams et al., 2000; Gray et al., 1999; Gutierrez and Cusick, 1997; Stepniewska et al., 2000

architectonic stains have been used to differentiate PIm but with the exception of acetyl cholinesterase (AChE, see below), these other stains have not been replicated between researchers or species (Cusick et al., 1993; Gray et al., 1999; Gutierrez et al., 2000; Gutierrez et al., 1995; Stepniewska and Kaas, 1997). Finally, PIm has been shown to connect to MT in all simian species studied namely: marmoset, cebus, squirrel, owl, and macaque monkeys (Kaas and Lyon, 2007; Soares et al., 2001; Stepniewska et al., 1999).

PIp and PIcm stain darkly for CB and lightly for CO thus allowing PIm to be differentiated. PIcm arches along the lateral border of PIm extending above the BrSC in macaque and squirrel monkeys (Cusick et al., 1993; Gray et al., 1999; Gutierrez et al., 1995; Stepniewska and Kaas, 1997; Stepniewska et al., 1999; Stepniewska et al., 2000). PIcm only comprises the medial part of the division PIc as described originally by Lin and Kaas (1979) with the lateral extent of PIc being described variously by different groups. Because PIcm lies next to a continuous area, it has been given two different names in two competing naming schemes. The nomenclature used here is from the Kaas lab (Stepniewska and Kaas, 1997; Stepniewska et al., 1999; Stepniewska et al., 2000) while the Cusick lab (Cusick et al., 1993; Gray et al., 1999; Gutierrez and Cusick, 1997; Gutierrez et al., 1995) has used the name Inferior pulvinar central division for the same division in their later work. PIcm has been consistently shown to stain lightly for AChE across researchers and species (Gray et al., 1999; Gutierrez et al., 1995; Stepniewska and Kaas, 1997). The name PIp has been used consistently to describe the most caudo-medial division of the inferior pulvinar that borders PIm medially and extends to or slightly above the BrSC in macaque and squirrel monkeys. The cebus represents an exception to the organization described above. In this primate Soares and colleagues (2001) claim that PIp has migrated to lie ventral to PIm.

Lateral to PIcm there is a area of inferior/lateral pulvinar larger than the combined size of the three subdivisions described above (Figure 3). The Kaas and Cusick groups (Cusick et al., 1993; Gray et al., 1999; Gutierrez and Cusick, 1997; Gutierrez et al., 1995; Kaas and Lyon, 2007; Stepniewska and Kaas, 1997; Stepniewska et al., 1999; Stepniewska et al., 2000; Weller et al., 2002) have divided this area differently based primarily on chemoarchitecture (Figure 4). Subsequently the Ungerleider lab (Adams et al., 2000) divided the area in question into 3 parts based on both chemoarchitecture and inferred retinotopy. Due to this difference in methodology the Kaas and Cusick models will be described below while the Ungerleider model will be covered when discussing the integration of mapped areas and architectonic areas.

The work by the Kaas and Cusick groups was done mostly in macaque and squirrel monkeys and is best compared in these species (Cusick et al., 1993; Gray et al., 1999; Gutierrez and Cusick, 1997; Gutierrez et al., 1995; Stepniewska and Kaas, 1997; Stepniewska et al., 1999; Stepniewska et al., 2000). In the Cusick model (Figure 4A) the area lateral to PIcm is divided into the pulvinar inferior lateral division (PIl) and the pulvinar inferior lateral division shell (PIl-s). PIl is present through the entire rostral caudal extent of the pulvinar while PIl-s is most visible in the middle half of the rostral caudal extent. PIl is distinguished from PIcm by lighter CB staining and darker AChE staining. In turn PIl-s is distinguished from PIl by possessing a high density of CB positive neurons and the presence of horizontally running fiber bundles (Gray et al., 1999). PIl also contains the occasional CB staining neuron and the presence of these neurons is a way to distinguish PIl from its dorsal neighbor PL, though this dorsal border can only be determined approximately in some sections (Gray et al., 1999). The dorsal border of PIl is at or above the level of the BrSC in both squirrel monkeys and macaque monkeys; this is taken as evidence that there are actually only two major divisions of the pulvinar: superior and inferior

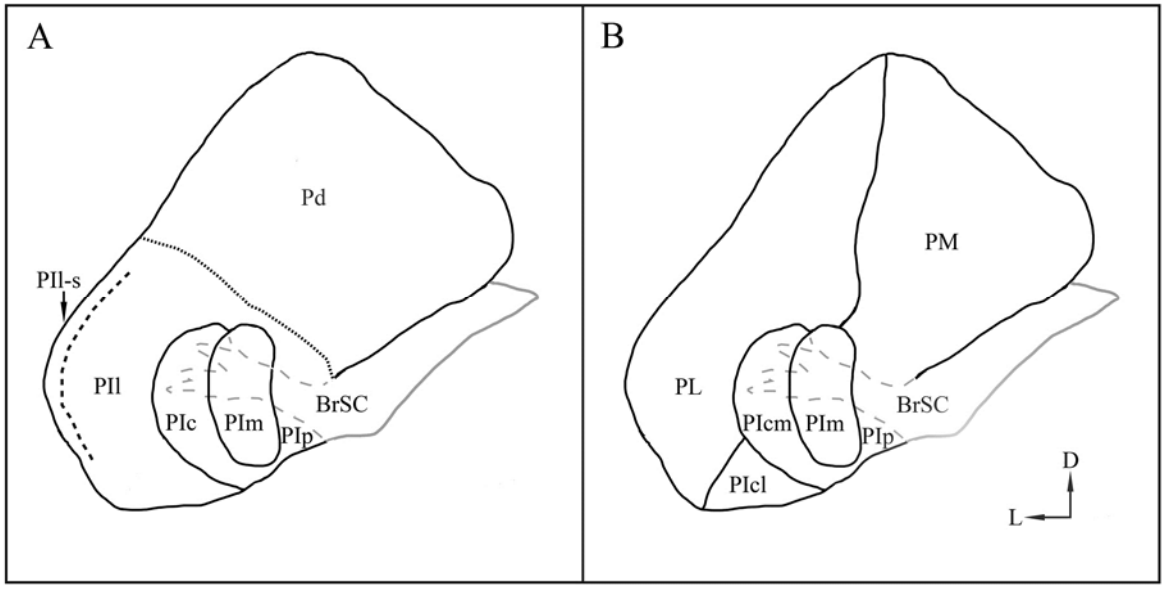

Figure 4.

Competing versions of pulvinar organization. Two competing versions of pulvinar organization shown in a schematic of a coronal section of macaque thalamus. Figure 4A shows Cusick lab's divisions of the pulvinar: PIp, PIm, inferior pulvinar central division (PIc), inferior pulvinar lateral division (PIl) and inferior pulvinar lateral division shell (PIl-s). Figure 4B shows Kaas lab's divisions of the pulvinar: PIp, PIm, PIcm, and inferior pulvinar central lateral division (PIcl). Note that PIcm and PIc are different names for the same division. The dashed line in figure 4A shows the border between PIl and PIl-s, which is more noticeable in sections anterior to this level of section and absent in sections more posterior to this level of section. The dotted line in figure 4A shows the border drawn by the Cusick lab between their re-imagined inferior pulvinar and the part of the pulvinar they describe and the dorsal pulvinar (Pd). Based on data from: Gray et al., 1999; Gutierrez and Cusick, 1997; Stepniewska and Kaas, 1997; Stepniewska et al., 2000

(Gray et al., 1999; Gutierrez et al., 1995). The superior division contains all of the tissue above the BrSC and the inferior division contains all the tissue below the BrSC including the consensus divisions as well as PIl and PIl-s (Figure 4A). The dorsal extent of PIl along with the difference in nomenclature represents one of the primary differences between the Cusick and Kaas models of pulvinar organization. The Kaas group divides the space lateral to PIcm between PL and a division they call the central lateral division of the inferior pulvinar (PIcl) (Figure 4B). Relative to the other divisions PIcl stains moderately for CB CO and AChE. It also possesses a minority of neurons that stain darkly for CB. The border between PL and PIcl lies ventral to the dorsal bound of the Cusick PIl subdivision in both the macaque and squirrel monkey. The dorsal ventral extent of PIcl varies relative to the BrSC in the rostral caudal axis especially in the squirrel monkey but also in the macaque. This variance does not occur for PIl in the Cusick model.

A resolution of differences between the Kaas and Cusick models remains elusive. Of note is the possibility that some of the divergent observations made may be due to species differences given that Stepniewska and Kaas used two subspecies of macaque and comparable figures from the two groups appear to be in different subspecies (compare gross features of figure 1 Gray et al., 1999 with figure 15 of Stepniewska and Kaas, 1997). Independent reports (Jones, 2007b; Lysakowski et al., 1986) confirm the possibility of a shell like structure in ACHE staining but contend that this structure extends well into the dorsal part of PL beyond the limits of PIl-s. Indeed the concept of a shell may be reaching some level of consensus with the Kaas group tentatively acknowledging its existence in more recent work (Kaas and Lyon, 2007).

Given that there is strong evidence for both chemoarchitectonic and visuotopic subdivisions of the pulvinar in simians, it is obvious to ask: are these subdivisions compatible?

To answer this question it is best to look at the three species where electrophysiological mapping data is available making the layout of the visuotopic maps clear. Hence, the discussion below will be limited to the macaque, owl and cebus monkeys.

Working in the macaque the Ungerleider lab used CB staining and retrograde tracing to understand the relationship between the visuotopic and chemoarchitectonic boundaries (Adams et al., 2000). This work represents the only attempt to reconcile these boundaries in a simian. Visuotopy was defined in the form of P1, P2, and P3 (see above; Adams et al., 2000; Ungerleider et al., 1984). P3 was shown to be coextensive with the consensus cemoarchitectonic divisions (PIp, PIm, and PIcm) while P1 and P2 were shown to lie within the lateral region where no consistent architectonic boundaries have been found. P1 and P2 are thought to be coextensive with Benders lateral map and inferior maps respectively (Adams et al., 2000; Ungerleider et al., 1984). This result was not surprising and previous investigators had been aware that the mapped area should lie lateral to PIcm (Gray et al., 1999; Gutierrez and Cusick, 1997; Stepniewska and Kaas, 1997).

In the Cebus the relationship between the chemoarchitectontic and visuotopic pulvinar divisions is less clear. As previously mentioned Gattass and colleagues (1978) showed the existence of two maps in the cebus. More recently Soares and colleagues (2001) demonstrated chemoarchitectonic divisions and showed the relationship to these functional areas. These areas were defined by tract tracing, and named P1, P2, and P3 after the fashion of the prior work by the Ungerleider lab (Adams et al., 2000; Ungerleider et al., 1984) in the macaque (see above). PIm and PIcm are clearly visible CB stained sections from the cebus. Other areas have been argued to exist, including PIp which it is suggested is situated ventral to PIm (Soares et al., 2001). These findings suggest homology between the cebus and the other primates (including the

macaque) that have chemoarchitectonically defined divisions of the inferior pulvinar. However, the anatomical boundaries and the functional divisions in the cebus do not correspond to those found in macaque. The most straightforward example of the difference is that the macaque P3 contains PIp, PIm and PIcm while the cebus P3 only contains PIm and PIp, and P1 contains PIcm as well as other more lateral divisions. In discussing the correspondence of the visuotopic maps, the authors state that the dorsal map is not coextensive with either a functional subdivision (though it shares territory with P2) or an architectonic subdivision (though it resides mostly in PL). P1, however, is claimed to be coextensive with the ventral map having the same medial border as PIcm. When the maps presented by Gattass and colleagues (1978) are directly compared with CB stained sections presented by Soares and colleagues (2001), this latter claim comes into question. Soares and colleagues (2001) show PIm and hence P3 sitting directly over the MGN, while Gattass and colleagues (1978) show the ventral map and hence P1 occupying the same space.

In the owl monkey the entire inferior pulvinar is proposed to be a single representation of the contralateral hemipfield (Allman et al., 1972). This same area is divided into at least 4 chemoarchitectontic divisions by Stepniewska and Kaas (1997) who were building on the tripartite division proposed by of Lin and Kaas (1979). Stepniewska and Kaas suggest that (as in the macaque) the map lies within the largest and most anterolateral subdivision (which they call PIcl). This is in effect a suggestion that Allman and colleagues (1972) misinterpreted or over interpreted their data. Given that Allman and colleagues made just as many penetrations in the supposedly un-mapped part of the pulvinar as they did in the mapped part of the pulvinar this suggestion seems one of convenience. It is perhaps most straight forward to admit that in the owl monkey a relationship between the map and chemoarchitectontic divisions is difficult to

surmise based on the current data. Overall, a conclusion that is not difficult to come to is that the new and old world monkeys seem to share many chemoarchitectonic divisions but differ in the arrangement of their visuotopic maps, and the relationship of these physeological maps to the chemoarchitectontic divisions.

During Bender's mapping of the macaque pulvinar, a visually active area lacking clear retinotopy was discovered. This area was later proposed as a functional subdivision named the dorsomedial lateral pulvinar (PDM) by Peterson and colleagues (1985). The full extent of PDM is unclear but it is centered in the lateral pulvinar of the macaque lying dorso-medial to the retinotopically mapped regions and likely extends into the medial pulvinar. PDM enjoys wide spread recognition in the literature though data dealing with the anatomic limits of this area are sparse (Jones, 2007b; Kaas and Lyon, 2007; Lyon et al., 2010). Though the correspondence is imprecise, it is possible that macaque PDM and the dorsal map of the cebus (see above) are analogous given their location to the main mapped region in these primates.

Recently, a new division has been proposed for the lateral pulvinar based purely on connectivity (Lyon et al., 2010). The pulvinar inferior lateral division (PIL) of Lyon and colleagues (2010) is located in the most inferior and lateral region of macaque PL and receives strong projections from MT and the third visual area (V3). PIL takes its name from the work of Cusick and colleagues (1993) where a division of the same name was proposed in squirrel monkey. PIL was the predecessor to PIL-s (Gutierrez et. al., 1995) and Lyon and colleagues (2010) call the area a "shell" leading the reader to assume they mean PIL-s. The use of the term PIL is somewhat confusing because according to Cusick (Cusick et al., 1993, Gutierrez et al., 1995) both PIL and PIL-s are defined primarily by chemoarchitectonics and extend at least to the level of the BrSC, whereas Lyon's PIL is defined by its connections and stays well below the

BrSC. Regardless of its name, a division like PIL (as defined by Lyon et al., 2011) is supported by previous studies showing the presence of MT, V3 and superior colliculus (SC) projections to this region in macaque (Benevento and Standage 1983, (Benevento and Standage, 1983; Lysakowski et al., 1986; Shipp, 2001). Further, an area similar to PIL can be distinguished by myelo and cyto architecture (Lysakowski et al., 1986) and possesses a particularly high concentration of SC to MT relay neurons (Berman and Wurtz, 2008; Berman and Wurtz, 2010; Berman and Wurtz, 2011). Interestingly, MT projecting neurons have been demonstrated in a similar location to PIL in the marmoset (Kaas and Lyon 2007).

Modern views on dividing the pulvinar: The medial divisions

Compared to the quantity of work that has gone toward dividing the inferior and lateral pulvinar, little has been done to delineate the organization of the medial pulvinar. Architectonic and physiologic data have been brought to bear on the organization of the medial pulvinar but a consensus has yet to emerge from these investigations. The connections of PM are not uniform, suggesting the existence of divisions (Cappe et al., 2009; Gutierrez et al., 2000). That said, because there is as of yet no consensus on division and no models based solely on connections, I will largely leave aside the discussion of the spatial pattern of connectivity in the medial pulvinar.

Gutierrez and colleagues (2000) have put forth perhaps the most comprehensive system for organizing the medial pulvinar (Figure 5). This work is from the Cusick lab and therefore seeks to incorporate the dorsal part of PL, a posterior part of LP and PM into the dorsal pulvinar and then subdivide the dorsal pulvinar. Working in macaque, they divided this area of the pulvinar into three divisions: the dorsal lateral pulvinar (PLd), the medial pulvinar lateral

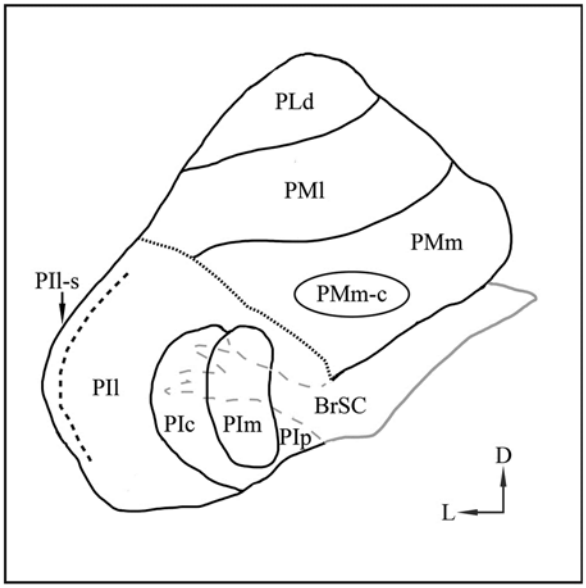

Figure 5.

Cusick lab's divisions of the pulvinar. A schematic of a coronal section depicting the Cusick lab's divisions of the pulvinar in the macaque. Divisions and conventions of the inferior pulvinar as in figure 4B. Divisions of the dorsal pulvinar are: dorsal lateral pulvinar (PLd), medial pulvinar lateral division (PMl), medial pulvinar medial division (PMm), and medial pulvinar medial division central division (PMm-c). Based on data from: Gray et al., 1999; Gutierrez et al., 2000; Gutierrez and Cusick, 1997

division (PMl), and the medial pulvinar medial division (PMm). These three main divisions were determined using staining for AChE, Pv, and CB. Pld stained lightly and densely for CB densely for Ache and Pv. PMl stained moderately for ACHE, Pv, and CB. Lastly, PMm stained moderately for CB and moderately to lightly for Pv and AChE. These divisions appear to stack one on top of the other with PLd being the most dorsal and PMm the most ventral. The three divisions lie in this configuration for nearly the entire rostral caudal extent of the pulvinar with the exception of the most caudal aspect where PLd disappears, leaving the other two divisions. Also, retrograde tracing from the parietal cortex is presented as evidence for the three subdivisions, while retrograde tracing from the temporal cortex is used to define a subcompartment within PMm called PMm central division (PMm-c).

Other groups besides Gutierrez and colleagues (2000) have used connections to suggest that PM might be divisible, but as mentioned earlier, no consensus has been reached on a scheme for dividing PM, and no single group's divisions have been adopted by others (Cappe et al., 2009; Jones, 2007b; Romanski et al., 1997). Further, placement of PDM represents another issue with the divisions presented by Gutierrez. Despite the acceptance of PDM as an entity, Gutierrez does not indicate how this division fits into his model or clarify the anatomical extent of PDM. Nonetheless, the presence of some segregation in PM's wide ranging connections is likely and PM represents fertile ground for future anatomical study.

Comparison of simians and prosimians

The pulvinar of prosimians (largely represented by the bush baby, *Otolemur garnettii*) now appears to bear many similarities to the pulvinar of simian primates; this understanding, however, has been long in coming. As mentioned above, early attempts at division split the bush

baby pulvinar into a superior and inferior division separated by the BrSC (Glendenning et al., 1975). This work also suggested that the caudo-medial portion of the pulvinar receives strong projections from the SC. Other studies of that era showed that more lateral areas receive strong (though not exclusive) projections from V1 (Raczkowski and Diamond, 1980; Raczkowski and Diamond, 1981). Wall and colleagues (1982) suggested the division of the inferior pulvinar of bush babies into two parts based on differences in the density of projections from MT. Since these classic studies, and until very recently, there has been little progress towards further division of the bush baby pulvinar. The difficulty in dividing the bush baby pulvinar stems from its uniformity when stained for most of the substances that differentiate the anthropoid pulvinar (Baldwin et al., 2013; Wong et al., 2009).

Three recent studies have updated the organization of the bush baby pulvinar (Baldwin et al., 2013; Wong et al., 2009; Li et al., 2013 i.e. Chapter III). These studies are unified in asserting that the bush baby pulvinar is similar to the pulvinar of other primates, having a large lateral part containing by two visuotopic maps (though of the 3 only Li et al., 2013 demonstrates the maps directly), a smaller caudo-medial tract bearing a resemblance to the consensus divisions of PIp, PIm and PIcm and a dorsal medial area suggestive of PM. These works also find consensus on the existences of differences between the bush baby pulvinar and the pulvinar of other primates, though the specifics of those differences are not agreed upon.

Early anatomical studies in the bush baby hinted at the presence of maps in the pulvinar but only recently were the existence of two maps electrophysiologically confirmed (Li et al., 2013; Wong et al., 2009). The larger of the two maps sits in a dorsal position and is completely encompassed by the dorsal pulvinar. The smaller map sits in a more ventral position and straddles the border (i.e. the BrSC) between the superior and inferior pulvinar (Li et al., 2013).

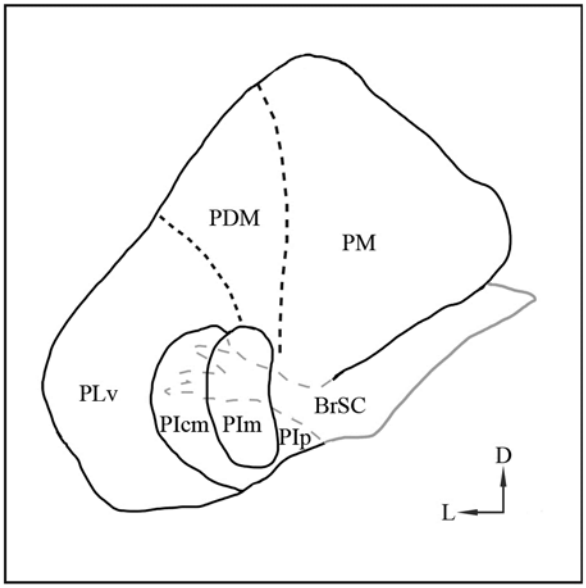

Figure 6.
Divisions of the pulvinar to be used to review connections and function. A schematic of a coronal section depicting the divisions of the pulvinar to be used for the remainder of this review in the macaque. Dashed lines represent the inexact borders between PLv, PDM, and PM. PLv = ventral lateral pulvinar

This location receives strong projections from V1 in a way reminiscent of the V1 projections to the mapped area in the macaque (Wong et al., 2009). The maps are both first order and share a border that includes central vision and the vertical meridian which is represented by a curved line at the most posterior extent of the maps. The horizontal meridian is represented as a sheet that runs perpendicular to the vertical meridian in roughly the parasagittal plane (Li et al., 2013). These features mean that the maps in the bush baby are arranged in a somewhat different manner than in the macaque. However, the overarching similarities to the maps in other primates are strong and this area has been judged a likely homologue to the maps in macaque (Baldwin et al., 2013; Li et al., 2013; Wong et al., 2009).

Along with the two maps some medial and posterior areas were found to lack clear retinotopy (Li et al., 2013). Part of this area stains strongly for Vglut2 mirroring the projections from the SC (Baldwin et al., 2013). This is a parallel to the strong Vglut2 staining that has been found in macaque PIp and PIcm (Balaram et al., 2013). Further, a previously unnoticed myelin circle analogous to the mark originally distinguishing PIm in owl monkey was found medial to the mapped area (Li et al., 2013). These data are strong evidence that at least some of the consensus regions found in other primates can be found in the bush baby, though the extent of the homology is still in debate. The dorsal aspect of the medial non-retinotopic area is reminiscent of PM in other primates though, as is the case for PM in general, the area is defined more by our lack of understanding than by any clear anatomical or physiological signature.

Summary of divisions

For the sake of clarity it is best to relate past work defining the connections and physiology of the pulvinar to a single set of divisions. As reviewed above, there is ample

evidence for several different sub-nuclei within the pulvinar. Nonetheless, judging the overall level of certainty for the divisions of the pulvinar is difficult. Some divisions have broad consensus while others are in varying levels of dispute. In anthropoid primates the three divisions of the inferior pulvinar (PIm, PIp and PIcm) seem the clearest, while the process of dividing the medial pulvinar has only just begun. When comparing to historical work, new small areas like PIp and PIl-s can pose a problem because their size creates uncertainty about whether they were studied. The specter of variation between species adds further difficulty. In the macaque the organization of the inferior pulvinar and the inferior part of the lateral pulvinar seem clear, while in other species less certainty exists. With these difficulties in mind, I will propose a set of pulvinar divisions. I emphasize that these divisions are made out of necessity and I am cognizant that additional work will be needed to fully understand the divisions of the pulvinar.

I will use broad divisions of the pulvinar for the purpose of describing both the connections and physiological properties presented in subsequent sections. Because the vast majority of work to be reviewed is for the macaque, I have biased the divisions selected towards those demonstrated for the macaque. Further, the second largest body of work in the pulvinar is in the spider monkey which shares striking similarities with the pulvinar of the macaque (Stepniewska et al., 2000). The divisions to be used will be described within the framework of macaque PL, PI, and PM (see figure 6). In this scheme PL is broken in two parts at the top of the BrSC (similar to the Cusick schema). The dorsal part of PL as well as the part of PM just above the inferior pulvinar is treated as a single subnucleus; this division is likely composed mostly of PDM and I will refer to it simply as PDM. PIp, PIm and PIcm will be recognized when these areas are distinguishable. The ventral part of PL that remains I will call PLv. This area

encompasses the visuotopic maps (P1 and P2), PIcl and PIl-s. PM is left largely as Olszewski envisioned it except where it has ceded room to PI and PDM. Some publications do not allow for small divisions to be distinguished; if this is the case I will simply refer to the Olszewski's divisions PI, PL, and PM. As reviewed above, Olszewski's divisions can be distinguished in most simians. The divisions described are used for all species except the owl monkey and prosimians where no clear lateral pulvinar exists. In owl monkey the medial divisions of PIp, PIm and PIcm will be specified and the area lateral to these divisions existing in both the inferior and dorsal pulvinar will be assumed to be analogous to the mapped areas in macaque, while the area of pulvinar dorsal to the PI complex will be assumed analogous to PM. In bush baby the pulvinar is divided into three parts: a lateral mapped area that, as reviewed above, is analogous to PLv and will be called PLv, a ventro-medial unmapped area (likely homologous to PIp and PIm) and a dorsal medial area (likely homologous to PM).

Connections

The following section discusses issues surrounding the connections of the PL, PI and PM. The first sub-section provides an overview of the pulvinar's connections and touches on issues of differential density of cortical and subcortical connections. The second sub-section traces the cortico-thalamo-cortical connections and discusses their components.

The pattern of pulvinar connection

The pulvinar has a vast array of connections to both cortical and subcortical areas. Within the telencephalon the pulvinar as a whole is connected to most if not all of the parietal

occipital and temporal cortices. Restricted elements of frontal cortex, limbic cortex and other telencephalic areas also receive from the pulvinar. Table 1 gives an accounting of the connections within PL, PI and PM. The pattern revealed by the table shows that the sub- nuclei of PI and PLv are most concerned with the visual areas lying within the occipital and temporal cortices. PDM is also connected with many visual areas but extends its connections into the posterior parietal cortex. Lastly, PM is connected with some parts of the posterior cortex, virtually all of the temporal lobe and portions of the frontal cortex and limbic system.

The pulvinar receives input from several subcortical areas outside the telencephalon. The SC and retina are the best documented of these (see table) but the pulvinar also receives other projections. These other subcortical inputs as a whole are not glutamatergic and resist being tabulated because their projection foci within the pulvinar are not yet fully charted, some having only been demonstrated in cat and prosimian. First among the sub cortical afferents to the pulvinar is the thalamic reticular nucleus which provides GABAergic feedback presumably to all parts of the pulvinar (Conley and Diamond, 1990). GABAergic projections are also provided by the nucleus of the optic tract in the pretectum (Baldauf et al., 2005; Lysakowski et al., 1986). The parabigeminal nucleus and parabrachial region contribute cholinergic projections to the pulvinar (Diamond et al., 1992; Lysakowski et al., 1986). Finally, the pulvinar is innervated by serotonergic and noradrenergic projections from the brain stem (Morrison and Foote, 1986).

Simply listing the areas that are connected to the pulvinar nuclei does not fully represent the pattern of connections. Shipp (2001) argued for different functional subcompartments within the visuotopic maps of macaque PLv. As discussed above, in the maps of the macaque pulvinar, the vertical and horizontal meridians are mapped as sheets, meaning that there is a third

		PI			PL		PM
		PIp	PIm	PIcm	PLv	PDM	PM
Sub cortical	retina	x	xx	x	0	0	0
Sub cortical	SC superficial	xx	x	xx	x	x	0
Sub cortical	SC deep	0	0	0	0	x	x
occipital	V1	0	0	x	xx	0	0
occipital	V2	x	x	x	xx	x	0
occipital	V3	x	x	x	x	x	0
occipital	V4	x	x	x	x	x	0
temporal	MT	x	xx	x	x	x	0
temporal	FST, MST	0	x	0	0	0	x
temporal	V4v, TEO	0	0	0	x	x	x
temporal	auditory belt, para-belt	0	0	0	0	0	x
temporal	TE, temporal pole	0	0	0	x	0	xx
posterior parietal	LIP, VIP, PO	0	x	x	0	x	x
frontal	FEF, 45	0	0	0	0	x	x
cingulate	posterior cingulate	0	0	0	0	0	x
limbic	amygdala, anterior cingulate, orbital frontal	0	0	0	0	0	x
insula	insula	0	0	0	0	0	x

Key: 0 =little or no evidence of projections, x = projections, xx = dense projections

Table 1. Connections of the Pulvinar

Presented below are the connections of PI, PL and PM to selected brain regions. Pip, PIm, PIcm and PLv are most connected with areas involved in the first stages of cortical visual processing. PDM is most connected with areas involved in the later stages of visual processing. PM is connected with frontal, temporal and auditory areas likely indicating that it may be divided further. The data in the table represents the interpretation of a large body of literature. The supplementary material at the end of this review provides a list of the areas connecting to the pulvinar followed by references in which these connections have been demonstrated. The course and fine divisions of the pulvinar are tabulated in rows 1 and 2 respectively. The course and fine divisions of much of the rest of the brain are tabulated in column 1 and 2 respectively. SC superficial = superior colliculus superficial layer, SC deep = superior colliculus deep layer, V1 = the primary visual cortex, V2 = the secondary visual cortex, V3 = the third visual area, V4 = forth visual area, MT = middle temporal area, FST = floor of the superior temporal sulcus, MST = middle superior temporal, V4v = ventral part of forth visual area, TEO= posterior part of inferotemporal cortex, LIP = lateral intraparietal area, VIP = ventral intraparietal area, PO = parieto-occipital cortex, FEF = frontal eye fields, 45 = brodmann's area.

dimension within the mapped area where an additional feature (besides the two dimensions needed to represent the retina) could be mapped (see also Li et al., 2013). Using tracer injections into V1, the secondary visual cortex (V2), the fourth visual area (V4), and MT Shipp (2001) argued that V1 and V2 projects to the entire mapped area but V4 and MT occupies separate compartments along the mapped area's third (non-visual) axis. This arrangement allows the V4 and MT recipient volumes to have full visual representations in both maps, but not overlap. These data suggest that output from the maps might be segregated between the dorsal and ventral processing streams (Shipp, 2001). Kaas and Lyon (2007) have also argued that pulvo-cortical connections segregate between the two visual streams but make their case from a different premise. They suggested that a single afferent area may differently innervate the multiple pulvinar sub- nuclei to which it projects and that when taken as a whole the projections to PLv and the sub-nuclei of PI appear to segregate. PLv was shown to associate with the cortical areas involved in the ventral stream while the PI complex was shown to associate with the dorsal stream (Kaas and Lyon, 2007 for review). The place of SC in these patterns of connections has been the focus of continuous debate but it has become apparent that the SC connects more to cells projecting to MT and V3 (dorsal stream areas), sends a few connections to cells projecting to V4 (a ventral stream area) and appears to provide no input to cells projecting to V2 or V1 (primary areas) (Lyon et al 2010).

Following the cortico-thalamo-cortico connections

The dorsal thalamus and cortex are tightly interlinked. The entire cortex receives dorsal thalamic projections and the entire dorsal thalamus receives cortical afferents. This relationship is specific such that if cortical area A projects to thalamic nucleus B then thalamic nucleus B will

send projections to cortical area A (Jones, 2007a for review). The pulvinar as part of the dorsal thalamus exhibits this property and the following section is devoted to describing the form of the projections between the thalamus and cortex as well as the patterns that exist within these projections.

The descending projections to the pulvinar come from two populations of pyramidal cells: larger cells located in layer V and smaller cells located in layer VI. There is evidence that within V1 the majority of cells projecting to the pulvinar are layer Vb cells (but see Conley and Raczkowski, 1990) while more anterior areas receive projections from layer Va and VI cells (Levitt et al., 1995; Lund et al., 1981; Lund et al., 1975; Raczkowski and Diamond, 1981; Rockland, 1996; Trojanowski and Jacobson, 1977). It has been suggested that layer VI neurons are feedback projections while layer V neurons are feed forward projections (Sherman and Guillery, 2006). In the visual system, this theory is based on the fact that V1 projections to the LGN originate in layer VI, and projections from V1 to pulvinar originate in layer V (Sherman and Guillery, 2006). Evidence for the theory is sparse in data pertaining to the connections between the extrastriate areas and the pulvinar. Some evidence can be derived from a study by Raczkowski and Diamond (1981) in bush baby which was done before much of the extrastriate cortex had been divided into modern functional divisions. In this study retrograde tracer was injected into various subnuclei in the pulvinar resulting in the labeling of layer V and VI cells in various parts of the cortex. No part of the cortex was labeled by every injection but when cells in V1 were labeled they were always in layer V and when cells in the inferotemporal cortex (IT) were labeled they were always in layer VI. The cortex between V1 and IT (remember modern subdivisions were not defined) showed a trend of having either layer V or VI cells (but not both) depending on what part of the pulvinar was injected. For example, if a given part of the extra

striate visual cortex had layer VI pulvinar projecting cells then there would always be a patch of layer V cells in a more posterior part of the cortex. If, however, a different injection labeled layer V cells in that same part of the cortex then there would always be a patch of layer VI cells in a more anterior area (Raczkowski and Diamond, 1981). This trend in the data supports the idea that layer V cells send feedforward projections while layer VI cells produce feedback projections. Examination of the arbors and boutons of layer V and VI cells provides further evidence of a functional division.

The two varieties of pulvinar projecting cells (layer V and VI) are assumed to connect to two varieties of pulvinar projections (round and elongated respectively) that are described below. It is worth noting that the evidence for this link in primates is largely correlative. The link in non-primates is strong, therefore I find the generalization to primates reasonable (reviewed Sherman and Guillery, 1996).

Using light microcopy (LM) in the macaque Rockland (1994; 1996; 1998) described two types of axons projecting from the temporal and occipital cortices to the pulvinar. The more numerous of these types had thin axons, elongated wide ranging arbors (1-3 mm covered) and small boutons while the less numerous variety had large axons, compact round (spherical with a diameter of 100-150 μm) arbors with large boutons. Rockland dubbed these projections elongated (E) and round (R), respectively. Of the cortical areas injected, the more posterior (V1) sent mostly R with some E projections to PI and PL, while somewhat more anterior areas (specifically the posterior inferotemporal area TEO and MT) sent mostly E and some R projections to PI and PL, and the most anterior areas injected (inferotemporal areas TE and TF) only sent type E projections (Rockland, 1996; Rockland, 1998). R projections from V1 tended to have 2-3 foci within the pulvinar while R projections from other visual areas had one focus

(Rockland, 1998). The temporal lobe areas sent either entirely type R projections or a mix of both types to PM (Rockland, 1996). Parallel work demonstrates both E and R type projections from macaque posterior parietal cortex to PM (Darian-Smith et al., 1999). In the studies described above these two types of arbors tended to overlap or lie either immediately adjacent to each other, though, interestingly this is not always the case in for somatosensory projections to PM (Darian-Smith et al., 1999; Rockland, 1994; Rockland, 1996; Rockland, 1998). E arbors tended to send collaterals to the TRN while R projections sent collaterals to the SC or pretectum (Rockland, 1998). This work was anticipated by work in rat and similar findings have been demonstrated in cat (Deschenes et al., 1994; Guillery et al., 2001).

Rockland's findings correlate well with prior work on both the LM and ultrastructural levels. Previous electron microscopy (EM) in the macaque and squirrel monkeys demonstrated at least 4 types of terminals (Mathers, 1972a; Mathers, 1972b; Ogren and Hendrickson, 1979a). The most numerous types had round vesicles and were relatively small (RS) as compared to a second variety that had round vesicles and a large size (RL). Further, two varieties of small terminals having flattened vesicles were identified, one variety (called P by Ogren and Hendrickson) had both pre and post synaptic specializations visible and sometime contained ribosomes while the second had only presynaptic specializations (called F by Ogren and Hendrickson). RL terminals tended to make contact on proximal dendrites while RS terminals tended to make contacts on more distal dendrites. Further, RL terminals often formed synaptic triads and sometimes formed glomeruli with P terminals and presumed relay neuron dendrites. Perhaps most importantly Mathers (1972b), working in squirrel monkey, demonstrated that both RL and RS terminals degenerated when large areas of the occipital and temporal lobes were ablated. This final finding contrasted with lesions of the primary sensory cortices that caused

only RS terminals in the LGN and MG to degenerate (Mathers, 72b). Studies from other thalamic nuclei, especially the LGN, have been used to suggest that RL and RS terminals are glutamatergic while P and F terminals are GABAergic and originate from the dendrites of local circuit neurons and GABAergic cell axons (either from local circuit neurons or TRN neurons) respectively (reviewed Jones, 2007a).

Recent work has confirmed the existence of RL and RS type terminals throughout the pulvinar but suggests that the size and origin of these terminals is not uniform. A key assumption of this work is that Vglut2 and Vglut1 transporters are markers of subcortical or cortical afferents; an assumption which appears to be well founded (Balaram et al., 2013). With this assumption in place researchers used both LM and EM methods to survey the thalamus for RL terminals and found that regions resembling PIp, PIcm and a part of the lateral pulvinar (likely corresponding to the lateral shell of the Cusick group) had RL terminations from a subcortical source presumably the SC (Rovo et al., 2012). Further it was demonstrated that PM had significantly smaller RL terminals than PL (Rovo et al., 2012). This work further emphasizes the dangers of treating the pulvinar as a single nucleus.

Authors working with Golgi stained cells have reported that the typical relay neuron in PI and PLv has a symmetric dendritic field of 150-600μm in diameter with the average field of ~ 500μm in diameter. Cell bodies in this area vary in diameter between 15 and 40μm with a typical soma size of ~30μm (Ogren and Hendrickson, 1979b). Similar results have been reported for relay neurons in PDM and PM and in general these neurons are similar to other relay neurons found in the thalamus (Darian-Smith et al., 1999; Ogren and Hendrickson, 1979b).

The Golgi studies described above do not support the concept of sub-classes of pulvinar relay cells. However, several investigators who have stained the pulvinar for CB have noted the

presence of very large projection neurons scattered unevenly through PL and PI (Gutierrez et al., 1995; Imura and Rockland, 2007; Stepniewska and Kaas, 1997). The core and matrix theory associates staining for Pv or CB with two classes of relay cells (reviewed Jones, 2007a). This theory is based largely on the primary thalamic nuclei but has been generalized to the rest of the thalamus. In the core and matrix theory CB containing projection cells are called matrix cells. CB containing relay cells (contrary to the data mentioned above) have been shown to have small cell bodies and project mostly to layer I with some projections to layers II and III. Pv containing cells, in contrast, are large and project to the middle layers (reviewed Jones, 2007a).

Projections from pulvinar relay neurons ascend through the internal capsule to the cortex, branching at least once along the route. As ascending axons leave the thalamus they branch and provide collaterals to the TRN (Conley and Diamond, 1990). In general after branching in the TRN, axons from the pulvinar do not branch again until the cortical target area is reached, but in a minority of cases pulvinar axons branch to innervate two cortical areas. Retrograde double labeling experiments have demonstrated cells that projected to V1 & V2, V1 & V4, and V4 & MT (Adams et al., 2000; Kennedy and Bullier, 1985; Lysakowski et al., 1988). Axons that project from PL to the extrastriate visual areas branch further after they reach their target areas, separating into 2-6 spatially discreet arbors (Rockland et al., 1999). Within V2 of the macaque, pulvinar projections to the middle layers are thicker in the CO rich stripes in macaque suggesting that the branching pattern of pulvinar axons may specifically target spatially separated functional units in the cortex (Levitt et al., 1995).

The projection pattern from the pulvinar to V1 is distinct compared to the pulvinar's projections to the other parts of the cortex. In V1 the pulvinar projects to layer I densely and layers II-III sparsely (Ogren and Hendrickson, 77; Chapter V). The axons projecting to layer I

ascend in a columnar manner until reaching layer I where they turn at right angles and run parallel to the cortical surface in the outer half of layer I forming arbors of predominantly en passant boutons (Chapter V). These boutons are of similar size to boutons found in layer I of the extrastriate cortex (Chapter V). Large injections into PLv demonstrate patchiness in the layer II-III projections in V1, at least in macaque, though the structural or functional units that these patches correlate with is unknown (Ogren and Hendrickson, 1977).

Pulvinar projections to areas outside V1 have similar termination patterns (Levitt et al., 1995; Rockland et al., 1999; Romanski et al., 1997; Marion et al., 2013, i.e. Chapter VI). In the areas examined the pulvinar forms arbors most densely along the border of layers III and IV with clear projections to layers I, III and IV. Some reports include descriptions of light projections in layers II, V and VI (Rockland et al., 1999). Investigation of projections from PL to various visual areas did find differences in the size of arbors and terminal fields. Area V4 had the largest arbors and terminal fields while MT had the smallest with V2/V3 lying somewhere in between (Rockland et al., 1999). Arbors were described as being most prominent in layers III and IV but a single axon could also innervate any or all of the other layers (Rockland et al., 1999). In V2 the arbors in layer I and layer IV appeared to originate from the same parent axons, however, layer 1 arbors appeared morphologically similar to V1 layer I pulvinar projections (though more spatially restricted), while layer IV arbors were much more columnar (Rockland et al., 1999; Chapter V). Further the boutons on layer I arbors were smaller when compared to their layer IV counterparts which were larger than the afferent cortical connections from V1 (Marion et al., 2013; Chapter V).

Function

As anticipated by their connections PI, PL and PM contain a variety of visually responsive neurons. The receptive field properties of the subnuclei appear to reflect their inputs from the cortex or SC and can be modulated by orienting and attention. Lesions of the pulvinar have differing effects and highlight that the role of the pulvinar in vision is far from settled. The first subsection below will discuss the visual receptive field properties of the pulvinar. The second subsection will review data pertaining to the role of the pulvinar in attention and orienting.

Receptive field properties

Conclusions from previous studies suggest that different subnuclei contain different proportions of visually responsive neurons and somewhat distinct receptive field properties. In the macaque monkey, the PI complex contains the most visually responsive cells (90%), followed by PLv (74%), then PDM (57%) and lastly PM with the fewest visually responsive cells (22%) (Maior et al., 2010; Petersen et al., 1985). Receptive field sizes in PI, PLv and PDM increase with eccentricity (Bender, 1982; Berman and Wurtz, 2010; Li et al., 2013; Petersen et al., 1985). For a given eccentricity the receptive fields of PI and PLv are similar in size and somewhat larger than V1 receptive fields (Bender, 1982; DeBruyn et al., 1993; Li et al., 2013; Petersen et al., 1985). PDM contains substantially larger receptive fields than PI or PLv (Peterson et al 85). Some parts of PM and perhaps also parts of PDM contain receptive fields that are bilateral, some of which verge on full field (~40 degrees in diameter) (Benevento and Port, 1995). Most cells in PLv appear to be binocular with a minority of monocular cells; the

proportion of monocular to binocular cells varies between bush baby and macaque (Bender, 1982; Li et al., 2013).

PI and PLv have many cells (proportions vary depending on the paper) that respond to light spots, oriented bars, and directional stimuli (Bender, 1982; Mathers and Rapisardi, 1973; Petersen et al., 1985; Robinson and Petersen, 1985). Thanks to the diligent work of Berman and Wurtz (2008; 2010; 2011) the connections of some of these cells are known. These researchers recorded in PL and PI and used orthodromic and antidromic stimulation from electrodes in SC (superficial layers) and MT to establish the connections of the cells recorded. Berman and Wurtz (2008; 2010; 2011) demonstrated that cells receiving projections from SC were sensitive to light spots (not bars), cells that projected to MT were not directionally selective, and cells that received projections from MT tended to be directionally selective. These data suggested that directionally selectivity in pulvinar cells in inherited from cortex and not from SC (Berman and Wurtz, 2008; Berman and Wurtz, 2010; Berman and Wurtz, 2011). PDM cells are also selective for orientation and direction though less is known about the connections that confer these properties (Petersen et al., 1985). More elaborate response properties have been reported for pulvinar neurons. Cells in PM and PDM have been shown to respond to complex geometric shapes and show color opponency (Benevento and Port, 1995; Nguyen et al., 2013). Further, within PM (of macaque) a group of cells responds to human faces and a minority of these cells codes for the emotional content of these faces (Maior et al., 2010).

Orienting and attention

Cells within the macaque pulvinar have been shown to alter their firing in response to several behavioral and cognitive states. Cells showing saccadic suppression, presaccadic

enhancement, postsaccadic enhancement and biphasic enhancement have been reported for PI, PLv and PDM (Benevento and Port, 1995; Berman and Wurtz, 2008; Berman and Wurtz, 2010; Berman and Wurtz, 2011; Petersen et al., 1985). Berman and Wurtz (2011) demonstrated that cells receiving input from SC exhibited saccadic suppression (but not attention effects) and some of these cells projected to MT. Attention has been shown to modulate activity in PI, PLv and PDM. Attention appeared to have a greatest influence on the cells of PDM (Bender and Youakim, 2001; Petersen et al., 1985).

Some studies of simians and humans with lesions in the pulvinar support a role for the nucleus in orienting and attention while many other simian studies do not clearly support a connection. Early studies of bilateral lesions show either no effect or effects on eye movements and attention(Bender and Baizer, 1984; Bender and Baizer, 1990; Bender and Butter, 1987; Chalupa et al., 1976; Chow, 1954; Leiby et al., 1982; Nagel-Leiby et al., 1984; Ungerleider et al., 1977; Ungerleider and Christensen, 1977; Ungerleider, 1979; Ungerleider and Pribram, 1977). Bender (1988) has argued that the effects seen during the bilateral studies are the result of disruptions of the BrSC. Evidence for this claim comes from studies that show a recapitulation of the lesion results only when lesioning methods disrupted fibers of passage (Bender and Baizer, 1990; Bender and Butter, 1987; Leiby et al., 1982). Lesions in these studies generally involve all of PI and PLv with some or all of PDM also being destroyed (Bender and Baizer, 1984; Bender and Baizer, 1990; Bender and Butter, 1987; Chalupa et al., 1976; Chow, 1954; Leiby et al., 1982; Nagel-Leiby et al., 1984; Ungerleider et al., 1977; Ungerleider and Christensen, 1977; Ungerleider, 1979; Ungerleider and Pribram, 1977).

In contrast to bilateral lesions, unilateral lesions (or inactivation) of the pulvinar have been shown to cause visual defects in both humans and monkeys. Human patients with

unilateral pulvinar lesions can suffer from acute hemineglect and show persistent deficits of varying degrees of severity in orienting and attention(Arend et al., 2008; Ogren et al., 1984; Rafal and Posner, 1987; Snow et al., 2009; Strumpf et al., 2012; Ward and Arend, 2007; Ward et al., 2002). In a classic study, deficits in reaction times in the contralesional hemisphere were demonstrated in patients with pulvinar lesions performing a cued reaction time task (Rafal and Posner, 1987). In recent studies more complex deficits have been explored. For example, paitents with pulvinar lesions were shown to perform a lateralized orientation discrimination task equaly well in both hemifields but the additon of flanking distractors (two patches of increased or decreased contrast) caused a greater detrement to performance in the contralesional hemisphere (Snow et al., 2009). Inevitably, these studies suffer from difficulty localizing the lesions and patient variability but none the less suggest a connection between the pulvinar and attention.

Two studies in macaque have used unilateral reversible GABAergic blockades of PDM to study the role of this nucleus in orienting and attention (Petersen et al., 1987; Wilke et al., 2010). Both report symptoms consistent with the biasing of attention to the hemisphere ipsilateral to the blockade. In one study, Petersen and colleagues (1987) used a saccade based variant of a cued reaction time task (Posner task) to demonstrate that monkeys made slower saccades to validly cued targets on the side contralateral to the blockade and faster saccades to invalidly cued targets on the side ipsilateral to the blockade. In a second study a more complex task was used but results were similar with faster saccades to targets ipsilateral to the blockade when compared to saccades made when only vehicle was injected, as well as a pronounced bias to saccade to targets ipsilateral to the blockade when targets were presented in in both hemispheres simultaneously (Wilke et al., 2010). Further blockade of PDM also appeared to cause the improper use of the

upper limb commiserate with problems with the sensory motor transform (Wilke et al., 2010). The difference between the effects of unilateral and bilateral lesions is curious and to my mind points to the presence of a hemispheric imbalance reminiscent of the Sprague effect (Sprague, 1966; Sprague and Meikle, 1965). Regardless of the reasons for the effects observed, the neglect seen in unilateral lesions of the pulvinar suggests that PLv and especially PDM are part of a network of areas responsible for attention.

How does the pulvinar participate in the cortical attentional network? A recent paper presents one possible mechanism. Saalmann and colleagues (2012) made simultaneous recordings from multiple visual areas in macaques preforming a cued flanker task. The task structure allowed for a period of time between the cue and the stimulus where attention was allotted to a particular spatial location without the presence of a stimulus. The researchers simultaneously recorded single units and LFPs in V4, TEO and PLv or PI. They used a measure called coherence which is the normalized Fourier transform of a cross correlogram to compare changes in synchrony between areas and conditions. The attended condition was shown to have increased coherence in alpha band frequencies between the LFPs in each of the areas (i.e. V4-pul, V4 – TEO and pul – TEO). Further there was an increase in coherence (in the alpha band) between the spikes in the pulvinar and the LFPs in V4 and TEO. Lastly, the researchers used conditional Granger causality (i.e. partial correlation with Granger causality) to demonstrate that the pulvinar Granger caused the attention associated increase in alpha band activity in both TEO and V4 but V4 and TEO had little influence on each other. This research was interpreted to mean that PLv and PI orchestrate the synchronization of cortical areas during attentional states. When interpreting this work it is important to keep in mind that most of the claims of the paper are based on comparisons of the attended and un-attended conditions during the delay period

between cue and response time when the monkey must remember where the cue appeared as well as attend to that position. Future work will be needed to determine if memory or attention are responsible for the effects observed. Also, the lack of orienting problems when the pulvinar is ablated bilaterally raises the possibility that PLv and PI are not necessary for all processes supporting attention. Regardless this is an interesting and potentially important paper and represents the most recent iteration of theories linking pulvinar function to synchrony, attention, or in this case, both (Saalmann and Kastner, 2011; Shipp, 2003; Shipp, 2004).

Drivers, Modulators and the Place of the Pulvinar in the Visual Hierarchy

What cells must fire for pulvinar cells to fire? What cells will fire if a pulvinar cell fires? These are basic and interesting questions though they are deceptively difficult to answer. At the heart of both questions is the concept of drive, which is a difficult term to define concisely, yet, one that is central in the thoughts of many neuroscientists. Sherman and Guillery have produced by far the most extensive theory of driving especially with regards to the pulvinar (Guillery and Sherman, 2002a; Guillery and Sherman, 2002b; Guillery and Sherman, 2011; Sherman, 2007; Sherman, 2012; Sherman and Guillery, 1996; Sherman and Guillery, 1998; Sherman and Guillery, 2002; Sherman and Guillery, 2006; Sherman and Guillery, 2011; Sherman and Guillery, 2013). Here, I will describe their theories and outline how they apply to the pulvinar.

Theories on Driving and Modulating

In mid-1990's the existence of cortico thalamo cortico loops was becoming apparent in the primate thanks to Rockland's work (1994; 1996; 1998) on E and R terminals (see above).

Also, not too long previously, the work of Fellaman and Van Essen (1991) had popularized the idea of deducing the hierarchical nature of the cortex using anatomy. In this environment, Sherman and Guillery (1996; 1998) proposed that the Drive (which in this initial case means the ability for one area to activate a second area) could be passed from the cortex to some thalamic nuclei then back to the cortex at an area higher in the hierarchy than the initial cortical area. Their deduction is based largely on generalizations from the anatomy and physiology of the LGN which will be reviewed below. Crick and Koch (1998), influenced by Sherman and Guillery, showed how the same conclusion could be reached from a theoretical stand point. They reasoned that if area X drives area Y either directly or indirectly, then area Y cannot drive area X because this positive feedback loop would cause out of control oscillations in the brain (Crick and Koch, 1998). This principal they named the "No Strong Loops Hypothesis". From this logic they reasoned that if a cortical area drove part of the pulvinar then that part of the pulvinar could not drive that cortical area; instead, it must drive a part of the cortex further up in the hierarchy to keep from forming a strong loop (Crick and Koch, 1998). I mention Crick and Koch because their ideas help clarify the initial conception of a driver; namely, for both Crick and Koch as well as Sherman and Guillery the initial idea of driving is that of one area relating to another (Crick and Koch, 1998; Sherman and Guillery, 1996).

Sherman and Guillery (1996) proposed several basic logical steps to get to the theory outlined above. This idea is based on concepts initially developed by Guillery (1995) but is stated in full in Sherman and Guillery's first review (Sherman and Guillery, 1996). First, they observe that in the primary sensory relays of the thalamus the drive is known to be the peripheral sense organs. Second, the anatomic and physiologic properties of the glutamatergic driving afferents (drivers) coming from the periphery to primary relay nuclei are well known and differ

from the properties of the descending glutamatergic afferents from layer VI of the cortex (modulators). Third, the form of the descending inputs from layer V of the cortex to the association nuclei (which includes the pulvinar) is similar to the form of the drivers in primary thalamic nuclei and it is known that the cortex is responsible for driving some association nuclei. Finally they suggest that there is no reason to assume that higher cortical sensory areas are driven by lower cortical sensory areas; higher sensory areas may be driven entirely by the thalamic association nuclei. In their 1996 review as well as in many subsequent reviews, Sherman and Guillery lay out a parametric approach for identifying driving or modulating projections (Table 2; Sherman and Guillery, 1996; Sherman and Guillery, 1998; Sherman and Guillery, 2002; Sherman and Guillery, 2006; Sherman and Guillery, 2011; Sherman and Guillery, 2013). Further, they suggest that all the primary relays be referred to as first order sensory relays and that the association nuclei should be called higher order thalamic relays. Higher order is used instead of second order to emphasize that information may pass through the thalamus many times during its processing.

In the time since their original publication, Sherman and Guillery have revised their theories in two ways. First, they now allow that there are some cortical areas that are driven in part by the direct projections from other cortical areas (Sherman and Guillery, 2011; Sherman and Guillery, 2013). Second, the projections that possess the properties of known drivers they have switched from calling 'driving projections' to calling them 'Class 1 projections' (Sherman and Guillery, 2011; Sherman and Guillery, 2013). Similarly the projections that possess the properties of glutamatergic modulators are now known as 'Class 2 projections' with non-glutamatergic modulators (a Class that developed through the years) being referred to specifically by the transmitter used (Sherman and Guillery, 2011; Sherman and Guillery, 2013).

Driver (Type 1)	**Modulator (Type 2)**
Thick axons	Thin axons
Little convergence onto target	Much convergence onto target
Large terminals on proximal dendrites	Small terminals on distal dendrites
Each terminal forms multiple contacts	Each terminal forms a single contact
Large excitatory postsynaptic potential	Small excitatory postsynaptic potential
Activates only Ionotropic receptors	Activates metabotropic receptors
Synapses show paired-pulse depression	Synapses show paired-plus facilitation
Creates sharp cross-correlogram	Creates sharp cross-correlogram

Table 2. Properties of Glutamatergic Drivers and Modulators
Adapted from Sherman and Guillery (2006)

The terms driver and modulator are retained in their writing but now refer purely to the concept of information flow (Sherman and Guillery, 2013). They define drivers as carrying the main message and modulators as incrementally changing that message (Sherman and Guillery, 2013). This change in nomenclature allows Sherman and Guillery to highlight that their classification schema can be used in contexts where the content of the information being passed between cells or areas is unknown (Sherman and Guillery, 2011; Sherman and Guillery, 2013). Also, this change in nomenclature marks a difficulty in defining all projections from one area as drivers of a second area because it turns out that the variables defined (class 1 and 2) are best used at the synapse or at the single cell level where as driving and modulating are concepts that are native to the level of whole areas or at least sub-compartments within an area (De Pasquale and Sherman, 2011; Petrof et al., 2012).

Drivers of the pulvinar

The Sherman and Guillery (1996; 1998; 2006) theory can be applied to projections entering and exiting the pulvinar to pick out likely drivers and modulators. It is perhaps best to admit up front that the anatomy of the pulvinar is not known in sufficient detail to place all parts of it precisely into a visual cortical hierarchy. Some statements can be made concerning what areas drive the pulvinar and what areas are driven by the pulvinar. First I will cover the projections to the pulvinar then move on to the ascending projections from the pulvinar.

As out lined in the connections section, the cortico- thalamic projections from layer 5 that have been examined in detail appear to fit some of the criterion for Class 1 projections (Levitt et al., 1995; Lund et al., 1981; Lund et al., 1975; Raczkowski and Diamond, 1981; Rockland, 1996; Trojanowski and Jacobson, 1977). Bender (1983) established that the inferior map in PLv loses

its visual responsiveness after V1 but not SC lesions, proving that PLv directly or indirectly gets its drive from V1. Recent work (also described in the 'Connections' section) suggests that PIcm and PIp along with parts of PLv receive projections from sub- cortical areas (likely SC) that resemble Class 1 projections (Rovo et al., 2012). Interestingly, there is somewhat contradictory work that shows retinal projections to PIm making Class 1 synapses on MT projecting relay cells (Warner et al., 2010). Also, cells in PI appear to inherit their motion sensitivity from MT suggesting that MT drives some of PI (Berman and Wurtz, 2010; Berman and Wurtz, 2011). In conclusion, given the prevalence of layer 5 projections running from V1 to PLv it seems likely that PLv is driven in part by V1. PLv, PDM, PM and some of PIm are likely all driven by cortex though which cortical area exactly remains to be resolved as more data are gathered. Some circuits in PI, especially in PIcm and PIp, are likely driven by the SC or perhaps the retina (Rovo et al., 2012; Warner et al., 2010).

The paths ascending from the pulvinar to the cortex are difficult to class into drivers and modulators. Data presented in this thesis and reviewed in the connections section suggests that projections from PLv to layer IV of V2 fit the form of Class 1 projections while terminals ending in layer I appear smaller, suggesting that they are more like Class 2 projections (Marion et al., 2013). As noted previously, these two populations of terminals appear to arise from the same axons in projections to V2 (Marion et al., 2013; Rockland et al., 1999). In cebus monkeys, GABAergic blockade of part of PLv during recordings of overlapping receptive fields in V2 led to mixed results with an increase in firing in some cells and a decrease in others in both the stimulus driven and spontaneous conditions (Soares et al., 2004). Perhaps these opposite results are due to the opposite effect of class 1 and 2 projections on different layers? Unfortunately, these results are difficult to interpret because the block in the pulvinar was partial, dropping the

responsiveness by only 40%. Also, the length of the blockade was substantially longer than anticipated and the cases were chronic with one experiment a week for about 20 weeks making it impossible to rule out compensatory changes in the pulvinar or cortex.

The afferent projections from the pulvinar to V1 are likely modulatory. As described in the connections section, the projections arise from PLv and terminate most densely in layer I and have small boutons relative to the layer IV projections of the pulvinar in V2 suggesting that they are Class 2 projections (Marion et al., 2013). The No Strong Loops Hypothesis also suggests that these projections should be modulatory because we know that PLv gets its drive either directly or indirectly from V1. Recent work by Purushothaman and colleagues (Purushothaman et al., 2012, i.e. Chapter IV) has demonstrated that the projections from PLv back to the cortex have a powerful effect on V1. In this study we demonstrated that visually driven activity in bush baby V1 cells was vastly diminished after blockade of a visuotopically overlapping region of PLv with a GABA agonist. This effect was especially pronounced for the transient component of the V1 cells response to the preferred orientation. Additionally, injection of PLv with a GABA antagonist had either an excitatory or inhibitory effect on V1 visual responses depending on how the injection, the V1 cells receptive field, and the stimuli were positioned (overlapping or not overlapping) relative to each other in the visual field.

The results reviewed above are important because they give us an idea of the type of information processing that might involve cortical modulators; yet the role of modulators appears under appreciated by Sherman and Guillery (1998; 2002; 2006; 2013). The concept that drivers carry the important information is central to Sherman and Guillery's theories. In their writing, the reader is repeatedly implored to follow the flow of information by defining the drivers (Sherman and Guillery, 1998; Sherman and Guillery, 2002; Sherman and Guillery, 2006;

Sherman and Guillery, 2013). On occasion this emphasis on driving is taken so far as to state that drivers are "information bearing," thus implying that modulators carry no information (Sherman, 2012). The suggestion that understanding the actions of modulators is somehow less important is very dangerous. Clearly modulators, both glutamatergic or otherwise have been implicated in a wide range of interesting behaviors (Kandel et al., 2000). The results reviewed above give important insights into the actions of glutamatergic modulators in the cortex and hopefully serve to provide some balance to research into drivers and modulators.

Supplementary Material

The section below consists of the references considered when compiling Table 1 listed by the area(s) in each data containing row of the table. References may be repeated if they apply to more than one row of the table.

Retina: (Cowey et al., 1994; Itaya and Van Hoesen, 1983; Mizuno et al., 1983; O'Brien et al., 2001; Warner et al., 2010)

SC superficial: (Baldwin et al., 2013; Benevento and Standage, 1983; Berman and Wurtz, 2008; Berman and Wurtz, 2010; Berman and Wurtz, 2011; Harting et al., 1980; Huerta and Harting, 1983; Lyon et al., 2010; Lysakowski et al., 1986; Mathers, 1971; Raczkowski and Diamond, 1981; Stepniewska et al., 1999; Stepniewska et al., 2000; Wong et al., 2009)

SC deep: (Baldwin et al., 2013; Benevento and Standage, 1983; Harting et al., 1980; Huerta and Harting, 1983; Lyon et al., 2010; Lysakowski et al., 1986; Mathers, 1971; Raczkowski

and Diamond, 1981; Stepniewska et al., 1999; Stepniewska et al., 2000; Wong et al., 2009)

V1: (Adams et al., 2000; Benevento and Davis, 1977; Benevento and Rezak, 1976; Carey et al., 1979; Conley and Raczkowski, 1990; Cooper et al., 1979; Dick et al., 1991; Glendenning et al., 1975; Huppe-Gourgues et al., 2006; Kaas and Lyon, 2007; Kaske et al., 1991; Kennedy and Bullier, 1985; Lin and Kaas, 1979; Lund et al., 1975; Lysakowski et al., 1988; Marion et al., 2013; Mizuno et al., 1983; Ogren and Hendrickson, 1976; Ogren and Hendrickson, 1977; Ogren and Hendrickson, 1979a; Raczkowski and Diamond, 1980; Rezak and Benevento, 1979; Rockland, 1998; Soares et al., 2001; Symonds and Kaas, 1978; Ungerleider et al., 1983; Wong et al., 2009)

V2: (Adams et al., 2000; Curcio and Harting, 1978; Dick et al., 1991; Kaas and Lyon, 2007; Kaske et al., 1991; Kennedy and Bullier, 1985; Levitt et al., 1995; Lin and Kaas, 1979; Livingstone and Hubel, 1982; Lund et al., 1981; Lyon et al., 2010; Marion et al., 2013; Ogren and Hendrickson, 1977; Raczkowski and Diamond, 1980; Rockland et al., 1999; Soares et al., 2001; Wong-Riley, 1977; Wong et al., 2009; Yeterian and Pandya, 1997)

V3: (Kaas and Lyon, 2007; Lyon et al., 2010; Marion et al., 2013; Raczkowski and Diamond, 1980; Shipp, 2001)

V4: (Adams et al., 2000; Lyon et al., 2010; Lysakowski et al., 1988; Raczkowski and Diamond, 1980; Rockland et al., 1999; Shipp, 2001; Soares et al., 2001; Yeterian and Pandya, 1997)

MT: (Adams et al., 2000; Berman and Wurtz, 2008; Berman and Wurtz, 2010; Cusick et al., 1993; Glendenning et al., 1975; Gray et al., 1999; Kaas and Lyon, 2007; Kaske et al., 1991; Lin and Kaas, 1979; Lin et al., 1974; Lyon et al., 2010; Raczkowski and Diamond, 1980; Rockland, 1998; Rockland et al., 1999; Shipp, 2001; Soares et al., 2001; Standage

and Benevento, 1983; Stepniewska et al., 1999; Ungerleider et al., 1984; Warner et al., 2010; Wong et al., 2009)

FST, MST: (Boussaoud et al., 1992; Kaas and Lyon, 2007)

V4v, TEO: (Baizer et al., 1993; Baleydier and Morel, 1992; Raczkowski and Diamond, 1980; Rockland, 1996; Trojanowski and Jacobson, 1976; Trojanowski and Jacobson, 1977; Webster et al., 1993; Yeterian and Pandya, 1989; Yeterian and Pandya, 1991)

Auditory belt, para-belt: (Cappe et al., 2009; de La Mothe et al., 2012; Gutierrez et al., 2000; Hackett et al., 2007; Hackett et al., 1998)

TE, temporal pole: (Baleydier and Morel, 1992; Markowitsch et al., 1985; Trojanowski and Jacobson, 1976)

LIP, VIP, PO: (Asanuma et al., 1985; Baizer et al., 1993; Baleydier and Morel, 1992; Cappe et al., 2009; Gutierrez et al., 2000; Lin and Kaas, 1979; Trojanowski and Jacobson, 1977; Yeterian and Pandya, 1985)

FEF, 45: (Asanuma et al., 1985; Cappe et al., 2009; Contini et al., 2010; Gutierrez et al., 2000; Romanski et al., 1997; Trojanowski and Jacobson, 1974; Trojanowski and Jacobson, 1976; Trojanowski and Jacobson, 1977)

Posterior cingulate: (Baleydier and Mauguiere, 1985; Yeterian and Pandya, 1988)

Amygdala, anterior cingulate, orbital frontal: (Romanski et al., 1997; Trojanowski and Jacobson, 1976; Yeterian and Pandya, 1988)

Insula: (Romanski et al., 1997)

Reference List

Adams MM, Hof PR, Gattass R, Webster MJ, Ungerleider LG. 2000. Visual cortical projections and chemoarchitecture of macaque monkey pulvinar. J Comp Neurol 419(3):377-393.

Allman JM, Kaas JH, Lane RH, Miezin FM. 1972. A representation of the visual field in the inferior nucleus of the pulvinar in the owl monkey (Aotus trivirgatus). Brain Res 40(2):291-302.

Arend I, Rafal R, Ward R. 2008. Spatial and temporal deficits are regionally dissociable in patients with pulvinar lesions. Brain 131(Pt 8):2140-2152.

Asanuma C, Andersen RA, Cowan WM. 1985. The thalamic relations of the caudal inferior parietal lobule and the lateral prefrontal cortex in monkeys: divergent cortical projections from cell clusters in the medial pulvinar nucleus. J Comp Neurol 241(3):357-381.

Baizer JS, Desimone R, Ungerleider LG. 1993. Comparison of subcortical connections of inferior temporal and posterior parietal cortex in monkeys. Vis Neurosci 10(1):59-72.

Balaram P, Hackett TA, Kaas JH. 2013. Differential expression of vesicular glutamate transporters 1 and 2 may identify distinct modes of glutamatergic transmission in the macaque visual system. J Chem Neuroanat 50-51:21-38.

Baldauf ZB, Wang S, Chomsung RD, May PJ, Bickford ME. 2005. Ultrastructural analysis of projections to the pulvinar nucleus of the cat. II: Pretectum. J Comp Neurol 485(2):108-126.

Baldwin MK, Balaram P, Kaas JH. 2013. Projections of the superior colliculus to the pulvinar in prosimian galagos (Otolemur garnettii) and VGLUT2 staining of the visual pulvinar. J Comp Neurol 521(7):1664-1682.

Baleydier C, Mauguiere F. 1985. Anatomical evidence for medial pulvinar connections with the posterior cingulate cortex, the retrosplenial area, and the posterior parahippocampal gyrus in monkeys. J Comp Neurol 232(2):219-228.

Baleydier C, Morel A. 1992. Segregated thalamocortical pathways to inferior parietal and inferotemporal cortex in macaque monkey. Vis Neurosci 8(5):391-405.

Bender DB. 1981. Retinotopic organization of macaque pulvinar. J Neurophysiol 46(3):672-693.

Bender DB. 1982. Receptive-field properties of neurons in the macaque inferior pulvinar. J Neurophysiol 48(1):1-17.

Bender DB. 1983. Visual activation of neurons in the primate pulvinar depends on cortex but not colliculus. Brain Res 279(1-2):258-261.

Bender DB. 1988. Electrophysiological and behavioral experiments on the primate pulvinar. Prog Brain Res 75:55-65.

Bender DB, Baizer JS. 1984. Anterograde degeneration in the superior colliculus following kainic acid and radiofrequency lesions of the macaque pulvinar. J Comp Neurol 228(2):284-298.

Bender DB, Baizer JS. 1990. Saccadic eye movements following kainic acid lesions of the pulvinar in monkeys. Exp Brain Res 79(3):467-478.

Bender DB, Butter CM. 1987. Comparison of the effects of superior colliculus and pulvinar lesions on visual search and tachistoscopic pattern discrimination in monkeys. Exp Brain Res 69(1):140-154.

Bender DB, Youakim M. 2001. Effect of attentive fixation in macaque thalamus and cortex. J Neurophysiol 85(1):219-234.

Benevento LA, Davis B. 1977. Topographical projections of the prestriate cortex to the pulvinar nuclei in the macaque monkey: an autoradiographic study. Exp Brain Res 30(2-3):405-424.

Benevento LA, Port JD. 1995. Single neurons with both form/color differential responses and saccade-related responses in the nonretinotopic pulvinar of the behaving macaque monkey. Vis Neurosci 12(3):523-544.

Benevento LA, Rezak M. 1976. The cortical projections of the inferior pulvinar and adjacent lateral pulvinar in the rhesus monkey (Macaca mulatta): an autoradiographic study. Brain Res 108(1):1-24.

Benevento LA, Standage GP. 1983. The organization of projections of the retinorecipient and nonretinorecipient nuclei of the pretectal complex and layers of the superior colliculus to the lateral pulvinar and medial pulvinar in the macaque monkey. JComp Neurol 217(3):307-336.

Berman RA, Wurtz RH. 2008. Exploring the pulvinar path to visual cortex. Prog Brain Res 171:467-473.

Berman RA, Wurtz RH. 2010. Functional identification of a pulvinar path from superior colliculus to cortical area MT. J Neurosci 30(18):6342-6354.

Berman RA, Wurtz RH. 2011. Signals conveyed in the pulvinar pathway from superior colliculus to cortical area MT. J Neurosci 31(2):373-384.

Boussaoud D, Desimone R, Ungerleider LG. 1992. Subcortical connections of visual areas MST and FST in macaques. Vis Neurosci 9(3-4):291-302.

Cappe C, Morel A, Barone P, Rouiller EM. 2009. The thalamocortical projection systems in primate: an anatomical support for multisensory and sensorimotor interplay. Cereb Cortex 19(9):2025-2037.

Carey RG, Fitzpatrick D, Diamond IT. 1979. Layer I of striate cortex of Tupaia glis and Galago senegalensis: projections from thalamus and claustrum revealed by retrograde transport of horseradish peroxidase. J Comp Neurol 186(3):393-437.

Chalupa LM, Coyle RS, Lindsley DB. 1976. Effect of pulvinar lesions on visual pattern discrimination in monkeys. JNeurophysiol 39(2):354-369.

Chow KL. 1954. Lack of behavioral effects following destruction of some thalamic association nuclei in monkey. AMA Arch Neurol Psychiatry 71(6):762-771.

Conley M, Diamond IT. 1990. Organization of the Visual Sector of the Thalamic Reticular Nucleus in Galago. Eur J Neurosci 2(3):211-226.

Conley M, Raczkowski D. 1990. Sublaminar organization within layer VI of the striate cortex in Galago. J Comp Neurol 302(2):425-436.

Contini M, Baccarini M, Borra E, Gerbella M, Rozzi S, Luppino G. 2010. Thalamic projections to the macaque caudal ventrolateral prefrontal areas 45A and 45B. Eur J Neurosci 32(8):1337-1353.

Cooper HM, Kennedy H, Magnin M, Vital-Durand F. 1979. Thalamic projections to area 17 in a prosimian primate, Microcebus murinus. J Comp Neurol 187(1):145-167.

Cowey A, Stoerig P, Bannister M. 1994. Retinal ganglion cells labelled from the pulvinar nucleus in macaque monkeys. Neuroscience 61(3):691-705.

Crick F, Koch C. 1998. Constraints on cortical and thalamic projections: the no-strong-loops hypothesis. Nature 391(6664):245-250.

Curcio CA, Harting JK. 1978. Organization of pulvinar afferents to area 18 in the squirrel monkey: evidence for stripes. Brain Res 143(1):155-161.

Cusick CG, Scripter JL, Darensbourg JG, Weber JT. 1993. Chemoarchitectonic subdivisions of the visual pulvinar in monkeys and their connectional relations with the middle temporal and rostral dorsolateral visual areas, MT and DLr. JComp Neurol 336(1):1-30.

Darian-Smith C, Tan A, Edwards S. 1999. Comparing thalamocortical and corticothalamic microstructure and spatial reciprocity in the macaque ventral posterolateral nucleus (VPLc) and medial pulvinar. J Comp Neurol 410(2):211-234.

de La Mothe LA, Blumell S, Kajikawa Y, Hackett TA. 2012. Thalamic connections of auditory cortex in marmoset monkeys: lateral belt and parabelt regions. Anat Rec 295(5):822-836.

De Pasquale R, Sherman SM. 2011. Synaptic properties of corticocortical connections between the primary and secondary visual cortical areas in the mouse. J Neurosci 31(46):16494-16506.

DeBruyn EJ, Casagrande VA, Beck PD, Bonds AB. 1993. Visual resolution and sensitivity of single cells in the primary visual cortex (V1) of a nocturnal primate (bush baby): correlations with cortical layers and cytochrome oxidase patterns. J Neurophysiol 69(1):3-18.

Deschenes M, Bourassa J, Pinault D. 1994. Corticothalamic projections from layer V cells in rat are collaterals of long-range corticofugal axons. Brain Res 664(1-2):215-219.

Diamond IT, Fitzpatrick D, Conley M. 1992. A projection from the parabigeminal nucleus to the pulvinar nucleus in Galago. J Comp Neurol 316(3):375-382.

Dick A, Kaske A, Creutzfeldt OD. 1991. Topographical and topological organization of the thalamocortical projection to the striate and prestriate cortex in the marmoset (Callithrix jacchus). Experimental Brain Research 84(2):233-253.

Felleman DJ, Van Essen DC. 1991. Distributed hierarchical processing in the primate cerebral cortex. Cereb Cortex 1(1):1-47.

Gattass R, Oswaldo-Cruz E, Sousa AP. 1978. Visuotopic organization of the cebus pulvinar: a double representation the contralateral hemifield. Brain Res 152(1):1-16.

Glendenning KK, Hall JA, Diamond IT, Hall WC. 1975. The pulvinar nucleus of Galago senegalensis. J Comp Neurol 161(3):419-458.

Gray D, Gutierrez C, Cusick CG. 1999. Neurochemical organization of inferior pulvinar complex in squirrel monkeys and macaques revealed by acetylcholinesterase histochemistry, calbindin and Cat-301 immunostaining, and Wisteria floribunda agglutinin binding. J Comp Neurol 409(3):452-468.

Guillery RW. 1995. Anatomical evidence concerning the role of the thalamus in corticocortical communication: a brief review. J Anat 187 (Pt 3):583-592.

Guillery RW, Feig SL, Van Lieshout DP. 2001. Connections of higher order visual relays in the thalamus: a study of corticothalamic pathways in cats. JComp Neurol 438(1):66-85.

Guillery RW, Sherman SM. 2002a. Thalamic relay functions and their role in corticocortical communication: generalizations from the visual system. Neuron 33(2):163-175.

Guillery RW, Sherman SM. 2002b. The thalamus as a monitor of motor outputs. Philos Trans R Soc Lond B Biol Sci 357(1428):1809-1821.

Guillery RW, Sherman SM. 2011. Branched thalamic afferents: what are the messages that they relay to the cortex? Brain Res Rev 66(1-2):205-219.

Gutierrez C, Cola MG, Seltzer B, Cusick C. 2000. Neurochemical and connectional organization of the dorsal pulvinar complex in monkeys. J Comp Neurol 419(1):61-86.

Gutierrez C, Cusick CG. 1997. Area V1 in macaque monkeys projects to multiple histochemically defined subdivisions of the inferior pulvinar complex. Brain Res 765(2):349-356.

Gutierrez C, Yaun A, Cusick CG. 1995. Neurochemical subdivisions of the inferior pulvinar in macaque monkeys. JComp Neurol 363(4):545-562.

Hackett TA, De La Mothe LA, Ulbert I, Karmos G, Smiley J, Schroeder CE. 2007. Multisensory convergence in auditory cortex, II. Thalamocortical connections of the caudal superior temporal plane. J Comp Neurol 502(6):924-952.

Hackett TA, Stepniewska I, Kaas JH. 1998. Thalamocortical connections of the parabelt auditory cortex in macaque monkeys. J Comp Neurol 400(2):271-286.

Harting JK, Huerta MF, Frankfurter AJ, Strominger NL, Royce GJ. 1980. Ascending pathways from the monkey superior colliculus: an autoradiographic analysis. JComp Neurol 192(4):853-882.

Huerta MF, Harting JK. 1983. Sublamination within the superficial gray layer of the squirrel monkey: an analysis of the tectopulvinar projection using anterograde and retrograde transport methods. Brain Res 261(1):119-126.

Huppe-Gourgues F, Bickford ME, Boire D, Ptito M, Casanova C. 2006. Distribution, morphology, and synaptic targets of corticothalamic terminals in the cat lateral posterior-pulvinar complex that originate from the posteromedial lateral suprasylvian cortex. J Comp Neurol 497(6):847-863.

Imura K, Rockland KS. 2007. Giant neurons in the macaque pulvinar: a distinct relay subpopulation. Front Neuroanat 1:2.

Itaya SK, Van Hoesen GW. 1983. Retinal projections to the inferior and medial pulvinar nuclei in the Old-World monkey. Brain Res 269(2):223-230.

Jones EG. 2007a. The Thalmus Cambridge: Cambridge University Press.

Jones EG. 2007b. The Thalmus Cambridge: Cambridge University Press.

Kaas JH, Lyon DC. 2007. Pulvinar contributions to the dorsal and ventral streams of visual processing in primates. Brain Res Rev 55(2):285-296.

Kandel ER, Schwartz JH, Jessell TM. 2000. Principles of Neural Science. New York.

Kaske A, Dick A, Creutzfeldt OD. 1991. The local domain for divergence of subcortical afferents to the striate and extrastriate visual cortex in the common marmoset (Callithrix jacchus): a multiple labelling study. Experimental Brain Research 84(2):254-265.

Kennedy H, Bullier J. 1985. A double-labeling investigation of the afferent connectivity to cortical areas V1 and V2 of the macaque monkey. J Neurosci 5(10):2815-2830.

Leiby CC, 3rd, Bender DB, Butter CM. 1982. Localization and detection of visual stimuli in monkeys with pulvinar lesions. Exp Brain Res 48(3):449-454.

Levitt JB, Yoshioka T, Lund JS. 1995. Connections between the pulvinar complex and cytochrome oxidase-defined compartments in visual area V2 of macaque monkey. Exp Brain Res 104(3):419-430.

Li K, Patel J, Purushothaman G, Marion RT, Casagrande VA. 2013. Retinotopic maps in the pulvinar of bush baby (Otolemur garnettii). J Comp Neurol.

Lin CS, Kaas JH. 1979. The inferior pulvinar complex in owl monkeys: architectonic subdivisions and patterns of input from the superior colliculus and subdivisions of visual cortex. JComp Neurol 187(4):655-678.

Lin CS, Wagor E, Kaas JH. 1974. Projections from the pulvinar to the middle temporal visual area (MT) in the owl monkey, Aotus trivirgatus. Brain Res 76(1):145-149.

Livingstone MS, Hubel DH. 1982. Thalamic inputs to cytochrome oxidase-rich regions in monkey visual cortex. Proc Natl Acad Sci U S A 79(19):6098-6101.

Lund JS, Hendrickson AE, Ogren MP, Tobin EA. 1981. Anatomical organization of primate visual cortex area VII. JComp Neurol 202(1):19-45.

Lund JS, Lund RD, Hendrickson AE, Bunt AH, Fuchs AF. 1975. The origin of efferent pathways from the primary visual cortex, area 17, of the macaque monkey as shown by retrograde transport of horseradish peroxidase. J Comp Neurol 164(3):287-303.

Lyon DC, Nassi JJ, Callaway EM. 2010. A disynaptic relay from superior colliculus to dorsal stream visual cortex in macaque monkey. Neuron 65(2):270-279.

Lysakowski A, Standage GP, Benevento LA. 1986. Histochemical and architectonic differentiation of zones of pretectal and collicular inputs to the pulvinar and dorsal lateral geniculate nuclei in the macaque. J Comp Neurol 250(4):431-448.

Lysakowski A, Standage GP, Benevento LA. 1988. An investigation of collateral projections of the dorsal lateral geniculate nucleus and other subcortical structures to cortical areas V1 and V4 in the macaque monkey: a double label retrograde tracer study. ExpBrain Res 69(3):651-661.

Maior RS, Hori E, Tomaz C, Ono T, Nishijo H. 2010. The monkey pulvinar neurons differentially respond to emotional expressions of human faces. Behav Brain Res 215(1):129-135.

Marion R, Li K, Purushothaman G, Jiang Y, Casagrande VA. 2013. Morphological and neurochemical comparisons between pulvinar and V1 projections to V2. J Comp Neurol 521(4):813-832.

Markowitsch HJ, Emmans D, Irle E, Streicher M, Preilowski B. 1985. Cortical and subcortical afferent connections of the primate's temporal pole: a study of rhesus monkeys, squirrel monkeys, and marmosets. J Comp Neurol 242(3):425-458.

Mathers LH. 1971. Tectal projection to the posterior thalamus of the squirrel monkey. Brain Res 35(1):295-298.

Mathers LH. 1972a. The synaptic organization of the cortical projection to the pulvinar of the squirrel monkey. J Comp Neurol 146(1):43-60.

Mathers LH. 1972b. Ultrastructure of the pulvinar of the squirrel monkey. J Comp Neurol 146(1):15-42.

Mathers LH, Rapisardi SC. 1973. Visual and somatosensory receptive fields of neurons in the squirrel monkey pulvinar. Brain Res 64:65-83.

Mizuno N, Takahashi O, Itoh K, Matsushima R. 1983. Direct projections to the prestriate cortex from the retino-recipient zone of the inferior pulvinar nucleus in the macaque monkey. NeurosciLett 43(2-3):155-160.

Morrison JH, Foote SL. 1986. Noradrenergic and serotoninergic innervation of cortical, thalamic, and tectal visual structures in Old and New World monkeys. J Comp Neurol 243(1):117-138.

Nagel-Leiby S, Bender DB, Butter CM. 1984. Effects of kainic acid and radiofrequency lesions of the pulvinar on visual discrimination in the monkey. Brain Res 300(2):295-303.

Nguyen MN, Hori E, Matsumoto J, Tran AH, Ono T, Nishijo H. 2013. Neuronal responses to face-like stimuli in the monkey pulvinar. Eur J Neurosci 37(1):35-51.

O'Brien BJ, Abel PL, Olavarria JF. 2001. The retinal input to calbindin-D28k-defined subdivisions in macaque inferior pulvinar. Neurosci Lett 312(3):145-148.

Ogren M, Hendrickson A. 1976. Pathways between striate cortex and subcortical regions in Macaca mulatta and Saimiri sciureus: evidence for a reciprocal pulvinar connection. Exp Neurol 53(3):780-800.

Ogren MP, Hendrickson AE. 1977. The distribution of pulvinar terminals in visual areas 17 and 18 of the monkey. Brain Res 137(2):343-350.

Ogren MP, Hendrickson AE. 1979a. The morphology and distribution of striate cortex terminals in the inferior and lateral subdivisions of the Macaca monkey pulvinar. J Comp Neurol 188(1):179-199.

Ogren MP, Hendrickson AE. 1979b. The structural organization of the inferior and lateral subdivisions of the Macaca monkey pulvinar. J Comp Neurol 188(1):147-178.

Ogren MP, Mateer CA, Wyler AR. 1984. Alterations in visually related eye movements following left pulvinar damage in man. Neuropsychologia 22(2):187-196.

Olszewski J. 1952. The Thalamus of the Macaca Mulatta: An Atlas for Use with the Stereotaxic Instrument. Basel: S. Karger.

Petersen SE, Robinson DL, Keys W. 1985. Pulvinar nuclei of the behaving rhesus monkey: visual responses and their modulation. J Neurophysiol 54(4):867-886.

Petersen SE, Robinson DL, Morris JD. 1987. Contributions of the pulvinar to visual spatial attention. Neuropsychologia 25(1A):97-105.

Petrof I, Viaene AN, Sherman SM. 2012. Two populations of corticothalamic and interareal corticocortical cells in the subgranular layers of the mouse primary sensory cortices. J Comp Neurol 520(8):1678-1686.

Purushothaman G, Marion R, Li K, Casagrande VA. 2012. Gating and control of primary visual cortex by pulvinar. Nat Neurosci 15: 905-912.

Raczkowski D, Diamond IT. 1980. Cortical connections of the pulvinar nucleus in Galago. J Comp Neurol 193(1):1-40.

Raczkowski D, Diamond IT. 1981. Projections from the superior colliculus and the neocortex to the pulvinar nucleus in Galago. J Comp Neurol 200(2):231-254.

Rafal RD, Posner MI. 1987. Deficits in human visual spatial attention following thalamic lesions. Proc Natl Acad Sci U S A 84(20):7349-7353.

Rezak M, Benevento LA. 1979. A comparison of the organization of the projections of the dorsal lateral geniculate nucleus, the inferior pulvinar and adjacent lateral pulvinar to primary visual cortex (area 17) in the macaque monkey. Brain Res 167(1):19-40.

Robinson DL, Petersen SE. 1985. Responses of pulvinar neurons to real and self-induced stimulus movement. Brain Res 338(2):392-394.

Rockland KS. 1994. Further evidence for two types of corticopulvinar neurons. Neuroreport 5(15):1865-1868.

Rockland KS. 1996. Two types of corticopulvinar terminations: round (type 2) and elongate (type 1). JComp Neurol 368(1):57-87.

Rockland KS. 1998. Convergence and branching patterns of round, type 2 corticopulvinar axons. JComp Neurol 390(4):515-536.

Rockland KS, Andresen J, Cowie RJ, Robinson DL. 1999. Single axon analysis of pulvinocortical connections to several visual areas in the macaque. J Comp Neurol 406(2):221-250.

Romanski LM, Giguere M, Bates JF, GoldmanRakic PS. 1997. Topographic organization of medial pulvinar connections with the prefrontal cortex in the rhesus monkey. Journal of Comparative Neurology 379(3):313-332.

Rovo Z, Ulbert I, Acsady L. 2012. Drivers of the primate thalamus. J Neurosci 32(49):17894-17908.

Saalmann YB, Kastner S. 2011. Cognitive and perceptual functions of the visual thalamus. Neuron 71(2):209-223.

Saalmann YB, Pinsk MA, Wang L, Li X, Kastner S. 2012. The pulvinar regulates information transmission between cortical areas based on attention demands. Science 337(6095):753-756.

Sherman SM. 2007. The thalamus is more than just a relay. Curr Opin Neurobiol 17(4):417-422.

Sherman SM. 2012. Thalamocortical interactions. Curr Opin Neurobiol 22(4):575-579.

Sherman SM, Guillery RW. 1996. Functional organization of thalamocortical relays. J Neurophysiol 76(3):1367-1395.

Sherman SM, Guillery RW. 1998. On the actions that one nerve cell can have on another: distinguishing "drivers" from "modulators". Proc Natl Acad Sci U S A 95(12):7121-7126.

Sherman SM, Guillery RW. 2002. The role of the thalamus in the flow of information to the cortex. Philos Trans R Soc Lond B Biol Sci 357(1428):1695-1708.

Sherman SM, Guillery RW. 2006. Exploring The Thalamuc And Its Role In Cortical Function. Cambridge: The MIT Press. 484 p.

Sherman SM, Guillery RW. 2011. Distinct functions for direct and transthalamic corticocortical connections. J Neurophysiol 106(3):1068-1077.

Sherman SM, Guillery RW. 2013. Functional Connections of Cortical Areas. Cambridge, Massachusetts: MIT press.

Shipp S. 2001. Corticopulvinar connections of areas V5, V4, and V3 in the macaque monkey: a dual model of retinal and cortical topographies. J Comp Neurol 439(4):469-490.

Shipp S. 2003. The functional logic of cortico-pulvinar connections. Philos Trans R Soc Lond B Biol Sci 358(1438):1605-1624.

Shipp S. 2004. The brain circuitry of attention. Trends Cogn Sci 8(5):223-230.

Snow JC, Allen HA, Rafal RD, Humphreys GW. 2009. Impaired attentional selection following lesions to human pulvinar: evidence for homology between human and monkey. Proc Natl Acad Sci U S A 106(10):4054-4059.

Soares JG, Diogo AC, Fiorani M, Souza AP, Gattass R. 2004. Effects of inactivation of the lateral pulvinar on response properties of second visual area cells in Cebus monkeys. Clin Exp Pharmacol Physiol 31(9):580-590.

Soares JG, Gattass R, Souza AP, Rosa MG, Fiorani M, Jr., Brandao BL. 2001. Connectional and neurochemical subdivisions of the pulvinar in Cebus monkeys. VisNeurosci 18(1):25-41.

Sprague JM. 1966. Interaction of cortex and superior colliculus in mediation of visually guided behavior in the cat. Science 153(3743):1544-1547.

Sprague JM, Meikle TH, Jr. 1965. The Role of the Superior Colliculus in Visually Guided Behavior. Exp Neurol 11:115-146.

Standage GP, Benevento LA. 1983. The Organization of Connections between the Pulvinar and Visual Area Mt in the Macaque Monkey. Brain Res 262(2):288-294.

Steele GE, Weller RE. 1993. Subcortical connections of subdivisions of inferior temporal cortex in squirrel monkeys. Vis Neurosci 10(3):563-583.

Stepniewska I, Kaas JH. 1997. Architectonic subdivisions of the inferior pulvinar in New World and Old World monkeys. VisNeurosci 14(6):1043-1060.

Stepniewska I, Qi HX, Kaas JH. 1999. Do superior colliculus projection zones in the inferior pulvinar project to MT in primates? Eur J Neurosci 11(2):469-480.

Stepniewska I, Ql HX, Kaas JH. 2000. Projections of the superior colliculus to subdivisions of the inferior pulvinar in New World and Old World monkeys. VisNeurosci 17(4):529-549.

Strumpf H, Mangun GR, Boehler CN, Stoppel C, Schoenfeld MA, Heinze HJ, Hopf JM. 2012. The role of the pulvinar in distractor processing and visual search. Hum Brain Mapp.

Symonds LL, Kaas JH. 1978. Connections of striate cortex in the prosimian, Galago senegalensis. J Comp Neurol 181(3):477-512.

Trojanowski JQ, Jacobson S. 1974. Medial pulvinar afferents to frontal eye fields in rhesus monkey demonstrated by horseradish peroxidase. Brain Res 80(3):395-411.

Trojanowski JQ, Jacobson S. 1976. Areal and laminar distribution of some pulvinar cortical efferents in rhesus monkey. J Comp Neurol 169(3):371-392.

Trojanowski JQ, Jacobson S. 1977. The morphology and laminar distribution of cortico-pulvinar neurons in the rhesus monkey. Exp Brain Res 28(1-2):51-62.

Ungerleider L, Ganz L, Pribram KH. 1977. Size constancy in rhesus monkeys: effects of pulvinar, prestriate, and inferotemporal lesions. Exp Brain Res 27(3-4):251-269.

Ungerleider LG, Christensen CA. 1977. Pulvinar lesions in monkeys produce abnormal eye movements during visual discrimination training. Brain Res 136(1):189-196.

Ungerleider LG, Christensen, C. A. 1979. Pulvinar lesions in monkeys produce abnormal scanning of a complex visual array. Neuropsychologia 17:493-501.

Ungerleider LG, Desimone R, Galkin TW, Mishkin M. 1984. Subcortical projections of area MT in the macaque. J Comp Neurol 223(3):368-386.

Ungerleider LG, Galkin TW, Mishkin M. 1983. Visuotopic organization of projections from striate cortex to inferior and lateral pulvinar in rhesus monkey. JComp Neurol 217(2):137-157.

Ungerleider LG, Pribram KH. 1977. Inferotemporal versus combined pulvinar-prestriate lesions in the rhesus monkey: effects on color, object and pattern discrimination. Neuropsychologia 15(4-5):481-498.

Walker AE. 1938. The Primate thalamus: University of Chicago Press.

Wall JT, Symonds LL, Kaas JH. 1982. Cortical and subcortical projections of the middle temporal area (MT) and adjacent cortex in galagos. J Comp Neurol 211(2):193-214.

Ward R, Arend I. 2007. An object-based frame of reference within the human pulvinar. Brain 130(Pt 9):2462-2469.

Ward R, Danziger S, Owen V, Rafal R. 2002. Deficits in spatial coding and feature binding following damage to spatiotopic maps in the human pulvinar. NatNeurosci 5(2):99-100.

Warner CE, Goldshmit Y, Bourne JA. 2010. Retinal afferents synapse with relay cells targeting the middle temporal area in the pulvinar and lateral geniculate nuclei. Front Neuroanat 4:8.

Webster MJ, Bachevalier J, Ungerleider LG. 1993. Subcortical connections of inferior temporal areas TE and TEO in macaque monkeys. J Comp Neurol 335(1):73-91.

Weller RE, Steele GE, Kaas JH. 2002. Pulvinar and other subcortical connections of dorsolateral visual cortex in monkeys. JComp Neurol 450(3):215-240.

Wilke M, Turchi J, Smith K, Mishkin M, Leopold DA. 2010. Pulvinar inactivation disrupts selection of movement plans. J Neurosci 30(25):8650-8659.

Wong-Riley MT. 1977. Connections between the pulvinar nucleus and the prestriate cortex in the squirrel monkey as revealed by peroxidase histochemistry and autoradiography. Brain Res 134(2):249-267.

Wong P, Collins CE, Baldwin MK, Kaas JH. 2009. Cortical connections of the visual pulvinar complex in prosimian galagos (Otolemur garnetti). J Comp Neurol 517(4):493-511.

Yeterian EH, Pandya DN. 1985. Corticothalamic connections of the posterior parietal cortex in the rhesus monkey. J Comp Neurol 237(3):408-426.

Yeterian EH, Pandya DN. 1988. Corticothalamic connections of paralimbic regions in the rhesus monkey. J Comp Neurol 269(1):130-146.

Yeterian EH, Pandya DN. 1989. Thalamic connections of the cortex of the superior temporal sulcus in the rhesus monkey. J Comp Neurol 282(1):80-97.

Yeterian EH, Pandya DN. 1991. Corticothalamic connections of the superior temporal sulcus in rhesus monkeys. Exp Brain Res 83(2):268-284.

Yeterian EH, Pandya DN. 1997. Corticothalamic connections of extrastriate visual areas in rhesus monkeys. J Comp Neurol 378(4):562-585.

CHAPTER III

RETINOTOPIC MAPS IN THE PULVINAR OF BUSH BABY (OTOLEMUR GARNETTII)

The study described in this chapter was published and is reproduced below without alterations: Li K, Patel J, Purushothaman G, Marion RT, Casagrande VA. 2013. Retinotopic maps in the pulvinar of bush baby (Otolemur garnettii). J Comp Neurol.

Introduction

The primate pulvinar is located at the dorsal posterior end of the thalamus and at least three subdivisions, or equivalent areas (Gattass et al., 1978), of the pulvinar can be identified: the inferior (PI), lateral (PL), and medial pulvinar (PM) (Walker, 1938, P.48-56; Emmers et al., 1963; Huerta et al., 1986; Wong et al., 2009). Most cells recorded in PL and PI were found to respond to simple visual stimuli (Bender, 1982; Petersen et al., 1985). PI and PL enjoy rich connections with the superior colliculus (SC), the parabigeminal nucleus and the primary visual cortex, as well as other early visual cortical areas of both the dorsal and ventral streams (Kaas & Lyon, 2007). Many functional roles have been proposed for these visual pulvinar subdivisions , including visual salience (Petersen et al., 1987), attention (Van Essen, 2005), visual stability (Robinson & Petersen, 1985; Berman & Wurtz, 2011), motion integration (Merabet et al., 1998),

temporal binding (Arend et al., 2008) and as a relay between cortical visual areas (Sherman, 2007; Theyel et al., 2010), among others.

The number and organization of retinotopic maps in the visual pulvinar are of great interest because of pulvinar's wide connections with visual cortical areas and its various proposed functions. The visual pulvinar has been electrophysiologically surveyed in the Old World simian macaque (Bender, 1981) and the New World simian cebus (Gattass et al., 1978). Two retinotopic maps were identified in both species. However, the positions and visual field representations of these maps were reported to differ. In macaque, one map was reported in ventro-lateral PL and the other was described as straddling the PI/PL border (Bender, 1981), while one was found in ventral PI/PL and the other in dorsal PL in cebus (Gattass et al., 1978). The relationship between these observed pulvinar maps in macaque and cebus monkeys remains unclear: 1) the positions of homologous retinotopic maps may have shifted between Old World and New World simian species, 2) true differences between the reported maps may have developed between the species, or 3) maps may not have been detected in the study of one of these species.

Compared to simians, prosimians are considered to be closer to the common ancestors of modern primates (Jerison, 1979) and generally have smaller and less differentiated pulvinar compared to simians (Raczkowski & Diamond, 1981) With knowledge of pulvinar retinotopy of a prosimian, the comparison between it and that of simians can help reveal the following: the common structure of primate pulvinar, the correspondence between reported pulvinar retinotopic maps in different primate species, and potentially, pulvinar features that have evolved solely in simians. Additionally, the functional features of simian pulvinar that are recently evolved are likely to have evolved separately for New and Old World simians, and may correlate with simians' expanded development of extrastriate cortex. The retinotopic organization of pulvinar,

however, has not been electrophysiologically examined in any prosimian species. In this study we used bush babies (Otolemur garnettii) as a representative species of prosimians. We electrophysiologically examined the retinotopy of its visual pulvinar and constructed 3D models of the maps from data across cases. We also compared the resulting functional maps with the chemoarchitecture of each pulvinar subdivision.

Materials and Methods

Animal Preparation

Six bush babies (Otolemur garnettii) of both sexes weighing 0.77-1.1 kg were used in this study. All experiments were performed according to a protocol approved by the Vanderbilt University Institutional Animal Care and Use Committee (IACUC). Some of these animals were used in multi-day terminal recording sessions while others underwent a series of 1-day survival recording sessions before a final 1-day terminal recording session.

Anesthesia was first induced with 20-40 mg/kg ketamine and 0.4-0.5 mg/kg xylazine, and maintained with 1-3% isoflurane during surgery. During the first session a 8 mm craniotomy and durotomy were performed over LGN at the Horsley-Clarke coordinates of anterior-posterior +3 and medial-lateral 7. After surgery, isoflurane was replaced by urethane in terminal sessions and propofol/nitrous oxide in survival sessions. Urethane was given intra-peritoneally, induced with a dose of 1.25 mg/kg and maintained with 0.25 mg/kg boosters every 2 hours. For propofol/nitrous oxide anesthesia, the animal was given propofol intra-venously at 2.5-6 mg/kg/hr first and then at 0.2-0.6 mg/kg/hr after the animal was stabilized. Once the animal was deeply anesthetized, it was given the muscle relaxant, vecuronium bromide, intravenously at 0.15

mg/kg/hr. While the animal was infused with vecuronium bromide, it was respired with 75% nitrous oxide in oxygen in the survival sessions, or room air in the terminal sessions. During the recording session the end tidal CO2 pressure was monitored and maintained between 35 and 50 mmHg. EEG and ECG were monitored to ensure a stable anesthetic plane, and the animals' toes were pinched periodically to help with ECG monitoring of anesthesia.

The animals pupils were dilated with 1% topical atropine solution. The eyes were focused onto a tangent screen 57 cm away using contact lenses of appropriate size and power. A map of the blood vessel pattern was reflected back on to the tangent screen from the tapetum to locate the optic disks, which were used to infer the locations of the area centralae.

A survival recording session usually lasted 10-12 hours, after which the brain opening was covered with tecoflex (artificial dura) for protection. A specially molded plastic cap of appropriate size was glued with dental cement over the craniotomy window, and the scalp was sutured closed. First vecuronium bromide infusion and then propofol anesthesia was withdrawn and the animal was monitored until it was fully awake, at which point it was given treats and the analgesic buprenorphine 0.01 mg/kg. After a survival session an animal was allowed at least two weeks to recover before another survival session was performed. All pulvinar mapping was done on the left hemisphere. Some of these animals received tracer injections in the right pulvinar for a related study.

Recording

We recorded extracellular single and multi-unit activity using epoxylite-coated tungsten microelectrodes (FHC Inc., Bowdoin, ME) with impedances ranging from 1 to 2.5 at 1 kHz. The signal was amplified and digitized with a Plexon multichannel acquisition processor (Plexon

Inc., Dallas, TX), and fed to a speaker after filtering. The high impedance of these electrodes ensured that we could differentiate between background hash and neural spikes.

The central vision representation of bush baby pulvinar was found by first looking for the central vision representation of LGN near the Horsley-Clarke coordinates of AP +3 and ML 7, and then moving 1.5 to 2 mm medially. The electrode was initially lowered 7-7.5mm from the cortical surface, then advanced in steps of 100 . At each location, we examined the visual responsiveness of cells using spots, bars and other light patterns projected on the tangent screen. At peripheral locations we used a hand held screen to roughly estimate the receptive field locations off-screen.

When we found any visual response with bright light spots, we used an ophthalmoscope to project confined light spots or light bars with clear borders and uniform luminance on the screen, to locate the receptive field. Recorded units were classified as vague, moderate or brisk by their visual responses. A brisk unit showed large clear spikes and a clear response similar to the response of V1 cells, with either no adaptation or fast recovery. A moderate unit showed a clear receptive field, spikes clearly larger than background hash and consistent recovery from adaptation. A vague unit showed correlation between visual stimulation and activity but either was hard to localize, showed very slow recovery from fatigue, or had small spikes barely larger than background hash. For most non-vague units we also tested the ocularity of their receptive field. We hand plotted the receptive field centers of vague units, the accurate receptive fields of the non-vague units, and separate receptive fields for the two eyes when they deviated.
At the end of each penetration, one or two lesions were made by passing 5 of current through the electrode tip for 10 seconds, with tip negative. Four to nine penetrations were made in each session. Penetrations were spaced 500 apart.

Histology and Tissue Reconstruction

At the end of each terminal recording session the animal was overdosed with Nembutal (>) and perfused transcardially with a saline rinse followed by a fixative consisting of 3% paraformaldyhyde, 0.1% glutaraldhyde and 0.2% picric acid (saturated solution, V/V) in 0.1M phosphate buffer (PB). Perfusions were done within five weeks of the first recording sessions so lesions left in the early sessions remained visible. The brain was blocked at AP +8 in the coronal plane in the Horsley-Clarke coordinates. The thalamus was coronally sectioned frozen at 52 . During the sectioning needle probe marks were left in the thalamus perpendicular to the cutting plane to facilitate reconstruction.

Sections from the first three animals were stained for Nissl substance, cytochrome oxidase (CO), acetylcholinesterase (AChE) and calbindin, in series, to reveal pulvinar subdivisions. In later cases only some of the four stains were used to facilitate reconstruction. CO staining was used in all cases. We employed a CO staining protocol that used 0.02% diaminobenzidine (DAB), 0.03% cytochrome C, 0.015% catalase, 2% sucrose, 0.03% nickel-ammonium-sulphate and 0.03% cobalt-chloride in 0.05M PB of 7.4pH. This method is based on the one used by Boyd and Matsubara (1996), and it allowed better differentiation, sharper contrast and faster reactions compared to the original method (Wong-Riley, 1979). Our staining for AChE followed the procedure of Geneser-Jensen and Blackstad (1971).

For immunostaining for calbindin (see also Table 1), sections were first incubated with 1:5000 calbindin D28k rabbit-anti-rat antibody (Swant Inc. Marly, Switzerland, Code No.: cb-38a, Lot No.: 9.03), then 1:200 biotin conjugated donkey anti-rabbit antibody, and later ABC standard elite kit (Vector laboratories Inc. Burlingame, CA). The immunostaining was visualized with

Antigen	Immunogen	Manufacturer	Species	Catalog No.	JCN antibody No.	Dilution
Calbindin	Recombinant rat cCalbindin D-28k	Swant (Belinzona, Switzerland)	Rabbit polyclonal	CB38	10000340	1:5,000
Donkey anti-Rabbit IgG Antibody, biotin-SP conjugate	Rabbit IgG	Millipore (Billerica, MA)	Donkey polyclona	AP182B		1:500

Table 1. Antibodies Used

0.05% DAB, 0.04% nickel-ammonium-sulfate and 0.003%. The primary antibody was polyclonal and was produced against recombinant rat calbindin D-28k. In normal concentration, the antibody yields only a single band at 28kDa for primate brain tissue (manufacturer product description: http://www.swant.com/pfd/Rabbit%20anti%20Calbindin%20D-28k%20CB38.pdf). As a postive control, a previous study had also shown a lack of stainning with this antibody in primate cortex tissue with calbindin antigen preabsorption (del Rio & DeFelipe, 1995). Additionally, the LGN of primates, including bush baby, has been shown to express calbindin D28k only in its koniocellular (K) cells but not in the magnocellular (M) or parvocellular (P) cells (Johnson & Casagrande, 1995; Hendry & Reid, 2000). This distribution pattern was perfectly reflected in our stained sections (see Fig 1D).

Two additional bush baby hemispheres were used in this study and each was blocked and sectioned as in the other six cases, but without electrophysiological recording. Sections from one of these cases were stained in series with CO and myelin, the other CO, AChE, calbindin and myelin. We used method of Gallyas (1979) for myelin staining. All photomicrographs of sections used in figures were enhanced in contrast, with their luminance decreased to compensate. The manipulations were done in GIMP 2.8.2 (www.gimp.org). Photomicrographs of myelin sections were digitally stretched in our figures to compare with other sections, as the myelin stained sections tended to shrink more than the others.

In the cases with pulvinar recordings, LGN, pulvinar and pulvinar subdivisions were manually reconstructed along with the penetrations. Sections were aligned based on large blood vessels and the marks left during cutting. The penetrations were located using the electrolytic lesions. Shrinkage factors were calculated for each penetration from the distance between lesions measured during experiment and measured on sections. Penetrations in the same animals were

found to show shrinkage factors within 10% of each other. In a few penetrations one of the lesions was not visible, in which case each of these penetrations was reconstructed assuming a shrinkage factor that equaled the average of other penetrations in the same animal. The sites of recorded units were deduced from their depths relative to the depths of the lesions.

Data Analysis

In our analysis the centers of recorded units' receptive fields were measured in a polar coordinate system, whose origin was on the contralateral area centralis (AC) and the unit vector of angle zero degrees horizontally pointed to the right. The coordinates for ipsilateral receptive fields were measured with a coordinate system centered on the ipsilateral AC. The shape of a receptive field was modeled as an ellipse with either a vertical or horizontal major axis. The eccentricity of receptive field centers' was translated from the distance on tangent screen to the angle from AC, and the area of receptive fields was translated accordingly.

The visual field representation at each recorded location of our penetrations was calculated as the gravity center of the centers of all receptive fields recorded at that location. However, for binocular units we did not include ipsilateral receptive field, and at locations with many single units of different visual response qualities (see above), we only included receptive fields with response qualities of the tier highest at that location.

We mapped 365 multi- or single unit locations in the pulvinar of 6 animals. Due to the limited coverage of the visual field when using a tangent screen, we only sampled units with receptive fields with eccentricities of less than 42 degrees. We focused our penetrations in PI and PL as previous studies showed that these areas are connected to V1 and V2 (Symonds & Kaas, 1978; Raczkowski & Diamond, 1980, 1981). In each penetration the electrode was lowered in

steps of 100 . At each depth, new units were identified based on differences in spike shapes and receptive field properties. Visual pulvinar was broadly surveyed in different animals, and data from all six cases were combined to construct the final maps. We observed differences in the relative positions of LGN and pulvinar in different animals. A gross difference of about also was observed in the position of thalamus as a whole, presumably due to small differences in ear canal height or orbital tissue thickness that impact the head position in the stereotaxic apparatus. Nevertheless, we were able to align the reconstructed models from different animals by the shape of brachium of the superior colliculus (brSC) and PI. Consequently, residual variations in PL/PI shape and retinotopic organization within each pulvinar nucleus were quite small.

Results

In this section we first present the chemoarchitectonic subdivisions we identified in bush baby pulvinar, to provide a reference frame for the location of the retinotopic maps. Major map features will then be described, together with representative electrode penetrations that demonstrate these features. And finally, we present an overall model that gives predictions of the receptive field progression that should be seen in any given penetration.

Architecture of the visual pulvinar

We determined the pulvinar subdivisions using CO, myelin, AChE and calbindin staining to compare the architectonic subdivisions to the physiological maps (Fig 1). The three large subdivisions of the bush baby pulvinar, PL, PI and PM, were found on sections stained with any of the four methods. The brSC was easily recognized by its dark horizontally oriented fibers in

myelin stained sections (Fig 1A), and as a lightly stained horizontal fiber bundle in sections stained with the other three methods (Figs 1B-D). This broad fiber bundle extended from the caudal end to the rostro-ventral border of pulvinar, separating PI from PL and PM. PI occupied the ventral half of pulvinar in the most posterior coronal sections, and became smaller in more anterior sections, disappearing at about the same anterior-posterior (AP) level as the middle of LGN. PL could be distinguished from PM with its darker myelin staining. PL also showed darker CO staining while PM appeared patchy and generally lighter with CO staining (Fig 1B). About half of the pulvinar area above brSC could be considered PL. Anteriorly, the border between the lateral posterior nucleus (LP) and PL, as well as the border between anterior pulvinar and PM, were hard to define based on the staining methods we used.

The inferior pulvinar of bush baby has been difficult to subdivide based on chemoarchitectonic features (Symonds & Kaas, 1978; Wong et al., 2009). At the medial end of brSC the area with dense fiber bundles grew wide and curved ventrally, separating PI from PM. In this heavily myelinated area a darkly stained circle was found consistently in myelin stained sections (arrowhead, Fig 1A). This circle extended dorsally into the PM/PL border. CO and AChE stained sections revealed a dark patch in the same area (Fig 1BC). These features were very similar to those described in the medial inferior pulvinar in owl monkeys (Lin & Kaas, 1979; Stepniewska & Kaas, 1997). Therefore, bush baby PI can be divided into medial (PIm) and central (PIc) zones, with PIm at the PI/PM/PL junction, and PIc occupying the rest of PI.

Additionally, we found two distinct areas in bush baby PIc, a large lateral region that stained lightly for myelin and darkly for both CO and AChE, as well as a ventro-medial region which stained darkly for myelin and lightly for both CO and AChE. These features resembled those described for the lateral (PIcl) and medial (PIcm) portions of PIc in simian species

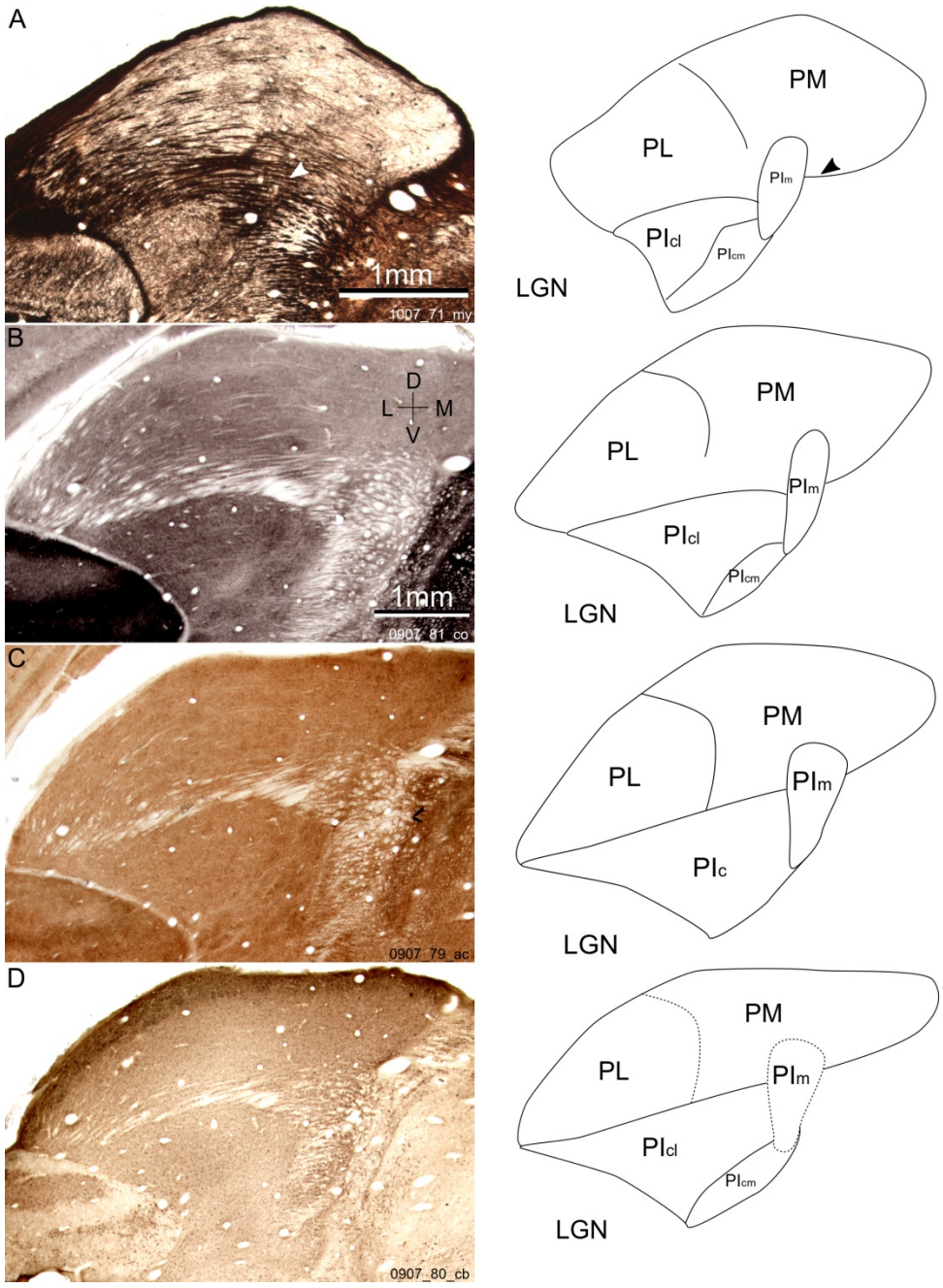

Figure 1.

A–D: Left: Coronal sections of bush baby pulvinar in two animals at comparable anterior–posterior levels. The four sections are stained for myelin, cytochrome oxidase (CO), acetylcholinesterase (AChE), and calbindin (CB), respectively. The myelin section showed more shrinkage during staining and was digitally stretched to match the other sections. Right: Line drawings of subdivision borders visible in the sections at left. Solid lines are clear borders between subdivisions; dotted lines show borders not obvious with that stain. The arrowheads in A show the location of the myelin circle. D, dorsal; L, lateral; V, ventral; M, medial. Subdivisions: PL, lateral pulvinar; PM, medial pulvinar; PIm, medial inferior pulvinar; PIc, central inferior pulvinar; PIcl, lateral part of PIc; PIcm, medial part of PIc; LGN, lateral geniculate nucleus.

(Lysakowski et al., 1986; Stepniewska & Kaas, 1997; Gray et al., 1999). However, one salient feature of PIcl/PIcm/PIm in simians is the alternate dark and light bands revealed by immunostaining for the calcium binding protein calbindin (Stepniewska & Kaas, 1997). Yet our calbindin staining (Fig 1D) showed only small differences between these subdivisions. Nevertheless, in keeping with prior schemes, we refer to the three subdivisions of bush baby inferior pulvinar as PIcl, PIcm, and PIm, from lateral to medial. Lacking connectional data, however, we cannot be certain that these subdivisions are homologous to the simian pulvinar subdivisions with the same names.

Visual Responses of Cells in PI and PL

Neurons in both PL and the lateral part of PI showed robust responses to simple visual stimuli. Almost all visually responsive cells showed localized receptive fields but a few responded over wide areas of the visual field. Most cells were better driven by light spots than light bars. The majority of cells we found responded to binocular input. Among the 126 cells on which we tested ocularity, 73 were binocular, 22 responded to ipsilateral eye stimulation and 31 cells responded to contralateral eye stimulation.. Additionally, 12 of the 73 binocular cells only responded when both eyes received visual stimulation simultaneously. In macaque only the ocularity of cells in PI has been reported (Bender, 1982). In the roughly equivalent area of bush baby pulvinar (the ventral map, as we will discuss below) we identified 21 binocular cells out of 36 that were tested for ocularity. Among the rest, 5 received from the ipsilateral eye and 10 the contralateral eye. The proportion of binocular cells is smaller in bush baby pulvinar than reported for macaque (Bender, 1982). Weak direction selectivity was observed for many neurons. Cells that responded either in a transient or a sustained manner to standing contrast were found in a

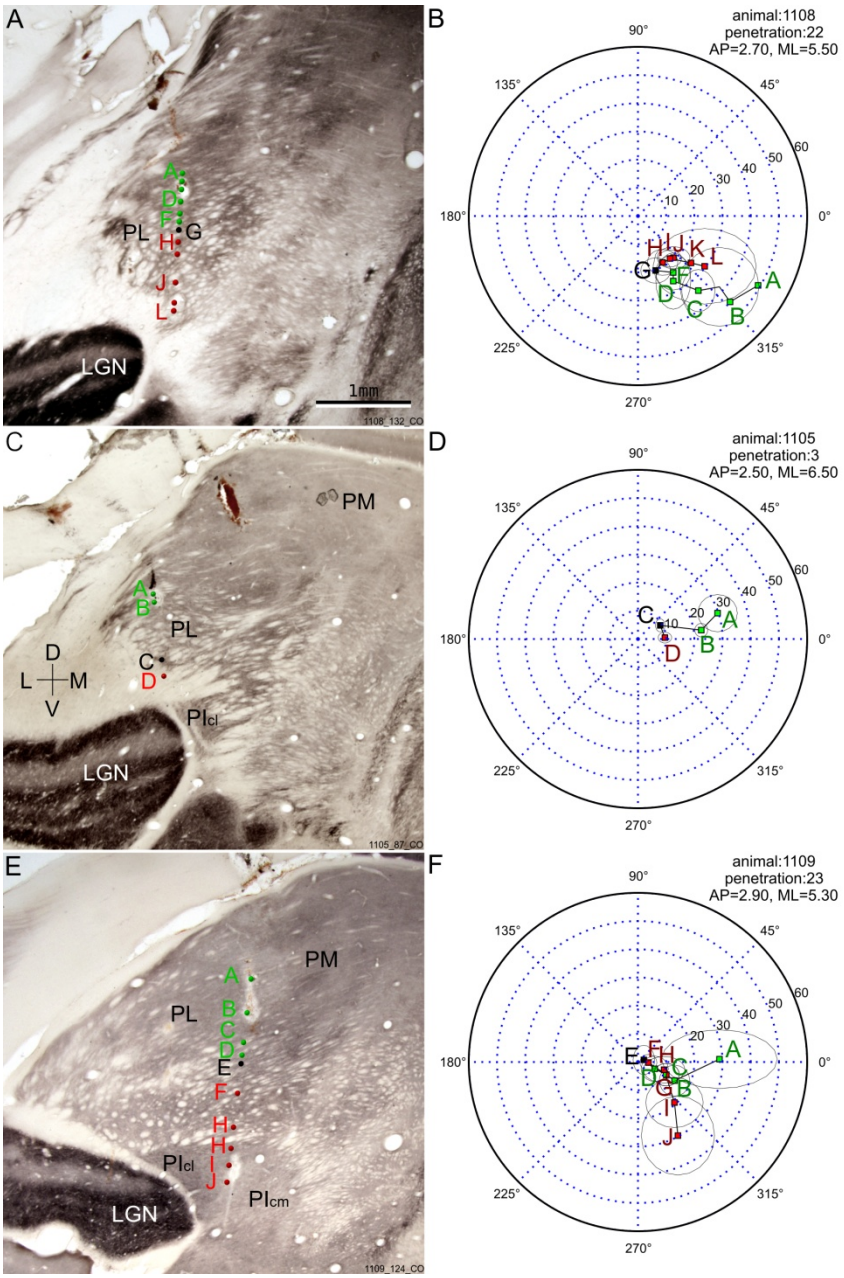

Figure 2.

Three representative penetrations from three different cases showing the reversals of receptive field progressions that reveal the two retinotopic maps. A,C,E: Reconstruction of example penetrations overlaid on coronal CO sections, with corresponding receptive field progression shown at right in B,D,F. B,D,F: Perimeter charts of penetrations with colored dots showing the receptive field centers of corresponding units whose locations in the brain are indicated in the sections at left. Green dots and green letters indicate units dorsal to the reversal point; red dots and red letters indicate units ventral to the reversal point. Black dots and letters label the reversal point. The top section is just anterior to PI; the other two sections are in the middle of PI. A trend for the receptive fields to shift gradually toward the vertical meridian (VM) then away from VM can be seen clearly. PL, lateral pulvinar; PI, inferior pulvinar; PM, medial pulvinar; LGN, lateral geniculate nucleus.

mixed population in PI and PL. A majority of visually driven cells showed strong adaptation to repeated stimulation, but there also were cells with strong facilitation. Most, although not all, of the cells' receptive fields appeared in the contralateral visual field. Collectively the receptive fields of recorded cells covered more than 60 degrees of the contralateral visual field. The receptive field positions of pulvinar neurons shifted systematically through the visual field as the electrode advanced ventrally, showing well organized visual field representations in most of PI and PL.

Dorsal and Ventral Retinotopic Maps

One major feature of the receptive field progressions observed in electrode penetrations was the reversal of progression. As the electrode passed through the visual pulvinar, the recorded receptive fields first progressed towards the vertical meridian (VM), then turned sharply and progressed away from VM. The reversal of receptive field progression in each penetration occurred at similar dorsal-ventral depths in pulvinar. This reversal marked a border between two visual field representations (see Figs 2B, 2D and 2F). Both the pulvinar areas above and below the region where progression reversals happened showed precise retinotopy, with each area representing the full contralateral field. Double representations were clearly demonstrated in some penetrations, where receptive fields in the same area of the visual field appeared before and after the reversal (see Fig 2F). As such, these progressions can be considered as evidence for two distinct retinotopic maps.

For convenience we refer to these maps, henceforth, as the dorsal and the ventral maps based on their relative positions in pulvinar. We used a 3-D wire frame volume that contained all cells included in the receptive field progression towards VM to represent the dorsal retinotopic

map, and another wire frame volume that contained all those progressing away from VM to represent the ventral map, as shown in Figure 3. The border between the two maps lay roughly on the PI/PL border at its posterior end, and extended anteriorly as a mostly horizontal sheet. In the anterior half of the maps, as PI became smaller, larger portions of the ventral map extended dorso-medially across brSC (Fig. 3B). The visual field representation of the dorsal and ventral maps was roughly continuous across the map border, as the receptive fields moved continuously even near the progression reversals.

The Central and Peripheral Representation

The representation of the central-peripheral axis of the visual field is shown with colored eccentricity contour representations in Figure 4AB. These contours were modeled as 3D volumes that contained all but a few (<5) recorded cells with receptive fields within 5, 10, or 15 degrees of the central vision. The two maps had adjoined central vision representations, located at the postero-medial end of both maps. Representative penetrations shown in Figure 4C-F and their reconstructions shown in Figure 4C'-F' demonstrated the two main features of the central-peripheral representation. First, in single penetrations cells closer to the border between the two maps had more central receptive fields, while cells on the dorsal surface of the dorsal map and the ventral surface of the ventral map had more peripheral receptive fields. Second, postero-medial penetrations had reversal points closer to central vision, and generally cells with more central receptive field than antero-lateral penetrations at comparable depths.

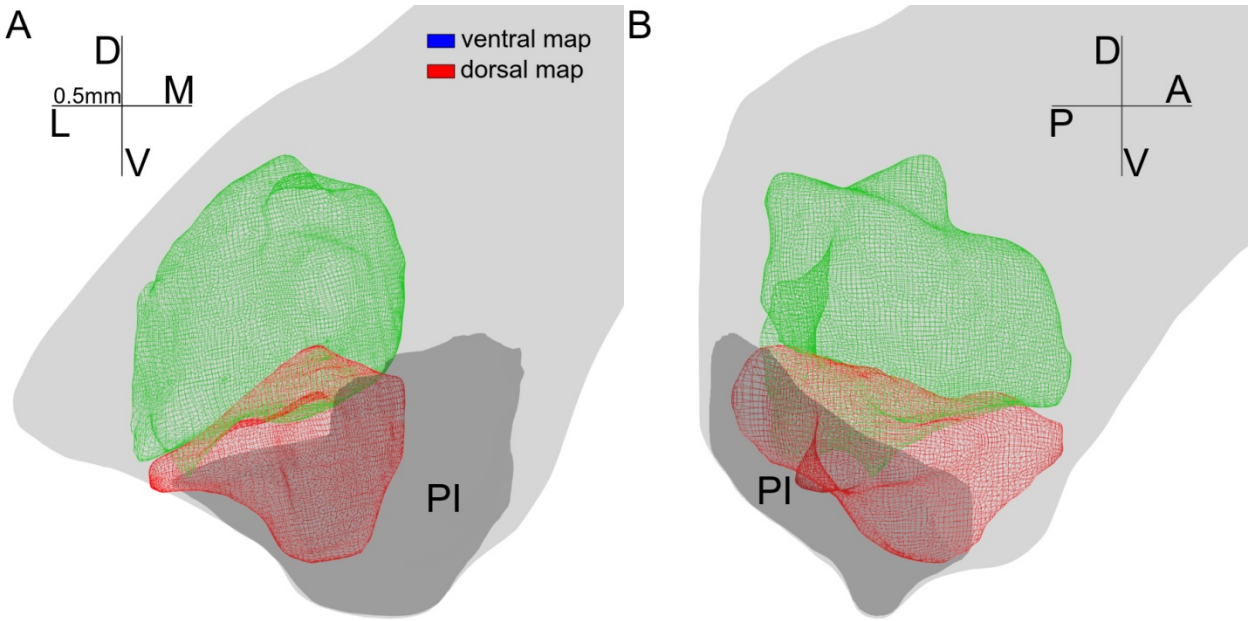

Figure 3.

3-D views of the dorsal (green) and ventral (red) map.The model of the dorsal map contains all recorded units showing receptive fields before the progression reversal. Similarly, the model of the ventral map contains all recorded units after the receptive progression reversal. Both models were smoothed, so a few (fewer than five for each structure) recording sites are left out. A coronal view is shown in A, and a parasagittal view is shown in B. Light gray shows the outline of the pulvinar. Dark gray shows the outline of the inferior pulvinar. D, dorsal; L, lateral; V, ventral; M, medial; A, anterior; P, posterior. Each arm of the compass is 0.5 mm in the model.

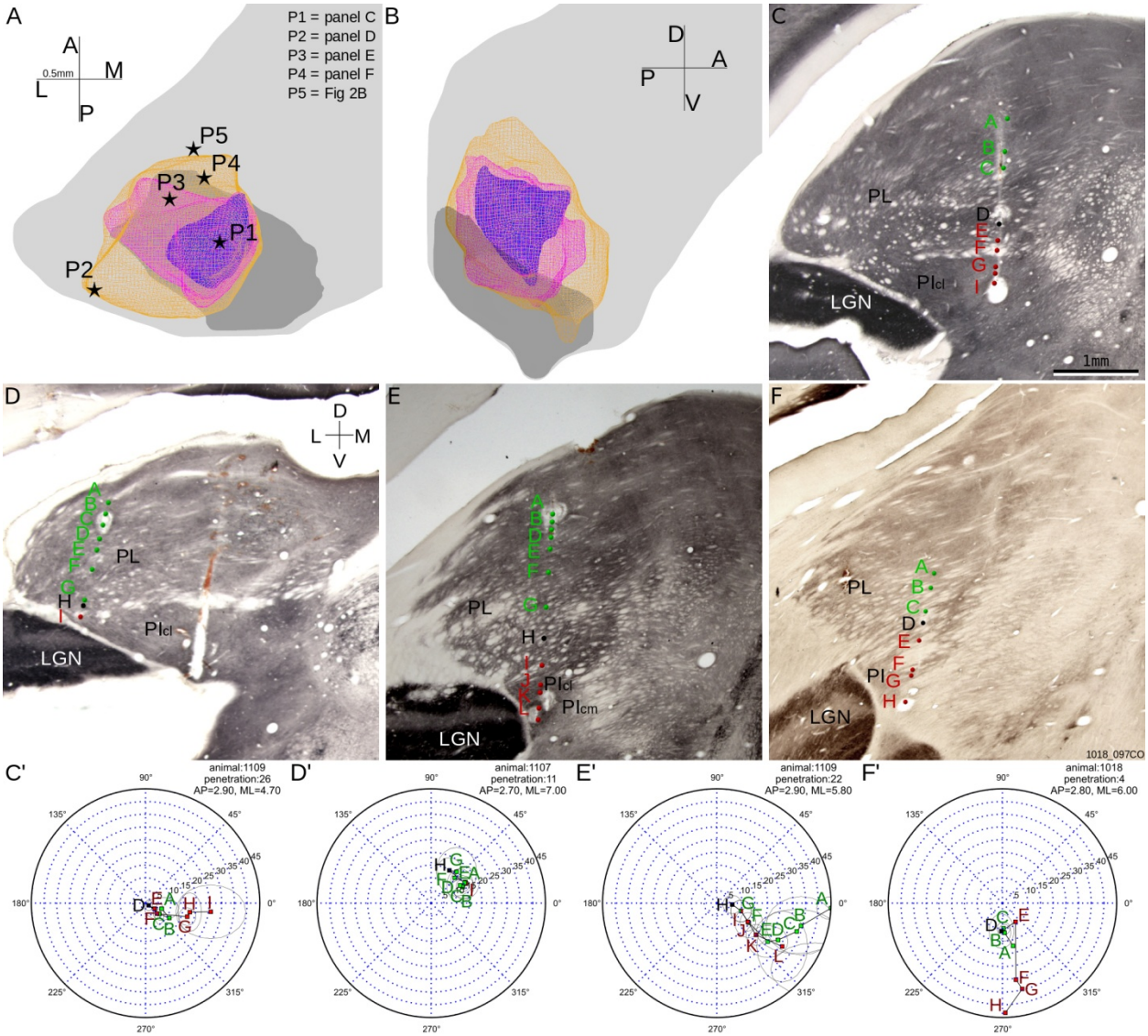

Figure 4.

Representation of the central–peripheral axis of the visual field. A,B: Horizontal (A) and parasagittal (B) views of the representations of visual field areas within 5° (blue), 10° (pink), and 15° (yellow) of the area centralis. Same conventions as in Figure 3. C–F: Reconstructions overlaid on coronal CO sections of example penetrations whose locations are shown in A, with the same conventions as in Figure 2. C′–F′: Perimeter charts of penetrations shown in C–F. PIcm, medial part of central inferior pulvinar; PIcl, lateral part of central inferior pulvinar.

The Horizontal Meridian Representation

Both maps represented the upper field in their lateral half and the lower field in their medial half, as shown in Figure 5. We deduced the horizontal meridian (HM) representation from the borders between these two volumes representing the upper and lower field in each map. The HM representation we get is a vertical sheet continuous between the dorsal and the ventral maps, as can be seen in Figures 5B, 5D and 6AB. Indeed, receptive field progressions roughly near HM were found along this border between the representations of two quadrants (Figures 2F and 6CD) Figure 6EF demonstrated that penetrations had lower field receptive fields medial to the sheet, and upper field receptive fields lateral to it.

There were two areas where the HM representation sheet was not flat. In the dorsal map the posterior end of the HM representation is convex toward the lateral side. This feature can be clearly seen from the overall shape of the border between the upper and lower field representations, as shown in Figure 6A Individual penetrations showed the same feature, as posterior penetrations (like Figure 6C) had dorsal map receptive fields at both side of HM but the progression showed strong fluctuation on elevation, while more anterior penetrations showed dorsal map receptive fields progressions flatter along HM (like Figures 2F and 6D). In the ventral map the ventral end of HM representation curved laterally. As a result vertical penetrations often showed receptive field progressions near an oblique radial line in the visual field (see Figure 4E and 6C) instead a horizontal line.

The Vertical Meridian Representation

The VM was represented as a curve on both the posterior and the medial edges of the border between the two maps. In the dorsal map, the representation of visual field areas near VM

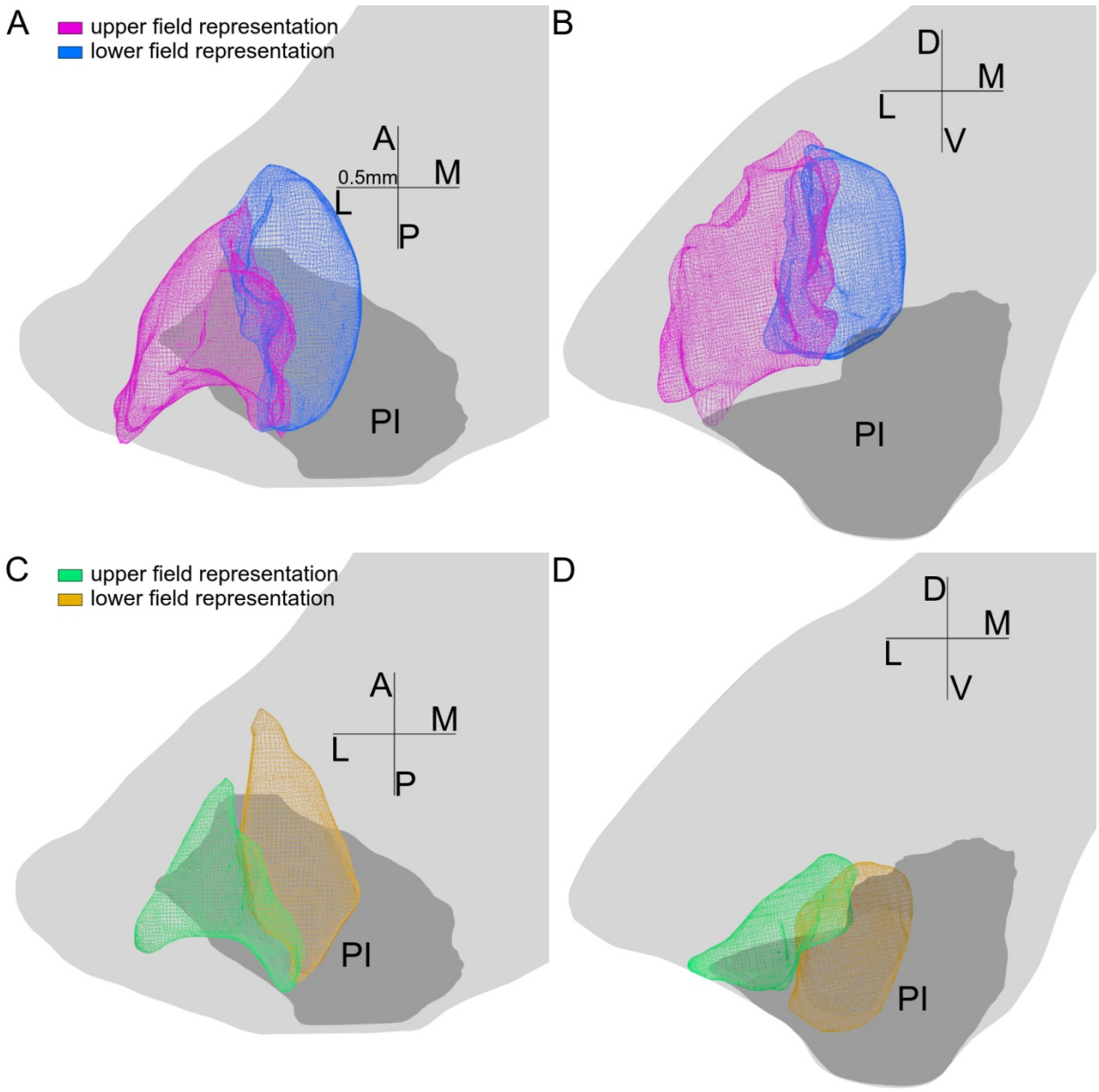

Figure 5.
Upper and lower field representations of each of the maps, with the same conventions as in Figure 3. A,B: Horizontal and coronal views of the upper (purple) and lower (blue) field representations of the dorsal map. C,D: Horizontal and coronal views of the upper (green) and lower (yellow) field representations of the ventral map. For both maps, the upper field representations lie on the lateral side and the lower field representations lie on the medial side of the maps.

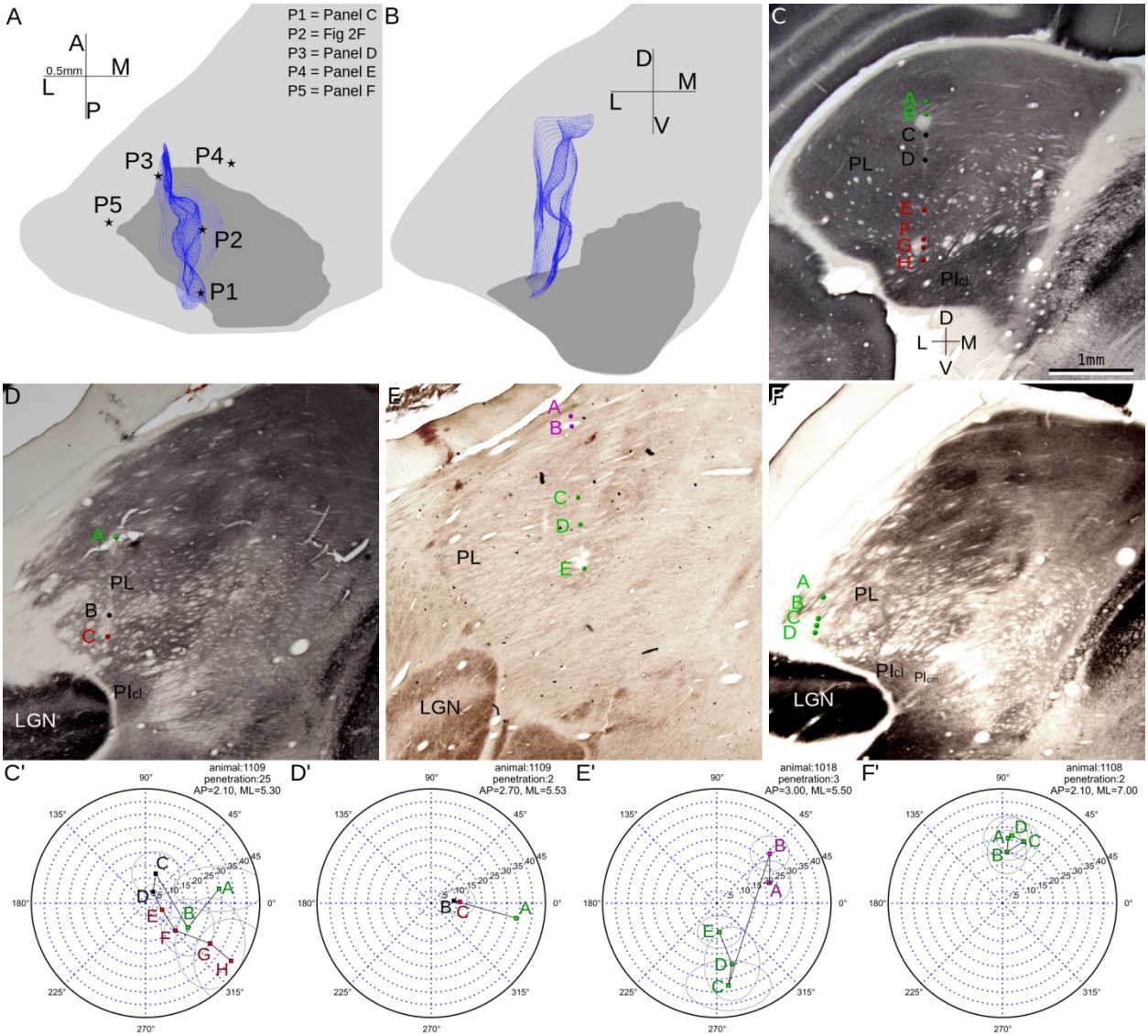

Figure 6.

Representation of the horizontal meridian (HM). A,B: Horizontal (A) and coronal (B) views of the HM representation (in blue), with the same conventions as in Figure 3. The HM representation was modeled as the border between the upper and the lower field representations of both maps. In A, each star shows the location of a penetration whose receptive field progression is shown in another panel as indicated in the table at top right. top C–F: Reconstructed penetrations overlaid on coronal CO sections, whose locations are indicated in A. Same conventions as in Figure 2. C′–F′: Receptive field progressions of the four penetrations shown in C–F, revealing features of the HM. Purple dots and letters indicate units outside of the two maps.

extended along the medial and the ventral surfaces of the map. Similarly, in the ventral map, the representation of near-VM area extended along the dorsal and medial surfaces. In other words, an iso-azimuth contour (see the 3 degrees contour shown in Figure 7AB) appeared as a rotated T shape on most of its coronal sections. Medial and posterior penetrations, like the ones shown in Figures 4E and 7C, showed reversal points closer to VM than anterior and lateral penetrations, representative penetrations of which shown in Figures 4E and 7D. A comparison between Figures 4E and 7E showed that penetrations farther from the VM representation tend to have receptive-field progressions with a wider angle from VM. The extension of near-VM representation on the border between the two maps was supported by the reversal of receptive field progressions observed in almost all our penetrations, where receptive fields moved towards VM and then away from VM. The extended near-VM representation on the medial border of both maps was demonstrated by penetrations there that showed receptive field progressions very close to VM. In this model, there should still be azimuth changes when moving dorsal-ventrally along the medial border of the maps. However, in the ventral map, since the medial border curves laterally, vertical penetrations got closer to the tilted medial border when going deeper. As a result, such penetrations showed receptive field progressions that were parallel to VM after reversal (see Figure 4F).

Overall Model

Coronal and horizontal cross-sections of the maps are shown in Figures 8 and 9, respectively. The three coronal sections shown in Figure 8B-D are drawn directly from a model which combines the models of eccentricity and quadrants representations at three anterior-

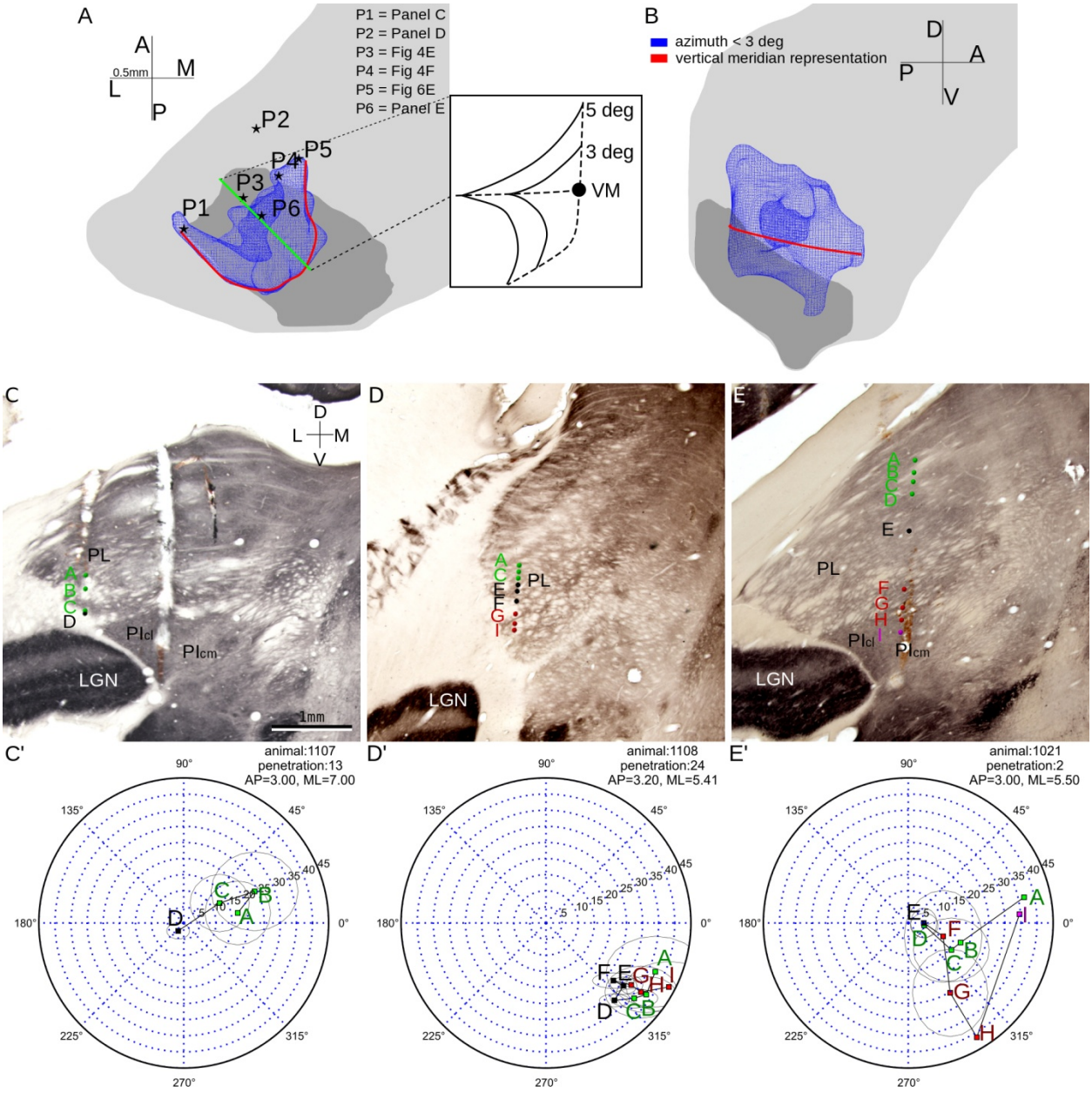

Figure 7.

Representation of the vertical meridian (VM). A,B: Horizontal (A) and coronal (B) views of the representation of the visual field area within 3° of VM in blue. The red line shows the representation of VM deduced from data. In A, each star shows the location of a penetration shown in C–E. C–E: Reconstructed penetrations overlaid on coronal CO sections. Locations of these penetrations are marked in A. Same conventions as in Figure 2. C′–F′: Receptive field progressions of penetrations shown in C–F.

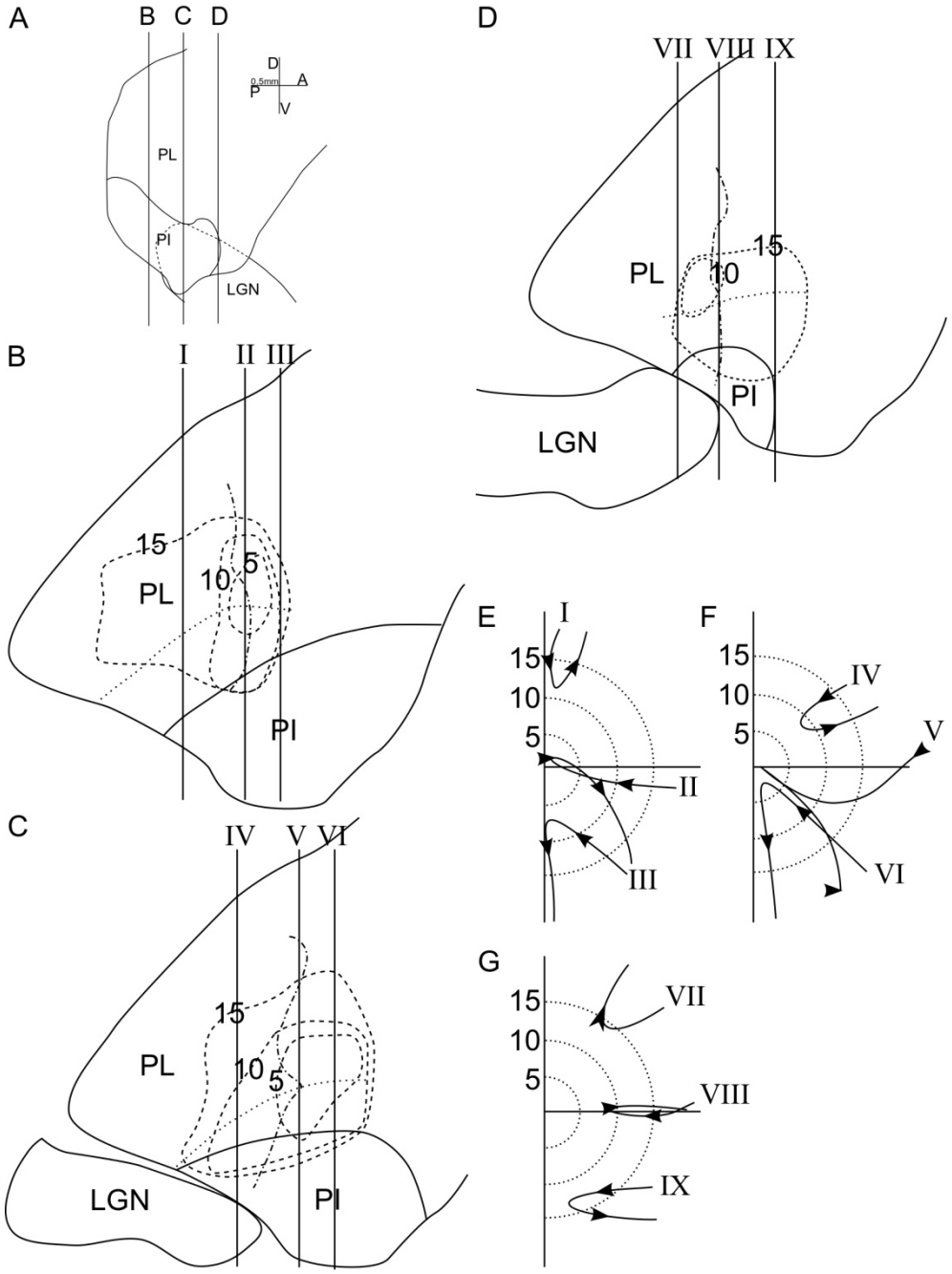

Figure 8.

Cross-sections of the map model. A: Location of coronal sections shown in B–D. B–D: Three coronal sections through the pulvinar at different anterior–posterior levels. Solid lines show the outline of the pulvinar and the PI/PL border. Dotted lines show the border between the two maps. Dashed lines show the iso-eccentricity contours at 5°, 10°, and 15° from central vision, as indicated by the number on each contour. Dotted-dashed lines show the border between upper and lower visual field representations. The vertical lines with roman numerals indicate the location of hypothetical penetrations with predicted receptive field progressions shown in E–G. E–G: Receptive field progressions predicted from the map model for hypothetical penetrations shown in B–D.

posterior levels marked in panel A. Hypothetical penetrations are marked on the coronal sections and their receptive field progressions, as predicted from the model, are shown in panels E-G.

At these anterior-posterior levels, both the representations of the upper and lower visual fields were present, so the 3 lateral hypothetical penetrations (I, IV, VII) were all in the upper field, and the 3 medial ones (III, VI, IX) were all in the lower field. The upper and lower field representations were not symmetric on the coronal plane. A larger upper field representation was found in the more posterior part of map, while a larger lower field representation was found at more anterior levels (compare panel B and D). The curvature of the HM representation at its posterior end caused the two posterior penetrations (II, V) to approach HM from the lower field and move into the lower field after the reversal. All of the representations at the posterior levels, and the medial penetrations at more anterior levels (I-III, VI, IX), were close to the VM representation, and therefore have reversal points close to VM.

Horizontal cross-sections through this combined model (Figure 9) showed clearly the retinotopic organization of the individual maps. The ventral cross-section (panel B) and the dorsal cross-section (panel D) showed the basic features of the ventral and the dorsal map, respectively. These features included a medio-posterior central vision representation, and an HM representation sheet that ran anterior-posteriorly. The cross-section in the middle (panel C) showed the transition between the dorsal and ventral maps. The border between the two maps was higher at its posterior end and lower at its anterior end. As a result, in horizontal cross-sections showing both maps, the dorsal map was anterior to the ventral map. The central vision representation fell between the maps and on the sheet representing HM.

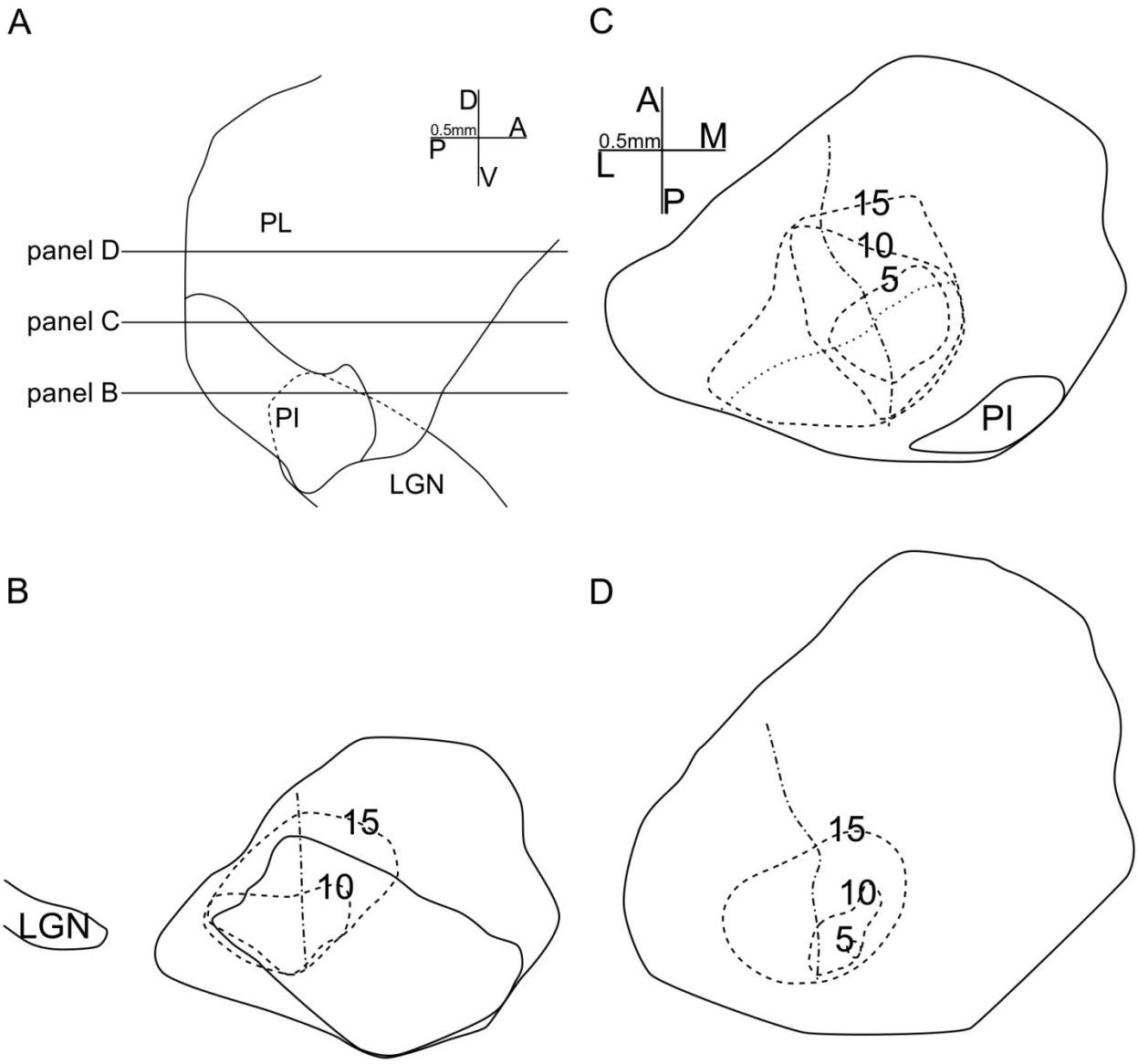

Figure 9.
Horizontal sections of the map model. A: Location of the horizontal sections shown in B–D. B–D: Solid lines show the outline of pulvinar with inferior pulvinar and LGN separately. Other conventions as in Figure 8.

Receptive Field Sizes in the Dorsal and Ventral Maps

It is of interest to determine if neurons in the two retinotopic maps have different receptive field sizes, as would be expected if the neurons in the two maps are dominated by different inputs or integrate information differently across the visual field. To test this hypothesis we chose penetrations with clear reversal points in their receptive field progressions, and assigned the units encountered before and after the reversal point to the two identified retinotopic maps. We only included cells with receptive fields within 30 degrees of central vision, to avoid bias in estimating the sizes of receptive fields near the edge of our screen, and in order to compare with similar data gathered in macaque pulvinar (Bender, 1981). The receptive field areas of these units were compared to the eccentricity of their receptive field centers in figure 10. As shown, more central receptive fields had smaller areas in both the dorsal and the ventral maps (Pearson r test, dorsal map: r=0.5194, p=4.23E-4; ventral map: r=0.5853, p=5.18E-6). Both maps showed similar slopes representing the increasing in receptive field size with eccentricity. The receptive field sizes of dorsal map cells were slightly larger than those of the ventral map cells (t-test, t=2.056, p=0.0426).

Compared to the two maps of macaque monkey lateral pulvinar (Bender, 1981, Fig.10), the maps in bush baby pulvinar had neurons with larger receptive fields for the same eccentricity. These pulvinar cells also featured receptive field sizes comparable to cells in bush baby V2 (Allison & Casagrande, 1994), and larger receptive fields than found in bush baby V1 cells (DeBruyn et al., 1993). The same relationship was found in macaque monkey, where pulvinar cell receptive fields were larger in size than V1 cells (Bender, 1981; Hubel & Wiesel, 1974), suggesting that if V1 provides the visual drive to these maps there is convergence of input to pulvinar.

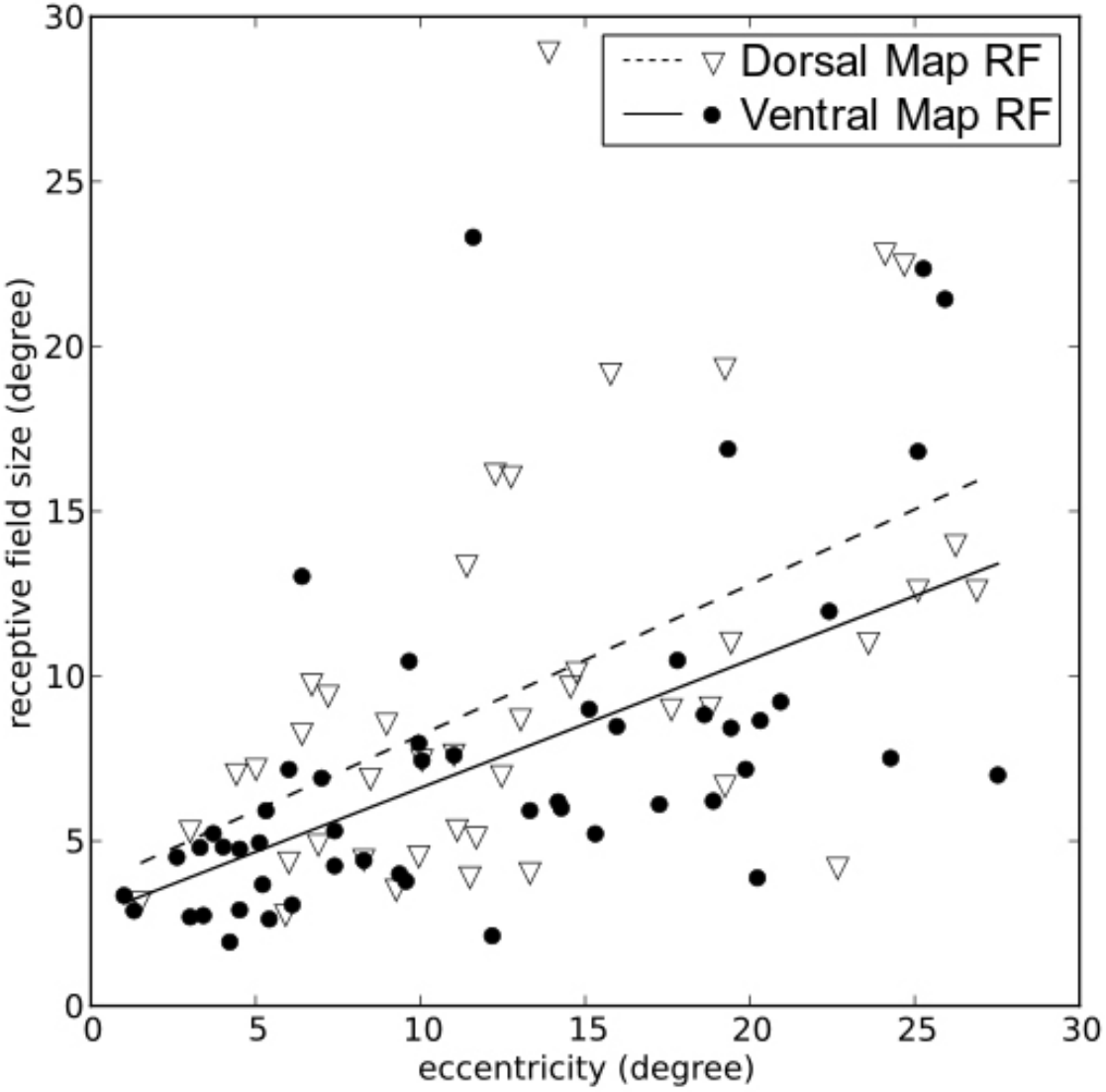

Figure 10.
Receptive field sizes as a function of the eccentricity of their centers. Only nonvague (moderate and brisk) units in penetrations showing clear reversals of RF progression were included in the analysis. Straight lines are linear regressions for the two classes of units. The eccentricities were translated from distance on the tangent screen to the view angle from area centralis, and the receptive field sizes were calculated as the square root of the area of the ellipses used to model the receptive fields. Receptive field sizes increase with eccentricity in both maps, and receptive fields in the dorsal map were slightly larger than those in the ventral map at comparable eccentricities.

Area Medial to the Two Maps

A few penetrations suggested that more visual areas may exist medial to the two identified maps. In these medial penetrations, receptive fields were encountered that were in a drastically different location than would be predicted in a typical receptive field progression through the dorsal and ventral maps. Some of these receptive fields were encountered at the beginning of some penetrations, before we entered the dorsal map (see Figure 4E). The rest were encountered deep in penetrations below cells showing receptive field progressions typical for the ventral map (see Figure 7E). Among the cells encountered after the ventral map, some also displayed very large receptive fields, often encompassing the full contralateral visual field. Others showed receptive fields located well into the ipsilateral visual field, or extending over VM into the ipsilateral visual field. In each of the latter cases the location of the optic disks was checked to ensure that the eyes had not moved.

DISCUSSION

In this study, we identified three architectonic subdivisions in bush baby PI. Two electrophysiologically defined retinotopic maps were found, one confined in PL and the other within ventral PL and PIcl, a new subdivision of PI. The central vision representations of both maps were found at the posterior end of the border between the two maps. We found that bush baby pulvinar receptive fields were slightly larger than those found in the macaque monkey, and they increased in size with eccentricity. We did not find qualitative differences in stimulus preferences between cells in the two maps. Below we discuss how the architectonic structure of bush baby PI and PL relate to their connection patterns and how their connections correlate with

the retinotopic maps. We compare the retinotopic pulvinar maps in bush baby with those found in the New and Old World simian species, represented by macaque and cebus monkey, respectively. Finally, we propose two models of retinotopic organization that can account for bush baby pulvinar maps and the maps described previously in macaque monkey.

Architecture and Connections

With both architectonic and retinotopic information, we were able to establish subdivisions within bush baby PI that appear consistent with the subdivisions described in simian species (Stepniewska & Kaas, 1997; Gray et al., 1999). We used the nomenclature established in owl monkey since it appeared to fit best with the bush baby subdivisions (see Lin & Kaas, 1979). These subdivisions also bear similarity with PI subdivisions described in other simians. In owl monkey, PIm is defined uniquely by a dark myelin circle (Lin & Kaas, 1979). In macaque, CO staining of PI showed four bands demarcating PIcl, PIcm, PIm and PIp with alternating dark and light staining from lateral to medial (Gutierrez et al., 1995; Stepniewska & Kaas, 1997). In bush baby PIm showed a myelin circle, while PIcl, PIcm and PIm showed dark, light and dark alternating CO bands, suggesting homology with these subdivisions in simians.

A number of connectional studies in bush babies and macaques also support the chemoarchitectonic subdivisions we found in this study. In bush baby, both V1 and MT have been reported to employ two separate connections with PI areas that we defined as PIcl and PIm (Symonds & Kaas, 1978; Wall et al., 1982; Wong et al., 2009). Some connections with the temporal cortices have been found exclusively in PIcm among PI subdivisions (Raczkowski & Diamond, 1980; Raczkowski & Diamond, 1981). In macaque, PIcl and PIm also have been reported to have separate connections with MT (Ungerleider et al., 1984) and receive separate

inputs from V1 (Gutierrez & Cusick, 1997). Also, several studies showed that V2 projects to PIcl (Kennedy & Bullier, 1985; Raczkowski & Diamond, 1980) but not PIm (O'Brien et al., 2002; Raczkowski & Diamond, 1980) in both bush baby and macaque. Some interspecies differences, however, have been reported to exist in the connection patterns between PI and higher visual areas. For example, the only PI subdivision that showed connections to DLr (the rostral area of the dorsolateral visual area, considered to overlap with V4 in macaque) was PIm in bush baby (Raczkowski & Diamond, 1981), and PIcm in macaque (Kaas & Lyon, 2007).

PL and PI have been reported to receive inputs from several subcortical visual areas, including the superficial layers of the superior colliculus (SC) and the parabigeminal nucleus (Diamond et al., 1992). Parabigeminal projections appeared to be located within PL and PIcl (Diamond et al., 1992). The superficial layers of the superior colliculus have been shown to project to the posterior half of PI, and to a thin dorsal layer in PL (Diamond et al., 1992). Baldwin et al. (2011) further reported two chemoarchitectonic subdivisions at the caudal end of PI that receive from SC. These areas were identified by immunostaining for the vesicular glutamate transporter 2 (vGluT2). We were unable to correlate these areas with the chemoarchitectonic subdivisions identified in this study. More subdivisions may be found in bush baby PI and PL but different chemoarchitectonic methods will be required.

Retinotopic Maps in Pulvinar and their connections with Visual Cortex

The map features we found electrophysiologically were consistent with those observed in connectional studies. As expected from the connectional patterns, we found that a localized point in the paracentral visual field was represented as a curved strip of cells in the pulvinar, running roughly anterior posterior. The two strips curve toward the border between the two maps at their

anterior ends, and meet at some point. Anatomical examples that are similar to cross-sections of the eccentricity contours shown in Figure 4B can be seen in Symonds and Kaas (1978) showing V1 projections and Carey et al. (1979) showing retrograde labeling from V1. In the latter study when a series of injections were made in V1 from the central to the peripheral representation, the strips of labeled pulvinar cells moved both anteriorly and away from the border between the dorsal and ventral maps (Carey et al., 1979). This pattern is consistent with the representation of central vision at the medio-posterior end of the border between the two visuotopic maps. Consistent with our findings concerning the upper and lower visual field representations, the lateral part of PI/PL has been reported to connect to lateral V1, which represents the upper visual field (Raczkowski & Diamond, 1981), while medial part of PI/PL has been reported to connect to medial V1, which represents the lower visual field (Raczkowski & Diamond, 1981; Conley & Raczkowski, 1990; DeBruyn et al., 1993). The central-peripheral and upper-lower field axes in our maps are also consistent with those inferred from pulvinar-MT connections (see Wall et al., 1982; Wong et al., 2009).

The two pulvinar visuotopic maps have cortical connections only with the early visual cortices. Both maps have major connections with V1, V2, V3, and to a lesser extent MT (Raczkowski & Diamond, 1981). Reciprocal connections with the temporal visual areas were reported to be restricted to either PM or the medial and ventral border of PI (Raczkowski & Diamond, 1980; Raczkowski & Diamond, 1981). Connections with the posterior parietal cortex were only found in PM (Glendenning et al., 1975; Raczkowski & Diamond, 1981).

Prosimian and simian pulvinar

The pulvinar of simians, particularly the pulvinar of anthropoid primates, is generally larger than that of studied prosimians (Chalfin et al., 2007). In the Old World simian macaque, the pulvinar is rotated laterally and posteriorly in comparison to that of the bush baby. Once these transformations have been accounted for, most architectonic and visuotopic map features appear to correspond nicely between these two species. In bush baby, the dorsal and ventral maps are found lateral to PIm, while in macaque they are found ventral, lateral and posterior to the MT recipient zone of PIm, consistent with an overall pulvinar rotation. The lateral map in macaque is analogous to the dorsal bush baby map we report here, and the inferior macaque map appears to correspond nicely to the ventral bush baby map. The upper field is represented laterally in both bush baby maps, and ventrally in both macaque maps. Under the same transformation the vertical sheet of HM representation in bush baby lies at a similar position in pulvinar as the mostly horizontal sheet of HM representation in macaque. Two major differences, however, exist between the two species. In macaque pulvinar, VM is represented on the border between the two maps, while in bush baby pulvinar VM is represented the posterior and media edges of that border. Additionally, in macaque the lateral map has a second order representation of the visual field. In other words, the representation of the horizontal meridian is split on the lateral surface of PL: the upper and lower visual field representations are not joined at the horizontal meridian. First order representations are those where adjacent points of the same hemifield always map to adjacent points in the brain such as in the primary visual cortex or middle temporal cortex. In contrast second order representations are maps that contain a discontinuity in their representation in the brain and adjacent points are not necessarily represented in adjacent pieces of tissue as is the case for the second visual area (V2) in primates

(Allman & Kaas, 1974) much like in V2, where the HM representation is split to form its anterior border. In bush baby, by contrast with macaque monkey, both pulvinar visuotopic maps appear to have first order representations.

The two maps in bush baby pulvinar are similar in visual field representation to the ventrolateral map in the New World cebus pulvinar. The ventrolateral cebus map reported in Gattass et al. (1978) may, in fact, consists of two individual retinotopic maps. Cebus pulvinar is rotated laterally and posteriorly compared to bush baby pulvinar, as in the macaque. Instead of being located at the medio-posterior pole as in bush baby pulvinar maps, the central vision representation of the ventrolateral pulvinar map is located on its latero-anterior border in cebus. If the bush baby pulvinar maps are rotated, most bush baby map features align nicely with those reported for the cebus ventrolateral map in pulvinar. These features include the shapes of both the VM and HM representations and their spatial relation (compare Figures 6A and 7A of this paper to Figures 4C and 5 in Gattass et al., 1978). Given its relation with the two bush baby pulvinar maps, the ventrolateral map in cebus pulvinar can be divided into two maps along the horizontal extension of the VM representation, where penetrations showed a reversal of receptive field progressions similar to the ones seen in bush baby. That border runs from the dorso-anterior end of the ventrolateral map to its ventro-posterior end. Since that border in cebus is not horizontal, however, double representations were not apparent in individual penetrations. Instead, anterior penetrations can be predicted to encounter cells in the ventral visuotopic map with receptive fields adjacent to those of belonging to posterior cells in the dorsal visuotopic map. Indeed, we can see examples of this double representation in the A+2 and A+0 penetrations in Figure 4 of Gattass et al. (1978), where the receptive fields in A+2 after the reversal matched the receptive fields in A+0 before the reversal. Additionally, the cebus dorso-medial map

appeared to be located in the equivalent position to the dorsal medial PL (Pdm) in macaque (Petersen et al., 1985), which might correspond to a separate map dorso-anterior to the dorsal map in bush baby. The latter would require more data to confirm, however.

A partial pulvinar map representing the visual field beyond 5 degrees from central vision had been reported in the inferior pulvinar of the simian species owl monkey (Allman et al., 1972). Given that owl monkey visual pulvinar has been reported to be similar to bush baby visual pulvinar in both connection patterns (Graham et al., 1979) and architectonic features (Allman et al., 1972; Lin and Kaas, 1979), it is not surprising that the partial map reported in owl monkey PI showed many features in common with the ventral map we identified in bush baby, including the relative location of upper-lower field representation and central-peripheral representation (Allman et al., 1972). The major difference is that owl monkey PI was reported to be fully occupied by a single retinotopic map, instead of having a medial section not included in the major map. This feature is in contrast to later connectional findings that PIm in owl monkey had its own visual field representation separate from the map in PIc (Lin and Kaas, 1979, Graham et al., 1979). It was likely that the sparse sampling in this early electrophyisiology study was not enough to distinguish the two separate maps in PIcl and PIm.

The second order representation reported in the lateral map of macaque pulvinar appears not to be shared by either cebus or bush baby. Given the orientation of the maps in bush baby, for the dorsal map to have a second order representation most vertical penetrations should have started with receptive fields near HM, yet only a small part of our observed penetrations showed this feature. The cebus ventrolateral pulvinar map is reported as having straight, parallel iso-elevation contours (Gattass et al., 1978). Regardless of whether cebus ventrolateral pulvinar map consists of one or two maps this result suggests that there is no second order map in this area.

The second order representation reported in macaque pulvinar map is thus specific to this species and suggests that this organization evolved separately in Old World simians.

A New Model for Maps in Thalamic Nuclei

The visual field is mapped onto the two dimensional sheet on the retina but is represented in a three dimensional volume in structures such as the pulvinar. Although the visual field is roughly represented the same way in different primates there are significant differences in detail. At least two models of visual field mapping exist in primate thalamus.

In the maps reported in macaque pulvinar the VM representation covers half the surface of the map. Both HM and VM are represented as curved sheets. The central vision is represented as a long curve on the intersection between HM and VM representations. Map features like the representations of VM, HM and the central vision are one dimension higher than the visual field features they represent: the central vision, a point, is represented as a curve, and VM, a line, is represented as a sheet. There exist perfect iso-projection curves for each of the two macaque pulvinar maps such that each point on the same curve represents the same location in the visual field (Bender, 1981). In other words, when sliced perpendicular to local iso-projection curves, each slab of the map contains the full representation of the contralateral visual field. The way the pulvinar maps represent the visual field as described in macaque is similar to that of V1 and LGN. In both of these areas, the visual field is mapped onto one surface, with a column made of cells from different layers representing the same point in the visual field. With this organization, different visual functions could potentially be carried out in different slabs of the same map. One such hypothesis concerning pulvinar states that more posterior slabs relay visual signals between

V1 and V2, while more anterior slabs relay signal between gradually higher levels in the visual hierarchy (Shipp, 2003, Fig.5-6).

In contrast to the macaque pulvinar maps, the central vision is represented as single points in both bush baby pulvinar maps, and VM is represented as a curve in both maps. In each of the maps, the representation of the elevation axis is parallel to the VM representation, and the azimuth axis is represented on the polar axis of a polar coordinate system on planes perpendicular to the VM representation. This organization leaves the polar angle as the iso-projection axis. The iso-projection curves are roughly concentric to the central vision representation and parallel to the HM representation. Unlike the organization described in macaque pulvinar, there is no obvious way to subdivide such maps into divisions with full visual field representations. As a result, cells with different functions are more likely to be mixed in bush baby pulvinar rather than clustered. Indeed we found cells with different visual responses mixed in bush baby pulvinar.

The partial inferior map reported in owl monkey pulvinar was described as resembling the one model represented by macaque pulvinar maps, with its representation of central vision on a line at the middle of its dorsal surface. However, details of that map near its central vision representation are lacking so we do not know whether this is indeed the case. As discussed in the previous section, cebus pulvinar maps showed a focal representation of central vision which fits more with the map model for bush baby than with that of the macaque monkey but again the data for the latter study are sparse so it is still unclear how the pulvinar maps are organized in either owl monkey or cebus monkey.

These two different types of visuotopic map organization are diagrammed in figure 11. Panel A shows a model of the macaque pulvinar inferior map abstracted from the diagrams in

Figure 11 of Bender (1981) , while in panel B the model shows how the visual field is mapped in the bush baby pulvinar. The difference in the shapes of certain map features, such as the central vision representation and VM, can be easily visualized. These models can be applied to other thalamic nuclei where 2-D sensory sheets are represented in a 3-D volume and where specific aspects of the sensory sheet are emphasized. For example, the map organization reflected in primate LGN conforms to the former model represented also by the macaque pulvinar. Cells with different functions achieve a higher level of clustering in the former model compared to the latter. This difference in pulvinar map organization may reflect the higher levels of differentiation in Old World simian pulvinar compared to both prosimian and New World simian pulvinar.

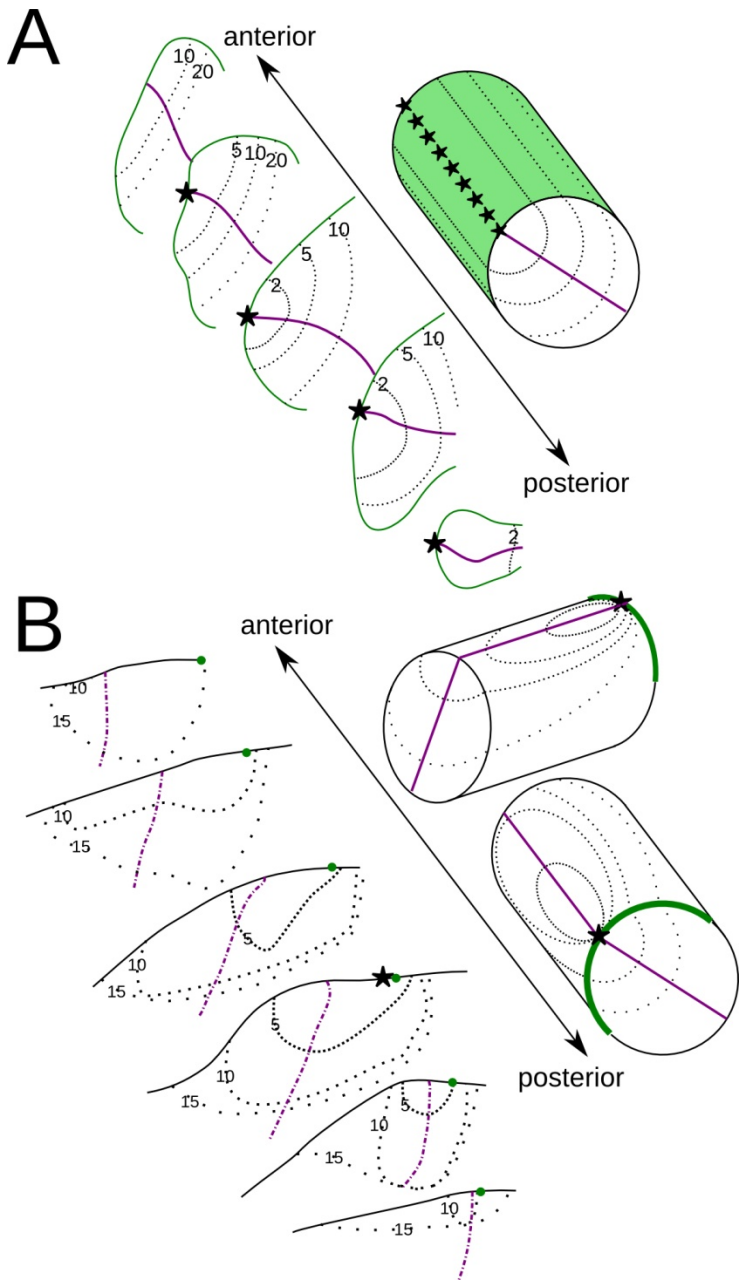

Figure 11.
Two ways in which a 2D contralateral visual field could be represented in a 3D brain structure. A: Retinotopy of the inferior map of the macaque pulvinar adapted from Figure 11 of Bender (1981) and a simplified model of that map at upper right. B: Retinotopy of the inferior map in bush baby pulvinar, along with its simplified model in two different views. In the simplified models, stars indicate central vision representations. Purple lines show the intersection of the horizontal meridian (HM) representations with the structure surface for the simplified model, and HM for the coronal sections. The vertical meridian (VM) is shown either as a green surface or a green line. Note that most of the visible intersection between HM and the surface in the left panel is also the intersection between the HM and VM representations, and thus the central vision representation. Thin dotted lines are iso-eccentricity contours, with lower eccentricity represented by denser dotted lines. The VM representation line in B is only on the structure surface, in contrast to all other lines representing the intersection between a plane in the structure and the structure surface. Numerals indicate eccentricities in degrees.

Other Acknowledgements

We wish to thank Mariesol Rodriguez and Julia Mavity-Hudson for assistance with histological preparations, Dmitry Yampolsky and Yaoguang Jiang for assistance with experiments, and Mary Feurtado for assistance with animal surgery.

Literature Cited

Allison JD, Casagrande VA. 1994. Receptive field structure of V2 neurons in the prosimian primate Galago crassicaudatus. Society for Neuroscience 20:1741 (Abs.).

Allman JM, Kaas JH. 1974. The organization of the second visual area (V II) in the owl monkey: a second order transformation of the visual hemifield. Brain Res 76:247–265.

Allman JM, Kaas JH, Lane RH. 1973. The middle temporal visual area (MT) in the bushbaby, Galago senegalensis. Brain Res 57:197–202.

Allman JM, Kaas JH, Lane RH, Miezin FM. 1972. A representation of the visual field in the inferior nucleus of the pulvinar in the owl monkey. Brain Res 40:291–302.

Arend I, Rafal RD, Ward R. 2008. Spatial and temporal deficits are regionally dissociable in patients with pulvinar lesions. Brain 131:2140–2152.

Baldwin MKL, Balaram P, Kaas JH. 2011. Superior colliculus connections and VGLUT2 expression within visual thalamus of prosimian galagos (Otolemur garnetti). Program No. 817.17. 2011 Neuroscience Meeting Planner. Washington, DC: Society for Neuroscience, 2011. Online.

Bender DB. 1981. Retinotopic organization of macaque pulvinar. J Neurophysiol 46:672–693.

Bender DB. 1982. Receptive-field properties of neurons in the macaque inferior pulvinar. J Neurophysiol 48:1–17.

Berman RA, Wurtz RH. 2011. Signals conveyed in the pulvinar pathway from superior colliculus to cortical area MT. J Neurosci 31:373–384.

Boyd JD, Matsubara JA. 1996. Laminar and columnar patterns of geniculocortical projections in the cat: relationship to cytochrome oxidase. J Comp Neurol 365:659–682.

Carey RG, Fitzpatrick D, Diamond IT. 1979. Layer I of striate cortex of Tupaia glis and Galago senegalensis: Projections from thalamus and claustrum revealed by retrograde transport of horseradish peroxidase. J Comp Neurol 186:393–437.

Chalfin BP, Cheung DT, Muniz JAPC, de Lima Silveira LC, Finlay BL. 2007. Scaling of neuron number and volume of the pulvinar complex in New World primates: comparisons with humans, other primates, and mammals. J Comp Neurol 504:265–274.

Conley M, Raczkowski D. 1990. Sublaminar organization within layer VI of the striate cortex in Galago. J Comp Neurol 302:425–436.

DeBruyn E, Casagrande VA, Beck PD, Bonds AB. 1993. Visual resolution and sensitivity of single cells in the primary visual cortex (V1) of a nocturnal primate (bush baby): correlations with cortical layers and cytochrome oxidase patterns. J Neurophysiol 69:3–18.

del Río MR, DeFelipe J. 1995. A light and electron microscopic study of calbindin D-28k immunoreactive double bouquet cells in the human temporal cortex. Brain Res 690:133-140.

Diamond IT, Fitzpatrick D, Conley M. 1992. A projection from the parabigeminal nucleus to the pulvinar nucleus in Galago. J Comp Neurol 316:375–382.

Emmers R, Akert K, Woolsey CN. 1963. A stereotaxic atlas of the brain of the squirrel monkey (Saimiri sciureus). 1st ed. University of Wisconsin Press Madison.

Van Essen DC. 2005. Corticocortical and thalamocortical information flow in the primate visual system. Prog Brain Res 149:173–185.

Gallyas F. 1979. Silver staining of myelin by means of physical development. Neurol Res 1:203–209.

Gattass R, Oswaldo-Cruz E, Sousa APB. 1978. Visuotopic organization of the cebus pulvinar: a double representation of the contralateral hemifield. Brain Res 152:1–16.

Geneser-Jensen FA, Blackstad TW. 1971. Distribution of acetyl cholinesterase in the hippocampal region of the guinea pig. Cell Tissue Res 114:460–481.

Glendenning K, Hall J, Diamond IT, Hall W. 1975. The pulvinar nucleus of Galago senegalensis. J Comp Neurol 161:419–457.

Gray DN, Gutierrez C, Cusick CG. 1999. Neurochemical organization of inferior pulvinar complex in squirrel monkeys and macaques revealed by acetylcholinesterase histochemistry, calbindin and Cat-301 immunostaining, and Wisteria floribunda agglutinin binding. J Comp Neurol 409:452–468.

Gutierrez C, Cusick CG. 1997. Area V1 in macaque monkeys projects to multiple histochemically defined subdivisions of the inferior pulvinar complex. Brain Res 765:349–356.

Gutierrez C, Yaun A, Cusick CG. 1995. Neurochemical subdivisions of the inferior pulvinar in macaque monkeys. J Comp Neurol 363:545–562.

Hendry SHC, Reid RC. 2000. The koniocellular pathway in primate vision. Annu Rev Neurosci 23:127–153.

Hubel DH, Wiesel TN. 1974. Uniformity of monkey striate cortex: a parallel relationship between field size, scatter, and magnification factor. J Comp Neurol 158:295–305.

Huerta MF, Krubitzer LA, Kaas JH. 1986. Frontal eye field as defined by intracortical microstimulation in squirrel monkeys, owl monkeys, and macaque monkeys: I. Subcortical connections. J Comp Neurol 253:415–439.

Jerison HJ. 1979. Brain, body and encephalization in early primates. J Hum Evol 8:615–635.

Johnson J, Casagrande VA. 1995. Distribution of calcium-binding proteins within the parallel visual pathways of a primate (Galago crassicaudatus). J Comp Neurol 356:238–260.

Kaas JH, Lyon DC. 2007. Pulvinar contributions to the dorsal and ventral streams of visual processing in primates. Brain Res Rev 55:285–296.

Kennedy H, Bullier J. 1985. A double-labeling investigation of the afferent connectivity to cortical areas V1 and V2 of the macaque monkey. J Neurosci 5:2815–2830.

Lin CS, Kaas JH. 1979. The inferior pulvinar complex in owl monkeys: architectonic subdivisions and patterns of input from the superior colliculus and subdivisions of visual cortex. J Comp Neurol 187:655–678.

Lysakowski A, Standage GP, Benevento LA. 1986. Histochemical and architectonic differentiation of zones of pretectal and collicular inputs to the pulvinar and dorsal lateral geniculate nuclei in the macaque. J Comp Neurol 250:431–448.

Merabet LU, Desautels A, Minville K, Casanova C. 1998. Motion integration in a thalamic visual nucleus. Nature 396:265–268.

O'Brien BJ, Abel PL, Olavarria JF. 2002. Connections of calbindin-D28k-defined subdivisions in inferior pulvinar with visual areas V2, V4 and MT in macaque monkeys. Thalamus & Related Systems 1:317–330.

Petersen SE, Robinson DL, Keys W. 1985. Pulvinar nuclei of the behaving rhesus monkey: visual responses and their modulation. J Neurophysiol 54:867–886.

Petersen SE, Robinson DL, Morris JD. 1987. Contributions of the pulvinar to visual spatial attention. Neuropsychologia 25:97–105.

Raczkowski D, Diamond IT. 1980. Cortical connections of the pulvinar nucleus in Galago. J Comp Neurol 193:1–40.

Raczkowski D, Diamond IT. 1981. Projections from the superior colliculus and the neocortex to the pulvinar nucleus in Galago. J Comp Neurol 200:231–254.

Robinson DL, Petersen SE. 1985. Responses of pulvinar neurons to real and self-induced stimulus movement. Brain Res 338:392–394.

Sherman SM. 2007. The thalamus is more than just a relay. Curr Opin Neurobiol 17:417–422.

Shipp S. 2003. The functional logic of cortico-pulvinar connections. Philos Trans R Soc Lond B Biol Sci 358:1605–1624.

Stepniewska I, Kaas JH. 1997. Architectonic subdivisions of the inferior pulvinar in New World and Old World monkeys. Vis Neurosci 14:1043–1060.

Symonds LL, Kaas JH. 1978. Connections of striate cortex in the prosimian, Galago senegalensis. J Comp Neurol 181:477–511.

Theyel B, Llano D, Sherman SM. 2010. The corticothalamocortical circuit drives higher-order cortex in the mouse. Nat Neurosci 13:84–88.

Ungerleider LG, Desimone R, Galkin TW, Mishkin M. 1984. Subcortical projections of area MT in the macaque. J Comp Neurol 223:368–386.

Walker AE. 1938. The Primate Thalamus. University of Chicago press.

Wall JT, Symonds LL, Kaas JH. 1982. Cortical and subcortical projections of the middle temporal area (MT) and adjacent cortex in galagos. J Comp Neurol 211:193–214.

Wong P, Collins CE, Baldwin MKL, Kaas JH. 2009. Cortical connections of the visual pulvinar complex in prosimian galagos (Otolemur garnettii). J Comp Neurol 517:493–511.

Wong-Riley M. 1979. Changes in the visual system of monocularly sutured or enucleated cats demonstrable with cytochrome oxidase histochemistry. Brain Res 171:11–28.

CHAPTER IV

GATING AND CONTROL OF PRIMARY VISUAL CORTEX BY PULVINAR

The study described in this chapter was published and is reproduced below without alterations: Purushothaman G, Marion R, Li K, Casagrande VA. 2012. Gating and control of primary visual cortex by pulvinar. Nat Neurosci 15: 905-912.

Introduction

The primate visual system is currently viewed as a rough hierarchy of 30 or more cortical areas[1-4]. Area V1 is at the bottom of this hierarchy and contains a representation of important elementary visual features. Synaptic inputs from LGN as well as intracortical circuits are thought to underlie this key visual representation[1,2]. This model of visual system organization and function is incomplete in at least two aspects[4]. First, the model does not take into account the significant input to V1 from pulvinar in elucidating V1 function[4-7]. Second, unlike cortico-cortical connections, cortico-pulvino-cortical projections are not hierarchical[4]. Lateral pulvinar receives input from infra-granular layer 5 of V1 and projects to supra-granular layers 1-3 of V1 as well as to layers 3-4 of the secondary visual area V2[5,8-10]. Supra-granular layers 2-3 of V1 also project to granular layer 4 of V2 (Supplementary Fig. 1)[5]. Besides each sub-nucleus of pulvinar (e.g., lateral pulvinar) projecting both forward and backward to multiple interconnected cortical

areas (e.g., V1 and V2), multiple sub-nuclei connect with the same cortical area[5]. In the absence of layers or columns within the sub-nuclei of pulvinar[5], this complex mesh of interconnections obscures the hierarchical position of pulvinar relative to V1 and V2[4]. Consequently, it is difficult to decipher the distinct function of each node along the cortico-pulvino-cortical pathway; it is also difficult to tease out the causal relationship between neural activity at different nodes[4,11]. Despite these complications, certain facts about the pulvinar nucleus make it necessary to address these two limitations. The pulvinar has expanded through evolution in proportion to the enlargement of higher visual and association cortices with which it connects[5-7]. Pulvinar lesions in monkeys and humans often result in profound visual deficits such as spatial neglect and impaired attention[12-20]. Human and monkey experiments have shown pulvinar activity to be correlated with aspects of spatial vision, visual salience, attention, and saccadic suppression[21-28]. Pulvinar atrophy is also characteristic of severe neuropsychiatric disorders and treatment of some of these disorders mitigates pathologies of the pulvinar[29]. That a single thalamic nucleus is associated with such a wide array of visual functions and causes such a variety of deficits when damaged are not easily explained. This motivates a better understanding of the position of pulvinar in the functional hierarchy of the visual system.

As a simple first step towards this goal, we studied the *net* effect of manipulating the activity of pulvinar neurons on their projection zone lowest in the cortical hierarchy, i.e., the supra-granular layers of V1. We locally excited or suppressed neural activity in the lateral sub-nucleus of pulvinar and measured the impact of these manipulations on the V1 target zone of the affected lateral pulvinar neurons. For comparison and control, we also monitored and manipulated LGN neural activity in similar manner.

Results

We measured the responses of neurons in superficial layers 2-3 of area V1 to high-contrast (50%) drifting sinusoidal gratings presented within the neurons' visual receptive fields (Methods and Supplementary Fig. 2). In each experiment, responses of multiple V1 neurons were simultaneously measured using a 100-electrode array implanted in one hemisphere. Receptive fields of neurons sampled by different electrodes of the array varied in size from 1° to 4° and were located within 6° of *area centralis* (AC). These measurements showed a characteristic brisk phasic response to onset of visual stimulation followed by a tonic response for the reminder of the stimulation (Fig. 1a).

Effect of reversible inactivation of lateral pulvinar

Using a microelectrode we found lateral pulvinar neurons whose receptive fields overlapped with a majority of V1 receptive fields sampled by the array. Centrally located lateral pulvinar receptive fields that satisfied this criterion varied in size from 1° to 6° and were within 6° of *area centralis*. We inactivated the lateral pulvinar neurons by infusing a small volume (0.5μL) of the GABA agonist Muscimol (Methods). We then repeated the V1 measurements. In 95% (156/164) of V1 neurons studied in 3 animals, the characteristic visually driven responses were almost completely abolished after the visuotopically matched region of lateral pulvinar was inactivated (Fig. 1a, b). This change occurred at all orientations of the sinusoidal grating (Fig. 1c). The average visual response decreased from 43.1 ± 2.9 spikes/sec (mean ± s.e.m) to 15.45 ± 1.8 spikes/sec (Fig. 1b), a significant change (Wilcoxon rank-sum test, P=0; n=164) of 64%. We quantified the visual responsiveness of V1 neurons by computing the ratio of post-stimulus peak

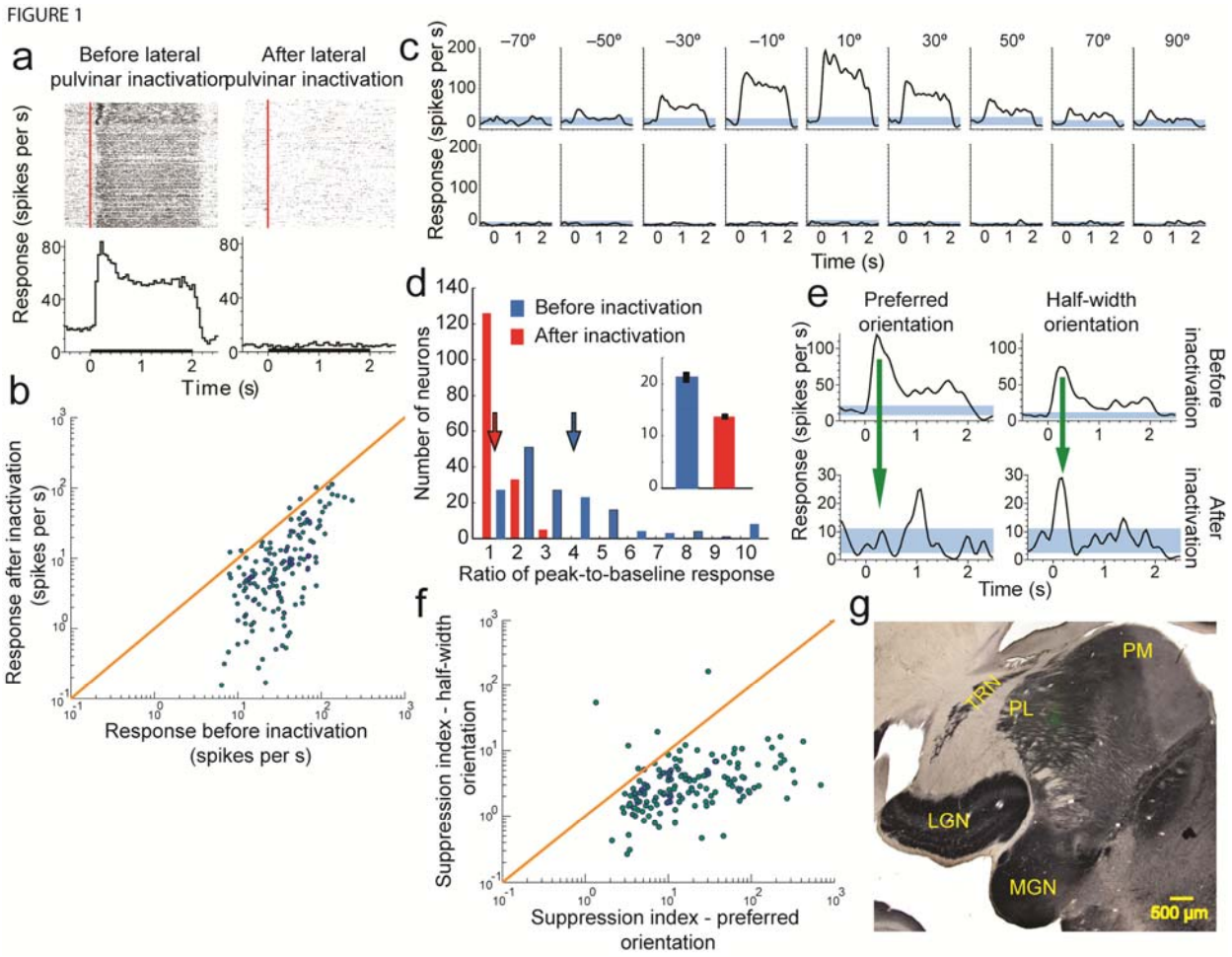

Figure 1.

Reversibly inactivating lateral pulvinar almost abolishes visual responses in supra-granular layers of V1. (a) Raster plots representing each spike as a dot and Peri-Stimulus Time Histograms (PSTHs) are shown for a sample neuron in layers 2-3 of V1 before (left column) and after (right column) lateral pulvinar inactivation. Red line on the raster plot shows visual input onset time and black line on the abscissa of the PSTH shows the visual input presentation time. Responses shown are for a drifting sinusoidal grating presented within the neuron's receptive field at 18 different orientations. (b) Comparison of the average input-driven response before and after lateral pulvinar inactivation for all 164 V1 neurons. (c) PSTHs are shown separately for 9 orientations at which this neuron was most responsive before lateral pulvinar inactivation. Blue bands represent 95% confidence interval around the mean baseline response measured before visual stimulation. (d) The phasic response, quantified as the ratio of peak-to-baseline activity, is shown for 164 V1 neurons before (blue) and after (red) lateral pulvinar inactivation. Inset shows baseline responses. (e) PSTHs are shown for a layer 3 V1 neuron before (top row) and after (bottom row) lateral pulvinar inactivation for the preferred orientation (left column) and half-width orientation (right column). Responses are shown at different scales for the top and bottom rows. (f) Comparison of suppression indices at preferred and half-width orientations for all 164 V1 neurons. (g) A composite figure showing the injection in lateral pulvinar. Coronal section of the left thalamus was stained for cytochrome oxidase (CO). A fluorescent image (green) was obtained with Alexafluor-488 conjugated streptavidin as probe for the BDA mixed with the muscimol injected in lateral pulvinar. The fluorescence image was used to create a vector mask for the CO image, thereby rendering transparent in the CO image all pixels with intensity above background in the fluorescent image. Fluorescence seen in the composite image is through these transparent pixels in CO. Fluorescence is localized well within lateral pulvinar and is more than 1 mm away from the TRN and LGN. LGN, lateral geniculate nucleus; MGN, medial geniculate nucleus; PL, lateral pulvinar; PM, medial pulvinar; TRN, thalamic reticular nucleus.

response to the pre-stimulus baseline (or background) response. This ratio changed significantly as a consequence of lateral pulvinar inactivation (Wilcoxon rank-sum test, P=0; n=164), with the average value decreasing by 300% from 4.01 ± 0.24 (mean ± s.e.m) to the near-baseline value of 1.34 ± 0.03 (Fig. 1d). Baseline V1 activity also changed significantly (Wilcoxon rank-sum test, P<0.001; n=164) decreasing by 36% after lateral pulvinar inactivation (inset, Fig. 1d).

After lateral pulvinar injection, the phasic component of V1 response was suppressed more strongly near the original preferred orientation of the neuron than near non-preferred orientations (Fig. 1e). We computed a suppression index as the divisive reduction in the ratio of the peak-to-baseline response that occurred with lateral pulvinar inactivation (Methods). Suppression at the preferred orientation (mean ± s.e.m = 0.11 ± 0.01) was about 5-fold stronger than at the half-width orientation (0.58 ± 0.10; Wilcoxon rank-sum test, $P< 10^{-30}$; n=164; Fig. 1f).

Spatiotemporal extent of the lateral pulvinar injections

To exclude cases in which the injection in lateral pulvinar diffused into the LGN or the thalamic reticular nucleus (TRN), we mixed the injected muscimol with biotinylated dextran amine (BDA) and probed it with Alexafluor-488 conjugated streptavidin (Methods). In the three cases described above, complete reconstruction of the thalamus showed the fluorescence was confined to lateral pulvinar within 500 μm of the injection, with no fluorescence in either the LGN or the TRN (Fig. 1g, Supplementary Figs. 3 4). Slight effusion along the path of injection observed in one case was also confined to dorsal lateral pulvinar and did not encroach on the TRN (Supplementary Fig. 4a).

Strong binding to $GABA_A$ receptors and high-affinity uptake into GABAergic neurons and astrocytes keep injected muscimol locally sequestrated[30,31]. Studies with [^{3}H] muscimol have found that even for large 1 μL injections of muscimol, the region of effectiveness remains confined to about 1 mm over several hours[30,31]. The 500 μm regions of fluorescence that resulted from 0.5 μL injections in our cases are in rough agreement with these measurements. However, some studies that used large volume (up to 2 μL) muscimol injections have reported that behavioural deficits sometimes changed or strengthened 1-2 hours after injection[32]. Effusion along the injection pipette or the slow spread of muscimol in the tissue at a rate of about 1-2 mm over 1-2 hours could account for these observations[32] (see Methods, "Injections"). To test the latter possibility, we studied the temporal dynamics of the effect of lateral pulvinar injections by measuring V1 visual responses in 15 minute intervals over several hours. These measurements showed that the average V1 visual response in the 15 minutes prior to the injection was 41.9 ± 6.1 spikes/sec (mean ± s.e.m). V1 visual responses started decreasing within a few minutes (< 5 min) of the injection and the average response between 20 min and 35 min after the lateral pulvinar injection was 10.4 ± 2.4 spikes/sec (Supplementary Figs. 5a), a significant change (Wilcoxon rank-sum test, $P<10^{-9}$; n=36) of 75% from the pre-injection response. Notably, there was no significant change in V1 visual responses thereafter for up to 125 minutes after the injection (Wilcoxon rank-sum test, $P>0.4$; Supplementary Fig. 5b, c,d; see also Supplementary Fig. 6). Because the LGN was 1.5-2.0 mm from the centre of the injection at the closest approach in our cases (Fig. 1g, Supplementary Figs. 3 and 4), at the rate of diffusion implied by the above-mentioned behaviour studies (~1 mm/hour), changes in V1 responses due to leakage into LGN could not have occurred sooner than 60-90 minutes after the injection. Therefore, in addition to

the histology, this analysis also showed our results to be consistent with the action of injected muscimol on proximal lateral pulvinar neurons rather than on the distant LGN neurons.

Our injections were made in the visuotopic region of lateral pulvinar that contained central receptive fields (Fig. 1g, Supplementary Figs. 3 and 4). The part of dorsomedial LGN closest to the centre of these lateral pulvinar injections represents the lower visual field; more central LGN receptive fields are located posterolaterally further away from the centre of these injections (Supplementary Fig. 4). As LGN and V1 receptive fields are retinotopically co-located, if the suppression of V1 responses were mainly due to leakage of muscimol into LGN, then V1 receptive fields in the lower field must necessarily be affected in order for the more central receptive fields to be affected. In the three cases described above, the injection almost completely suppressed visual responses in central V1 receptive fields. However the more eccentric a V1 receptive field was in the lower field, the more responsive it was to visual stimulation (Supplementary Fig. 7). This spatial gradient of the effect of the injection on V1 is also consistent with proximal action of muscimol on lateral pulvinar rather than its leakage into LGN.

LGN activity during inactivation of lateral pulvinar

To further ensure LGN input to V1 was not accidentally disrupted by the lateral pulvinar injection, we performed two more direct controls. First, we injected into lateral pulvinar a fluorophore conjugated muscimol (FCM, Methods) instead of the muscimol-BDA mixture. FCM is a single molecule in which the muscimol terminus binds to the GABA receptor and the BODIPY® TMR-X terminus fluoresces near 572 nm, allowing us to determine the spatial extent of inactivation directly from the fluorescence (Fig. 2a, Methods).

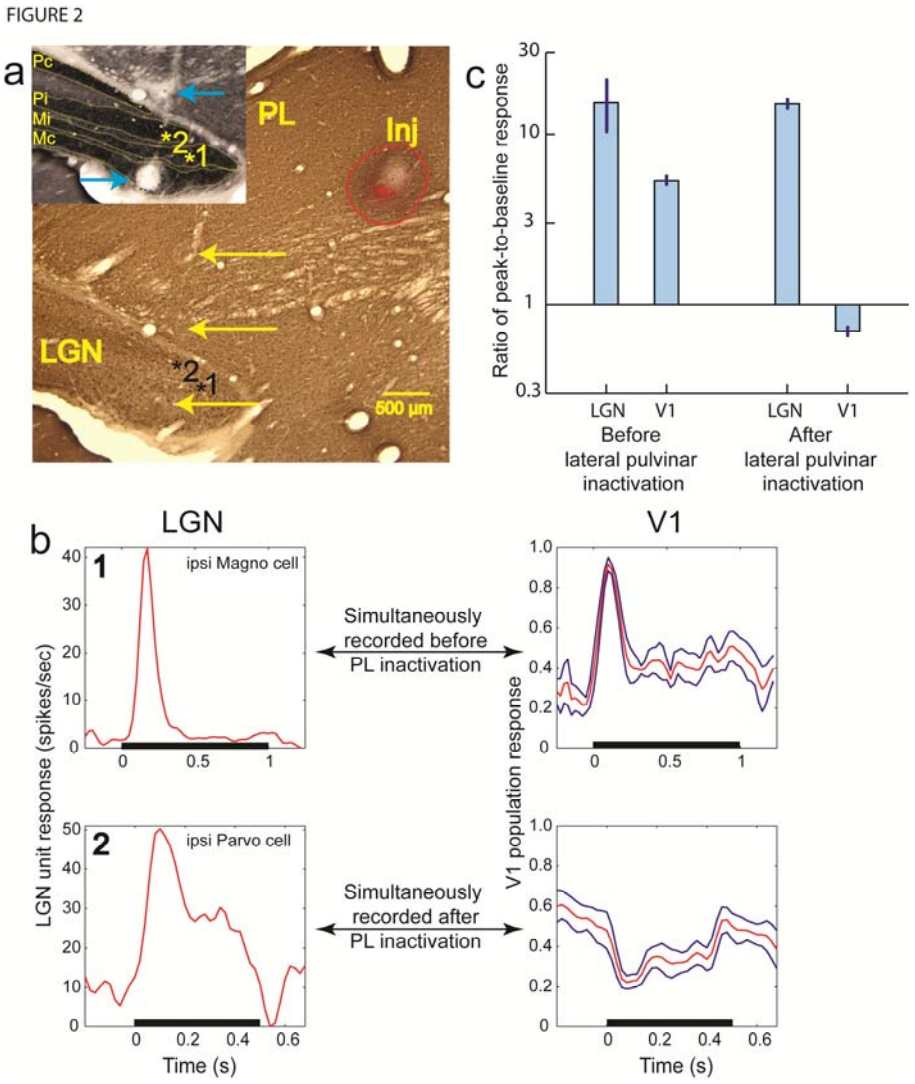

Figure 2.

Absence of V1 output in the presence of LGN input. (a) Composite figure of the injection, created using the method mentioned above (Fig. 1g). Coronal section of left thalamus was stained for Calbindin. The injection in lateral pulvinar is labeled "Inj". Red fluorescence is from fluorophore conjugated muscimol that was injected to inactivate this region of lateral pulvinar. The red outline shows the overall extent of the injection reconstructed from several successive sections through the thalamus. Region of inactivation is identical to the red fluorescent region, which is about 2 millimeters away from the LGN. The track from the electrode approaching LGN measurements sites is visible on the left. Yellow arrows mark 3 electrical lesions made along the electrode track for locating measurement sites in LGN. Inset shows the CO stained adjacent section with LGN layers marked and labeled. Blue arrows mark the 2 most ventral lesions. Numbers on the marked sites correspond to the numbers on the PSTHs shown in (b). (b) PSTHs measured at 2 LGN sites are shown along with simultaneously measured V1 responses before lateral pulvinar inactivation (top row) and after (bottom row). PSTH of a LGN neuron from the ipsi magnocellular layer in site 1 shows a brisk-onset transient response to a 1 second long visual stimulation of its receptive field. The mean normalized PSTH of 7 supra-granular V1 neurons, whose receptive fields completely overlapped that of the simultaneously measured LGN neuron (on the left), is shown in red. Blue lines show 1 s.e.m. Measurements at site 2 in the ipsi parvocellular layer were made after the lateral pulvinar injection. PSTH measured at this LGN site is shown along with the mean normalized PSTH of the simultaneously measured V1 responses. (c) Average ratio of peak-to-baseline response is shown for 8 LGN and 52 V1 neurons before lateral pulvinar inactivation; 14 LGN and 84 V1 neurons after lateral pulvinar inactivation. Error bars show 1 s.e.m.

Second, we monitored the integrity of LGN input to V1 by simultaneously measuring visual responses from LGN and V1 neurons both before and after the lateral pulvinar injection. To ensure that the measured LGN activity was largely responsible for the V1 activity assessed by the array, we selected LGN neurons with receptive fields completely overlapping those of the sampled V1 neurons[33]. One example is shown for measurements made before lateral pulvinar injection (Fig. 2b, top row). Simultaneously measured responses for an ipsilateral magnocellular LGN neuron (site "1" in layer Mi, Fig. 2a) and 7 superficial layer V1 neurons (Fig. 2b, top row) all of whose receptive fields were completely overlapping were both brisk, with peak-to-baseline ratios of 18 and 3.68 ± 0.02, respectively. Another example is shown for measurements made after lateral pulvinar injection (Fig. 2b, bottom row). The LGN response of this ipsilateral parvocellular neuron (site marked "2" in layer Pi, Fig. 2a) was still brisk, with peak-to-baseline ratio of 17 but the simultaneously measured V1 responses were suppressed, with a peak-to-baseline ratio of 0.46 ± 0.18 (Fig. 2b, bottom row).

Several LGN sites were sampled both before and after the lateral pulvinar injection. For each site, responses of a LGN neuron were measured simultaneously with several V1 neurons whose receptive fields overlapped that of the LGN neuron. The peak-to-baseline ratio did not change significantly for LGN neurons after lateral pulvinar injection (Wilcoxon rank-sum test, $P>0.39$; before lateral pulvinar injection: $n=8$, mean ± s.e.m = 15.31 ± 5.25; after lateral pulvinar injection: $n=14$, 15.08 ± 0.02; Fig. 2c). For V1 neurons, the ratio changed significantly after lateral pulvinar injection (Wilcoxon rank-sum test, $P< 10^{-6}$; before lateral pulvinar injection: $n = 52$, mean ± s.e.m = 5.32 ± 0.24; after lateral pulvinar injection: $n = 84$, 0.70 ± 0.04; Fig. 2c). These two controls showed that the integrity of LGN input to V1 was not compromised by the lateral pulvinar injection. The post-injection measurements included in the above analyses started

37 min after lateral pulvinar injection and finished 3 hours later. Throughout this period, LGN was robustly responsive to visual stimulation.

Sham and GABA injections

To verify that the mechanics of making the injection did not compromise V1 measurements (e.g., by displacing the electrode array during the insertion of the injectrode; see Methods), we performed 2 additional controls. First, while measuring the visual responses of V1 neurons with the array, we inserted the injectrode at the Horseley-Clarke co-ordinates for lateral pulvinar (Methods) and made a sham injection of the muscimol+BDA cocktail at a distance of 1.2 mm above the dorsal surface of lateral pulvinar (Fig. 3a; 1 animal). Peak-to-baseline ratios did not change significantly after the injection ($n = 44$, Wilcoxon rank-sum test, $P>0.5$; Fig. 3b). This confirmed that the injection process did not adversely affect V1 measurements.

Second, we injected into lateral pulvinar the fast and short acting native inhibitory transmitter GABA instead of the slow and long acting $GABA_A$ receptor agonist muscimol. Each injection of 0.4 μL of GABA in lateral pulvinar resulted in an immediate and drastic reduction in the visual responses of superficial layer V1 neurons (Fig. 3c). When injection was paused, stimulus-driven activity was immediately and fully restored in these neurons (Fig. 3c). We examined the responses of V1 neurons averaged within three distinct epochs: 1. pre-injection (~200 Sec – 1200 sec, Fig. 3c) 2. peri-injection (~1200 sec – 1600 sec, Fig. 3c) and 3. post-injection (~1600 sec – 2800 sec, Fig. 3c). Average response significantly changed (Wilcoxon rank-sum test, $P<0.007$, $n = 31$) from the pre-injection period (10.2 ± 1.7 spikes/sec) to the peri-injection period (5.4 ± 1.4 spikes/sec), a decrease of 47%. Average response also significantly changed (Wilcoxon rank-sum test, $P<10^{-4}$, $n = 31$) from the peri-injection period to the post-

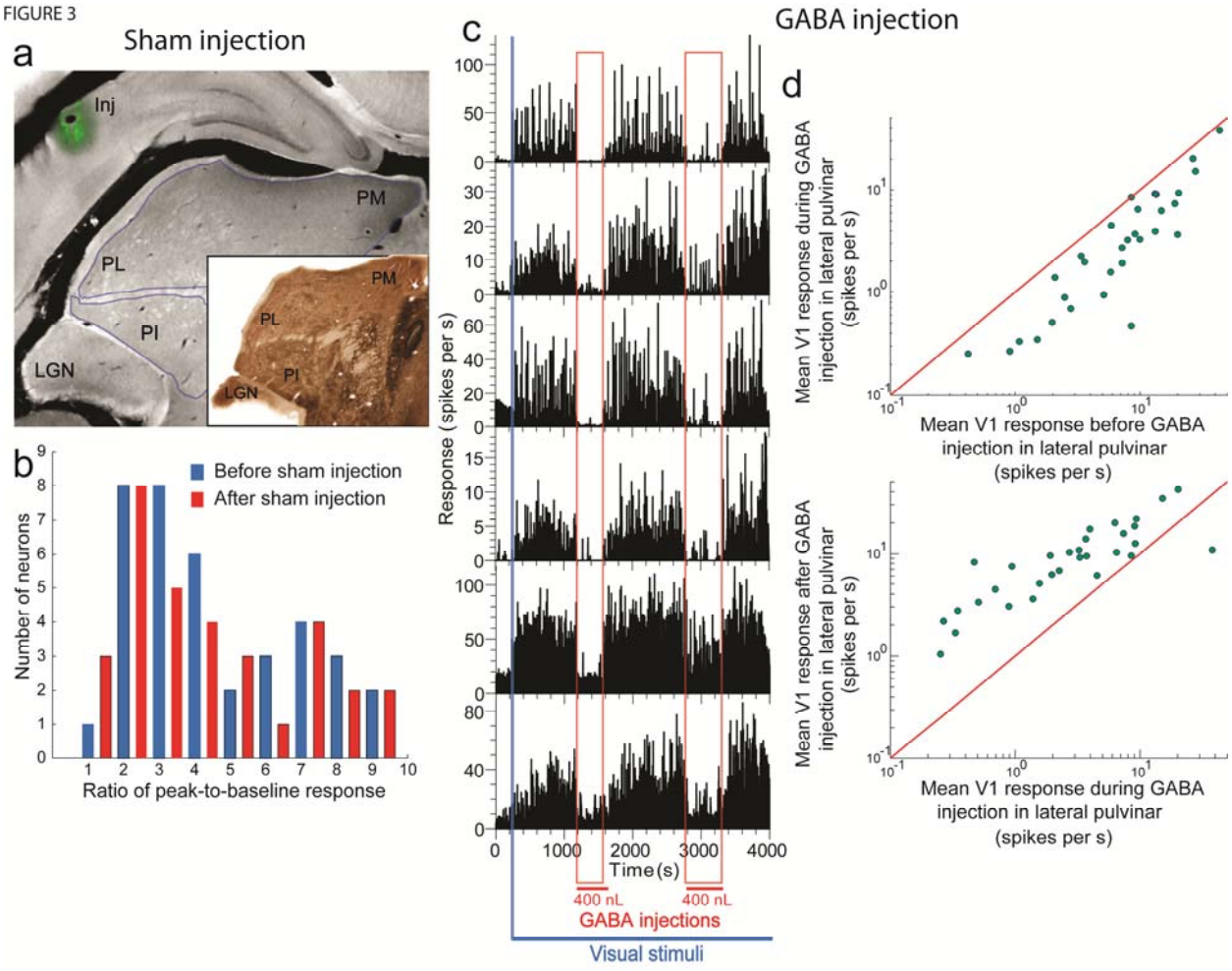

Figure 3.

The process of lateral pulvinar injection does not compromise the integrity of V1 measurements. (a) Coronal section showing sham injection (Inj) above lateral pulvinar. (Inset) Adjacent section stained for AChE. (b) Ratio of peak-to-baseline response for 44 V1 neurons from layers 2-3 before (blue) and after (red) sham injection. (c) Effect of injecting in lateral pulvinar short-acting GABA on visually driven responses for layer 2-3 V1 neurons. The blue bar represents the beginning of presentation of the visual stimuli sequence consisting of a 1-second presentation of a drifting sinusoidal grating and a 1 second inter-stimulus interval. During this continuous visual stimulation of V1 neurons, two 400 nL injections of GABA were made in lateral pulvinar, about 1500 seconds apart. The time period of each injection is shown marked by the vertical red band. (d) Comparisons of mean V1 responses during the pre-injection and peri-injection periods (top) and the mean V1 responses during the peri-injection and post-injection periods (bottom). LGN, lateral geniculate nucleus; PL, lateral pulvinar; PM, medial pulvinar; PI, inferior pulvinar.

injection period (10.9 ± 1.7 spikes/sec), an increase of 101%. This quick and complete recovery once again confirmed that the injection process did not compromise V1 measurements. The almost instantaneous effect that these small volume (400 nL) GABA injections had on V1 responses also fairly effectively ruled out leakage into LGN as the source of suppression of V1 responses. Histology confirmed the injections were within lateral pulvinar and did not leak into LGN (Supplementary Fig. 8). Additionally, this experiment also showed that injecting $GABA_A$ receptor ligands with different molecular structures into lateral pulvinar obtain similar effects on V1 responses. Finally, the results of this experiment are consistent with a previous study that reported reduction in V1 responses after injection of GABA into the Lateral Posterior (pulvinar) complex of the cat[34].

Effect of focal excitation of lateral pulvinar

We also measured visual responses in supra-granular V1 layers while focally exciting lateral pulvinar neurons (2 animals). Drifting sinusoidal gratings were presented inside V1 receptive fields at the lower contrast of 14% (to reduce saturation effects) and at near-optimal orientations. To excite lateral pulvinar, we injected 0.4 μL of the $GABA_A$ receptor antagonist Bicuculline Methiodide (BMI). We compared V1 measurements from a 10 minute interval prior to the injection with measurements from a 13-15 minute interval after the injection (Fig. 4a). V1 receptive fields sampled by the array overlapped those of the injected lateral pulvinar neurons to varying extents. The baseline activity of all V1 neurons whose receptive fields were within 4°-6° of the injected lateral pulvinar receptive fields changed significantly after injection (53 neurons from 2 animals; Wilcoxon rank-sum, $P<0.008$), with an average increase of 72%.

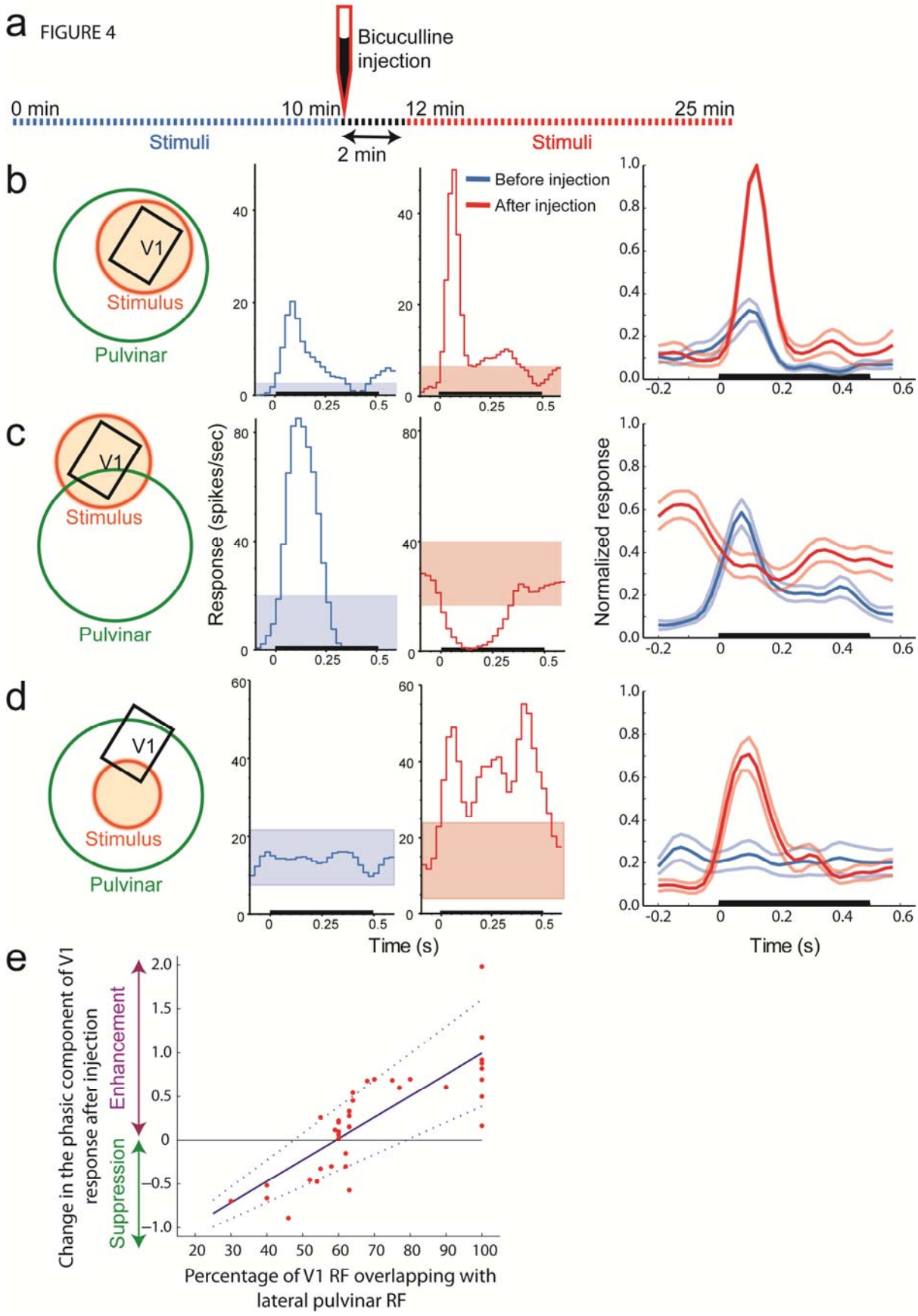
a
FIGURE 4
Bicuculline injection
0 min
10 min
12 min
25 min
Stimuli
2 min
Stimuli
b
V1
Stimulus
Pulvinar
Before injection
After injection
c
V1
Stimulus
Pulvinar
Response (spikes/sec)
Normalized response
d
V1
Stimulus
Pulvinar
Time (s)
Time (s)
e
Change in the phasic component of V1 response after injection
Enhancement
Suppression
Percentage of V1 RF overlapping with lateral pulvinar RF

Figure 4.

Exciting lateral pulvinar neurons responsive to a region boosts responses of V1 neurons to this region and suppresses responses to surrounding region. (a) Timing of response measurements and the injection of BMI. (b) In one subset of V1 neurons studied, V1 receptive fields (black) were enveloped by the injected lateral pulvinar receptive fields (green) and visual stimulation (orange) was centered on the V1 receptive fields. Visual responses of a V1 neuron with receptive field inside the excited lateral pulvinar receptive field are shown before (blue) and after (red) lateral pulvinar excitation. Colored bands represent 95% confidence interval about the baseline response. Last column shows the normalized responses of 14 V1 neurons in this subset, averaged over the pre-injection (thick blue line) and post-injection (thick red line) periods. Lighter lines represent 1 s.e.m. (c) In the second subset of V1 neurons studied, visual stimulation (orange) was centered about their receptive fields (black) that overlapped with the injected lateral pulvinar receptive fields by less than 60%. Brisk visual responses obtained before lateral pulvinar injection (blue) were suppressed after the injection (red). Last column shows the average PSTHs for the pre-injection (blue) and post-injection (red) periods. The average PSTH before lateral pulvinar injection in this case (last column, thick blue line) appears slightly larger than that seen in (b) due to normalization with respect to smaller post-injection responses. (d) In the third subset of V1 neurons, visual stimulation (orange) was centered about the lateral pulvinar receptive field and was marginal for the V1 receptive fields. V1 receptive fields were enveloped by the injected lateral pulvinar receptive fields. V1 neurons that hardly responded to the marginal stimulation of their receptive fields before lateral pulvinar injection (blue) showed a vigorous response after (red) the injection. (e) Change in the ratio of peak-to-baseline response is shown plotted on a logarithmic scale against the percentage of V1 receptive field overlapping with excited lateral pulvinar receptive field. Regression result is shown as the continuous blue line and the dotted lines represent 95% confidence interval for the estimate of the regression slope.

For each V1 neuron, we normalized PSTHs over the entire 25 minute measurement period including the pre- and post-injection intervals (Fig. 4a). Normalized PSTHs were then averaged across neurons for the pre- and post-injection periods separately. In V1 neurons whose receptive fields were fully enveloped by the injected lateral pulvinar receptive fields and were fully stimulated by the visual stimulus (Fig. 4b), the ratio of peak-to-baseline response changed significantly (Wilcoxon rank-sum, $P<10^{-30}$; n=14), increasing by 232% from 2.8 ± 0.40 to 9.3 ± 0.02 (Fig. 4b). V1 neurons whose receptive fields overlapped those of the injected lateral pulvinar neurons by less than ~60% showed a suppression of response as a consequence of the injection (Fig. 4c). The peak-to-baseline ratio changed significantly (Wilcoxon rank-sum, $P<0.007$; n=22; Fig. 4c), decreasing by 83% to 0.47 ± 0.01. In V1 neurons whose receptive fields were fully enveloped by the injected lateral pulvinar fields but were only marginally stimulated by the visual stimulus that was centered on the lateral pulvinar receptive fields (Fig. 4d), the peak-to-baseline response changed significantly (Wilcoxon rank-sum, $P<0.01$; n=17), increasing by 483% from 1.2 ± 0.08 to 7.05 ± 0.60 (Fig. 4d). This latter group of V1 neurons behaved as if their receptive fields had either enlarged or shifted towards the center of the injected lateral pulvinar receptive fields or both (Fig. 4d). For fully stimulated V1 receptive fields (i.e., Figs. 4b and 4c), a regression analysis showed the effect of the receptive field overlap on the peak-to-baseline ratio to be significant (R^2=0.64; F=66.5; P=0; *variance*=0.13). In order to classify V1 receptive fields unambiguously into these three qualitative categories (Figs. 4b, c, d), only V1 neurons whose receptive fields were less than half the size of the injected lateral pulvinar receptive field were selected for these post-hoc analyses.

Histology showed the BMI injections were localized within lateral pulvinar and did not diffuse into LGN (Supplementary Fig. 9). All three types of significant changes observed in V1

responses (i.e., Figs. 4b, c, d) occurred within minutes (~2 min) of small volume (400 nL) BMI injections in lateral pulvinar. This quick onset was consistent with the observed changes in V1 being due to the action of injected material on proximal lateral pulvinar neurons rather than due to leakage into distant LGN neurons. To further verify that leakage of the excitatory agent into LGN was not involved in kindling V1 neurons, we performed a control in which we injected the LGN first and lateral pulvinar next with ibotenic acid, a glutamate agonist, and observed the effect on neurons in the supra-granular layers of V1 (Fig. 5a). Baseline activity was continuously measured with an electrode array in layers 2-3 of V1. We injected a large 1.8 μL volume of ibotenic acid into all layers of LGN covering the region of visual space spanned by the receptive fields of V1 neurons sampled by the array. LGN excitation by ibotenic acid first produced a burst of 8-fold increase in V1 activity (Figs. 5b; Wilcoxon rank-sum, P=0, n=39). The excitotoxic apoptosis of LGN neurons that followed caused a significant change in V1 baseline activity (Wilcoxon rank-sum, $P<10^{-30}$, n=39), with an average decrease of 85%. After allowing 30-60 minutes for the apoptotic lesion of LGN to complete, we injected 1.0μL of ibotenic acid into lateral pulvinar (Fig. 5a). Despite the significantly lower baseline activity, V1 neurons again showed a burst of 14-fold increase in activity following this lateral pulvinar injection (Figs. 5b; Wilcoxon rank-sum, P=0, n=39). Fluoro-Jade C® staining of degenerating neurons confirmed the location and extent of excitotoxic lesions in LGN and lateral pulvinar (Fig. 5a; Methods). The results of this control experiment fairly effectively ruled out LGN's involvement in the excitatory kindling of V1 neurons and are consistent with the report that electrical stimulation of pulvinar elicits positive BOLD response in V1 of the macaque[35].

FIGURE 5

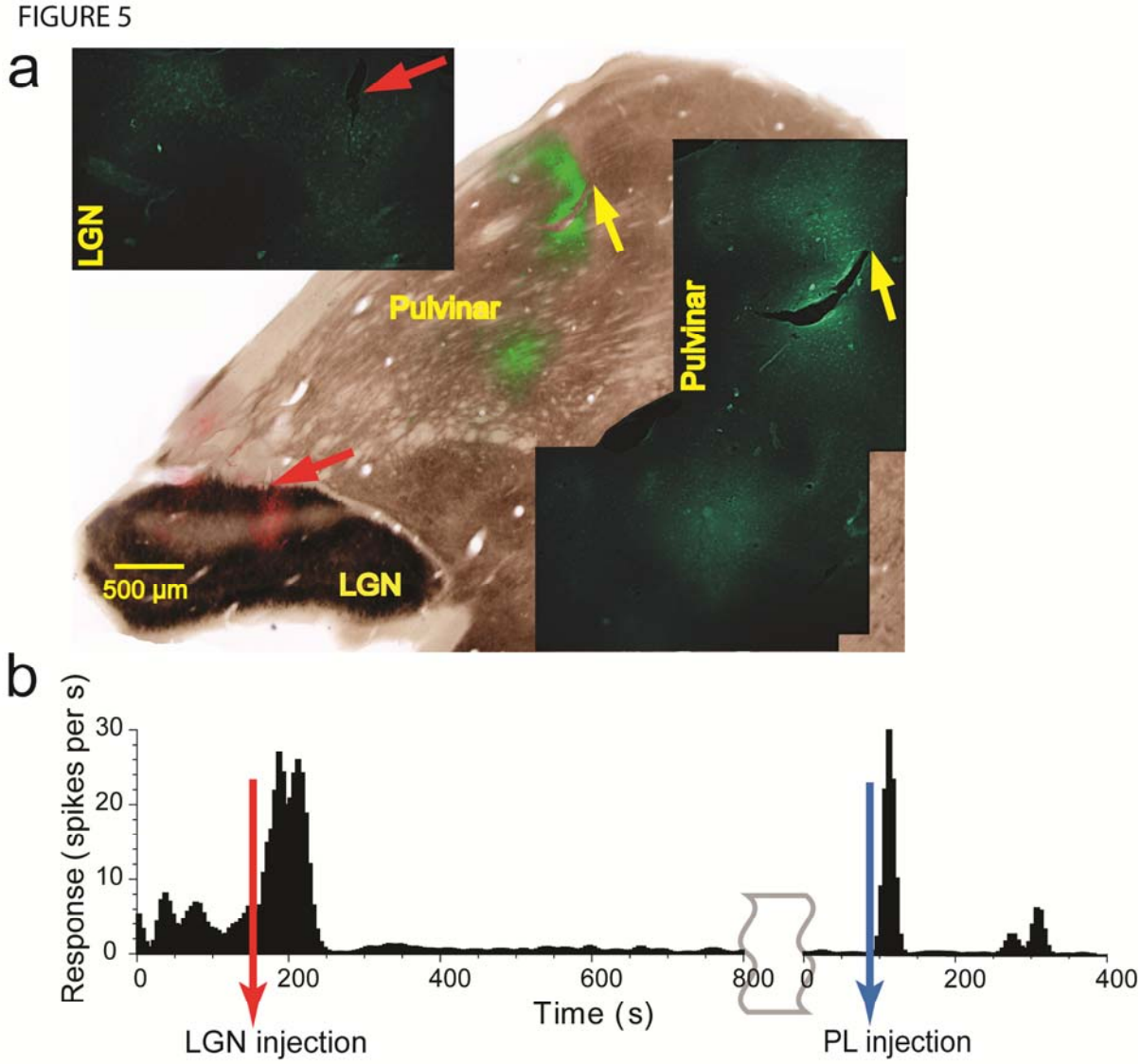

Figure 5.
Kindling of V1activity by lateral pulvinar excitation after LGN lesion. (a) Composite image showing the injections, created using the method mentioned above (Fig. 1g). Coronal section stained for AChE showing ibotenic acid injections in false colors, green in lateral pulvinar and red in LGN. Insets show regions of injections stained with Fluoro-Jade C® in higher magnification. Individual degenerating cells are seen labeled. (b) Changes in the baseline response of a supra-granular V1 neuron due to the injection of ibotenic acid in LGN and lateral pulvinar. The lateral pulvinar injection was made 30 mins after the end of the timeline shown for the LGN injection.

Discussion

Our data show that removal of lateral pulvinar input can almost extinguish visual responses in the primary visual cortex and prevent the associated visual information from propagating beyond V1. The data also show that lateral pulvinar neurons can strongly boost V1 visual responses in the region of their receptive fields while suppressing responses to the surrounding region. These results suggest that the higher-order thalamic nucleus pulvinar plays a critical and integral part in the functioning of the visual cortex[36].

The spatial proximity of lateral pulvinar to LGN in the thalamus posed considerable technical challenges in our study. Taken together, the extensive histological analyses of the injections (Fig. 1g, Fig. 2a, Supplementary Figs. 3, 4, 8 and 9), the temporal dynamics of changes in V1 responses following the injection of muscimol in lateral pulvinar (Supplementary Figs. 5 and 6), the spatial gradient of changes in visual responses across the central 6° of V1 following the injection of muscimol in lateral pulvinar (Supplementary Fig. 7), the use of fluorescent muscimol to directly determine the spatial extent of inactivation from fluorescence (Supplementary Fig. 2a), direct simultaneous measurement of LGN and V1 responses following lateral pulvinar injections (Figs. 2b and 2c), the almost instantaneous effects that small volume (400 nL) injections of GABA and BMI had on V1 responses, and the excitatory kindling of V1 from lateral pulvinar after LGN lesion all implicate the manipulation of neural activity in lateral pulvinar as the cause of the observed effects in V1. However, as mentioned in Introduction, these experiments measured the *net* effect of manipulating lateral pulvinar activity on V1 and do not allow us to distinguish between the direct effect that lateral pulvinar exerts on V1 and the indirect effect exerted via pathways through higher visual cortex[4,36,37]. Nevertheless, our data

reveal a surprisingly powerful scheme of control that the pulvinar can exercise over information processed and propagated within the visual cortex. Overall, our results illustrate a wide range of modulatory functions of a higher-order thalamic nucleus in cortical information processing[36]. Below, we briefly discuss possible relationships of these functions to circuits on the one hand and behavior on the other.

A role for lateral pulvinar in sustaining visual responses

How can lateral pulvinar effectively suppress geniculo-fugal visual input to V1? Quantitative accounting of our results requires more information, particularly about pulvinar afferents in V1 and the nature of lateral pulvinar's influence on V1 via the indirect pathway through extrastriate areas. However, some qualitative explanations can be suggested for how the direct pulvino-V1 circuit might be responsible for the observed effects. Several experimental and computational investigations indicate that a balanced combination of inhibitory and excitatory inputs underlies cortical neural responses[38-43]. Within this framework, our results could be accounted for if pulvinar provides potent excitatory synapses to V1. Many neurons in supra-granular layers that receive a disynaptic signal from the LGN will also receive a slightly delayed, quadrisynaptic geniculo-fugal signal via these lateral pulvinar synapses (Supplementary Fig. 10). Layer 5 cells in V1 that project to lateral pulvinar also receive input from supra-granular layers via their apical dendrites[44]. The resulting circuit may be lumped and depicted as consisting of a "loop" for computational purposes (Supplementary Fig. 10) though the system is clearly far more complex[36,45]. Under normal conditions, this pulvino-V1 "loop" might be necessary to drive and sustain the stimulus-evoked response. When lateral pulvinar is inactivated, the loss of the few but potent excitatory inputs from lateral pulvinar could result in a net inhibition that prevents visual

responses from fully emerging. Stronger inhibition at the preferred orientation of the neuron as postulated in some V1 models[42,43] would yield greater suppression of the visual response for the preferred orientation after lateral pulvinar inactivation.

A second possibility is that a gating signal from lateral pulvinar acts multiplicatively on the geniculo-fugal feed-forward excitatory signal. Setting this lateral pulvinar gating signal low would suppress the geniculo-fugal excitatory input. These two possibilities are not mutually exclusive as lateral pulvinar could gate feedforward excitatory inputs in a circuit with balanced net excitation and inhibition to the same effect. Thus, including lateral pulvinar inputs in current models of V1 circuitry and function might account for some of our results.

Pulvinar and control of bottom-up salience for attention

Lesion or chemical inactivation of pulvinar often results in deficits of visual attention[12-20,23,24]. Electrophysiological and imaging assays of pulvinar neural activity have also shown links to visual attention[6,20,23-26]. Furthermore, pulvinar has reciprocal connections with both prefrontal and visual cortices[5]. These facts suggest a role for pulvinar in mediating visual attention which requires coordinated control of top-down and bottom-up signal flows[46]. Specifically, pulvinar sub-nuclei interconnected with early visual areas could control stimulus-driven or bottom-up salience of visual responses in conjunction with goal-driven or top-down signals received via the sub-nuclei interconnected with pre-frontal and parietal areas[15,47,48].

A network model of visual attention has postulated that pulvinar controls and routes information within the window of attention up the visual cortical hierarchy by gating feedforward synapses[48]. Our data show that lateral pulvinar can control and gate V1 neural activity in a manner consistent with its hypothesized role in controlling bottom-up salience for

selective attention. When the spatiotemporal context of a visual stimulus autonomously enhances its salience in conflict with behavioural or top-down goals, lateral pulvinar can suppress neural responses to this stimulus in early visual cortex (Fig 1), thus biasing the competition in favour of behaviourally-relevant stimuli[46]. When the window of attention is on a particular set of visual inputs, lateral pulvinar can boost neural responses to these inputs while simultaneously suppressing responses to surrounding inputs (Fig 4), thus gating and routing attended signals up the cortical hierarchy[48]. This analogy between our results and models of visual attention has an important caveat. The large changes in activity observed in our experiments as a consequence of direct pharmacological manipulation of lateral pulvinar need not necessarily be commensurate with the magnitude of neural effects measured in behavioural experiments in which changes in activity are governed not only by engaging or disengaging attention but also by other variables like attentional load, the spatiotemporal window of attention, and fixational eye movements.

Behavioral consequences of pulvinar inactivation

Our data show strong suppression of V1 visual responses following the reversible inactivation of a retinotopic region of lateral pulvinar. There are important caveats in inferring the behavioral consequences of this result. Reversible inactivation or lesion of pulvinar in awake behaving animals and humans may or may not reveal a scotoma depending on many factors including whether the affected region is restricted to parts of pulvinar that connect with early visual cortex or if it covers other sub-nuclei as well (e.g., in the macaque ventro-lateral and centro-lateral but not dorsomedial part of the lateral pulvinar connect to areas V1 and V2[5]), whether the subject is fixating or free-viewing, whether viewing is binocular or monocular (if pulvinar inactivation/lesion is unilateral), the retinotopic size of the affected area relative to the

range of allowed fixational eye movements, and whether measurements are made after possible reorganization[16-18]. Another critical issue in the emergence of a scotoma is the size of the affected region and the nature of the background against which it is assessed[49]. Lesions to sub-nuclei connected to higher cortical areas (e.g., the dorsomedial part of lateral pulvinar[5]) are likely to have different types of behavioral consequences reflecting the functional properties of their projection zones[20,12-16]. Therefore, while it is hard to predict what the behavioral consequences of our results might be, our data clearly show that higher-order thalamic nuclei such as the pulvinar have a much more significant and key role to play in the cortical processing of sensory information than previously thought.

Acknowledgments

We thank Julia Mavity-Hudson for the histology, Steven Walston, Yaoguang Jiang, Dmitry Yampolsky, Julia Mavity-Hudson, Jay Patel, and David Rinker for help with experiments, Dmitry Yampolsky for technical and computational assistance, and Mary Feurtado for veterinary assistance. We thank Drs. Ford Ebner, Jon Kaas, Romesh Khumbani, Jeff Schall, Pascal Wallisch, and King-Wai Yao for their suggestions and comments on the work. Supported by NIH grants R01-EY01778, P30-EY008126, T32-EY07135, and P30-HD15052.

Methods

Ten adult prosimian primates (*Otolemur garnettii*) of both sexes weighing 0.9-1.3 kgs were used in these experiments according to approved protocols from the IACUC at Vanderbilt University.

Anesthesia was induced by an intraperitoneal injection of 30% Urethane solution (1.25 gms/kg) and maintained with 20% of induction dose every 2 hours. Neuromuscular blockade was achieved with Vencuronium bromide (0.5-1.0mg/kg/hr). Animals respired room air via a ventilator, supplemented with O_2 as necessary, to maintain expired CO_2 at 4%. Pupils were dilated with 2% cyclopentolate drops and contact lenses with sufficient power and 3-mm pupils were fitted to keep the monitor in clear focus on the retina.

Electrophysiology

V1 measurements were made using an electrode array. The dura was reflected and a Cyberkinetics 100 electrode array (Blackrock microsystems, Salt Lake City, UT) was pneumatically inserted over V1 and secured with 1% agarose in saline. Spikes were collected using a Bionics multichannel neural data acquisition system (Salt Lake City, UT) and sorted offline using Bayesian clustering methods (Plexon Inc). LGN and pulvinar measurements were made with single electrodes using a 16-channel Plexon Multichannel Acquisition Processor (Dallas, TX). Simultaneous measurements in V1 and LGN were made using differential mode recordings on both multichannel systems with common reference. We included in the analyses every neuron whose stimulus-driven PSTH (before lateral pulvinar injection) deviated outside the 95% confidence interval about the mean baseline response (for the analyses following the BMI injections, an additional selection criterion based on receptive field size was used as mentioned in that Results sub-section).

Receptive field mapping

In order to accurately map receptive fields, we used a modified version of Bishop's plotting table method (Bishop P.O, Henry, G.H, & Smith, C.J. *J. Physiol*., **216**, 39-68, 1971). Optic disks and retinal

blood vessels were back reflected with a fiber-optic light source and plotted on a tangent screen 57 cm in front of the eyes. *Area centralis* (AC) was marked relative to the optical disk for each eye. Throughout the experiment, the positions of retinal landmarks were periodically checked for residual drifts of the paralyzed eyes. Stimuli such as moving lines, flashing lines, and flashing spots were created using a projector with analog controls and back projected onto the tangent screen. V1 receptive fields were then accurately hand mapped using these stimuli and plotted on the tangent screen along with retinal landmarks and the AC. Using a 45° mirror, the receptive fields, AC, and retinal landmarks were then precisely transferred to a CRT monitor on which experimental stimuli were presented.

Visual Stimuli

Visual stimuli were generated using a VSG 2/5 system (Cambridge Research, U.K.) and presented on a 22 inch Sony CRT display at 120 HZ refresh rate. Sinusoidal gratings at the behaviorally optimal spatial (0.5 cycles/degree) and temporal frequency (2 Hz) were presented at orientations varying from 0° to 170° in steps of 10°. Each orientation, randomly selected, was presented for 1 second followed by a 1 second inter-stimulus interval during which the monitor was at the mean luminance of 12 cd/m^2. Gratings covered V1 receptive fields of interest, were presented at 50% contrast in lateral pulvinar inactivation experiments, and at 14% contrast in experiments in which lateral pulvinar was excited. Simultaneous V1 and LGN measurements were made by finding an LGN neuron whose receptive field was completely inside V1 receptive fields of interest. A circular patch of light at high contrast (>90%) was flashed inside the LGN receptive field for 0.5-1 second followed by an equal duration inter-stimulus interval during which the monitor was at the mean luminance of 12 cd/m^2.

Injections

The central representation of LGN was first found using a single electrode, often by aiming for the posterior pole of the LGN at the Horsley-Clarke coordinates of AP +3 and ML +7. Central representation in lateral pulvinar was then found by moving 1.5 mm more medial (see Atlas of bush baby thalamus/pulvinar: http://www.psy.vanderbilt.edu/faculty/Casagrande/CasagrandeLab/BUSHBABYATLAS2.pdf). Receptive fields of lateral pulvinar neurons at this site were then accurately plotted. The electrode was replaced with a custom injectrode back-filled with the required cocktail. Previously mapped receptive fields were found again with the injectrode. The injectrode was then lowered by about 100 μm so that the tip of the pipette and not just the tip of the electrode reached the target. The injectrode was then pulled back by 100 μm and the cocktail was slowly infused. Pulling back the injectrode in this manner helps create a "pocket" within which the injected material stays confined, as indicated by dozens of cases of histology performed in our lab. Muscimol injections contained a 66.7mM solution of Muscimol (114MW; Sigma Aldrich) in a 1.6% solution of BDA (10000MW; Invitrogen). GABA injections contained a 25mM solution of GABA (103MW; Sigma Aldrich) in a 1.6% solution of BDA. Bicuculline injections contained a 5mM solution of BMI (509MW; Sigma Aldrich) in a 1.6% solution of BDA. Fluorophore conjugated muscimol injections contained 1 mg of muscimol, BODIPY® TMR-X conjugate (Invitrogen) dissolved in 1 ml of 0.9% saline. Ibotenic acid injections contained a 5mg/ml solution of ibotenic acid (158MW; Sigma Aldrich).

Histology

Sodium pentobarbital (Nembutal, 50-75 mg/kg) was used for euthanasia. Animals were perfused through the heart with a saline rinse containing 0.05% sodium nitrite, followed by a fixative (2% paraformaldehyde in 0.1M phosphate buffer or 3% Paraformaldehyde, 0.1% Gluteraldehyde and 0.2% saturated picric acid) and a 10% sucrose solution. The brain was blocked coronally with a blade mounted at a known coordinate in a stereotax. The occipital cortex was removed and flattened between slides in 0.1M phosphate buffer with 30% sucrose. Flattened pieces were frozen and tangentially sectioned. The surface vasculature was preserved in the first 100µm-150µm section. The remaining tissue was sectioned at 52µm. The thalamus was cut coronally. All sections were placed in 20% glycerol in 0.1M Tris buffered saline (TBS) and frozen at -70° C until staining. Cytochrome oxidase (CO) staining was used to confirm that the array was in the primary visual cortex (Supplementary Fig. 2). CO staining was performed by incubating sections in 0.2% DAB (D5636, Sigma), 0.3% Cytochrome C (250600, Calbiochem), 0.15% Catalase (C40, Sigma), 2% Sucrose, 0.03% $CoCl_2$ and 0.03% $NiNH_4SO_3$ in 0.05M Phosphate Buffer at 40° C for 1-4 hours until well differentiated. Tangential slices of the primary visual cortex stained for CO were successively examined to confirm that the electrode tips were within layers 2-3 (Supplementary Fig. 2). *AChE* The standard method of Karnovsky and Roots[50] was used. Sections were preincubated in 0.1 M Acetate buffer (pH 6.6), 0.1M Sodium Citrate, 20mM $CuSO_{4,}$,10^{-3} M IsoOMPA, and 5mM $K_3Fe(CN)_6$ for 45 minutes. Sections were then incubated in a fresh solution as above with the addition of 0.1% ATHCH iodide overnight, rinsed in 0.1M Phosphate buffer, mounted on gelatinized slides, defatted, and cover-slipped with DPX. *BDA* To visualize BDA injected in the cocktails, sections were rinsed 3 times in TBS, placed into 1:400 Alexafluor-488 conjugated Streptavidin (Invitrogen) in a buffer consisting of 0.1%

Sodium azide, 0.2% Triton X 100 and 0.5% cold water fish gelatin for 2 hours, rinsed once in the same buffer, then twice in TBS. Sections were mounted and cover-slipped with Vectashield (Vector). *Fluoro-Jade® C* Sections were rinsed 3 times in TBS, mounted on subbed slides from distilled water (DH_2O), and placed on a 50° C slide warmer for a minimum of 30 minutes. They were then placed into 80% ethanol-1% Sodium hydroxide for 5 minutes, rinsed for 2 minutes in 70% ethanol, 2 minutes in DH_2O and then placed into 0.06% potassium permanganate in DH_2O for 10 minutes. They were rinsed in DH_2O for 2 minutes and transferred into a solution of 0.0001% Fluoro-Jade® C (Millipore) and 0.1% acetic acid in DH_2O. Slides were rinsed 3 times in DH_2O, dried on the slide warmer for a minimum of 5 minutes, cleared in Citrisolve (Fisher) for 5 minutes and cover-slipped.

Data Analysis

PSTHs were computed by aligning responses to stimulus onset, binning spikes in 50 ms intervals, and smoothing the binned averaged spike rate with a 150 ms wide sliding Gaussian window. The ratio of peak-to-baseline response was estimated as the ratio of the post-stimulus peak of the PSTH to the pre-stimulus PSTH values averaged over the 500 ms prior to stimulus onset. Suppression index at an orientation was estimated as the ratio of the peak-to-baseline value before injection to its value after injection.

Supplementary Figures

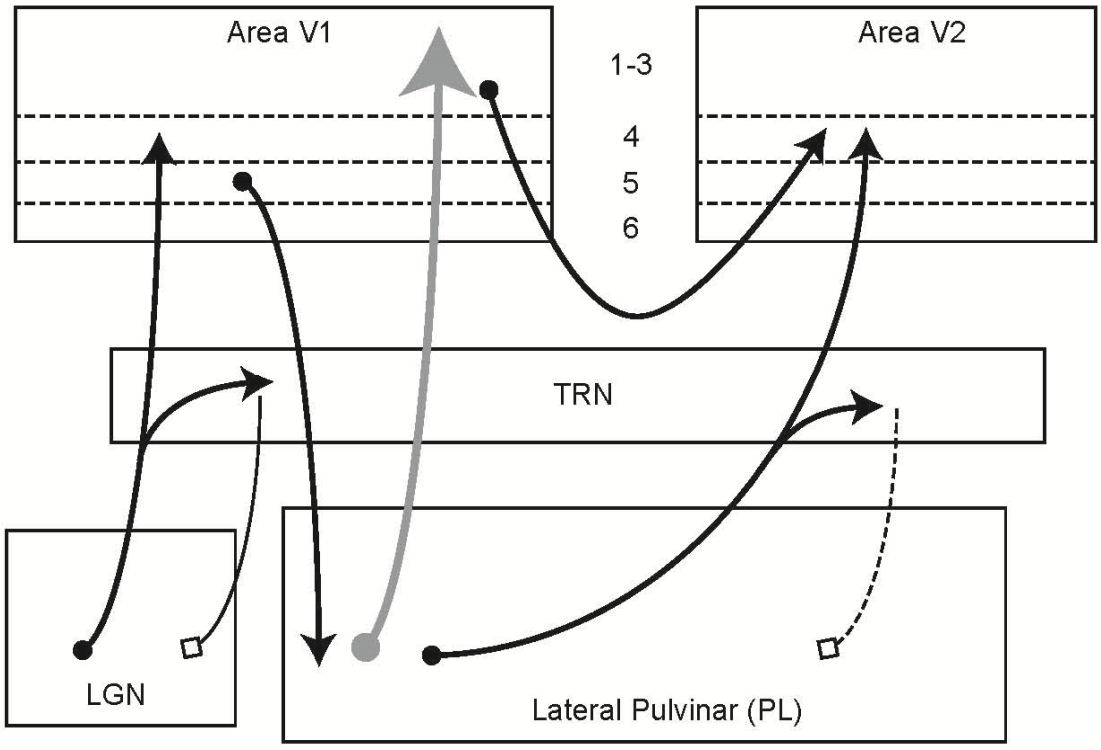

Supplementary Figure 1.
Thalamo-cortical connections relevant to the experiments Parvo- and magnocellular layers of LGN provide the driving input to layer 4 of V1. Collaterals of these projections terminate in the TRN, which projects back to the LGN in a spatio-topic manner. Layer 5 of V1 sends driving input to lateral pulvinar, which projects back to layers 1-3 of V1 in primates. In distantly related mammals like cats, the presumed homologue of this projection is confined to layer 1. Lateral pulvinar also projects to layer 4 of V2 as does area V1 from its output layers 2-3. Projections from lateral pulvinar to layer 4 of extrastriate areas send collaterals to the TRN which projects back to lateral pulvinar in a spatio-topic manner. Projections from TRN back to LGN and lateral pulvinar originate from separate regions of TRN.

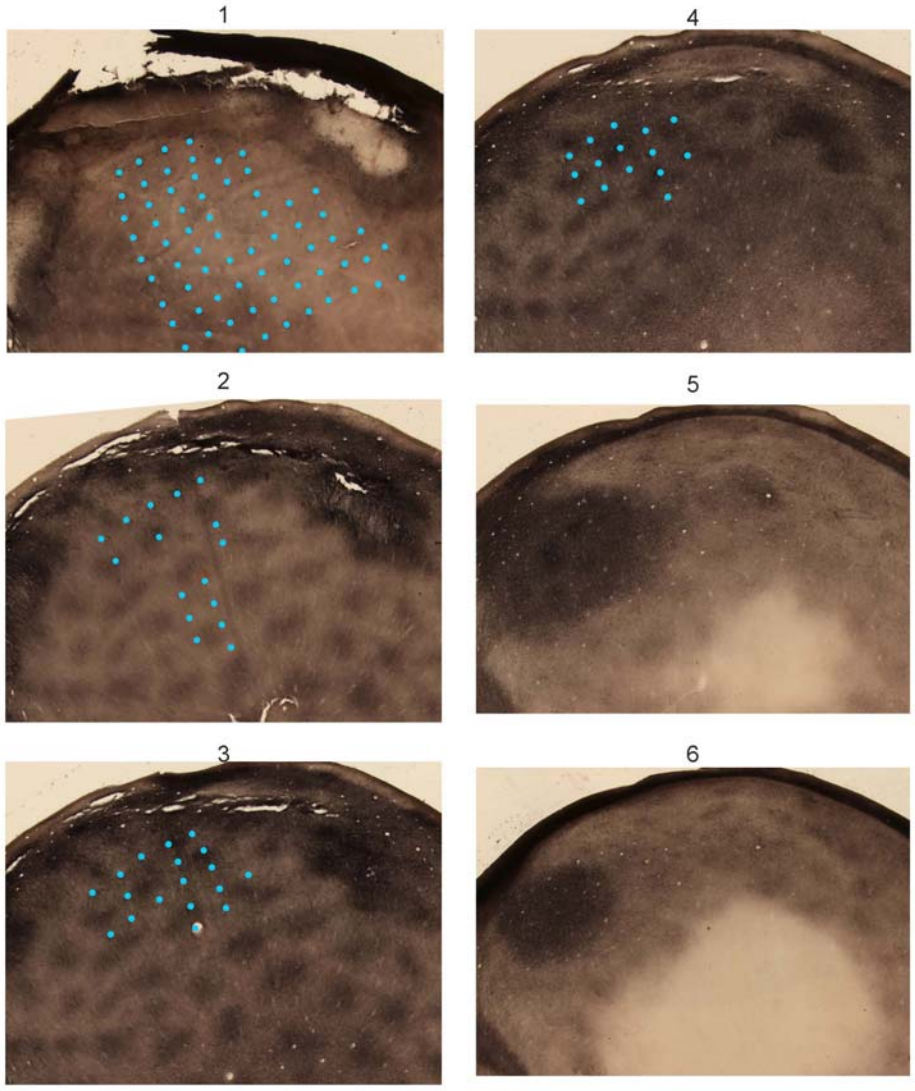

Supplementary Figure 2.
Placement of the multi-electrode array in layers 1-3 of V1Tangential sections of flattened, CO-stained V1 are shown with sections 1 through 6 representing the most dorsal, superficial layers to the most ventral, infragranular layers successively. Note that the CO blobs (dark patches) are centered in layer 3 and are not evident in layer 4 where CO stains uniformly. Blue dots are reconstructed electrode locations. Vasculature can be seen in Section 1 and CO blobs can be seen in sections 2 through 4. Thus, layer 4 starts between section 5 and 6. The electrode tips disappear with the CO blobs, showing that the tips were confined to layers 1-3.

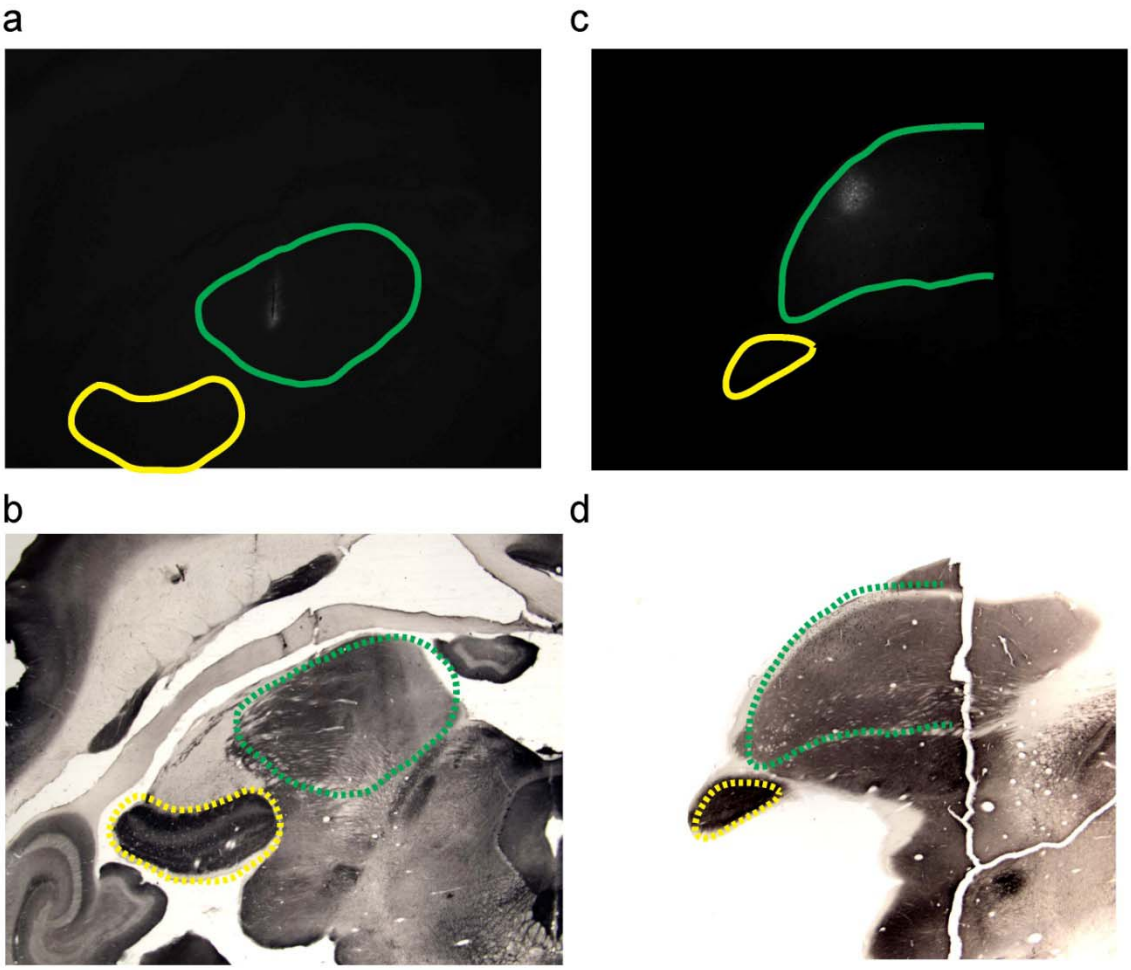

Supplementary Figure 3.
The injection was confined to lateral pulvinar and was widely separated from the LGN and the TRN. (a) Micrograph showing fluorescence from the muscimol+BDA injection. Lateral pulvinar is outlined in green and LGN in yellow. The outlines were created using a bright field image of the same sections. (b) Bright field LM image of the adjacent section stained for CO. The outlines shown in (a) are shown at the same spatial locations as dotted lines, in the same color. The two slices were aligned using several fiducial marks including blood vessels and artificial probes placed during tissue sectioning. Comparing (a) and (b), it is clear that fluorescence is confined to lateral pulvinar. (c) and (d) Similar images from the third and last case in which muscimol+BDA was injected.

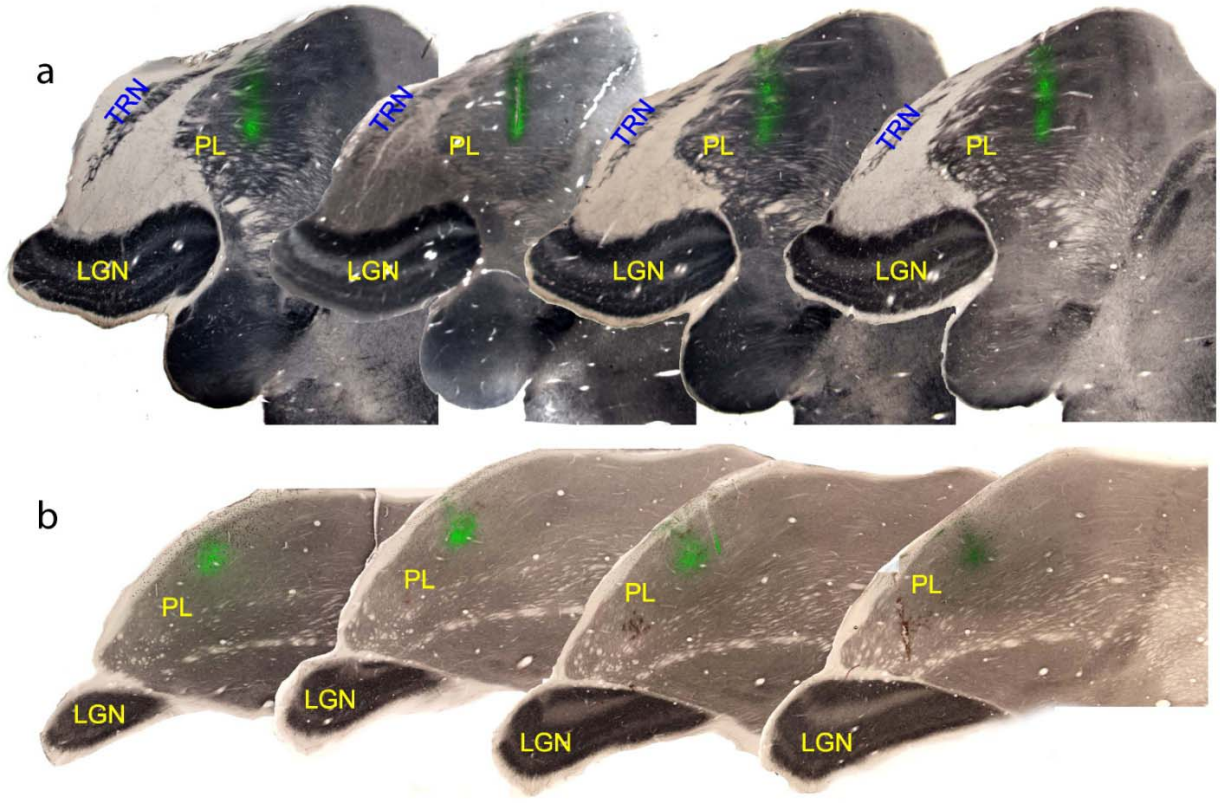

Supplementary Figure 4.

The injection was confined to lateral pulvinar and was widely separated from the LGN and the TRN. Part of the reconstruction of thalamus is shown for two cases. From left to right the sections represent anterior to posterior. Composite images were created as described above (see legend for Fig. 1g). Bright field images are of CO stained sections. Green fluorescence is from the muscimol+BDA injection. It is confined to the region of lateral pulvinar that contains the central visuotopic map. (a) It is clear that the injection was quite far from the LGN and the TRN. (b) TRN was not yet visible even in the most posterior section of this case.

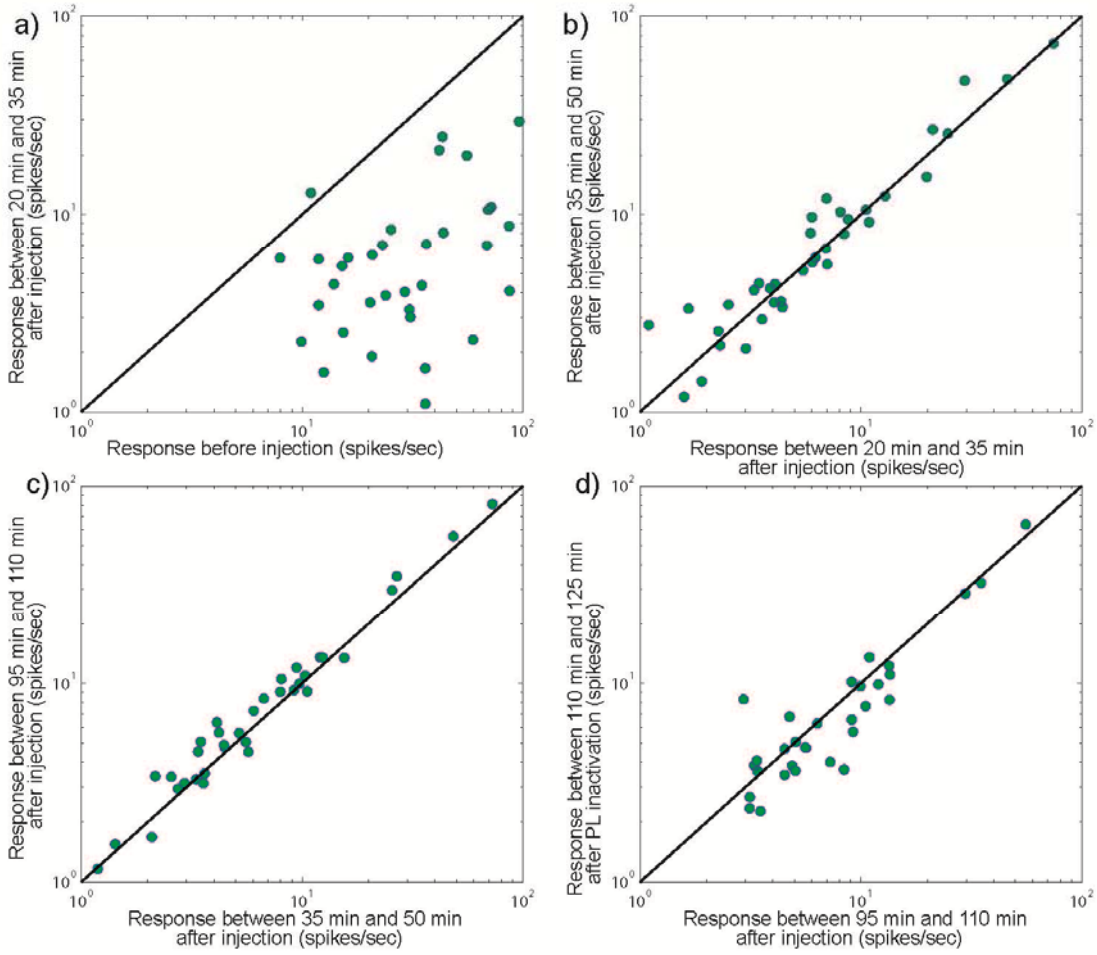

Supplementary Figure 5.

Temporal dynamics of changes in V1 responses following muscimol injection in lateral pulvinar. (a) Comparison of V1 responses before and after lateral pulvinar injection. V1 responses were averaged over the 15 minute interval prior to the injection and from 20 min to 35 min post-injection. (b), (c), and (d) Comparisons of average V1 responses in 15 minute intervals through the 125 minutes following the injection showed that almost all the change in V1 responses occurred within 35 minutes of the injection.

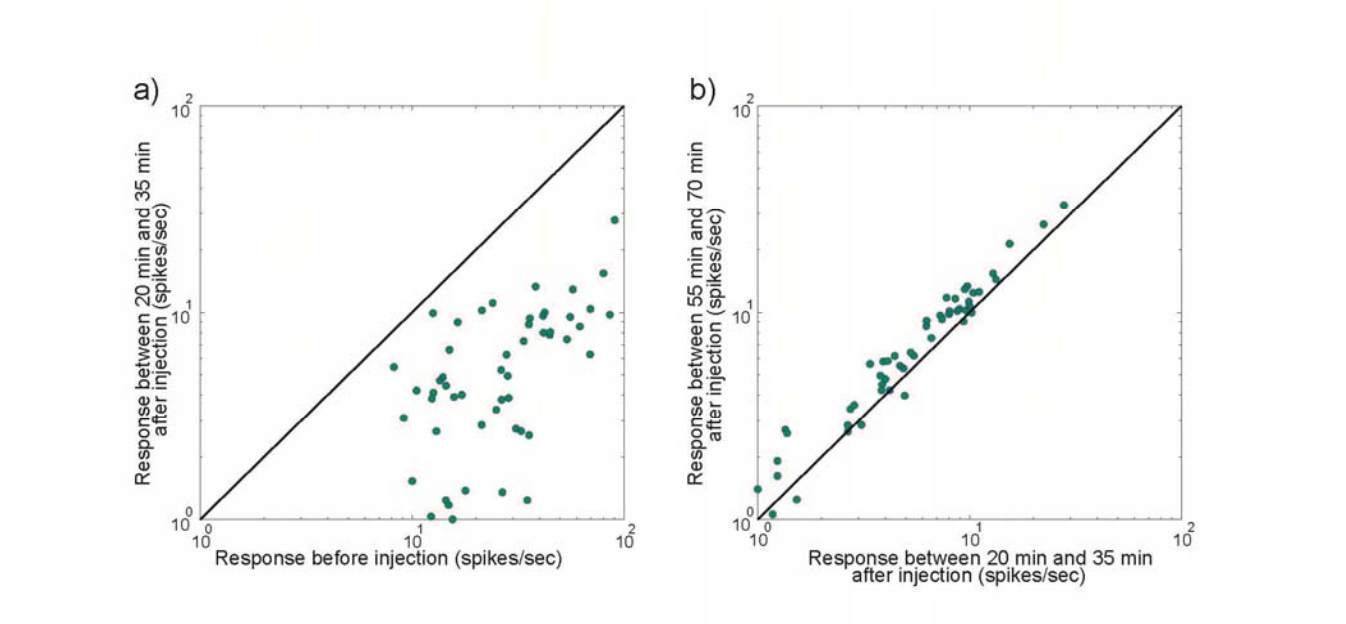

Supplementary Figure 6.
Temporal dynamics of changes in V1 responses following muscimol injection in lateral pulvinar. Same as Supplementary Figure 5, for another case of muscimol injection.

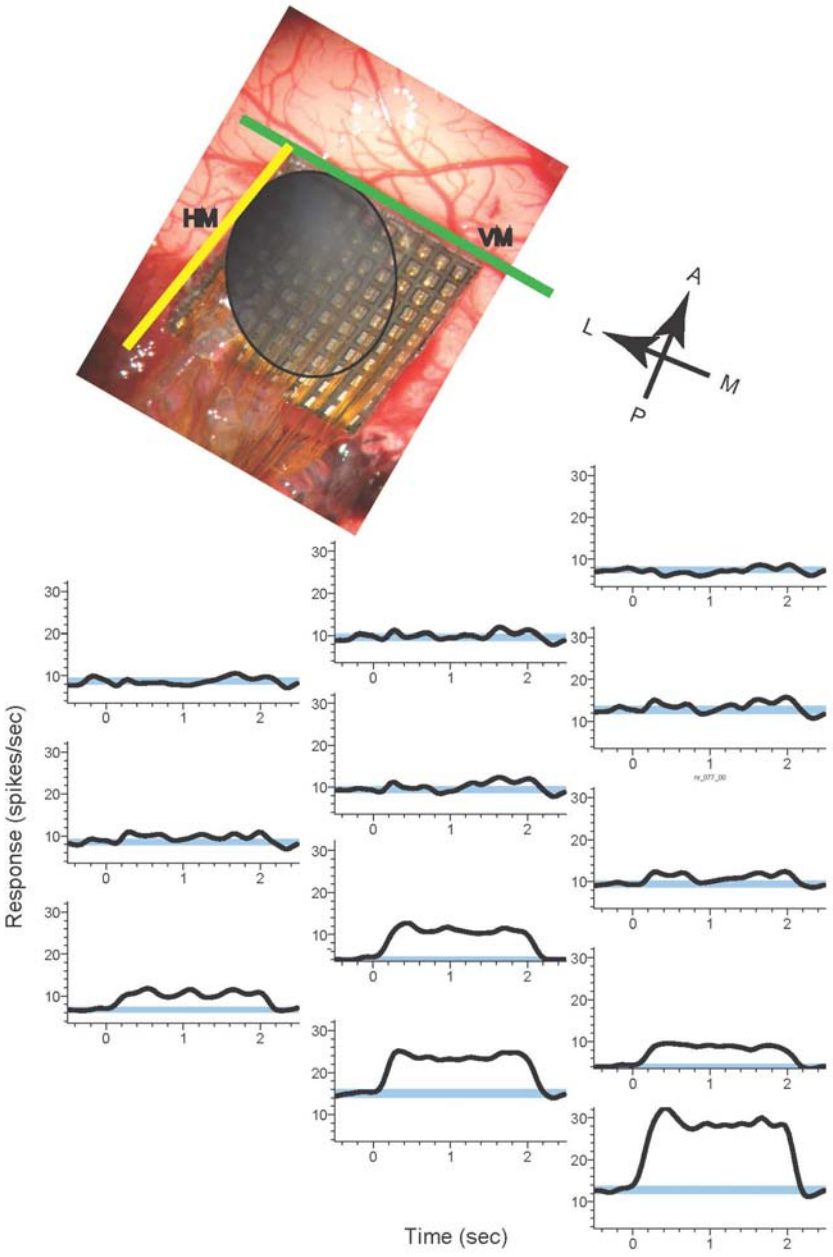

Supplementary Figure 7.

Spatial extent of influence in V1 of a focal muscimol injection in lateral pulvinar. The array placement on V1 is shown at the top. CO staining confirmed the array to be entirely inside V1 and the top row of electrodes to be roughly parallel to the V1-V2 border, marked by the vertical meridian (VM) in green. The spatiotopic region and extent in V1 of the corresponding region of injection in lateral pulvinar is shown schematically by the black oval. Receptive fields of V1 neurons near the darkest part of the oval entirely overlapped with the lateral pulvinar receptive field at which the injection was made. Electrodes further away from this corner of the array sampled V1 receptive fields that were further away from the injected lateral pulvinar receptive field. Simultaneously measured PSTHs for V1 neurons sampled by electrodes near the bottom edge of array are shown below. In all 3 animals studied, input-driven V1 responses increased gradually as the distance of their receptive fields increased from the lateral pulvinar receptive field at which the injection was made. No rebound was observed in the region of V1 sampled by the array.

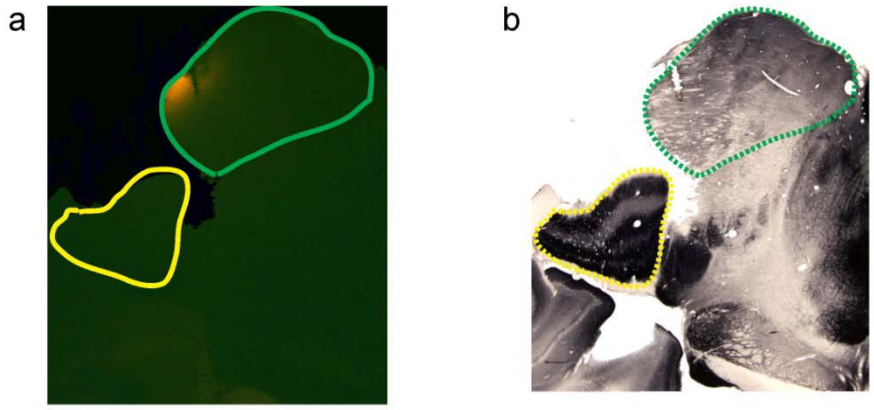

Supplementary Figure 8.
The injection was confined to lateral pulvinar and was widely separated from the LGN and the TRN. Same as Supplementary Figure 3; sections shown are for the GABA injection case

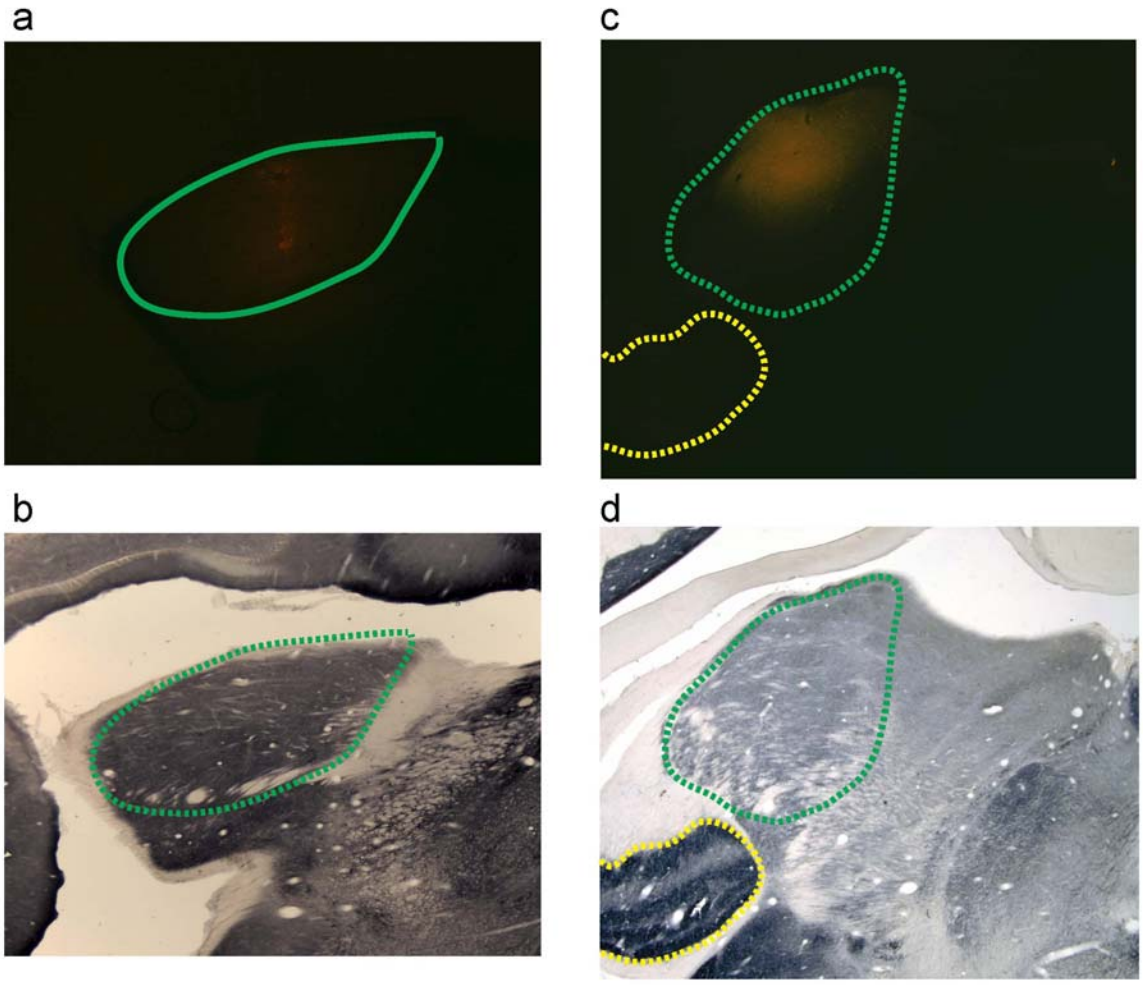

Supplementary Figure 9.
The injection was confined to lateral pulvinar and was widely separated from the LGN and the TRN. Same as Supplementary Fig. 3; sections shown are for the two BMI injection cases

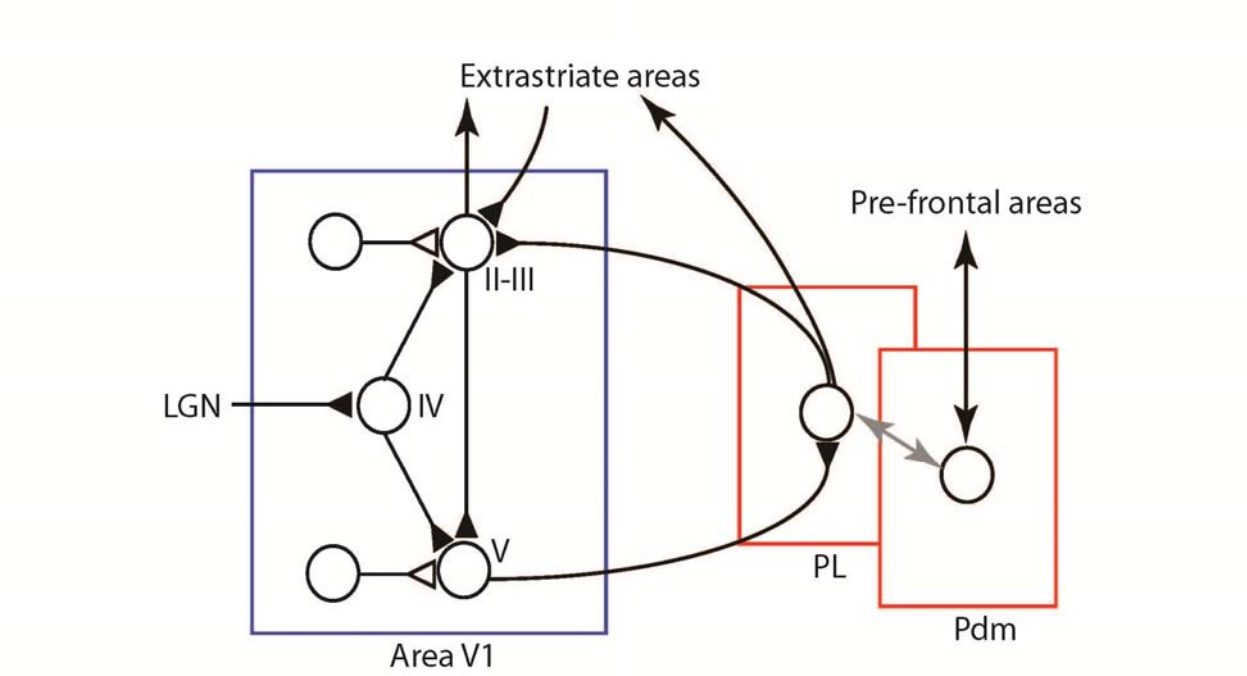

Supplementary Figure 10.
A putative role for pulvino-V1 circuit in controlling visual responses and bottom-up salience. A simplified, lumped representation of major, known V1-pulvino-V1 and intra-V1 connections in the primate are shown. Open synapses represent lumped inhibition and closed synapses, excitation. Net excitation and inhibition might be roughly balanced. In supra-granular layers, sparse but strong excitatory synaptic inputs from lateral pulvinar are included in this balance. Net inhibition might be broadly tuned at the preferred orientation of the neuron. Under normal conditions, the V1-pulvinar-V1 "loop" sustains the development of the visual response over time. Inactivating PL will yield the pattern of results obtained in our study. Other sub-nuclei such as Pdm connect with higher cortical areas shown to be involved in top-down control of selective attention. Intra-pulvinar interactions between different sub-nuclei might occur through large interneurons (grey arrow), the TRN, or through overlap of visuotopic maps in architectonically distinct sub-nuclei. This might allow for coordination of top-down and bottom-up signals in selective attention (see Discussion).

References

1. Kandel, E. R., Schwartz, J. H., & Jessell, T. M. *Principles of Neural Science* (New York: McGraw-Hill, 2000).
2. Purves, D., Augustine, G.J. & Fitzpatrick, D. *Neuroscience*. (Sinauer Associates, 2004).
3. Van Essen, D. C., Anderson, C. H. & Felleman. D. J. Information processing in the primate visual system: An integrated systems perspective. *Science* **255**, 419-423 (1992)
4. Felleman, D.J. & Van Essen, D.C. Distributed hierarchical processing in primate cerebral cortex. *Cereb. Cortex* **1**, 1-47 (1991).
5. Kaas, J. H. & Lyon, D. C. Pulvinar contributions to the dorsal and ventral streams of visual processing in primates. *Brain. Res. Rev*. 55, 285-296 (2007).
6. Petersen, D. L. & Robinson, S. E. Pulvinar and visual salience *Trends Neurosci.* 15, 127-132 (1992)
7. Casanova, C. The visual functions of the pulvinar. In: Werner, J. S. & Chalupa, L. M. (Eds) *The Visual Neurosciences* (Cambridge, MA: MIT Press, 2004).
8. Benevento, L.A., & Rezak M. The cortical projections of the inferior pulvinar and adjacent lateral pulvinar in the rhesus monkey (Macaca rnulatta): An autoradiographic study. *Brain Res*. **108** 1-24 (1976).
9. Rezak, M., & Benevento, L. A. A comparison of the projections of the dorsal lateral geniculate nucleus, the inferior pulvinar and adjacent lateral pulvinar to striate cortex (area 17) in the macaque monkey. *Brain Res*. **167**, 19-41 (1979).
10. Ogren M. P. & Hendrickson A.E. The distribution of pulvinar terminals in visual areas 17 and 18 of the monkey. *Brain Res*. **137**, 343–350 (1977).

11. Crick, F.C. & Koch, C. Constraints on cortical and thalamic projections: The no- strong-loops hypothesis, *Nature* **391**, 245-250 (1998).

12. Ward R., Danziger S., Owen V. & Rafal R Deficits in spatial coding and feature binding following damage to the human pulvinar. *Nature Neurosci* **5**, 99–100 (2002).

13. Karnath H-O., Himmelbach M. & Rorden C. The subcortical anatomy of human spatial neglect: putamen, caudate nucleus, and pulvinar. *Brain* **125**, 350–360 (2002).

14. Arend, I., Machado, L., McGrath, M., Ro, T., Ward, R. & Rafal, R. The role of the human pulvinar in visual attention and action: evidences from temporal order judgment, saccade decision and anti-saccade tasks. *Progress in Brain Research*, **171**, 475–483 (2008).

15. Snow, J.C., Allen, H.A., Rafal, R.D. & Humphreys, G.W. Impaired attentional selection following lesions to human pulvinar: Evidence for homology between human and monkey. *Proc Natl Acad Sci USA*.**106**, 4054–4059 (2009).

16. Chalupa LM. A review of cat and monkey studies implicating the pulvinar in visual function. *Behav Biol*; **20**, 149–67 (1977).

17. Ungerleider, L. G. & Christensen, C. A. Pulvinar lesions in monkeys produce abnormal scanning of a complex visual array. *Neuropsychologia* **17,** 493–501 (1979).

18. Bender, D. B. & Butter, C. M. Comparison of the effects of superior colliculus and pulvinar lesions on visual search and tachistoscopic pattern discrimination in monkeys." *Exp Brain Res* **69**, 140-154 (1987).

19. Rafal R.D. & Posner M.I. Deficits in human visual spatial attention following thalamic lesions. *Proc Natl Acad Sci USA* **84**, 7349–7353 (1987).

20. Wilke M., Turchi J., Smith K., Mishkin M. & Leopold D.A. Pulvinar inactivation disrupts selection of movement plans. *J. Neurosci*. **30**, 8650-8659 (2010).

21. Fischer J. & Whitney D. Precise discrimination of object position in the human pulvinar. *Hum Brain Mapp.* 30, 101-111 (2009).

22. Smith, A.T., Cotton, P.L., Bruno, A. & Moutsiana, C. Dissociating vision and visual attention in the human pulvinar. *J. Neurophys* **101**, 917 – 925 (2009).

23. Desimone, R., Wessinger, M., Thomas, L. & Schneider, W. Attentional control of visual perception: Cortical and subcortical mechanisms. *Cold Spring Harbor Symposium on Quantitative Biology*, **55**, 963–971 (1990).

24. Petersen S.E., Robinson D.L. & Morris J.D. Contributions of the pulvinar to visual spatial attention. *Neuropsychologia*. **25**, 97–105 (1987).

25. Bender D.B. & Youakim M. The effect of attentive fixation in macaque thalamus and cortex. *J. Neurophys.* **85**, 219-234 (2001).

26. Kastner S et al. Functional imaging of the human lateral geniculate nucleus and pulvinar. *J Neurophysiol*. 91, 438-448 (2004).

27. Wilke M., Mueller K.M. & Leopold D.A. Neural activity in the visual thalamus reflects perceptual suppression. *Proc Natl Acad Sci U S A*. **106**, 9465-9470 (2009).

28. Berman, R.A. & Wurtz, R.H. Signals conveyed in the pulvinar pathway from superior colliculus to cortical area MT. *J. Neurosci*. **31**, 373-384 (2011).

29. Ivanov, I. et al. Morphological abnormalities of the thalamus in youths with attention deficit hyperactivity disorder. *Am J Psychiatry*. **167**, 397–408 (2010).

30. Mize, R. R. & White, D. A. [^{3}H]Muscimol labels neurons in both the superficial and deep layers of cat superior colliculus. *Neurosci. Letters*, **104**, 31-37 (1989).

31. Martin, J.H. Autoradiographic estimation of the extent of reversible inactivation produced by microinjection of lidocaine and muscimol in the rat. *Neurosci. Lett*. **127**, 160–164 (1991).

32. Hikosaka, O. & Wurtz, R. H. Modification of saccadic eye movements by GABA-related substances II. Effects of muscimol in monkey substantia nigra pars reticulata. *J.Neurophysiol*. **53**, 292-308 (1985).

33. Reid, R. C. & Alonso, J. M. Specificity of monosynaptic connections from thalamus to visual cortex. *Nature* **378**, 281–284 (1995).

34. Molotchnikoff, S. & Shumikhina, S. The lateral posterior-pulvinar complex modulation of stimulus-dependent oscillations in the cat visual cortex. *Vision Res*., **36**, 2037-2046 (1996).

35. Logothetis NK, Augath M, Murayama Y, Rauch A, Sultan F, Goense J, Oeltermann A, & Merkle H. The effects of electrical microstimulation on cortical signal propagation. *Nature Neurosci*. **13**, 1283–1291 (2010).

36. Sherman S.M. & Guillery R.W. Distinct functions for direct and transthalamic corticocortical connections *J Neurophysiol*. **106**, 1068–1077 (2011).

37. De Pasquale R. & Sherman S. M. Synaptic Properties of Corticocortical Connections between the Primary and Secondary Visual Cortical Areas in the Mouse. *J Neurosci*. **31**, 16494-16506 (2011).

38. McCormick, D. A., Shu, Y. S. & Hasenstaub, A. Balanced recurrent excitation and inhibition in local cortical networks. in *Excitatory-Inhibitory Balance: Synapses, Circuits, Systems* (ed. Hensch, T.) (Kluver Academic Press, New York, 2003).

39. Ferster, D. Orientation selectivity of synaptic potentials in neurons of cat primary visual cortex. *J. Neurosci*. **6**, 1284–1301 (1986).

40. Softky, W. R. & Koch, C. The highly irregular firing of cortical cells is inconsistent with temporal integration of random EPSPs. *J Neurosci* **13**, 334-350 (1993).

41. Borg-Graham, L., Monier, C., & Fregnac, Y. Visual input evokes transient and strong shunting inhibition in visual cortical neurons, *Nature*, **389**, 369-373 (1998).

42. Somers, D. C., Nelson, S. B., & Sur,M. An emergent model of orientation selectivity in cat visual cortical simple cells. *J. Neurosci.,* **15**, 5448–5465 (1995).

43. Mariño J., Schummers, J., Lyon, D.C., Schwabe, L., Beck, O., Wiesing, P., Obermayer K., & Sur, M. Invariant computations in local cortical networks with balanced excitation and inhibition. *Nat. Neurosci.* **8**, 194-201 (2005).

44. Callaway, E. M. Local circuits in primary visual cortex of the macaque monkey. *Ann. Rev. Neurosci.* **21**, 47-74 (1998).

45. Rockland, K.S. Convergence and branching patterns of round, type 2 corticopulvinar axons. *J. Comp. Neurol*. **390**, 515–536 (1998).

46. Desimone, R. & Duncan, J. Neural mechanisms of selective visual attention. *Ann. Rev. Neurosci.* **18**, 193–222 (1995).

47. Van Essen, D.C. Cortico-cortical and thalamo-cortical information flow in the primate visual system. In: *Cortical Function: A View from the Thalamus*, V. A. Casagrande, R. Guillery, M. Sherman, eds., Progress in Brain Research *149*: 173-185 (Elsevier, 2005)

48. Olshausen, B.A., Anderson, C.H., & Van Essen, D.C. A neurobiological model of visual attention and invariant pattern recognition based on dynamic routing of information. *J. Neurosci.*, **13**, 4700–4719 (1993)

49. Ramachandran, V.S. & Gregory, R. Perceptual filling in of artificially induced scotomas in human vision. *Nature* **350**: 699-702, (1991)

50. Karnovsky, M. J. & Roots L. A 'direct coloring' thiocholine method for cholinesterases. *J. Histochem. Cytochem*., **12**, 219-220 (1964).

CHAPTER V

A MORPHOLOGICAL INVESTIGATION OF PULVINAR PROJECTIONS TO LAYER I OF VISUAL AREAS 1, 2, AND 3

Introduction

Investigation into the function of thalamo-cortical projections has traditionally focused on the primary sensory nuclei and their role in relaying information from the sensory periphery to the cortex. This tactic has been successful in establishing that all primary sensory nuclei send dense projections to layer III/IV of the primary sensory corteses and that these connections are central in the feed forward transfer of information (Sherman and Guillery, 1998; Sherman and Guillery, 2006 book p8-13; Jones, 1998). The role of layer III/IV projections in feed forward sensory processing is backed by analysis of cortico-cortical projections that further suggest that the superficial and deep layer projections between cortical areas are important in feedback processes (Felleman and van Essen). Along with cortico-cortical inputs both superficial and deep layers of many if not all cortical areas receive input from the thalamus in primates and cats (Jones 2007 p92-113). Indeed every thalamic nucleus tested sends projections to layer I of its cortical targets (Jones 2007 p92-113). What is the role of this thalmo-cortical layer I input in cortical processing and communication? Since Layer I is also the target of feedback cortical projections it is tempting to suggest that these are feedback projections but this cannot be

uniformly true given that the primary sensory thalamic nuclei send projections to layer I. One theory concerning the function of thalamic layer I inputs is that their projections are so called nonspecific or diffuse projections (Jones 1998; Jones 2007 p92-113). Such projections act in a permissive manner allowing the cells they contact to be brought to threshold by other inputs perhaps in service of processes like synchrony (Jones 2001). Along these same lines it has been suggested that these projections be considered under the heading of modulatory connections (Sherman 2012). Alternate views grounded in slice physiology suggest that layer I inputs have a much stronger effect and may in fact cause cells or at least their apical dendrites to create action potentials and therefore would qualify as a type of driving input (Larkum et al 1999; Schwindt and Crill 1999; Larkum et al 1999).

The pulvinar nucleus of the thalamus sends projections to layer I of cortex where it terminates broadly, mostly located in the occipital and temporal cortex including the primary and a number of visual areas including primary visual cortex (V1), secondary visual cortex (V2), visual area number three (V3), visual area number four (V4) and the middle temporal area (MT) (Rockland 1999). These layer I projections from pulvinar are always accompanied by robust layer III-IV projections in extrastriate cortex (Rocklnad 1999). In contrast in area V1 pulvinar only projects to layers I-III but primarily to layer I (Ogren and Hendrickson 1977; Rezak and Benevento 1979, Benevento et al 1976). This property of providing strong layer I projections to one area while providing layer I, III and IV projections to other areas (while not unique to the pulvinar) allows for these projections to be used to ask a number of interesting questions. Central among these questions is how similar the effect of layer I and layer IV projections might be on postsynaptic targets. Will pulvinar synapses in layer I be weak in keeping with a role to provide small modulatory effects to many cells or will these synapses be more robust like their

layer IV counterparts (Marion et al 2013)? Also, what differences can be observed between the layer I pulvinar projections to V1 and those terminating in the extrastriate visual areas. Are all pulvinar projections to layer I morphologically similar? In this study we sought to provide some answers to these questions by examining and comparing the morphology of projections to layer 1 in V1 with projections to extrastriate areas V2 and V3. Additionally, we compared the layer 1 projections in V1 to those known to drive the cortex from the lateral geniculate nucleus (LGN) which terminate primarily in layer IV of V1.

Methods

Subjects

Ten bush babies (*Otolemur garnettii*) of both sexes ranging in age from 6 months to 6 years were used. These animals were cared for according to the National Institutes of Health Guide for the Care and Use of Laboratory Animals and according to a protocol approved by the Vanderbilt University Institutional Animal Care and Use Committee.

Surgery and Tracer Injections

Since all of the cases were used as part of a previously published study (Marion et al., 2013), where the methods are described in detail, only a brief summary will be provided here. Under sterile procedures, the animals were anesthetized (propofol and nitrous oxide) and were given a muscle relaxant (Vecuronium bromide). The placement of tracers was established by visual evoked potential mapping of the lateral and inferior pulvinar. Tracer injections were made using pressure through “injectrodes” manufactured in-house which allowed recording and

injections to be made at the same locations. 300-450 nl of biotinylated dextran (BDA), dextran conjugated to Alexa-fluor 488 (dex 488), and dextran conjugated to Alexa-fluor 568 (dex 568) were injected. Animals were revived and survived 2-4 weeks before being perfused transcardially with aldehyde fixative.

Tissue processing, tracer visualization and case selection

The brain was blocked in the coronal plane before removing. It was then removed, frozen on dry ice and stored at −70°C until used. All cases were cut frozen using a sledge microtome at a section thickness of 30 to 52 μm. To visualize BDA, sections were placed in 1:400 or 1:500 streptavidin Alexa-fluor 488 or streptavidin Alexa-fluor 568 (Invitrogen) in tris-buffered saline (TBS) for 2 hours, then rinsed three times in TBS, mounted, and coverslipped with Vectashield (Vector). Dex 568 and dex 488 needed no additional processing to be visualized. Cytochrome oxidase (CO) staining was performed by using methods described previously (Boyd and Matsubara, 1996). Cases were considered successful if injections were localized to the areas of interest and produced projections dense enough to reveal clearly the cortical layer targeted.

Case reconstruction

In successful cases (N=9) a series of florescent sections (every 3rd or 6th section) was developed and examined for areas of interest (injection sites and projection foci). The laminar and nuclear borders of these areas and areas of interest in bouton quantification (below) were confirmed by digitally overlaying (Adobe Photoshop) florescent images of the areas of interest with bright field images of adjacent CO sections.

Section and confocal stack location

Sections that were selected for layer I bouton quantification came from the center of projection foci. For layer I of V2 the center of the foci were easily determined by eye but in layer I of V1 the numerous long distance projections made locating the center of the projection difficult hence sections containing multiple layer II/III arbors were chosen under the assumption that the presence of the much less common arbor type indicated the center of the projection. Confocal stacks for layer I V2 bouton quantification were taken from the center of the layer I projections. Confocal stacks for layer I V1 bouton quantification were taken from parts of layer I directly above a layer II/III projection or in the section of layer I that lay between the columnar locations of 2 layer II/III projections. Data for layer IV V2 bouton quantification came from a previous study (Marion et al. 2013). Some stacks from which these data were collected were located in the center of the projection foci (as determined by eye) while others were taken from more peripheral parts of the projection foci. No significant difference was found between bouton sizes measured in the center of the projection foci and those measured in the periphery; they were therefore combined and treated equally.

Acquisition of bouton size data

High powered confocal stacks of boutons were taken at the locations described above using a Zeiss 510 confocal microscope equipped with a 63x 1.4 NA objective. Once a stack had been acquired an observer naive to the origin of the stack was recruited to identify the boutons within the image. The areas at half maximum intensity of the boutons in the stack were then measured and recorded. In rare cases some boutons appeared to be smaller than the resolution of the microscope (0.07 μm^2). In these cases the boutons were not quantified. In the majority of the

stacks more boutons were present than were needed for the analysis (as determined by eye). Two strategies were employed to limit the number of boutins quantified: 1) the naive observer was asked only to select boutons within a column representing the central ~50% of the stack. 2) Alternatively, a column containing the central ~25 boutons chosen was measured.

Statistical Analysis

The bouton areas for each projection type (layer I V1, layer I V2, and layer IV V2) in each case were considered a single sample. Three samples were collected for layer IV V2 (n=24, 27, 36), two samples were collected for layer I V2 (n=16, 22) and four samples were collected for layer I V1 (n=26, 23, 25, 23). Data for each projection type was treated as a single population and these populations were compared to each other using a Kruskal Wallis test followed by rank sum tests with α levels corrected for multiple comparisons by the Bonferroni method (α levels provided in results). In an effort to understand the data more completely, a frequency distribution of the three populations was produced and inspected. These inspections showed that the layer I V1 data was skewed more than the other data. This skew was quantified using the using the nonparametric skew statistic which was calculated by subtracting the median from the mean and dividing by the standard deviation.

Results

Injection reconstruction

Injections of label in pulvinar were limited to PL and have been described in detail previously in Marion et. al (2013). Briefly, nine successful pulvinar injections were made in 6

cases. Reconstructed injections consisted of tracks where injections were made at one or two points along the track. Injections tended to be widest in the dorsal ventral axis with the largest injection being approximately 1.1 mm in the dorsal ventral axis. Electrophysiological recordings from the tip of the injectrodes along with images of the sections (both CO and fluorescent) containing the injections were compared with the bush baby visiotopic maps of pulvinar (Li et al.,2013), confirming that the vast majority of all injections fell within the dorsal pulvinar map. A typical tract in which two injections were made is presented in figure 1.

Overview of projections from pulvinar to cortex

Projections from the pulvinar to the cortex were observed in areas V1, V2, V3, MT and a number of other areas lying in the occipital, parietal and temporal cortices (see also Rockland 1999). Pulvinar axons that terminated in V1 (Figure 2) tended to ascend through the layers in a vertical, columnar manner generally without branching in other layers and were only seen to arborize once they reached layer I(see below for exception). Typically these axons made a right angle in lower layer I and then arborized in the outer half of layer I. These axons then travelled for great distances forming en passant boutons and branching occasionally (figure 3A). Although we could not fully reconstruct these axons it was clear that they many often arborized over a distance of more than two ~400 μm columns in V1. The border between the upper and

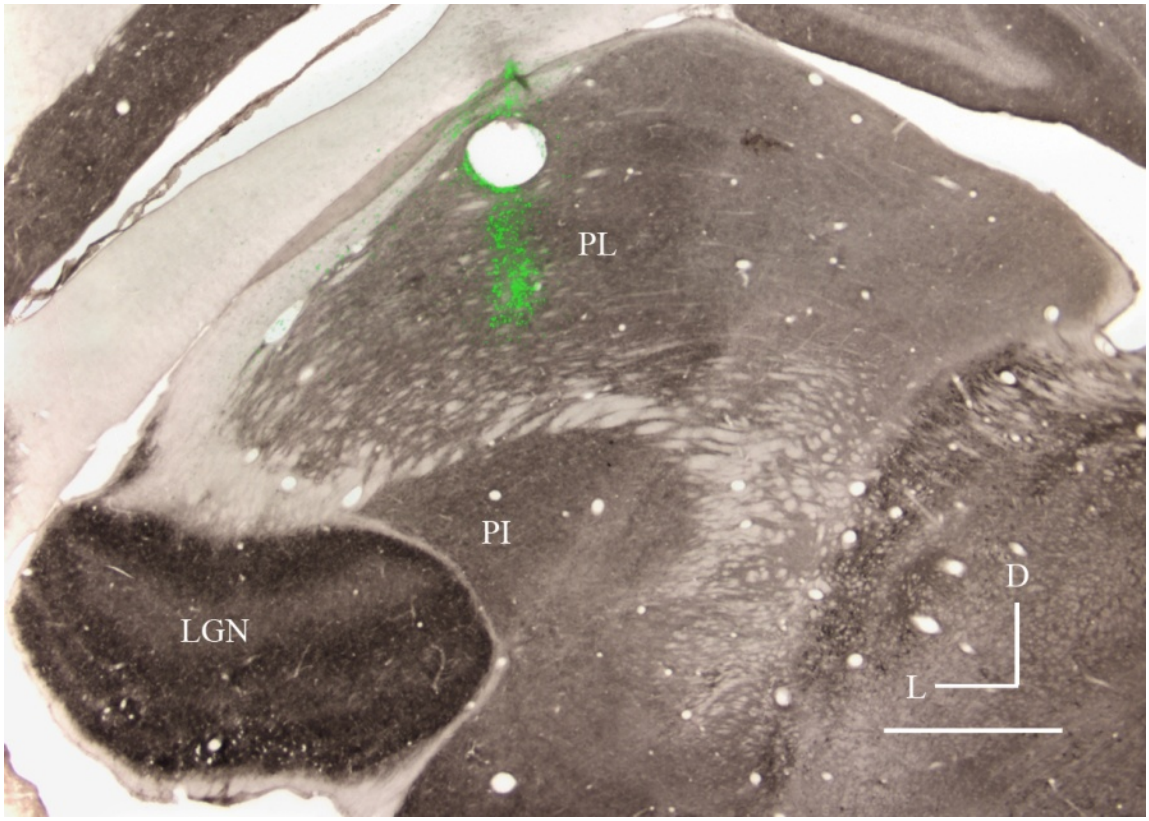

Figure 1.
Overlay of adjacent coronal cytochrome oxidase (CO) and florescent sections showing an example injection sites in pulvinar (green, biotinylated dextran). The pulvinar injection was centered on the central vision representation in lateral pulvinar (PL). PI, inferior pulvinar; D, dorsal; L, lateral. Scale bar = 1 mm.

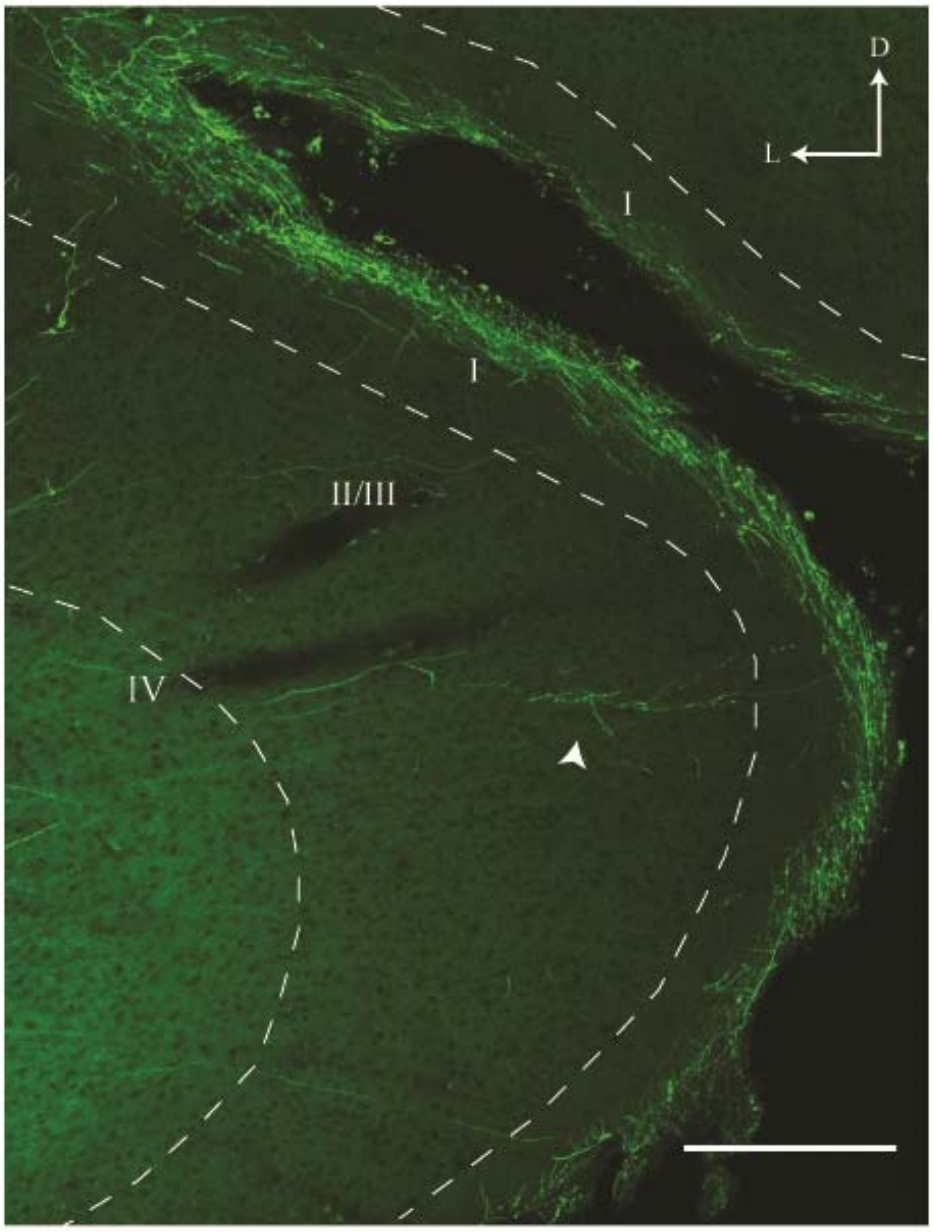

Figure 2.
Confocal photomicrograph of pulvinar projections (green) to the calcarine fissure in primary visual cortex (V1). Pulvinar axons can be seen to form arbors in a dense band in the outer half of layer 1. Occasional arbors are also observed in the upper part of layers 2-3 (arrow). D, dorsal; M, Medial. Scale bar = 200 μm.

lower halves of layer I was also a common place for axons to branch where they would send collaterals off in opposite directions. Less commonly observed were axons that ascended to the very top of layer I without turning at right angles to arborize tangentially. A few axons did produce boutons as they passed through the inner half of layer I but extensive arbors were never seen. Infrequently, axons were observed to form arbors in layers II/III. These arbors had a different appearance and like the arbors ending in layer IV (see Florence and Casagrande, 1987), these tended to remain confined to single vertical column (figure 3B).

Projections to extrastriate areas V2 and V3 had a similar form with the predominance of projections terminating in layer III-IV and a small number of projections terminating in lower layer II and upper layer I. The axons extending to layer I branched in a similar manner as described for V1 running in the outer half of layer I (figure 4). The tangential spread of the V2 and V3 layer I projections , unlike the projections to layer I of V1 tended to remain confined to the width a column and matched the width of the main projection to layers III and IV directly below them. The configuration of the axon arbors in V2 and V3 suggested that these arbors in layer I arose as branches from axons whose main projection was within layers III and IV although no detailed reconstructions were done to rule out the possibility that some axons terminated as a separate population only in layer I. It is also noteworthy that we never observed axons that passed through layers III and IV that did not have boutons as would be predicted if they were a separate population that bypassed layers III and IV to terminate only in layer I. In contrast, no pulvinar axons in V1 were observed that had boutons in layers III and 4.

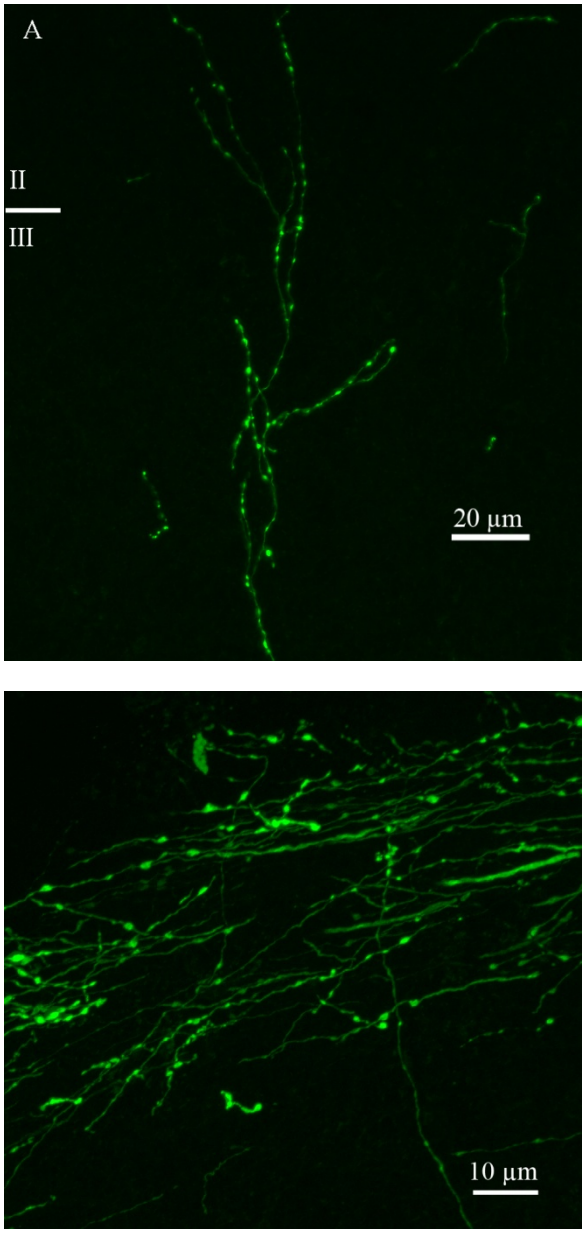

Figure 3.
High power confocal photomicrographs of pulvinar projections to layer I (**A**) and layer 2/3 (**B**) of the primary visual cortex (V1). Axons in layer I tended to run within a single sub layer while axons in layer II/III tended to arborize perpendicular to the layer. Note that the images are at different scales, see scale bar labels in the images. Cortical surface is represented by dashed line in **A**. In **B** layer boundaries are not within the plain of the image and cortical surface lies above the top of the image.

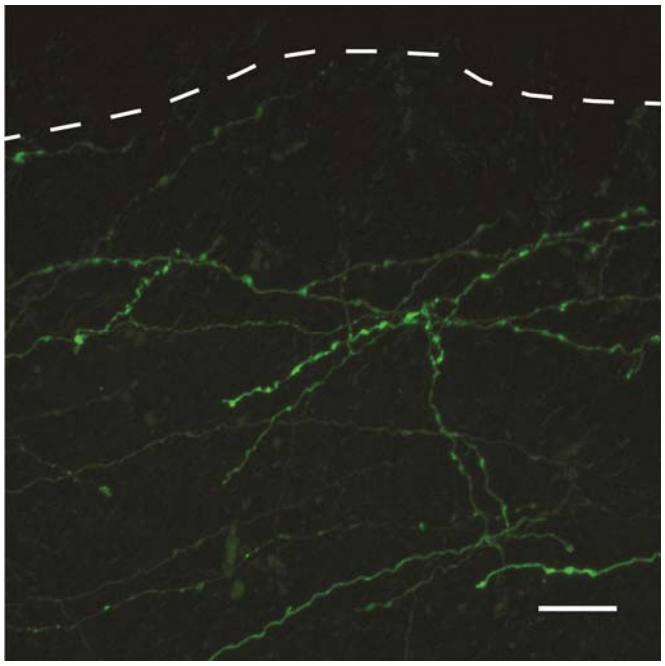

Figure 4.
High power confocal photomicrographs of pulvinar projections (green) to layer I of the secondary visual cortex (V2). Axons forming terminals in layer II/III preceded to the outer part of layer I where they arborized in a similar, albeit more restricted way, to the axons from pulvinar to V1. See text for details. Cortical surface is represented by dashed line. Scale bar = 10 μm.

Comparison of bouton sizes in V1 and V2

There is evidence that the size of presynaptic enlargements might act as a proxy measurement for post synaptic strength (Pierce and Lewin, 1994; Sherman and Guillery, 1996; Marion et. al. 2013). With this in mind we closely examined and quantified the boutons on pulvinar projections to layer I in V1 and layers I and IV in V2. The vast majority of boutons observed were of the en passant type with only an occasional stalk like terminal. As presented in previous work, the layer IV boutons in V2 have a median area of 0.48 μm^2 with a mean of 0.47 μm^2 (SEM=0.002 μm^2, n=87) (Marion et. al. 2013). Boutons in Layer I of V1 were measured in 4 samples in 4 cases and found to have median area of 0.33 μm^2 with a mean of 0.38 μm^2 (SEM=0.001 μm^2, n=97). Due to the sparseness of boutons in layer I of V2 only 2 samples in 2 cases could be quantified yielding median areas of 0.34 μm^2 with a mean of 0.33 μm^2 (SEM=0.004 μm^2, n=38). A Kruskal-Wallis test indicated that the samples varied significantly ($H=20.51$, 2 d.f., $p<0.01$). A rank sum test was then used to determine that the size of l layer I boutons in V1 and V2 were not significantly different ($p>0.05$). Layer I boutons form both V1 and V2 were smaller than those found in layer IV of V2 (rank sum test with Bonferroni correction for 3 comparisons, $p<0.001$). Non-parametric testing was favored because skew was apparent in some of the data. To quantify this we used the statistic of nonparametric skew finding the skewedness for layerIV of V2, layer I of V1 and layer I of V2 to be -0.03, 0.26, and -0.05 respectively. Clearly, the distribution of bouton sizes in layer I of V1 tended to be more skewed than the samples from V2 and in a opposite direction. The implications of this result are considered in the Discussion.

Discussion

The purpose of this study was to describe the pulvinar projections to layer I of V1 and compare these projections to the pulvinar projections to the extrastriate cortex specifically V2 and V3. Our primary findings were: 1) Pulvinar projections to V1 were concentrated in layer I where they formed a dense band of fibers that ran horizontally across several cortical columns in the outer half of the layer. 2) Pulvinar projections to layer I of V2 and V3 were similar to the layer I projections seen in V1 in that they ran horizontally and had similar small boutons unlike those in V1 they were less dense, were more confined within columns and most appeared to form as collaterals of axons terminating mainly in layers III and IV. 3) All projections to layer I in these visual areas were strikingly different from the projections to Layers III and IV in V2 and V3 in that they have different arborization patterns and smaller boutons.

Comparison with prior results

Our findings are in accord with past results showing that the majority of pulvinar projections to V1 occur in the upper part of layer I with additional terminations in layers II-III (Ogren and Hendrickson 1977; Rezak and Benevento 1979, Benevento et al 1976). The form of these projections fits with the general patterns shown by Layer I thalamo-cortical projections from other nuclei in that they parallel the cortical surface, span mutual columns, have en passant boutons and often have collaterals in layer III-IV (Lachica and Casagrande 1992; Rockland et. al. 1999; Rubio-Garrido et. al. 2009; Carey et al. 1979). Our data indicate that there are at least two types of pulvinar projections to V1: those that terminate only in layer I and those that terminate in layers I, II and III. Further, it appears that unlike those terminating in V1 projections to layer I

of V2 and V3 may arise as collaterals of axons that primarily terminate in the middle layers. There is precedence for different types of thalamo-cortical layer I projections. At least two classes of K-cells exist in the galago and the macaque (Lachica and Casagrande 1992; Casagrande et. al. 2007), and multiple classes of layer I terminating thalamic projections appear to exist in the rodent (Rubio-Garrido et. al. 2009).

The size of boutons in a projection has been shown to correlate with the number and size of synapses and with post synaptic efficacy (Pierce and Lewin, 1994; Sherman and Guillery, 1996; Marion et. al. 2013). By this criterion our quantitative data indicate that layer I projections may have less efficacious synapses than those terminating in layer IV. To our knowledge, no comparable measurements have been made comparing layer I bouton sizes with those in layer IV elsewhere in the brain. We are, however, able to compare the current data to prior measurements of parvo and magno projections to layer IV of V1. Pulvinar projections to V2 have already been demonstrated to have similar size boutons as parvo projections and somewhat smaller boutons as compared to magno projections. Both layer 1 projections appear to be have smaller boutons than either parvo or magno projections to Layer IV of V1 lending further support to the concept that layer IV thalamo-cortical projections are dominate over there layer I counterparts.

It is important to recognize that the different populations of boutons do not appear to have the same distribution. In the strictest sense, this violates one of the assumptions of the Kruskal-Wallis test and the rank-sum test (from which the Kruskal-Wallis is derived) that we used (Fagerland and Sandvik 2009). We acknowledge this point but are comfortable interpreting the boutons in layer I of V1 and V2 are smaller than those measured in layer IV of V2 because the effect of skew on the results of a Kruskal-Wallis test occurs in degrees and our p values are small enough that it is unlikely that they could be generated purely by the effects of differing

distributions (Fagerland and Sandvik 2009). Though it is clear that both the pulvinar projections to layer I have smaller boutons than the pulvinar projections to layer IV it is less certain that these projections are identical given the differences in there morphology and that the samples of bouton size for the two layer I projections appear to come from populations with different shapes.

Functional implication:

Sherman and Guillery (1998) have laid out a straightforward set of criteria for classifying glutamatergic projections into two types: Drivers (class 1) and modulators (class 2). Among the properties used to classify projections is bouton size and location of synapse relative to the soma. Within Sherman and Guillery's framework our data suggest that layer I projections are modulators and as such are involved in gain control and other processes that shape but do not carry the sensory signals being transmitted between areas. The idea that projections to layer I are modulatory has a long history and fits with Jones's (1998) idea of layer I projections as paralemniscal (a.k.a matrix) and thus less involved with specific feed forward processes. The purpose of these modulatory projections is still unclear. Some investigators (Jones 2001) have suggested as a class projections to layer I may be involved with the synchronization of signals across cortical columns or layers. In the specific case of the pulvinar the argument has been made that such projections could be involved in the gating of signals based on attention (Purushothaman et al., 2012). Complicating these straightforward views of layer I function is the specter of multiple classes of layer I projections possibly serving distinct functions. It is unclear if different types of layer I projections have different patterns of connections and this information is likely necessary before generalizations can be made. Whatever the purpose of these types of

projections, their presence in both archaecortex and in the 3 layered cortex of turtles suggests that one of these functions could have an ancient origin (Belekhova et. al. 2003; Heller and Ulinski 1987; Hall and Ebner 1970; Jones 2007 p117-119).

Reference List

Belekhova MG, Kenigfest NB, Minakova MN, Rio JP, Reperant J. 2003. [Calcium-binding proteins in the thalamus of turtles. Analysis of the thalamic organisation according to the theory of "core-matrix" and in the connection with the problem of homology of the amniote thalamic nucleus]. Zh Evol Biokhim Fiziol 39(6):504-523.

Benevento LA, Rezak M. 1976. The cortical projections of the inferior pulvinar and adjacent lateral pulvinar in the rhesus monkey (Macaca mulatta): an autoradiographic study. Brain Res 108(1):1-24.

Boyd JD, Matsubara JA. 1996. Laminar and columnar patterns of geniculocortical projections in the cat: relationship to cytochrome oxidase. J Comp Neurol 365(4):659-682.

Carey RG, Fitzpatrick D, Diamond IT. 1979. Thalamic projections to layer I of striate cortex shown by retrograde transport of horseradish peroxidase. Science 203(4380):556-559.

Casagrande VA, Yazar F, Jones KD, Ding Y. 2007. The morphology of the koniocellular axon pathway in the macaque monkey. Cereb Cortex 17(10):2334-2345.

Fagerland MW, Sandvik L. 2009. The Wilcoxon-Mann-Whitney test under scrutiny. Stat Med 28(10):1487-1497.

Felleman DJ, Van Essen DC. 1991. Distributed hierarchical processing in the primate cerebral cortex. Cereb Cortex 1(1):1-47.

Florence SL, Casagrande VA. 1987. Organization of individual afferent axons in layer IV of striate cortex in a primate. J Neurosci 7(12):3850-3868.

Hall WC, Ebner FF. 1970. Thalamotelencephalic projections in the turtle (Pseudemys scripta). J Comp Neurol 140(1):101-122.

Heller SB, Ulinski PS. 1987. Morphology of geniculocortical axons in turtles of the genera Pseudemys and Chrysemys. Anat Embryol (Berl) 175(4):505-515.

Jones EG. 1998. Viewpoint: the core and matrix of thalamic organization. Neuroscience 85(2):331-345.

Jones EG. 2001. The thalamic matrix and thalamocortical synchrony. Trends Neurosci 24(10):595-601.

Jones EG. 2007. The Thalmus Cambridge: Cambridge University Press.

Lachica EA, Casagrande VA. 1992. Direct W-like geniculate projections to the cytochrome oxidase (CO) blobs in primate visual cortex: axon morphology. J Comp Neurol 319(1):141-158.

Larkum ME, Kaiser KM, Sakmann B. 1999a. Calcium electrogenesis in distal apical dendrites of layer 5 pyramidal cells at a critical frequency of back-propagating action potentials. Proc Natl Acad Sci U S A 96(25):14600-14604.

Larkum ME, Zhu JJ, Sakmann B. 1999b. A new cellular mechanism for coupling inputs arriving at different cortical layers. Nature 398(6725):338-341.

Li K, Patel J, Purushothaman G, Marion RT, Casagrande VA. 2013. Retinotopic maps in the pulvinar of bush baby (Otolemur garnettii). J Comp Neurol.

Marion R, Li K, Purushothaman G, Jiang Y, Casagrande VA. 2013. Morphological and neurochemical comparisons between pulvinar and V1 projections to V2. J Comp Neurol 521(4):813-832.

Ogren MP, Hendrickson AE. 1977. The distribution of pulvinar terminals in visual areas 17 and 18 of the monkey. Brain Res 137(2):343-350.

Pierce JP, Lewin GR. 1994. An ultrastructural size principle. Neuroscience 58(3):441-446.

Purushothaman G, Marion R, Li K, Casagrande VA. 2012. Gating and control of primary visual cortex by pulvinar. Nat Neurosci 15(6):905-912.

Rezak M, Benevento LA. 1979. A comparison of the organization of the projections of the dorsal lateral geniculate nucleus, the inferior pulvinar and adjacent lateral pulvinar to primary visual cortex (area 17) in the macaque monkey. Brain Res 167(1):19-40.

Rockland KS, Andresen J, Cowie RJ, Robinson DL. 1999. Single axon analysis of pulvinocortical connections to several visual areas in the macaque. J Comp Neurol 406(2):221-250.

Rubio-Garrido P, Perez-de-Manzo F, Porrero C, Galazo MJ, Clasca F. 2009. Thalamic input to distal apical dendrites in neocortical layer 1 is massive and highly convergent. Cereb Cortex 19(10):2380-2395.

Schwindt P, Crill W. 1999. Mechanisms underlying burst and regular spiking evoked by dendritic depolarization in layer 5 cortical pyramidal neurons. J Neurophysiol 81(3):1341-1354.

Sherman SM. 2012. Thalamocortical interactions. Curr Opin Neurobiol 22(4):575-579.

Sherman SM, Guillery RW. 1996. Functional organization of thalamocortical relays. J Neurophysiol 76(3):1367-1395.

Sherman SM, Guillery RW. 1998. On the actions that one nerve cell can have on another: distinguishing "drivers" from "modulators". Proc Natl Acad Sci U S A 95(12):7121-7126.

Sherman SM, Guillery RW. 2006. Exploring The Thalamuc And Its Role In Cortical Function. Cambridge: The MIT Press. 484 p.

CHAPTER VI

MORPHOLOGICAL AND NEUROCHEMICAL COMPARISONS BETWEEN PULVINAR AND V1 PROJECTIONS TO V2

The study described in this chapter was published and is reproduced below without alterations: Marion R, Li K, Purushothaman G, Jiang Y, Casagrande VA. 2013. Morphological and neurochemical comparisons between pulvinar and V1 projections to V2. J Comp Neurol 521(4):813-832.

Introduction

A fundamental problem in neuroscience is to define the flow of information from the sensory periphery through the brain. For primary sensory nuclei of the thalamus, such as the lateral geniculate nucleus (LGN), the "feedforward" direction of information flow is clear: signals are sent to the LGN of the thalamus which, in turn, are combined to activate cells in primary visual cortex (V1). This is despite the fact that both LGN and V1 receive numerous other connections from many brain areas both subcortical and cortical (Casagrande and Kaas, 1994; Casagrande and Norton, 1991). The question is "who drives and who modulates?" a question that is more complicated for thalamic nuclei and cortical areas which are not directly connected to the periphery. The primate pulvinar and the secondary visual area (V2) are

exemplars of this problem. The visual pulvinar receives its drive from V1 (Bender, 1983), the lateral and inferior portions of the visual pulvinar and V1 send outputs to V2, (Casagrande and Kaas, 1994; Kaas and Lyon, 2007 for review). As seen in Figure 1A there are two routes by which feedforward information can travel from V1 to V2. The traditional view is that feedforward information flows from LGN to V1 and from there to V2 and other extrastriate areas in a hierarchical manner (Felleman and Van Essen, 1991; Goodale and Milner, 1992; Mishkin and Ungerleider, 1982). One alternative view is that for each cortical area, the main drive comes from the thalamus with cortico-cortical connections providing a modulatory input (Sherman and Guillery, 1998; Sherman and Guillery, 2002; Sherman, 2007). How can one decide between these alternatives? Rockland and Pandya (1979) argued that feedforward (potential driving connections) in cortex are distinct from feedback (modulatory connections) based on the cells of origin and the layers of termination of their axons. Their data showed that feedforward visual system connections are found within the middle layers of cortex (layers III and IV) while feedback connections are found in the supragranular layers, especially layer I, and in infragranular layers. These anatomical distinctions were subsequently used, in part, by Felleman and Van Essen (1991) to construct the now well-known dorsal and ventral hierarchies of cortical visual areas in macaque monkeys highlighted in many neuroscience textbooks. These cortical hierarchies continue to be referenced to each other based on the original criterion of laminar terminations of their inputs and outputs. At the level of the LGN and V1, however, driving connections have been distinguished from modulatory connections based on a number of additional anatomical criteria. Examples include the sizes, positions and arrangements of boutons and the protein content of these boutons (for review see Sherman and Guillery, 1998; Sherman and Guillery, 2002; Sherman, 2007).

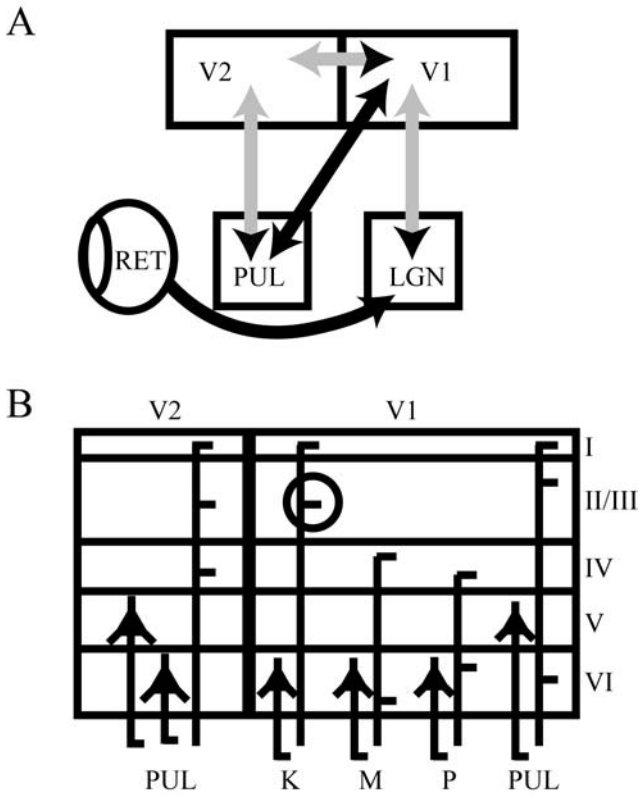

Figure 1.

Schematic summary of relevant connections between the eye (RET), lateral geniculate nucleus (LGN), lateral pulvinar (PUL) and primary (V1) and secondary (V2) visual cortical areas in bush baby. (A) Connections between areas are indicated by single or double-headed arrows. The connections compared in this study are indicated by green arrows. (B) Details of known primary connections between V1 and V2 and PUL and the individual layers of the LGN, the koniocellular (K), magnocellular (M) and parvocellular (P). Projections to cortex are indicated by horizontal line segments within the cortical layers which are indicated by roman numerals. Projections back to thalamus are indicated by connections from individual black cells in cortical layers V and VI. The open circle in V1 layers II/III indicates the location of a cytochrome oxidase blob in V1. Data for this figure were taken from Lachica and Casagrande, 1992, Florence and Casagrande, 1987; Ichida et al. 2012; Raczkowski and diamond, 1981; Collins et al.,2001 and unpublished observations.

Thus, the primary goal of this study was to examine and compare the two key inputs to V2 that could serve as drivers for this area, input from the lateral pulvinar (hereafter referred to simply as pulvinar) and input from V1 (see Symonds and Kaas, 1978; Wong et al., 2009). Prior studies have shown that inputs from both sources end in layer IV of V2 in macaque, bush baby and other primates consistent with the criterion for feedforward connections (Adams et al., 2000; Collins et al., 2001; Cragg, 1969; Cusick and Kaas, 1988; Felleman and Van Essen, 1991; Gattass et al., 1981; Kaske et al., 1991; Kennedy and Bullier, 1985; Kuypers et al., 1965; Lund et al., 1981; Mettler, 1935; O'Brien et al., 2001; Preuss et al., 1993; Rockland and Pandya, 1979; Shipp, 2003; Sincich and Horton, 2002; Tigges et al., 1973; Wong et al., 2009; Zeki, 1969). Hence, both inputs are possible drivers. Additionally, studies have shown that cells in primate V2 lose responsiveness following removal of V1 (Schiller and Malpeli, 1977), so V2 could be either driven directly by V1 or indirectly via the pulvinar (or both). Since LGN input to V1 is a known driver, we used the characteristics of this pathway for comparison, focusing here on axon distribution, bouton size, and the presence or absence of the vesicular glutamate transporter number 2 (Vglut2) and the calcium binding protein, parvalbumin (PV). The latter proteins are strongly expressed in the LGN axons within layer IV of V1 (Blumcke et al., 1991; DeFelipe and Jones, 1991; Nahmani and Erisir, 2005).

Methods

Overview

Ten bush babies (Otolemur garnettii) of both sexes, also known as “greater galagos”, were used in this study. Animal ages ranged from 6 months to 6 years with the median age being between 1 and 2 years. Four animals were optically imaged, 5 animals received injections in V1,

4 animals received injections in the LGN and all animals received injections in the pulvinar. In total 11 hemispheres were examined. All of the animals were cared for according to the National Institutes of Health Guide for the Care and Use of Laboratory Animals and according to the guidelines of the Vanderbilt University Institutional Animal Care and Use Committee under an approved protocol.

Anesthesia, Surgery, and Recovery

All surgical procedures were carried out under aseptic conditions and all survival procedures were performed under sterile conditions. Prior to surgery, anesthesia was induced with 2-4% isoflurane in O2. During this period animals were given intramuscular Dexamethasone to control for brain swelling, (1mg/kg), Glycopyrollate (Robinul) to reduce salivation and fluid accumulation (0.015mg/kg) and Naxcel as an antibiotic (2.2 mg/kg). Two venous catheters were inserted, the pupils were dilated with 2% cyclopentolate (Cyclogyl) and/or 1% atropine drops and contact lenses were placed in the eyes to protect the corneas. The heart rate and temperature were monitored continuously and the temperature was regulated using a water circulating heating pad and heat packs. After intubation animals were mounted in a stereotaxic apparatus and connected to CO2 and heart monitors and baseline measures of ECG, heart rate and CO2 were taken. Once the animal was stable under anesthesia, a midline incision was made and the skull exposed. In the initial surgery a craniotomy of ~10 mm in diameter was performed over either pulvinar or LGN and in some cases another craniotomy was made over the primary visual cortex (V1). After each craniotomy, the dura was cut and retracted. At the end of each surgery, artificial dura (Tecoflex®) and a protective cap of thermoplastic and dental cement

were placed over the craniotomies. In subsequent surgeries the brain was accessed by removal of the protective cap and the artificial dura.

Before an experiment was performed, the animal was switched to an anesthesia consisting of 75% N2O along with Propofol delivered at ~10 mg/kg/h if given during surgery, which was reduced during the experiments to 4-7 mg/kg/h. During the transition between anesthetic methods the animal was maintained temporarily on Propofol and isoflurane at the levels previously described. After the animal's physiological state was stable under Propofol/N2O anesthesia, neuromuscular blockade was induced with IV injection of 1mg/kg of Vencuronium bromide and maintained throughout the experiments with Vencuronium bromide (0.6 mg/kg/h) in a 5% dextrose lactated Ringers solution. Animals were artificially ventilated with a mixture of 75% N2O, 23.5% O2, and 1.5% CO2 that was delivered at a rate of 35-40 breaths/min in a volume sufficient to maintain the peak expired CO2 at 3.5-4%. Contact lenses with sufficient power were used to bring the animal to focus at a viewing distance of 28.5 cm or 57 cm. Retinal landmarks including the optic disks and areae centralii were plotted using back reflection of the blood vessel pattern from the tapetum at the beginning of each experiment. At this juncture one of two experiments could be performed, either optical imaging or visual evoked potential mapping and tracer injections. Both experimental procedures are described below.

At the end of each tracer injection or optical imaging session, animals were weaned from the ventilator and anesthetic after infusion of the paralytic agent was stopped and were watched carefully until they were capable of eating and drinking on their own. These animals also were given the analgesic buprenorphine (Buprenex 0.01 mg/kg) and the antibiotic, ceftiofur sodium (2.2 mg/kg) postoperatively. In some cases additional terminal experiments for a separate set of studies were performed before the animals were perfused.

Optical imaging

Our imaging equipment and procedures have been previously described (Khaytin et al., 2008; Xu et al., 2005; Xu et al., 2004). After a V1 craniotomy was performed and the dura removed and replaced with Tecoflex®, the opening was covered with 1% agarose in saline, and sealed with a glass cover-slip. Cortical reflectance changes following stimulus presentation were imaged using an Optical Imager 2001 system (Optical Imaging Inc., Mountainside, NJ). Visual stimuli were presented on a 21 inch monitor (Sony FD Trinitron, F400, Sony, Tokyo, Japan) at 120Hz (non-interlaced mode, background luminance = 30 cd/m2) using the VSG 2/5 stimulus generator (Cambridge Research Systems, Rochester, UK) synchronized with the imaging system. A macroscope consisting of two front-to-front tandem Nikon lenses (50 mm/50 mm or 50 mm/135 mm) magnified the cortex for the CCD camera. The image was focused at about 500-600 μm below the cortical surface and the diaphragm was closed by one or two f-stops. The light source was filtered at 540 nm to acquire a reference image of the surface vasculature and 611 nm to collect functional data. Raw images for each trial were normalized by the image acquired during a blank screen condition at the start of the trial (Crair et al., 1997). Visual topography of V1 was determined by use of retinotopically restricted rectangular windows, disks and rings of different sizes containing 100% contrast square-wave gratings (0.5 c/deg fundamental spatial frequency) presented at 2 orthogonal orientations and drifted at 2 Hz. Analysis was performed using WinMix (Optical Imaging Inc.).

Visuotopic mapping and tracer injections

Animals received tracer injections in the LGN, pulvinar and/or V1. The basic connections for LGN, pulvinar, V1 and V2 in bush baby are shown in Figure 1B. All tracer

injection experiments began by initially visuotopically mapping the location of the lateral geniculate nucleus (LGN) using tungsten microelectrodes (~1 MΩ, FHC) and stimulating with spots or bars of light on a tangent screen. LGN single and multi unit receptive fields were hand mapped and these data were used to estimate the relative stereotactic location of the area of interest (either in LGN or pulvinar) where the next penetration would be placed. In all but two of the hemispheres additional locations were mapped until a location was found that represented central vision. After a desirable location was found the electrode was retracted and an injectrode (made in house using 2-4 MΩ tungsten microelectrodes joined with a glass pipette with a tip diameter of 15-30 μm fitted with a plunger) was inserted at the location of the previous penetration. The injectrode was used to confirm the visuotopic location using either multiunit or single unit recording. This location was then injected with tracer. There were three hemispheres where this procedure was not followed. In the first case after the initial LGN visuotopic mapping penetration the pulvinar and LGN were injected without further electrophysiological mapping. In the second case the sterotaxic coordinates from one hemisphere that had been mapped were used to guide injectrode penetrations and injections in the opposite hemisphere. In the last case two injectrode penetrations were made into the LGN, one guided by electrophysiological mapping and a second guided stereotaxically and using the same injectrode as the first. All injections made in the thalamus were pressure injections and in all cases silicone oil was initially pulled into the tip of the injectrode to prevent leakage of the tracer during the penetration. However, if the injectrode was used to make mulitple injections the silicone oil was not replenished between injections. Injections generally were 300 nl of tracer (although in two cases 400 or 450 nl was used) and 100-200 nl of silicone oil injected slowly over a period of ~20-30 min. The tracers used in the thalamic injections were biotinylated dextran (BDA),

dextran conjugated to Alexa-fluor 488 (dex 488) and dextran conjugated to Alexa-fluor 568 (dex 568). The dextran portion of each of these tracers had a molecular mass of 10,000 u and all were purchased from Invitrogen. All dextran based tracers were used at 10% in 0.01 M phosphate buffer (PB pH 7.35-7.45).

Following injection of the thalamus, some animals received one or more injections into V1. In 4 cases these injections were guided by prior visuotopic mapping using optical imaging, while in one case the injections were guided stereotaxically. Cases received between 1-7 injections in 1, 3 or 4 penetrations. Both pressure and iontophoretic injections were placed in V1 containing dex 568 or the plant lectin, Phaseolus vulgaris leucoagglutinin (PHAL, Vector), respectively. Iontophoretic injections consisted of 7 or 15 minutes of 7 μA current alternating at 5 sec on, 5 sec off. Pressure injections consisted of 100 to 200 nl of tracer. The majority of injections were placed between 300 and 500 μm from the cortical surface, though some injections were confirmed to be as deep as 900 μm or extended just below the surface.

Perfusion, cutting and processing

Two to four weeks after injections were placed, the animals were administered a lethal dose of sodium pentobarbital and perfused transcardially with a saline rinse followed by a fixative consisting of 3% paraformaldyhyde, 0.1% glutaraldhyde and 0.2% picric acid (saturated solution v/v) in 0.1M PB. The brain was blocked in the coronal plane at a known AP coordinate with the head in a stereotaxic apparatus, and following blocking, the brain was removed. The brain was then cryoprotected, allowing the tissue to equilibrate overnight in 30% sucrose in 0.1M PB at room temperature. The brain was then frozen on dry ice and stored until use at -70°C. All cases were cut in the coronal plane using a sliding microtome. In all except 3 cases, sections

were 40 µm thick, in the others the sections were 30 or 52 µm. In several cases some of the cut sections were processed immediately (see below); in all cases some or all sections were re-frozen in a solution of 30% glycerol in 0.1 M Tris buffered saline (TBS pH 7.35-7.45), or 30 % ethylene glycol and 30% sucrose in 0.1 M in TBS, and stored at either -70°C or -20°C respectively until processed. The processing steps resulting in fluorescent sections were typically done using TBS.

Immunohistochemistry

Two buffers were repeatedly used in the immunohistochemical processes: blocking buffer (bb), consisting of 3% normal donkey serum, 2% cold water fish gelatin, 0.1% Triton X-100 and 0.1% sodium azide in TBS, and antibody buffer (ab), consisting of 0.5% cold water fish gelatin, 0.2% Triton X-100 and 0.1% sodium azide in TBS. To visualize an antigen of interest (Vglut2, PV, or PHAL) the sections were rinsed 3 times, placed in bb for 1 hour, then placed in primary diluted with ab for 12-48 hrs (see table 1 for dilution). The sections were then rinsed 3 times in ab and placed in secondary antibody (see table 2) diluted using ab for 2 hours. The sections were then rinsed one time in ab and two times in TBS before mounting. Sections were stored in the dark at 4oC. Occasionally for ease of dilution, the Alexa-fluor secondary antibodies were used at 1:500; no difference was seen in the resulting staining and staining at the typical concentration. Primary absent controls showed a uniform lack of staining.

Antibody characterization

The mouse monoclonal anti-parvalbumin antibody is specific and does not react with other members of the EF-hand family (technical information provided by Sigma-Aldrich). As in

Primary Antibody	Type	Dilution	incubation duration	Source	Cat #	Antigen specificity
anti-vesicular glutamate transporter 2	Monoclonal	1:5000	0.5 days	Millipore	MAB5504	Rat hypothalamus (Hrabovszky et. al. 2006), grey squirrel thalamus and superior coliclous (Baldwin et. al. 2011), Rat cortex (Fremeau et. al. 2001)
anti-parvalbumin	Monoclonal	1:1000	1-4 days	Sigma	P3088	Rat cortex (Celio, 1990; Kawaguchi and Kubota, 1997)
anti-*Phaseolus vulgaris* leucoagglutinin	Polyclonal (rabbit)	1:2000	1.5 days	Vector	AS-2300	N.A.

Table 1. Primary Antibodies

Secondary antibody	type	Dilution	Source	Cat #
Alexa-fluor 488	Donkey anti-rabbit	1:400	Invitrogen	A10042
Alexa-fluor 568	Donkey anti-rabbit	1:400	Invitrogen	A21206
Alexa-fluor 647	Donkey anti-mouse	1:400	Invitrogen	A31571
DyLight 698	Donkey anti-mouse	1:500	Jackson	715495-150

Table 2. Secondary Antibodies

all other species examined PV morphologically identifies specific classes of cells in bush baby thalamus and cortex (Johnson and Casagrande, 1995; Wong and Kaas, 2010).Staining using anti-PHAL (table 1) and the procedure above failed to result in stained processes in control sections lacking PHAL indicating primary antibody specificity.

In western blots of bush baby cerebellum and V1 tissue, the mouse monoclonal anti-Vglut2 recognizes a single band at 56kDa, the expected molecular weight (technical information provided by Millipore; Balaram, 2012 personal communication). This antibody shows that this protein is distributed in a similar way in the cortex of tree shrew, bush baby and macaque monkey suggesting that the same protein is being recognized across these distantly related species (Balaram et al., 2011; Hackett and de la Mothe, 2009; Wong et al., 2009; Wong and Kaas, 2010).For all combinations of primary and secondary antibodies used, omission of the primary antibody resulted in a complete lack of staining indicating specificity of the secondary antibodies.

Visualization of dextran based tracers and cytochrome oxidase (CO)

Dex 568 and dex 488 could be visualized after cutting without additional processing. To visualize BDA, sections were placed in 1:400 or 1:500 Streptavidin Alexa-fluor 488 or Streptavidin Alexa-fluor 568 (Invitrogen) for two hours then rinsed three times in TBS, mounted and coverslipped with Vectashield (Vector Laboratories Inc.). CO staining was done using methods described previously (Boyd and Matsubara, 1996).

Identification and reconstructions of injection and projection sites

Cases were considered successful if injections were localized to the areas of interest and injections produced projections dense enough to clearly reveal what cortical layer the projection targeted. In all successful cases an initial set of sections (every 3rd section in 2 cases, or every 6th section for all other cases) was developed for the tracers injected into that case. Then these sections were inspected in series for the injection sites and their extent, and the locations and extents of axon terminations, centers of most dense projection and regions where axonal projections in V2 from pulvinar and V1 came into close proximity or overlapped. To determine the laminar and nuclear (thalamus) locations of the fluorescent injection and projection sites, a series of adjacent sections were reacted to visualize CO and this set used to confirm areal borders and to align bright field images of CO sections with fluorescent micrographs of injection and projection sites (using Photoshop) so that placement could be confirmed.

Selection of sections analyzed

After an initial survey of sections was taken (see above), sections (either from the initial series of sections or from sections reacted subsequently) were chosen for further analysis using confocal microcopy at high power (63X of 1.4 numerical aperture). Sections chosen were for one of two types of analysis, either co-localization analysis (to determine if projections to V1 or V2 co-localized with parvalbumin or Vglut2), or bouton size analysis (to determine the size of boutons on projections to V1 or V2). Sections selected for co-localization analysis of Vglut2 or parvalbumin with a projection of either V1-V2, pulvinar-V2 or LGN-V1 had good staining in expected areas (layer IV of V1 for Vglut2 and many stained cells and processes through the cortex for parvalbumin) and sufficient density of the axonal projections of interest so that

multiple axons in layer IV could be sampled. These samples were chosen from at least two cases for each projection type (V1-V2, pulvinar to V2 or LGN to V1). Except in two cases, sections were chosen for bouton size analysis because they had low background staining and contained the densest center of the projection foci. In the remaining two cases, sections were chosen for bouton size analysis because they had low background staining and contained an area where projections from pulvinar and V1 came into close proximity to each other (< 40 μm), and had a significant numbers of boutons.

Microscopy and image analysis

Images were collected using bright field, fluorescent and confocal microcopy. A Zeiss LSM 510 confocal microscope with a motorized stage was used to montage a large portion of the sections so that areal and layer data could later be confirmed by alignment with an adjacent CO section. When data pertaining to Vglut2 or parvalbumin were collected, location within the cortical layers was determined by eye at the time of image acquisition from low power fluorescent micrographs of the area of interest. Images for bouton analysis were aligned with a montaged image of the fluorescent section and with a CO section so that a more exact estimation of the layers could be made. Alignment of sections was performed in Photoshop using the vasculature and the outline of the edge of the sections. Levels were adjusted in all photomicrographs subsequently displayed.

Bouton size analysis

High power confocal stacks destined for bouton size analysis were, in most cases, taken from the center of projection foci or in two cases from areas where projections from pulvinar and

V1 came into close proximity to each other (< 40 μm). In three cases the stack collected contained many more boutons than needed for analysis (as determined by eye), and in these cases analysis was limited to a cube centrally located in the stack, drawn by eye, and containing ~ 50% of the volume of the stack. Once high power stacks had been obtained, they were converted to grey scale and given to a naive observer who was instructed to pick out boutons. Boutons were defined as enlargements on axon shafts or terminals that were larger than the local average width of the axon and did not occur at points where the axon branched. Once the observer had selected the boutons for analysis, the stack was transferred into Metamorph (Molecular Devices). To measure the area of a given bouton inside Metamorph, first the brightest point within the bouton was found, then working within that plane of the stack, the image was thresholded at half the intensity level of the brightest point and the software was used to automatically circle the thresholded area and record the result. This process was repeated until all the boutons in a stack or designated sub-region were measured. This process is the areal analog to measuring full width at half maximum. If a bouton had a maximum intensity at or above the saturation point of the intensity range, that bouton was excluded from analysis. Such exclusions, however, happened infrequently because during the collection of the high power stacks destined for bouton size analysis, care was taken to minimize the number of pixels that were at saturated intensity within the axons.

During analysis the data were double checked to make sure that no areas were measured that exceeded the limit of the microscope's resolution. The theoretical limit of lateral resolution was calculated using equation 1 where r is the lateral resolution and λ is the wavelength of the light measured and N.A. is the numerical aperture of the objective (see http://www.olympusconfocal.com/theory/resolutionintro.html for more information).

Equation 1: $r = 0.4 \lambda / N.A.$

In our case λ is either 488 nm or 547 nm and N.A. is 1.4. The lateral resolution was then treated at the radius of a circle and the area of the resulting area of the circle was calculated and compared against the data. No datum was smaller than the area of the circle for the wavelength of the light measured.

In practice the resolution limit of a microscope should be determined experimentally. The management at the Vanderbilt Cell Imaging Shared Resources Core has measured the full width at half maximum resolution in the systems we used to be approximately 300 nm. When extrapolated into two dimensions a radius of 150 nm yields a circle with an area of approximately 0.07 μm2. No data measured were equal to or smaller than this area.

Co-localization analysis

To quantify the portion of Vglut2 or PV containing boutons in a population, 2 stacks for each projection type (LGN to V1, V1 to V2, pulvinar to V2) containing the greatest density of projections from two separate cases were chosen from the volume of data that had already been collected. In stacks used to quantify PV only the first 10 (3.41um) optical sections beginning at the tissue surface were used for the analysis. This was done because of PV signal drop off deeper in the tissue. Then each bouton within each stack was ranked on a scale of certainty of overlap with 3 categories: clearly co-localizing, clearly not co-localizing, and uncertain degree of co-localization.

Statistics

The bouton areas for each projection type (LGN to V1, V1 to V2, pulvinar to V2) in each case were considered as a single sample. Each sample was tested to see if it violated the assumption of being normally distributed using Lilliefors test (Matlab on line documentation, MathWorks Inc.). Only 2 of the 11 samples were not normally distributed ($p<0.05$), hence we have assumed for statistical comparison that the data are normally distributed but provide both means and medians for the 2 samples that were not normally distributed. In sample pairs where a t-test was to be performed, a two sample F-test was first administered. If the F-test was significant ($p<0.05$) then the samples were subsequently compared using a Student's t-test; otherwise the samples were compared using Welch's t-test. A uniform α level of 0.05 was adopted except in the case of multiple t-tests performed after an ANOVA in which case the α level (0.05) was corrected using the Bonferroni method where the α level is divided by the number of possible comparisons (in this specific case 6) before it was compared with the p-value obtained. The variability of all samples is reported as standard errors of the mean (SE).

Results

Thalamic injections

Nine successful pulvinar injections were made in 6 cases. Reconstructions of these injections showed that the sizes of these injections varied between 350 and 1100 μm in diameter and tended to be wider in the dorsal/ventral than in the other two dimensions. In each penetration, either one or two injections were made in the Pulvinar. In the cases where a second injection was made, it was always in the same penetration as the first. Figure 2 shows a typical

single injection in the lateral pulvinar. Injections were always located at or above the level of the brachium of the superior colliculus, which has traditionally been used to architectonically subdivide the lateral or superior pulvinar from the inferior pulvinar in bush baby (Diamond et al., 1992; Glendenning et al., 1975; Kaas and Lyon, 2007; Raczkowski and Diamond, 1980; Raczkowski and Diamond, 1981; Stepniewska, 2004; Symonds and Kaas, 1978; Wong et al., 2009). Pulvinar neural responses measured at the tip of the injectrode prior to the injection showed that the ventral injection was made at a visuotopic location within 20 deg of area centralis (AC). Within the injected part of pulvinar, there are two retinotopic maps (Li et al., 2011), one dorsal and one ventral, which are joined at their central vision representation at the vertical meridian. All of the injections were made at or dorsal to the most central point in the penetration. Histological analysis of the injections suggested that the center of the injection site tended to fall slightly dorsal to the end of the injectrode track, likely indicating a tendency for the tracer to pool in the space above the tip. Therefore, although involvement of the ventral map cannot be excluded, the bulk of our projections come from the dorsal map within PL. In all cases selected for further analyses (see Methods), a large number of brightly labeled cells (see Figure 2) were seen in the pulvinar, with a significant number of clearly labeled axons leaving the pulvinar. Furthermore, in all of these cases, only a few scattered cells along the injection track were seen to have taken up the label and none of these appeared to have labeled axons.

Successful BDA injections into the LGN were placed at 8, 12-15 and ~20º eccentricities in 2 cases. Two injections involved all layers (see Figure 2), while one involved the medial aspect of M layers alone. All injections resulted in a large number of brightly labeled LGN cells (see Figure 2) with significant numbers of axons leaving the LGN.

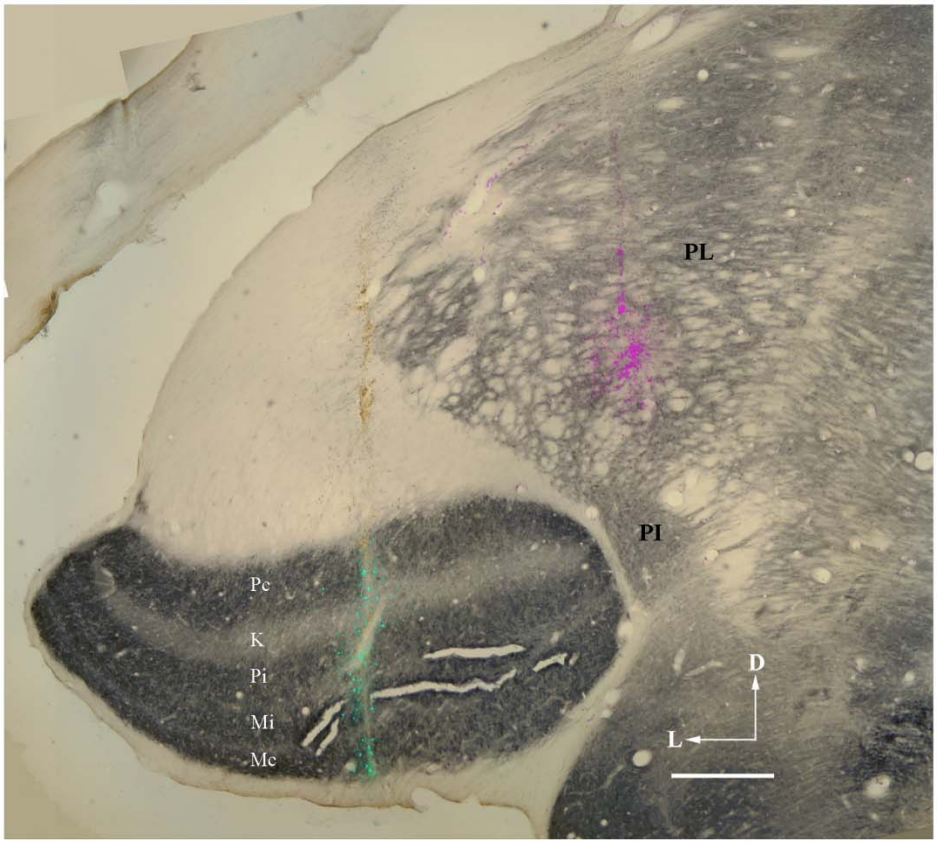

Figure 2.
A coronal cytochrome oxidase (CO) section through the thalamus showing examples of injection sites in lateral geniculate nucleus (LGN) (green, biotinylated dextran [BDA]) and pulvinar (magenta, dextran conjugated to Alexafluor 568 [dex 568]) taken on the same section as a fluorescent image prior to CO staining. The LGN injection in this case involved all layers. The pulvinar injection was centered on the central vision representation in lateral pulvinar (PL). M, magnocellular; P, parvocellular; K, koniocellular; c, contralateral; i, ipsilateral; PI, inferior pulvinar; PL, lateral pulvinar; D, dorsal; L, lateral. Scale bar = 500μm.

V1 injection sites

Nineteen injections were made in V1 in 5 cases. Complete reconstructions of these fluorescent injections and comparison with adjacent sections stained for CO showed that they were 120-400 μm in size and were centered in different layers of V1 mainly in layer III and were always confined to V1 based on the density of CO staining in layer IV and the presence of CO blobs in layer IIIB. Injections into V1 were all placed within the area representing 10º of AC as evidenced by both the OI data used to place the injection (Figure 3A) and by comparison with past mapping studies of V1 in the bush baby (DeBruyn et al., 1993; Xu et al., 2007; Xu et al., 2005). An example of a superficial injection is shown in Figure 3B. These injections resulted in dense labeling in V2. One or two injections were placed per penetration. Most injections were centered on the superficial layer as shown in Figure 3B although, when multiple injections were made in the same penetration, deep layer involvement was common.

Pulvinar projections to V2

Projections from PL were seen in the temporal, parietal and occipital cortices (data not shown). The bulk of these projections were to cortical layers III and IV except in area V1 where there were sparse projections to layers III and IV and dense projections to layer I. For this study, we focused on PL projections to area V2. Projections outside of area V2 will be considered in future studies. V2 received strong projections from the pulvinar, and like other areas of the extrastriate cortex, the bulk of the projections running to V2 terminated in layers III and IV (see Figure 4A), with the area of greatest density in layer IV. Projections from the pulvinar tended to be organized in a columnar manner, particularly in layer III where they were almost always oriented perpendicular to the laminar structure. In addition, patchiness was observed in the

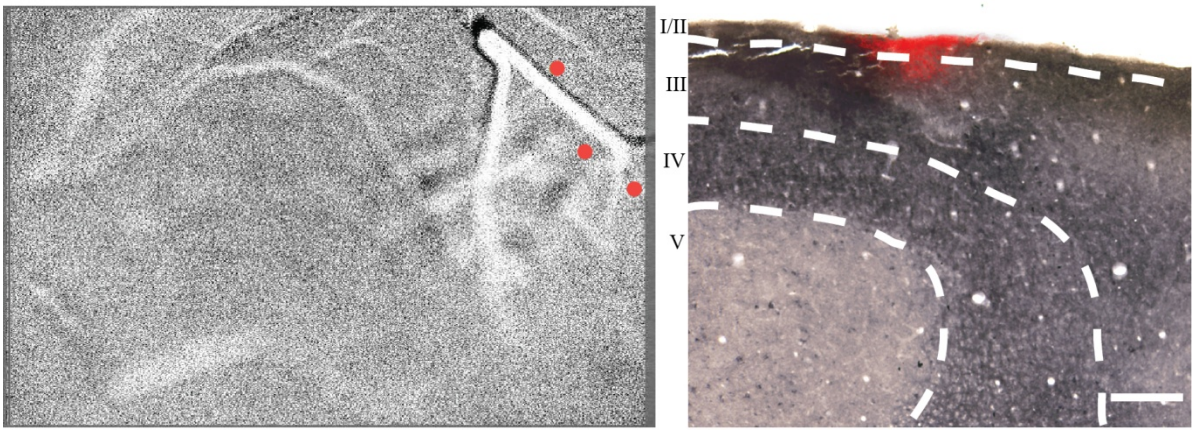

Figure 3.

(A) Differential optical imaging of primary visual cortex (V1) viewed from the surface showing the activation resulting from the presentation of orthogonal drifting square wave gratings limited to a 5º circular window placed on *area centralis* (AC). This differential image allowed us to place the plant lectin *Phaseolus vulgaris* leucoagglutinin (PHAL) injections (red dots) near central vision. Scale bar = 2.75mm. (B) An example of an injection site (red) shown on a CO stained section. Since AC is represented laterally in V1 of bushbaby this section shows a slightly tangential view of the layers. CO blobs (arrow) can also be seen in layer III in the section. Scale bar = 250µm.

projections from the pulvinar to the cortex, with one or two injections leading to 3-5 patches of projections. Curiously, the distinctness of the patches varied from case to case, and no correlation between the distinctness of the patches and the placement of the injections in the pulvinar was observed. In areas where the projections from the pulvinar were densest, a layer I projection also was observed. The layer I projection tended to emanate from the top of the densest parts of the projections in the layers below and then spread out, running parallel to the laminar structure of the cortex within layer I.

V1 projections to V2

Projections from V1 were observed in V2 as well as in an area anterior to V2 assumed to be V3 (see Fan et al., 2012 for review). In both areas, the bulk of the projections terminated in layers III and IV (see Figure 4B), with the area of greatest density in layer IV. In this respect, the projections from V1 to V2 were similar to those from pulvinar to V2, however, two subtle differences were observed at low power. First, pulvinar projections to layer III of V2 tended to extend in a more radial fashion than V1 projections. Second, no V1 projections were observed in layer I of V2 whereas pulvinar projections to the same layer were repeatedly observed. This latter difference could be due to the fact that individual injections in V1 were smaller than those in the pulvinar, yielding a less dense overall projection pattern.

LGN projections to V1

Figure 4C shows dense layer IV projections from the LGN to V1 as has been widely reported (see Casagrande and Kaas, 1994 for review). We observed these projections in both layer IVα and layer IVβ indicating the involvement of both M and P pathways (Florence and

Casagrande, 1987). Sparse projections of small caliber axons also were observed in layers III and I confirming involvement of the K layers.

Quantitative comparisons of projections to V2

Figure 5A shows projections from V1 (green) and pulvinar (magenta) in close proximity within the same flattened confocal stack taken from layer IV of V2. Both projections have similar fine morphology with many en passant (beads on a string) boutons and occasional stalk-like boutons. As seen in Figure 5A, axons and boutons tended to be larger in projections coming from the pulvinar. Figure 5B shows a quantification of bouton sizes for pulvinar and V1 in three cases. In case 09-02, pulvinar boutons (n=24) had a mean area of 0.52 μm2 (±0.04 SE) and V1 boutons (n=52) had a mean area of 0.39 μm2 (±0.03 SE) and a median of 0.33 μm. In case 09-07, pulvinar boutons (n=36) had a mean area of 0.46 μm2 (±0.03 SE) and V1 (n=8) boutons had a mean area of 0.21 μm2 (±0.03 SE). In case 09-08, pulvinar boutons (n=27) had a mean area of 0.44 μm2 (±0.03 SE) and V1 boutons had a mean area of 0.34 μm2 (±0.03 SE). In each case, the difference between the size of V1 boutons and pulvinar boutons was found to be significant ($p < 0.05$) using Student's t-test in cases 09-02 and 09-08 and using Welch's t-test in case 09-07 (because samples were shown to have unequal variances, see Methods). Boutons measured in cases 09-07 and 09-08 were taken from locations where the axons from V1 and pulvinar innervated the same region of V2 (in areas such as the one pictured in Figure 5A). Therefore, the difference in bouton size is not the result of the two projections to V2 representing different eccentricities. The boutons in case 09-02, however, were taken from non-overlapping projection centers located ~3mm apart thus indicating that the size differences are not specific to the cortical locations where projections overlap.

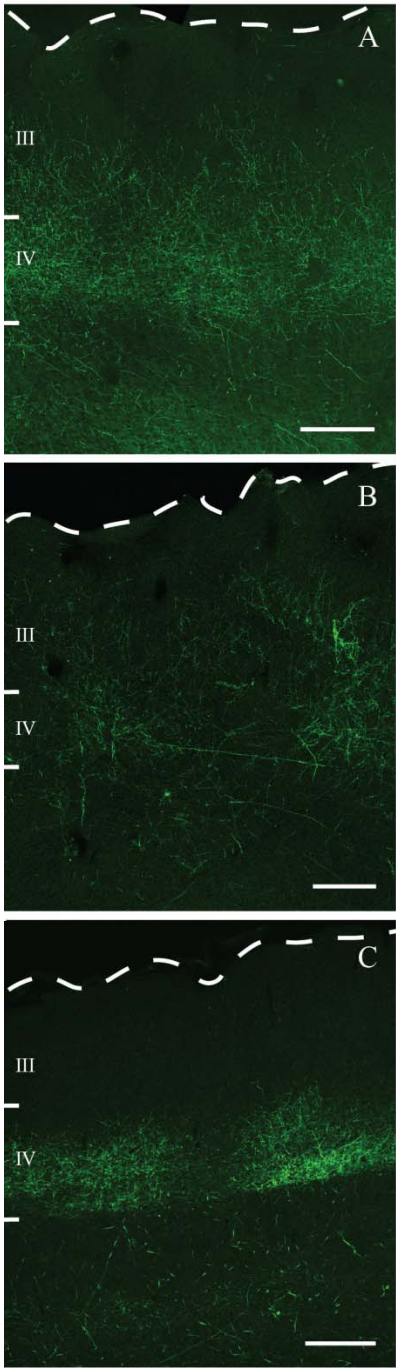

Figure 4.

Confocal photomicrographs of projections (green) to secondary visual cortex (V2) from pulvinar (A) and V1 (B) and from the LGN to V1 (C). Comparison of these projection patterns shows that all projections are centered in cortical layer IV but show different overall patterns of termination within layer IV and the other layers. Note that the LGN injection in this case was restricted to the ipsilateral parvocellular (P), koniocellular (K) and magnocellular (M) LGN layers given that ocular dominance columns can be seen clearly throughout the depth of layer IV. The K layer projections to layer III blobs and layer I of V1 were not present in this section. Images A and B are taken from a part of V2 on the dorsal surface of the cortex while image C is taken from a part of V1 near the posterior pole located on the ventral surface of the brain. In image A and B dorsal is towards the top and lateral is towards the left. In image C dorsal is towards the bottom and lateral is towards the right. See text for details. Scalebars = 200μm

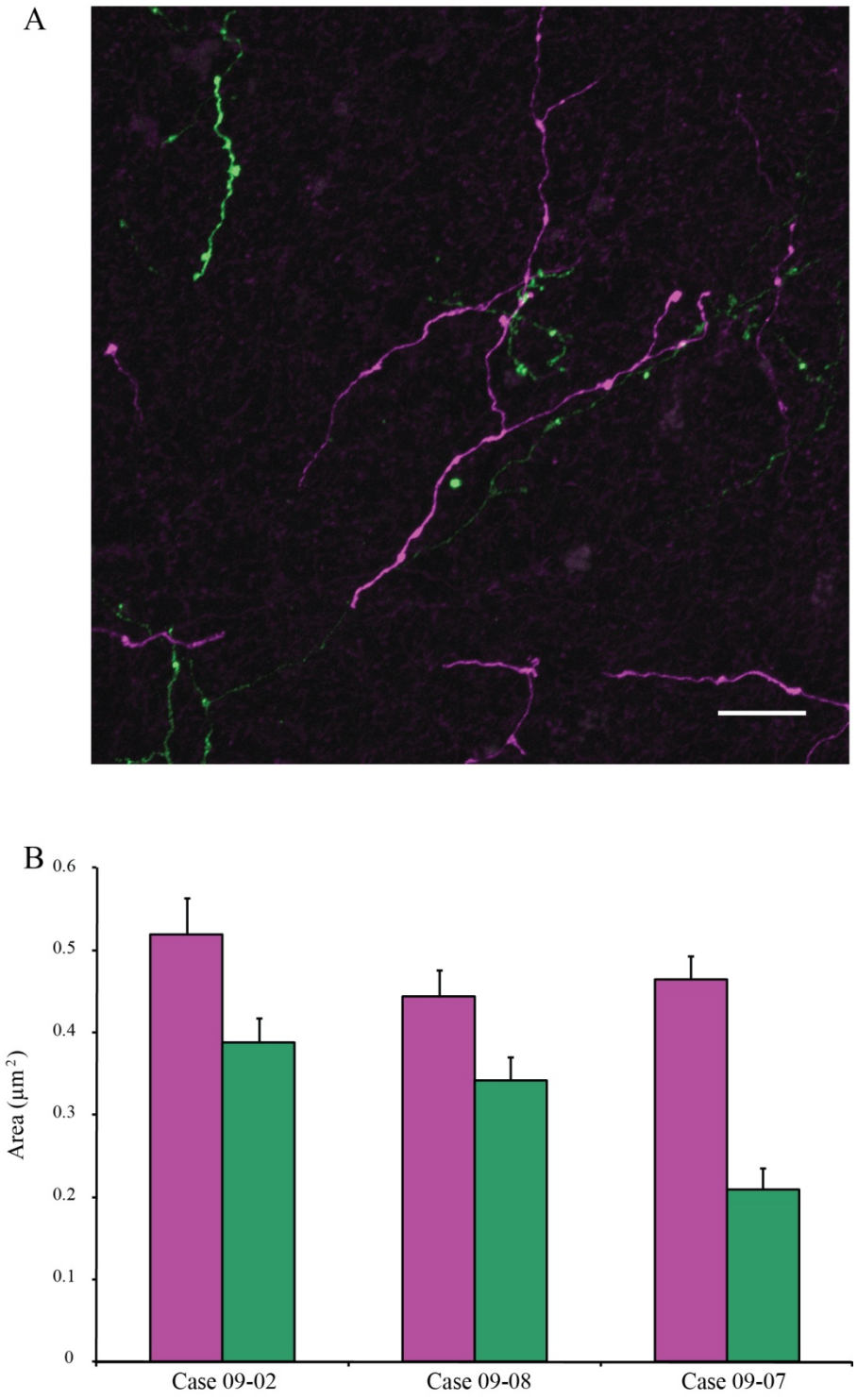

Figure 5.
Pulvinar boutons were larger than V1 boutons in V2. (A) Boutons in V2 from the pulvinar (magenta, BDA) and V1 (green, PHAL) shown in a high power confocal photomicrograph (scale bar = 10 µm, flattened stack). (B) The cross-sectional areas of boutons on projections from pulvinar (magenta) and V1 (green) to V2 were quantified in three cases. A t-test revealed that the pulvinar boutons were significantly larger in every case ($p < 0.05$).

Quantitative comparisons of projections from LGN to V1

In order to compare our findings in V2 to known thalamocortical driving projections, we examined the projections from the LGN to layer IV of V1. Figure 6A shows large en passant boutons in layer IVα (IVCα of Brodmann, 1909) of V1 resulting from a BDA injection in the LGN. Boutons areas in layer IVα (M cell projections) and layer IVβ (P cell projections) were quantified and compared to bouton areas of pulvinar and V1 projections to V2 (shown in Figure 5B). As Figure 6B depicts, M boutons in V1 (n = 110 from 2 cases) were found to have a mean area of 0.70 μm2 (±0.03 SE) while P boutons in V1 (n = 41 from 1 case) were found to have a mean area of 0.52 μm2 (±0.03 SE) and a median of 0.52 μm2. We compared these results with the findings of bouton areas in V2 depicted in Figure 5B; as seen in Figure 6B. When collapsed across three cases, pulvinar boutons (n=87) had a mean area of 0.47 μm2 (±0.02 SE) and V1 boutons (n=88) had a mean area of 0.36 μm2 (±0.02 SE). A one-way ANOVA run on the M LGN, P LGN, pulvinar and V1 bouton areas described above found significant variation ($F(3, 322) = 40.13$, $P = 0$). Student's t-tests with Bonferroni correction show that both the LGN projections to V1 and the pulvinar projections to V2 have larger boutons than the V1 projections to V2 ($p<0.05$); further, the boutons on M LGN projections to V1 are larger than boutons on both the P LGN projections to V1 and the pulvinar projections to V2 ($p<0.05$). The sizes of boutons on P LGN projections to V1 and pulvinar projections to V2, however, were not significantly different (Welch's t-test $P > 0.05$).

Control for tracer type

In the cases where boutons were quantified, the majority (14 of 16) of injections in V1were made with PHAL while all injections in the thalamus were made with dextran based

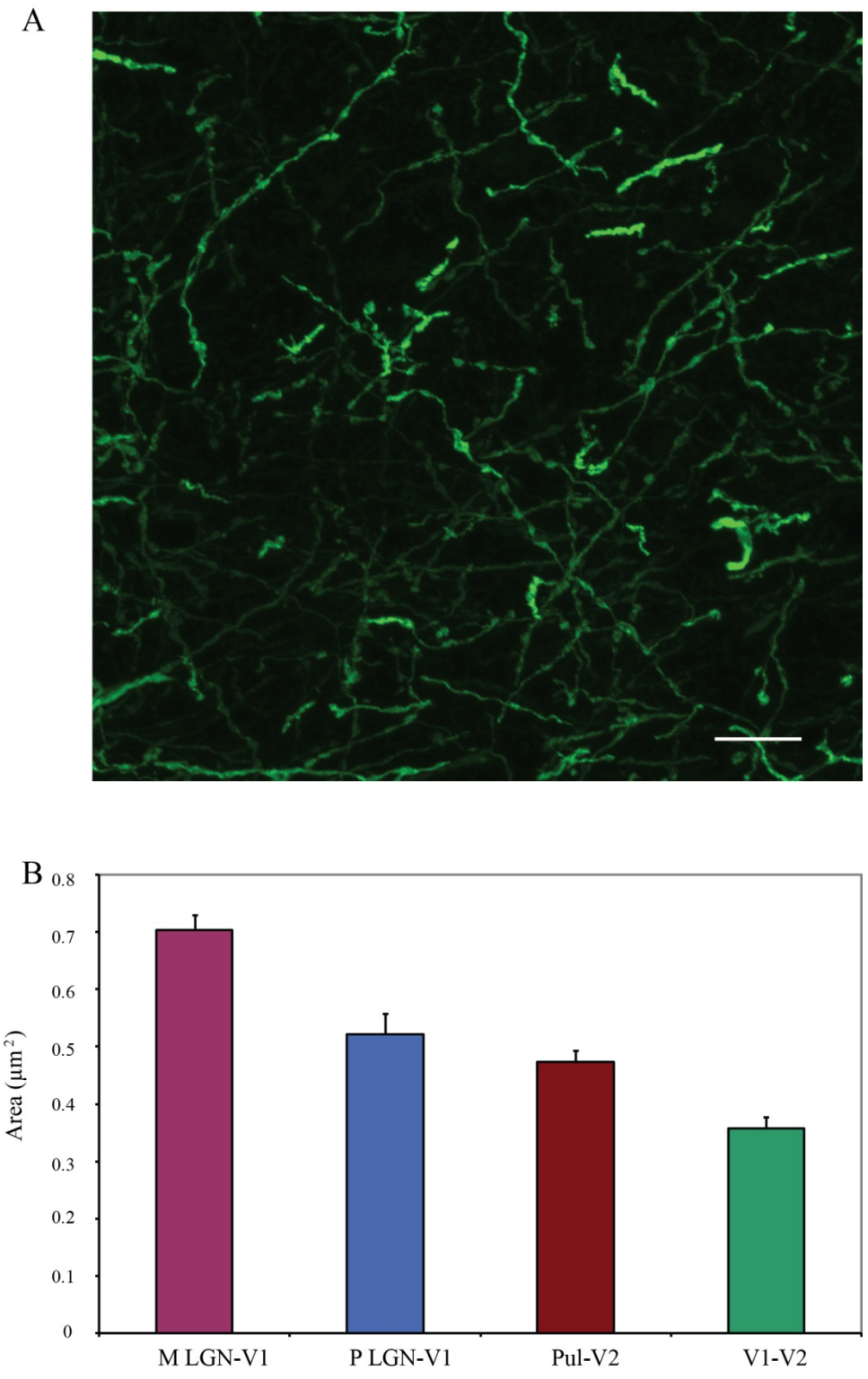

Figure 6.

LGN boutons in layer IV of V1 varied in size. Those from the M layers of LGN to IVα are shown in (A). These boutons are significantly larger than any boutons within layer IV of V2 from either V1 or pulvinar. (scale bar = 10 μm, flattened stack). (B) LGN P projections to layer IVβ of V1, however, did not differ in size from pulvinar to V2 boutons. (t-test $p > 0.05$).

tracers. To control for the possibility that tracer type might affect the measurements of bouton size, we examined a case where both dex 568 and PHAL were injected into V1 in the same area. As seen in Figure 7A, the resulting projections in V2 share the same fine morphology using either tracer type. Boutons on these projections were quantified and the results are shown in Figure 7B. The boutons on dex 568 projections (n=23) had a mean area of 0.28 μm2 (±0.02 SE) while boutons on PHAL projections (n=9) had a mean area of 0.30 μm2 (±0.02 SE). A Student's t-test showed no difference between these two populations ($p > 0.05$).

Co-localization of parvalbumin in thalamic axons

Parvalbumin has been found to co-localize with known driving axons from LGN to V1 layer IV (Blumcke et al., 1991; DeFelipe and Jones, 1991; Jones and Hendry, 1989; van Brederode et al., 1991). At low power, PV staining revealed brightly labeled cells and processes in both V1 and V2, likely due to the presence of GABAergic interneurons known to express parvalbumin (Johnson and Casagrande, 1995). These cells and processes were particularly dense in layers II, III and IV in the bush baby. Examination at high power showed that PV co-localized with projections from the LGN to V1 in layer IVα and IVβ (parts of both sub-layers are shown in Figures 8A, B, C, D). Interestingly, some geniculo-V1 processes did not contain any PV and many of those that did contain PV appeared to contain less PV (i.e. were more dimly labeled) compared to surrounding non-geniculofugal processes (presumably belonging to GABAergic interneurons). In V2, the axons from V1 (Figures 9A, B, C, D) and those from pulvinar (Figures 10A, B, C, D) rarely co-localized with PV. In order to compare the amount of co-localization seen in each projection type (LGN-V1, V1-V2 and pul-V2), we chose one confocal stack from 2 cases (see Methods) and determined for each of the boutons in a stack whether that bouton

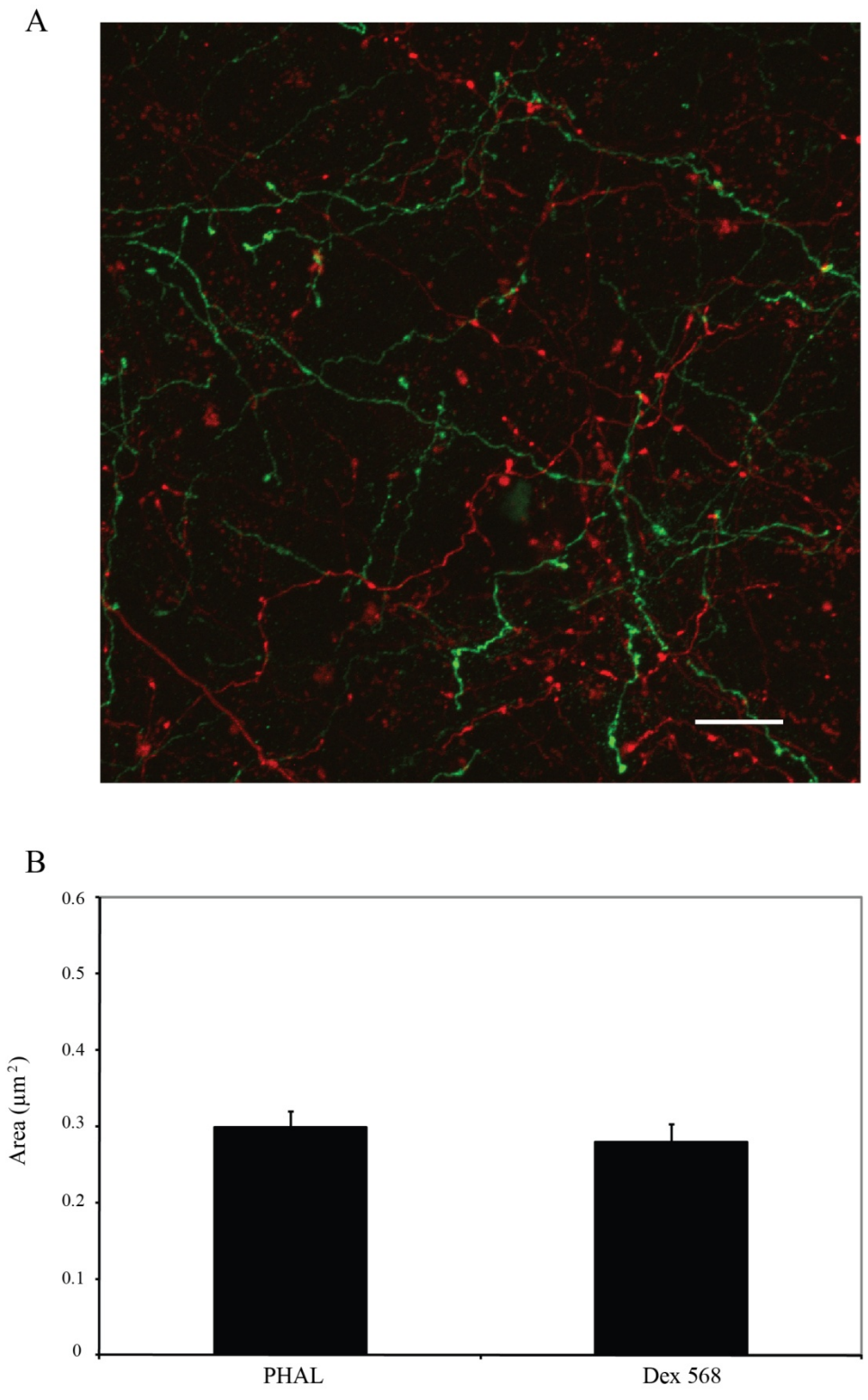

Figure 7.
Morphology revealed by dextran and PHAL tracing of the same projection is indistinguishable. (A) Projections from V1 labeled with dex 568 (magenta) and PHAL (green) in a high power confocal micrograph (scale bar = 10 μm, flattened stack) of V2. (B) The cross-sectional areas of projections from V1 to V2 traced with dex 568 are the same size as boutons on the same projections traced with PHAL (t-test $p > 0.05$).

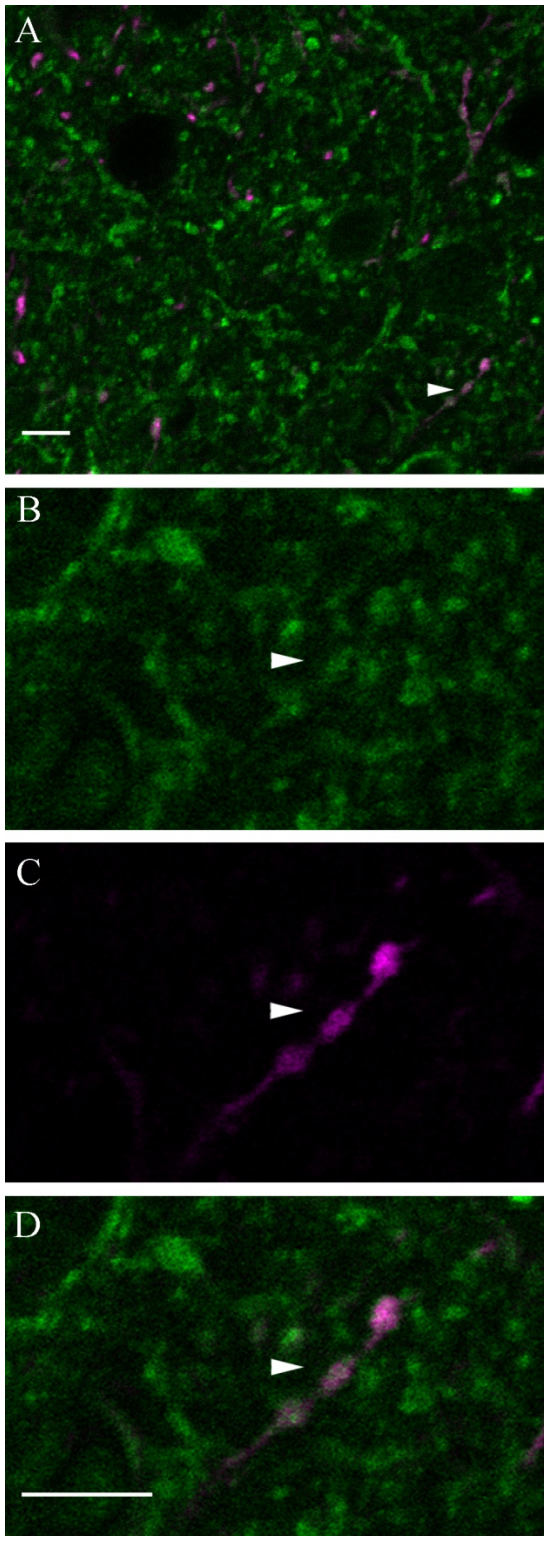

Figure 8.
Single plane confocal photomicrograph of LGN axons and parvalbumin (PV) in V1 (A). Higher magnification views from the same image (B-D) of a single axon indicated by the white arrowhead in all four panels. PV (green A, B, D) and LGN axons (Magenta A, C, D) co-localize (A, D). A striking structural congruency in the separate channels (compare B and C) was found for the majority of processes. See text for more details. Scale bars = 5 µm.

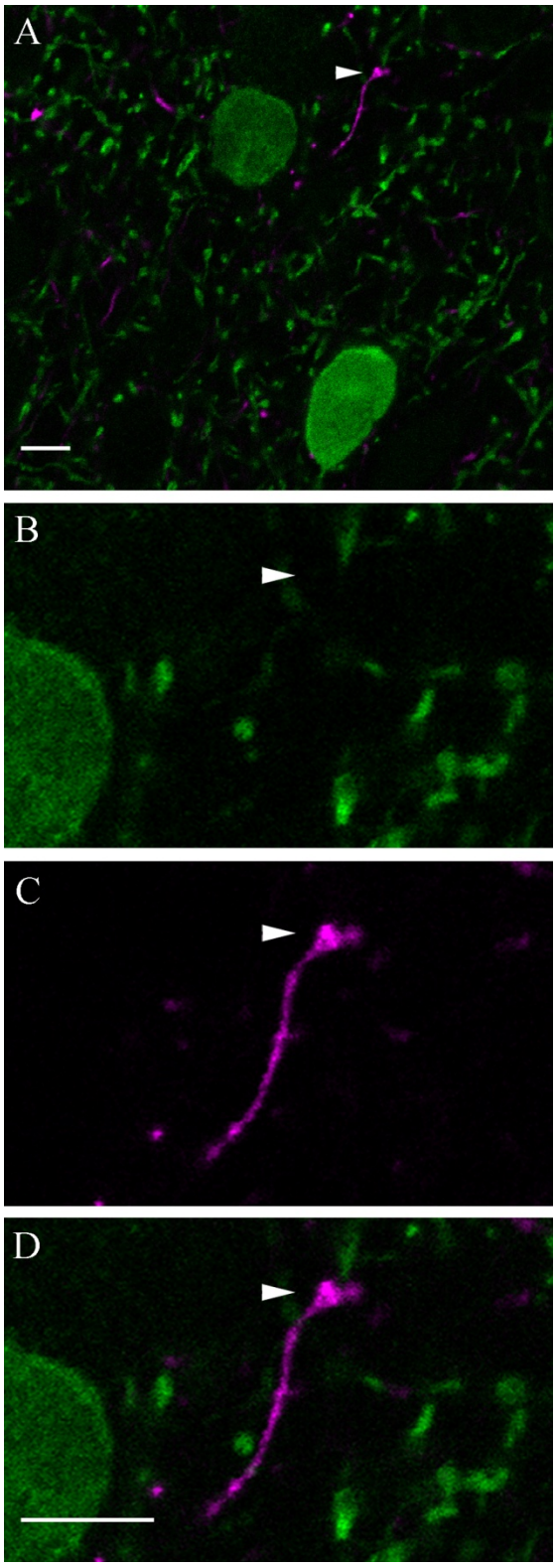

Figure 9.

Single plane confocal photomicrograph of V1 axons and parvalbumin (PV) in V2 (A). Higher magnification views from the same image (B-D) of a single axon indicated by the white arrowhead in all four panels. PV (green A, B, D) and V1 axons (Magenta A, C, D) do not co-localize (A, D). See text for more details. Scale bars = 5 μm.

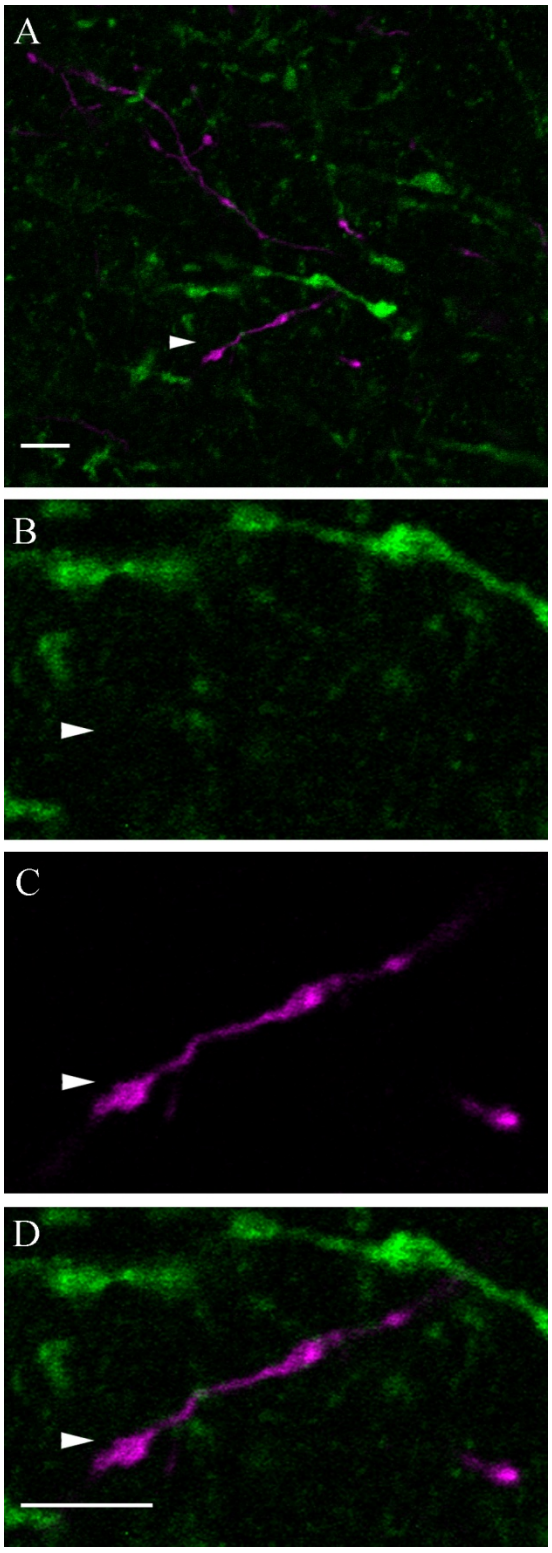

Figure 10.
Single plane confocal photomicrograph of pulvinar axons and parvalbumin (PV) in V2 (A). Higher magnification views from the same image (B-D) of a single axon indicated by the white arrowhead in all four panels. PV (green A, B, D) and pulvinar axons (Magenta A, C, D) do not co-localize (A, D). See text for more details. Scale bars = 5 µm.

co-localized with PV. Although in V1 LGN axons and boutons co-localized with PV, this analysis focused on boutons because these structures are larger and more readily resolved. Of the boutons examined on LGN to V1 projections, 78% (n=119) clearly co-localized with PV while 2% (n=3) clearly did not co-localize and a remaining 20% (n=31) of boutons examined had an ambiguous degree of overlap. These results contrast with the results of the same analysis conducted on boutons on pulvinar to V2 projections where 1% (n=1) clearly co-localized with PV while 69% (n=49) clearly did not co-localize and a remaining 30% (n=21) of boutons examined had an ambiguous degree of overlap. Similar to the pulvinar to V2 projections, in the V1 to V2 projections, 5% (n=5) clearly co-localized with PV, while 73% (n=73) clearly did not co-localize and a remaining 22% (n=21) of boutons examined had an ambiguous degree of overlap.

Co-localization of Vglut2 in thalamic boutons.

When viewed at low power, Vglut2 was seen to brightly label puncta in V1 layer IV with all other parts of V1 and V2 appearing dim in comparison. In V2, however, it was clear that layers III and IV showed increased staining compared to the other layers although this staining as mentioned, was weaker than that seen in V1 layer IV. No labeled cell bodies were observed in the cortex in any layer. Examination at high power showed that Vglut2 expressed as discreet puncta in both V1 and V2 (Figure 11 B, E, and H). In V1, Vglut2 (Figure 11B) was seen to co-localize (Figure 11C) with boutons on projections from the LGN in layer IVα (Figures 9A and C) and IVβ (not shown). In V2, boutons on axons from V1 (Figures 9D and F) rarely co-localized (Figure 11F) with Vglut2 (Figures 11E and F), while boutons on axons from the pulvinar (Figures 11G and I) frequently co-localized (Figure 11I) with Vglut2 (Figures 11H and

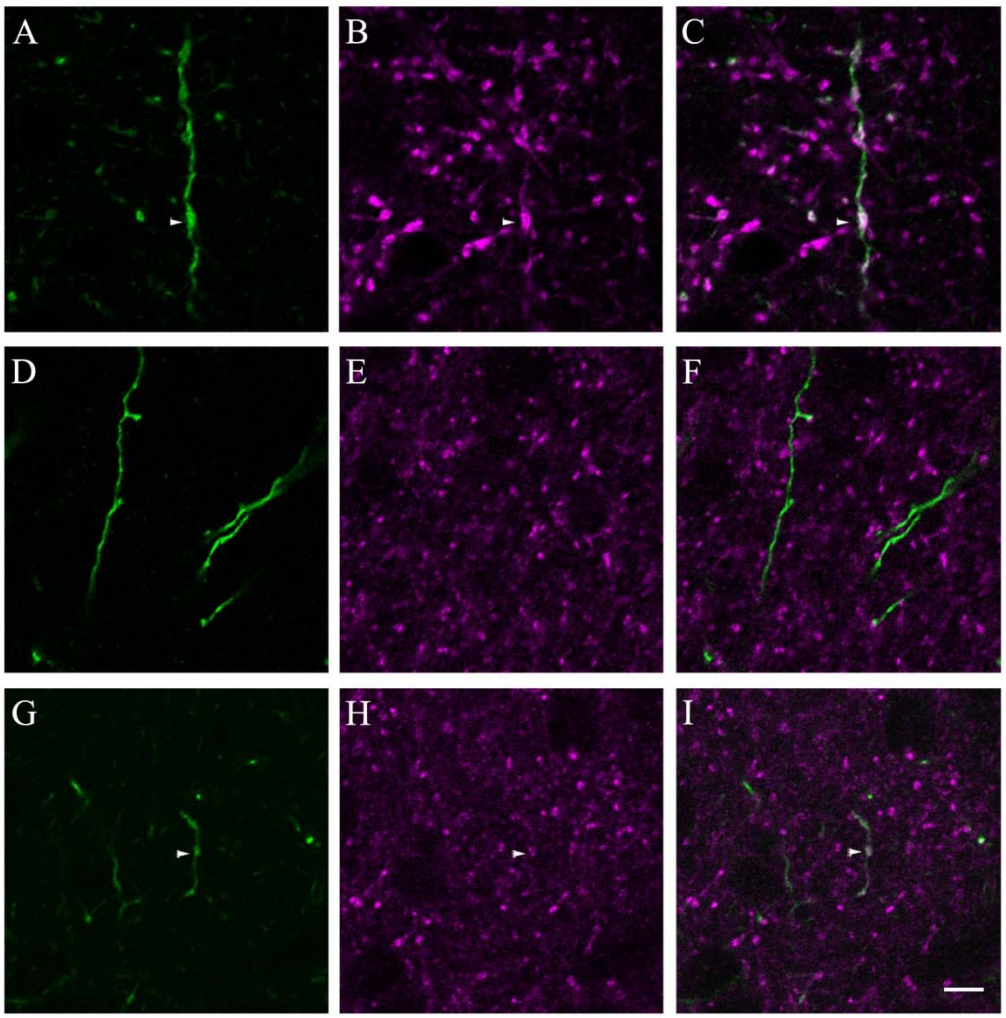

Figure 11.
LGN boutons in V1 (green, A, C) and vesicular glutamate transporter 2 (Vglut2) (magenta, B, E, F) co-localize (white, C). Similarly, pulvinar (green, G, I) boutons and Vglut2 co-localize in V2 (white, I) but V1 boutons in V2 (green, D,F) rarely co-localized with Vglut2 (F). Scale bar = 5 μm.

I). In order to compare the amount of co-localization seen in each projection type (LGN-V1, V1-V2 and pul-V2), we chose one stack from each of 2 cases (see Methods) and determined for each of the boutons in a stack whether that bouton co-localized with Vglut2. Of the boutons examined on LGN to V1 projections, 70% (n=119) clearly co-localized with Vglut2 while 12% (n=20) clearly did not co-localize and a remaining 18% (n=31) of boutons examined had an ambiguous degree of overlap. These results are similar to the results of the same analysis conducted on boutons on pulvinar to V2 projections where 60% (n=176) clearly co-localized with Vglut2 while 20% (n=58) clearly did not co-localize and a remaining 20% (n=59) of boutons examined had an ambiguous degree of overlap. Of the boutons on V1 to V2 projections, only 6% (n=3) clearly co-localized with Vglut2, while 73% (n=39) clearly did not co-localize and a remaining 20% (n=11) of boutons examined had an ambiguous degree of overlap.

Discussion

Our primary goal for this study was to examine and anatomically compare the two main inputs to bush baby visual area V2 that could serve as drivers for this area, namely, inputs from the pulvinar and inputs from V1. Since the LGN input to V1 is a known driver, we compared its key characteristics to the two potential driving pathways to V2. Our main findings were as follows: 1) both V1 and pulvinar pathways to V2 had some characteristics of driver inputs such as their relative density and terminal patterns in layer IV of V2 and 2) both V1 and pulvinar pathways to V2 were distinct from LGN to V1 layer IV inputs in several ways (see Figure 12). Both pulvinar and V1 inputs to layer IV of V2 showed irregular patches and extended densely into layer III. Also, unlike LGN projections to layer IV of V1 that contain the calcium binding

protein parvalbumin, neither pulvinar nor V1 axons in V2 contained this protein. Pulvinar axons, however, were more like LGN axons in two ways: their boutons were as large as the majority of LGN boutons, namely P boutons, and, like LGN boutons in V1, the majority of pulvinar boutons in V2 contained the glutamate transporter Vglut2. By contrast, V1 boutons were significantly smaller than either pulvinar boutons in V2 or LGN boutons in V1 and V1 to V2 boutons rarely showed any evidence of Vlgut2.

Below we consider the significance of these results in light of findings of others and in light of the Sherman and Guillery (1998) hypothesis that higher order thalamic nuclei could act as drivers of extrastriate cortex.

Laminar organization of inputs to V2

Others have shown in simian and prosimian primates that the primary inputs to V2 are from V1 and pulvinar and that these inputs end principally in V2 layer IV and lower layer III (Adams et al., 2000; Collins et al., 2001; Cragg, 1969; Cusick and Kaas, 1988; Felleman and Van Essen, 1991; Gattass et al., 1981; Kaske et al., 1991; Kennedy and Bullier, 1985; Kuypers et al., 1965; Lund et al., 1981; O'Brien et al., 2001; Preuss et al., 1993; Rockland and Pandya, 1979; Shipp, 2003; Sincich and Horton, 2002; Tigges et al., 1973; Wong et al., 2009; Zeki, 1969; for reviews see Casagrande and Kaas, 1994; Kaas and Lyon, 2007). Additionally, bush baby V2, like V2 in other primates gets a variety of inputs from higher order cortical visual areas including MT, V3, the dorsal medial area (DM/V3a) and the dorsal lateral visual area (DL/V4) among others as well as other subcortical sources (Casagrande and Kaas, 1994; Collins et al., 2001). The latter inputs, however, do not uniquely target layer IV and tend to terminate above and below layer IV (see Felleman and Van Essen, 1991 for review). Most of these inputs are far less

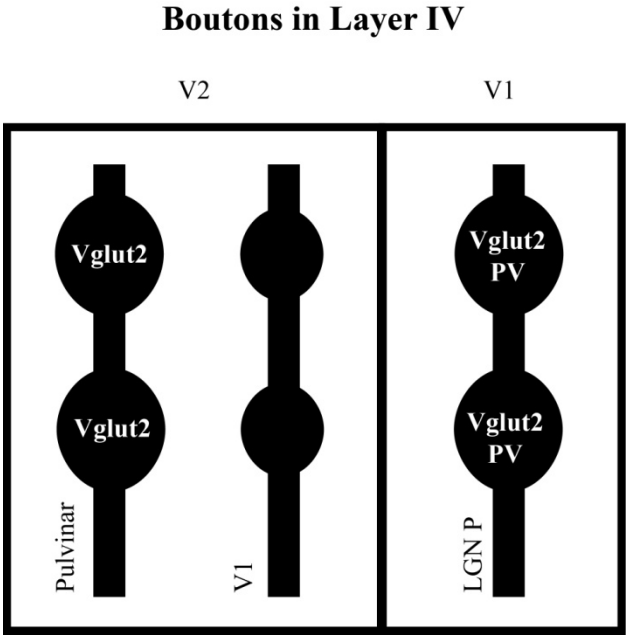

Figure 12.
Schematic summary of the main results. Axons with two boutons each from pulvinar and V1 in layer IV of V2 are shown on the left and an axon with two boutons from a P LGN cell in layer IV of V1 is shown on the right. The LGN boutons contain both PV and Vglut2, the pulvinar boutons contain only Vglut2 and the V1 boutons contain neither protein. See text for details.

dense in their distribution than either input to V2 from pulvinar or from V1 (Sincich and Horton, 2002). V2 of bush baby also shows a similar second order visuotopic organization to that seen in simian primates (Rosa et al., 1997; Xu et al., 2007; Xu et al., 2005). One difference that has been noted between prosiman bush babies and simian primates is in the compartmental organization in V2 which does not appear to exhibit clear thick and thin stripes as defined by CO or areas of weak orientation selectivity as seen in simian primates (Collins et al., 2001; Condo and Casagrande, 1990; 2007; Xu et al., 2005). Nevertheless, studies of the cortical connections of V2 in bush baby have reported clear evidence of a compartmental organization in V2 based on retrograde labeling following tracer injections into a variety of visual areas (Boyd and Casagrande, 1999; Collins et al., 2001). In our material we found clear regions of overlap between boutons from pulvinar and V1 in layer IV of V2 but also regions without overlap. No differences were noted between regions where these inputs overlapped and where they did not but we cannot rule out the possibility that one or the other input dominates functionally in specific compartments of V2 especially since our data show a patchy pattern of input to V2 from either pathway. Previous studies in macaque and squirrel monkey have demonstrated that pulvinar projects most densely to the CO dark stripes (both thick and thin) with very little input between these zones (Adams et al., 2000; Curcio and Harting, 1978; Levitt et al., 1995; Livingstone and Hubel, 1982; Ogren and Hendrickson, 1977; Sincich and Horton, 2002; Wong-Riley, 1977; Wong-Riley and Carroll, 1984) and data in several simians have document functional differences between V2 compartments although not a property that unifies the CO thick and thin stripes (see Roe and Ts'o, 1995 for review). Therefore, it remains possible that both V1 and pulvinar drive V2 but that they dominate in different compartments for functional reasons that remain to be elucidated.

Bouton Size

Increased bouton size has been has been correlated with an increased amount of release machinery associated with transmitters and is presumed to cause a greater post synaptic effect (Pierce and Lewin, 1994). Further, in comparisons between retino-geniculate and cortico-geniculate inputs, larger boutons have been found on the driving retino-geniculate afferents (see Sherman and Guillery, 1996 for review) while corticogeniculate afferents clearly act as modulators of the main message. Prior work in macaque monkey already had suggested that lateral pulvinar axons in V2 had larger boutons than boutons on axons from V1 in V2 (Rockland et al., 1999). These qualitative observations, however, were never quantified and came from different cases where injections were not matched for visuotopic eccentricity. Therefore, in the latter study it was never certain whether the differences seen could also reflect known differences related to visuotopy in V1 and V2 (Tootell et al., 1988; Vanduffel et al., 2002; Xu et al., 2007). Controlling for these factors, we quantitatively showed that boutons on pulvinar axons in V2 in bush baby are significantly larger than boutons on axons from V1, confirming and extending the earlier observations in macaque monkeys. When we compared the boutons found in V2 to those present on geniculo-cortical projections, we found that boutons on axons from pulvinar were similar in size to boutons on P LGN axons in layer IV of V1, although both populations were significantly smaller in size than boutons found on M axons in layer IV of V1. Our confocal finding that the M axons have larger boutons than those found on P axons also confirmed prior ultrastructural measurements made in the macaque and cat (Freund et al., 1989; Freund et al., 1985). Our findings also show that boutons on LGN to V1 projections are larger than those on V1 to V2 projections as would be suggested by comparing the work of Anderson and Martin (2009) to the work of Freund et al. (1989).

Neurochemical Content of Boutons

Parvalbumin has been shown to co-localize with geniculo-cortical projections (Blumcke et al., 1991; DeFelipe and Jones, 1991; Jones and Hendry, 1989; van Brederode et al., 1991). Our data show that, as in macaque monkeys, parvalbumin is located in the M and P LGN axons in layer IV of bush baby. Parvalbumin also is found in axons from relay cells in the medial geniculate nucleus projecting to A1 and in axons from cells in the ventrobasal nucleus projecting to S1 (Jones and Hendry, 1989; Wong and Kaas, 2010). Correlative studies using single labeling of axons and PV also have suggested that PV could occur in axons between thalamus and motor cortex (Melchitzky et al., 1999). Most of this protein, however, is found in the cell bodies and processes of interneurons in V1 and other cortical areas both in bush babies and other primate species (see Johnson and Casagrande, 1995). Also, interestingly, the calcium binding content of thalamic cells is not necessarily reflected in their axon content since koniocellular LGN relay cells contain calbindin and project to the CO blobs of V1, but the CO blobs clearly contain the highest amount of parvalbumin while the interblobs contain higher amounts of calbindin (Blumcke et al., 1991; Johnson and Casagrande, 1995). In both of the latter cases the density differences of these calcium binding proteins is reflected in the processes of cortical interneurons, not direct projections from thalamus. Therefore, the presence of the calcium binding proteins parvalbumin and calbindin in excitatory thalamic relay cells does not always correlate with the presence of this protein in their axons nor its cortical distribution in interneurons (see also Negyessy and Goldman-Rakic, 2005). Our data provide no evidence of parvalbumin in the axons from pulvinar to V2, nor evidence of parvalbumin in the axons from V1 to V2. Since virtually all parvalbumin positive cells in V1 are GABAergic interneurons and not excitatory relay cells, the latter result is not surprising. On the other hand parvalbumin is

present in some neurons of the lateral pulvinar in both bush babies and other primates (Gutierrez et al., 2000; Imura and Rockland, 2007; Jones and Hendry, 1989). We can't, of course, say if these particular cells send axons to V2 but it is highly likely that they were involved in our thalamic injections. So why is parvalbumin uniquely present in thalamic axons to primary sensory cortex layer IV? Parvalbumin has been associated with cells known to have a relatively high firing rate in cortex (Kawaguchi and Kubota, 1993). No data is available directly for thalamic relay cells providing cell by cell correlations between parvalbumin and firing rate but P and M LGN cells in bush baby have higher firing rates than K cells (Norton and Casagrande, 1982) perhaps requiring more effective calcium buffering in their axons as a result.

Vglut2 is one of three vesicular glutamate transporters, the others being Vglut1 and Vglut3 (see Fremeau et al., 2004 for review). In the visual system Vglut2 has been found to co-localize with retino-geniculate and geniculo-cortical afferents in the rat and ferret, respectively (Land et al., 2004; Nahmani and Erisir, 2005) while Vglut1 is found mainly in connections from cortex such as those projecting back to the LGN (Yoshida et al., 2009). Also, the Vglut2 expression pattern in the brain has been correlated with cell types that have a high probability of release, a property that has been speculated to be important in driving projections (Fremeau et al., 2004; Sherman and Guillery, 2011). Nevertheless, not every driving connection expresses Vglut2, the central example being the layer V projection to the pulvinar (Wei et al., 2011). Additionally, in mouse some thalmocortical axons have been found to contain both Vglut1 and Vglut2 (Graziano et al., 2008). This finding does not discount Vglut2 as a mark of driving, but instead points to the possibility of more than one type of driving connection. This concept of multiple types of drivers is developing in the literature and will be discussed in greater detail below (Sherman and Guillery, 2011; Viaene et al., 2011; Wei et al., 2011). We find that most

pulvinar projections to V2 express Vglut2 while V1 projections to V2 almost never express Vglut2. The frequency of expression was similar for the pulvinar and LGN projections to V2 and V1, respectively, but the intensity of expression was quite different, with the LGN projections showing stronger staining for Vglut2 in layer IV of V1. This novel finding fits with a recent in situ hybridization study in bush baby that showed mRNA expression of Vglut2 in both LGN and pulvinar cells with the LGN cells having substantially stronger expression (Balaram et al., 2011).

Multiple driver classes

This study grew out of the theoretical framework proposed by Sherman and Guillery (1998; 2002) that originally sought to define glutamatergic inputs as driving or modulatory using a parametric approach originally applied to the early stages of the visual system. In recent years the Sherman lab and other groups have begun to refine the original hypothesis. One important development has been data indicating that there are likely to be multiple types of cortical drivers (Sherman and Guillery, 2011; Viaene et al., 2011; Wei et al., 2011). Another development suggests that, at least in the mouse, there are both driver and modulator class reciprocal connections from the primary sensory cortices to adjoining cortices (Covic and Sherman, 2011; De Pasquale and Sherman, 2011). This second point finds some support from the work of Soares et al. (2004), who, working in the cebus monkey, showed a mixture of both excitation and inhibition of V2 responses after pulvinar blockade with GABA. It is easy to imagine a scenario where removal of one of two drivers to an area would result in a mix of excitation and inhibition. The latter results, however, are difficult to interpret given that, under normal circumstances, GABA effects last a very brief period (see Allison et al., 2000; Nealley and Maunsell, 1994), but

much longer time periods were reported by Soares et al. (2004). Regardless, in the case of cortico-cortical connections the question remains whether the present work supports more than one class projecting from V1 and V2. If this were the case one would potentially expect to find a bimodal distribution in the sizes of boutons on V1 to V2 axons. The present data, however, are unimodal and so cannot support this hypothesis, at least using this single original metric. Although our data do not support multiple populations within the V1 to V2 projections we cannot reject the possibility that V1 to V2 projections and pulvinar to V2 projections represent different types of driving connections particularly given the patchy distribution of projections from V1 and from pulvinar to V2 (see above).

Functional Considerations

Both the presence of Vglut2 and large bouton size have been linked to higher probability of transmitter release, a characteristic necessary for fidelity of information transfer (Covic and Sherman, 2011; Fremeau et al., 2004). By contrast, the presence of the other primary vesicular glutamate transporter (Vglut1) and small bouton size have been linked to low probability of release and various types of plasticity, especially potentiation (Balschun et al., 2010; Covic and Sherman, 2011; Fremeau et al., 2004). The latter appear to define, at least morphologically, the V1 to V2 axons. Caution is needed obviously in drawing functional conclusions from these metrics particularly given the compartmental specialization of V2 in primates and the possibility of multiple classes of drivers. Nevertheless, our anatomical data on bouton sizes and axonal Vglut2 suggest that PL projections to V2 are more similar to geniculo-V1 projections than are V1 projections to V2.

Traditionally, it has been thought that cortico-cortical feedforward projections, like the ones from V1 to V2, are responsible for driving a cortical area to respond to external sensory stimulation. Sherman and Guillery have hypothesized that secondary thalamic nuclei, such as the pulvinar, drive higher sensory cortex (e.g., V2) while cortico-cortical connections may modulate this driven activity (Sherman and Guillery, 1998; Sherman and Guillery, 2002). Our anatomical data on bouton sizes and axonal Vglut2 suggest that PL rather than V1 might be the driver of neural activity in V2. Furthermore, our recent study demonstrated that PL also powerfully controls and gates the information outflow from V1 to extrastriate areas (Purushothaman et al., 2012). Thus, it appears that PL is situated not only to directly activate V2 but also to control the V1 signals that influence V2. Taken together, these two studies emphasize a critical role for thalamocortical connections in determining the propagation of sensory information through the cortex.

Acknowledgments

We would like to acknowledge: Mariesol Rodriguez, Mary Feurtado, and Maria Tamborski for valuable technical support in the execution of experiments. We would like to acknowledge Mary Feurtado for valuable technical support in the execution of experiments and her continued dedication to our bush baby colony. We would like to acknowledge Julia Mavity-Hudson for technical support in every aspect of the project.

Experiments and data analysis were performed in part through the use of the VUMC Cell Imaging Shared Resource. We are grateful for this core's excellent equipment and personnel.

Literature Cited

Allison JD, Melzer P, Ding Y, Bonds AB, Casagrande VA. 2000. Differential contributions of magnocellular and parvocellular pathways to the contrast response of neurons in bush baby primary visual cortex (V1). Vis Neurosci 17(1):71-76.

Adams MM, Hof PR, Gattass R, Webster MJ, Ungerleider LG. 2000. Visual cortical projections and chemoarchitecture of macaque monkey pulvinar. J Comp Neurol 419: 377-393.

Anderson JC, Martin KA. 2009. The synaptic connections between cortical areas V1 and V2 in macaque monkey. J Neurosci 29(36):11283-11293.

Balaram P. 2012. Vglut2 western. In: Marion R, Casagrande A, editors. p 1.

Balaram P, Takahata T, Kaas JH. 2011. VGLUT2 mRNA and protein expression in the visual thalamus and midbrain of prosimian galagos (Otolemur garnetti). Eye and Brain 2011: 5-15.

Baldwin MK, Wong P, Reed JL, Kaas JH. 2011. Superior colliculus connections with visual thalamus in gray squirrels (Sciurus carolinensis): evidence for four subdivisions within the pulvinar complex. J Comp Neurol 519(6):1071-1094.

Balschun D, Moechars D, Callaerts-Vegh Z, Vermaercke B, Van Acker N, Andries L, D'Hooge R. 2010. Vesicular glutamate transporter VGLUT1 has a role in hippocampal long-term potentiation and spatial reversal learning. Cereb Cortex 20: 684-693.

Bender DB. 1983. Visual activation of neurons in the primate pulvinar depends on cortex but not colliculus. Brain Res 279: 258-261.

Blümcke I, Hof PR, Morrison JH, Celio MR. 1991. Parvalbumin in the monkey striate cortex: a quantitative immunoelectron-microscopy study. Brain Res 554: 237-243.

Boyd JD, Casagrande VA. 1999. Relationships between cytochrome oxidase (CO) blobs in primate primary visual cortex (V1) and the distribution of neurons projecting to the middle temporal area (MT). J Comp Neurol 409: 573-591.

Boyd JD, Matsubara JA. 1996. Laminar and columnar patterns of geniculocortical projections in the cat: relationship to cytochrome oxidase. J Comp Neurol 365: 659-682.

Brodmann K. 1909. Vergleichende lokalisationlehre der grosshirnrinde in ihren prinzipien dargestelt auf des zellenbaues. Leipzig: JA Barth.

Casagrande VA, Kaas JH. 1994. The afferent, intrinsic, and efferent connections of primary visual cortex in primates. In: Peters A, Rockland KS, editors. Primary Visual Cortex of Primates. New York: Plenum. p 201-259.

Casagrande VA, Norton TT. 1991. The lateral geniculate nucleus: A review of its physiology and function. In: Leventhal AG, editor. In The Neural Basis of Visual Function. London: MacMillan. p 41-84.

Celio MR. 1990. Calbindin D-28k and parvalbumin in the rat nervous system. Neuroscience 35(2):375-475.

Collins CE, Lyon DC, Kaas JH. 2003. Responses of neurons in the middle temporal visual area after long-standing lesions of the primary visual cortex in adult new world monkeys. J Neurosci 23(6):2251-2264.

Collins CE, Stepniewska I, Kaas JH. 2001. Topographic patterns of v2 cortical connections in a prosimian primate (Galago garnetti). J Comp Neurol 431: 155-167.

Condo GJ, Casagrande VA. 1990. Organization of cytochrome oxidase staining in the visual cortex of nocturnal primates (Galago crassicaudatus and Galago senegalensis): I. Adult patterns. J Comp Neurol 293: 632-645.

Covic EN, Sherman SM. 2011. Synaptic properties of connections between the primary and secondary auditory cortices in mice. Cereb Cortex 21: 2425-2441.

Cragg BG. 1969. The topography of the afferent projections in the circumstriate visual cortex of the monkey studied by the Nauta method. Vision Res 9: 733-747.

Crair MC, Ruthazer ES, Gillespie DC, Stryker MP. 1997. Ocular dominance peaks at pinwheel center singularities of the orientation map in cat visual cortex. J Neurophysiol 77: 3381-3385.

Curcio CA, Harting JK. 1978. Organization of pulvinar afferents to area 18 in the squirrel monkey: evidence for stripes. Brain Res 143: 155-161.

Cusick CG, Kaas JH. 1988. Surface view patterns of intrinsic and extrinsic cortical connections of area 17 in a prosimian primate. Brain Res 458: 383-388.

DeBruyn EJ, Casagrande VA, Beck PD, Bonds AB. 1993. Visual resolution and sensitivity of single cells in the primary visual cortex (V1) of a nocturnal primate (bush baby): correlations with cortical layers and cytochrome oxidase patterns. J Neurophysiol 69: 3-18.

DeFelipe J, Jones EG. 1991. Parvalbumin immunoreactivity reveals layer IV of monkey cerebral cortex as a mosaic of microzones of thalamic afferent terminations. Brain Res 562: 39-47.

De Pasquale R, Sherman SM. 2011. Synaptic properties of corticocortical connections between the primary and secondary visual cortical areas in the mouse. J Neurosci 31(46):16494-16506.

Diamond IT, Fitzpatrick D, Conley M. 1992. A projection from the parabigeminal nucleus to the pulvinar nucleus in Galago. J Comp Neurol 316: 375-382.

Fan RH, Baldwin MK, Jermakowicz WJ, Casagrande VA, Kaas JH, Roe AW. 2012. Intrinsic signal optical imaging evidence for dorsal V3 in the prosimian galago (Otolemur garnettii). J Comp Neurol.

Felleman DJ, Van Essen DC. 1991. Distributed hierarchical processing in the primate cerebral cortex. Cereb Cortex 1: 1-47.

Florence SL, Casagrande VA. 1987. Organization of individual afferent axons in layer IV of striate cortex in a primate. J Neurosci 7: 3850-3868.

Fremeau RT, Jr., Voglmaier S, Seal RP, Edwards RH. 2004. VGLUTs define subsets of excitatory neurons and suggest novel roles for glutamate. Trends Neurosci 27: 98-103.

Fremeau RT, Jr., Troyer MD, Pahner I, Nygaard GO, Tran CH, Reimer RJ, Bellocchio EE, Fortin D, Storm-Mathisen J, Edwards RH. 2001. The expression of vesicular glutamate transporters defines two classes of excitatory synapse. Neuron 31(2):247-260.

Freund TF, Martin KA, Soltesz I, Somogyi P, Whitteridge D. 1989. Arborisation pattern and postsynaptic targets of physiologically identified thalamocortical afferents in striate cortex of the macaque monkey. J Comp Neurol 289(2):315-336.

Freund TF, Martin KA, Whitteridge D. 1985. Innervation of cat visual areas 17 and 18 by physiologically identified X- and Y- type thalamic afferents. I. Arborization patterns and quantitative distribution of postsynaptic elements. J Comp Neurol 242(2):263-274.

Gattass R, Gross CG, Sandell JH. 1981. Visual topography of V2 in the macaque. J Comp Neurol 201: 519-539.

Glendenning KK, Hall JA, Diamond IT, Hall WC. 1975. The pulvinar nucleus of Galago senegalensis. J Comp Neurol 161: 419-458.

Goodale MA, Milner AD. 1992. Separate visual pathways for perception and action. Trends Neurosci 15: 20-25.

Graziano A, Liu XB, Murray KD, Jones EG. 2008. Vesicular glutamate transporters define two sets of glutamatergic afferents to the somatosensory thalamus and two thalamocortical projections in the mouse. J Comp Neurol 507(2):1258-1276.

Gutierrez C, Cola MG, Seltzer B, Cusick C. 2000. Neurochemical and connectional organization of the dorsal pulvinar complex in monkeys. J Comp Neurol 419: 61-86.

Hackett TA, de la Mothe LA. 2009. Regional and laminar distribution of the vesicular glutamate transporter, VGluT2, in the macaque monkey auditory cortex. J Chem Neuroanat 38: 106-116.

Hrabovszky E, Kallo I, Turi GF, May K, Wittmann G, Fekete C, Liposits Z. 2006. Expression of vesicular glutamate transporter-2 in gonadotrope and thyrotrope cells of the rat pituitary. Regulation by estrogen and thyroid hormone status. Endocrinology 147(8):3818-3825.

Ichida J, Casagrande VA. 1999. The morphology and distribution of intracellularly labeled corticogeniculate projection cells in bush baby. Society for Neuroscience. p 1424.

Imura K, Rockland KS. 2007. Giant neurons in the macaque pulvinar: a distinct relay subpopulation. Front Neuroanat 1: 2.

Johnson JK, Casagrande VA. 1995. Distribution of calcium-binding proteins within the parallel visual pathways of a primate (Galago crassicaudatus). J Comp Neurol 356: 238-260.

Jones EG, Hendry SH. 1989. Differential Calcium Binding Protein Immunoreactivity Distinguishes Classes of Relay Neurons in Monkey Thalamic Nuclei. Eur J Neurosci 1: 222-246.

Kaas JH, Lyon DC. 2007. Pulvinar contributions to the dorsal and ventral streams of visual processing in primates. Brain Res Rev 55: 285-296.

Kaske A, Dick A, Creutzfeldt OD. 1991. The local domain for divergence of subcortical afferents to the striate and extrastriate visual cortex in the common marmoset (Callithrix jacchus): a multiple labelling study. Exp Brain Res 84: 254-265.

Kawaguchi Y, Kubota Y. 1993. Correlation of physiological subgroupings of nonpyramidal cells with parvalbumin- and calbindinD28k-immunoreactive neurons in layer V of rat frontal cortex. J Neurophysiol 70: 387-396.

Kawaguchi Y, Kubota Y. 1997. GABAergic cell subtypes and their synaptic connections in rat frontal cortex. Cereb Cortex 7(6):476-486.

Kennedy H, Bullier J. 1985. A double-labeling investigation of the afferent connectivity to cortical areas V1 and V2 of the macaque monkey. J Neurosci 5: 2815-2830.

Khaytin I, Chen X, Royal DW, Ruiz O, Jermakowicz WJ, Siegel RM, Casagrande VA. 2008. Functional organization of temporal frequency selectivity in primate visual cortex. Cereb Cortex 18: 1828-1842.

Kuypers HG, Szwarcbart MK, Mishkin M, Rosvold HE. 1965. Occipitotemporal Corticocortical Connections in the Rhesus Monkey. Exp Neurol 11: 245-262.

Lachica EA, Casagrande VA. 1992. Direct W-Like Geniculate Projections to the Cytochrome-Oxidase (Co) Blobs in Primate Visual-Cortex - Axon Morphology. journal of comparative neurology 319(1):141-158.

Land PW, Kyonka E, Shamalla-Hannah L. 2004. Vesicular glutamate transporters in the lateral geniculate nucleus: expression of VGLUT2 by retinal terminals. Brain Res 996: 251-254.

Levitt JB, Yoshioka T, Lund JS. 1995. Connections between the pulvinar complex and cytochrome oxidase-defined compartments in visual area V2 of macaque monkey. Exp Brain Res 104: 419-430.

Li K, Patel J, Purushothaman G, Marion RT, Yampolsky D, Jiang Y, Mavity-Hudson JA, Casagrande VA. 2011. Retinotopic organization of pulvinar in a prosimian primate. Society for Neuroscience Program No. 269.20/HH29.

Livingstone MS, Hubel DH. 1982. Thalamic inputs to cytochrome oxidase-rich regions in monkey visual cortex. Proc Natl Acad Sci U S A 79: 6098-6101.

Lund JS, Hendrickson AE, Ogren MP, Tobin EA. 1981. Anatomical organization of primate visual cortex area VII. J Comp Neurol 202: 19-45.

Melchitzky DS, Sesack SR, Lewis DA. 1999. Parvalbumin-immunoreactive axon terminals in macaque monkey and human prefrontal cortex: laminar, regional, and target specificity of type I and type II synapses. J Comp Neurol 408(1):11-22.

Mettler FA. 1935. Corticofugal fiber connections of the cortex of Macaca mulatta. J Comp Neurol 61: 221-256.

Mishkin M, Ungerleider LG. 1982. Contribution of striate inputs to the visuospatial functions of parieto-preoccipital cortex in monkeys. Behav Brain Res 6: 57-77.

Nahmani M, Erisir A. 2005. VGluT2 immunochemistry identifies thalamocortical terminals in layer 4 of adult and developing visual cortex. J Comp Neurol 484: 458-473.

Nealey TA, Maunsell JHR. 1994. Magnocellular and Parvocellular Contributions to the Responses of Neurons in Macaque Striate Cortex. Journal of Neuroscience 14(4):2069-2079.

Negyessy L, Goldman-Rakic PS. 2005. Subcellular localization of the dopamine D2 receptor and coexistence with the calcium-binding protein neuronal calcium sensor-1 in the primate prefrontal cortex. J Comp Neurol 488(4):464-475.

Norton TT, Casagrande VA. 1982. Laminar organization of receptive-field properties in lateral geniculate nucleus of bush baby (Galago crassicaudatus). J Neurophysiol 47: 715-741.

O'Brien BJ, Abel PL, Olavarria JF. 2001. The retinal input to calbindin-D28k-defined subdivisions in macaque inferior pulvinar. Neurosci Lett 312: 145-148.

Ogren MP, Hendrickson AE. 1977. The distribution of pulvinar terminals in visual areas 17 and 18 of the monkey. Brain Res 137: 343-350.

Pierce JP, Lewin GR. 1994. An ultrastructural size principle. Neuroscience 58(3):441-446.

Preuss TM, Beck PD, Kaas JH. 1993. Areal, modular, and connectional organization of visual cortex in a prosimian primate, the slow loris (Nycticebus coucang). Brain Behav Evol 42: 321-335.

Purushothaman G, Marion R, Li K, Casagrande VA. 2012. Gating and control of primary visual cortex by pulvinar. Nat Neurosci 15: 905-912.

Raczkowski D, Diamond IT. 1980. Cortical connections of the pulvinar nucleus in Galago. J Comp Neurol 193: 1-40.

Raczkowski D, Diamond IT. 1981. Projections from the superior colliculus and the neocortex to the pulvinar nucleus in Galago. J Comp Neurol 200: 231-254.

Rockland KS, Andresen J, Cowie RJ, Robinson DL. 1999. Single axon analysis of pulvinocortical connections to several visual areas in the macaque. J Comp Neurol 406:221-250.

Rockland KS, Pandya DN. 1979. Laminar origins and terminations of cortical connections of the occipital lobe in the rhesus monkey. Brain Res 179(1):3-20.

Roe AW, Ts'o DY. 1995. Visual topography in primate V2: multiple representation across functional stripes. J Neurosci 15: 3689-3715.

Rosa MG, Casagrande VA, Preuss T, Kaas JH. 1997. Visual field representation in striate and prestriate cortices of a prosimian primate (Galago garnetti). J Neurophysiol 77: 3193-3217.

Schiller PH, Malpeli JG. 1977. The effect of striate cortex cooling on area 18 cells in the monkey. Brain Res 126: 366-369.

Sherman SM. 2007. The thalamus is more than just a relay. Curr Opin Neurobiol 17: 417-422.

Sherman SM, Guillery RW. 1996. Functional organization of thalamocortical relays. J Neurophysiol 76: 1367-1395.

Sherman SM, Guillery RW. 1998. On the actions that one nerve cell can have on another: distinguishing "drivers" from "modulators". Proc Natl Acad Sci U S A 95: 7121-7126.

Sherman SM, Guillery RW. 2002. The role of the thalamus in the flow of information to the cortex. Philos Trans R Soc Lond B Biol Sci 357(1428):1695-1708.

Sherman SM, Guillery RW. 2011. Distinct functions for direct and transthalamic corticocortical connections. J Neurophysiol 106: 1068-1077.

Shipp S. 2003. The functional logic of cortico-pulvinar connections. Philos Trans R Soc Lond B Biol Sci 358 : 1605-1624.

Sincich LC, Horton JC. 2002. Pale cytochrome oxidase stripes in V2 receive the richest projection from macaque striate cortex. J Comp Neurol 447: 18-33.

Soares JG, Diogo AC, Fiorani M, Souza AP, Gattass R. 2004. Effects of inactivation of the lateral pulvinar on response properties of second visual area cells in Cebus monkeys. Clin Exp Pharmacol Physiol 31(9):580-590.

Stepniewska I. 2004. The Pulvinar Complex. In: Kaas JH, Collins CE, editors. The Primate Visual System. Boca Raton: CRC press. p 53-80.

Symonds LL, Kaas JH. 1978. Connections of striate cortex in the prosimian, Galago senegalensis. J Comp Neurol 181: 477-512.

Tigges J, Tigges M, Kalaha CS. 1973. Efferent connections of area 17 in Galago. Am J Phys Anthropol 38: 393-397.

Tootell RB, Switkes E, Silverman MS, Hamilton SL. 1988. Functional anatomy of macaque striate cortex. II. Retinotopic organization. J Neurosci 8: 1531-1568.

van Brederode JF, Helliesen MK, Hendrickson AE. 1991. Distribution of the calcium-binding proteins parvalbumin and calbindin-D28k in the sensorimotor cortex of the rat. Neuroscience 44: 157-171.

Vanduffel W, Tootell RB, Schoups AA, Orban GA. 2002. The organization of orientation selectivity throughout macaque visual cortex. Cereb Cortex 12: 647-662.

Viaene AN, Petrof I, Sherman SM. 2011. Properties of the thalamic projection from the posterior medial nucleus to primary and secondary somatosensory cortices in the mouse. Proc Natl Acad Sci U S A 108(44):18156-18161.

Wei H, Masterson SP, Petry HM, Bickford ME. 2011. Diffuse and specific tectopulvinar terminals in the tree shrew: synapses, synapsins, and synaptic potentials. PLoS One 6(8):e23781.

Wong-Riley MT. 1977. Connections between the pulvinar nucleus and the prestriate cortex in the squirrel monkey as revealed by peroxidase histochemistry and autoradiography. Brain Res 134: 249-267.

Wong-Riley MT, Carroll EW. 1984. Quantitative light and electron microscopic analysis of cytochrome oxidase-rich zones in V II prestriate cortex of the squirrel monkey. J Comp Neurol 222: 18-37.

Wong P, Collins CE, Baldwin MK, Kaas JH. 2009. Cortical connections of the visual pulvinar complex in prosimian galagos (Otolemur garnetti). J Comp Neurol 517: 493-511.

Wong P, Kaas JH. 2010. Architectonic subdivisions of neocortex in the Galago (Otolemur garnettii). Anat Rec (Hoboken) 293: 1033-1069.

Xu X, Anderson TJ, Casagrande VA. 2007. How do functional maps in primary visual cortex vary with eccentricity? J Comp Neurol 501: 741-755.

Xu X, Bosking WH, White LE, Fitzpatrick D, Casagrande VA. 2005. Functional organization of visual cortex in the prosimian bush baby revealed by optical imaging of intrinsic signals. J Neurophysiol 94(4):2748-2762.

Xu X, Collins CE, Kaskan PM, Khaytin I, Kaas JH, Casagrande VA. 2004. Optical imaging of visually evoked responses in prosimian primates reveals conserved features of the middle temporal visual area. Proc Natl Acad Sci U S A 101(8):2566-2571.

Yoshida M, Satoh T, Nakamura KC, Kaneko T, Hata Y. 2009. Cortical activity regulates corticothalamic synapses in dorsal lateral geniculate nucleus of rats. Neurosci Res 64(1):118-127.

Zeki SM. 1969. Representation of central visual fields in prestriate cortex of monkey. Brain Res 14(2):271-291.

CHAPTER VII

CONCLUSIONS AND FUTURE DIRECTIONS

In the chapter that follows I discuss the broader implications of the data presented in this thesis. I take as a starting point the conclusions of each of the chapters that presented new data and expand these concepts with an eye to placing the pulvinar within the context of the visual hierarchy using the ideas of Sherman and Guillery (1996; 1998). Along the way I will offer some ideas on the types of experiments that I think should be done in the future.

Maps and Loops of the Pulvinar

In chapter II our primary findings showed that there are two retinotopic maps in the bush baby pulvinar. We also provided, for the first time, a model comparing the organization of retinotopic maps in pulvinar across primates and show how this model can be generalized to explain similarities and differences in thalamic visuotopic maps. We also demonstrated, using cytoarchtecture, the presence of areas resembling PIcl and PIm extending past anatomical work in the bush baby (Wong et al., 2009). As reviewed in chapters II and III available data strongly suggests that there are 2 maps in the lateral aspect of the macaque pulvinar (Adams et al., 2000; Bender, 1981). Further we also suggest in chapters II and III that data from the ventrolateral pulvinar in the cebus monkey originally interpreted as suggesting a single map may actually

indicate two maps. Taken together, these data indicate that all three branches of the primate lineage (New World, Old World and prosimians) likely possess two retinotopic maps that lie in the posterior lateral aspect of the pulvinar.

The findings in chapter III offer clarity as to the number of maps in the V1 recipient zone of the pulvinar but also raise questions. First among these questions: how do maps of different visual cortical areas connect to the visuotopic maps in PL and PI? If cells in V4 and MT, for example, project to populations of pulvinar relay cells that are intermixed, there is the possibility of the mixing of the two cortical signals. In macaque the vertical meridian and horizontal meridian of the two maps are represented as sheets (Bender, 1981). This means that multiple volumes of cells can be generated within the two maps each having a full visual field representation (reviewed chapters II and III). Previous researchers have proposed that relay cells projecting to the two different visual streams (specifically V4, and MT) are serviced by different volumes within the maps of the pulvinar thus keeping the signals from intermixing (Shipp, 2001). In the bush baby this arrangement of inputs seems unlikely because *area centralis* is represented by a single point or small volume of cells instead of as a line as it is in macaque (see Chapter 3 Figure 11). If inputs must share a small volume to represent central vision they are, by default, not segregated by distance. Does this represent a significant species difference between macaques and bush babies? What arrangement of inputs might be expected in New World monkeys? Does the pulvinar in different species relate differently to the dorsal and ventral processing streams? These are important questions if we wish to understand how much pulvinar function might have been changed by evolution, and will take a substantial amount of additional research to answer.

The Pulvinar as a Gate

In chapter IV we showed that pulvinar cells are part of a powerful gain control mechanism that affects cells with overlapping receptive fields in layer II/III of V1. Because many cells in layer II/III of V1 project forward in the visual hierarchy, we theorized that pulvinar inputs have a gating effect on information coming from V1 to other cortical areas. It is important to interpret these data in context. For example, because unilateral and bilateral lesions of the pulvinar have produced different results in attentional and orienting paradigms it is unclear whether identical results would be obtained if these experiments were repeated in awake animals or using bilateral pulvinar block (see chapters II and IV for review). Repeating these experiments in the awake preparation with both unilateral and bilateral blockade are excellent future steps to investigating the mechanism and perceptual implications of these data.

Sherman and Guillery (Sherman and Guillery, 2006; Sherman and Guillery, 2013) consider gating effects like the one shown in chapter IV to be a type of modulation. In chapter V we demonstrate that the direct projections between the retinotopically mapped area of the pulvinar (the area blocked in chapter IV) to V1 terminate primarily in layer I and fit the profile of class 2 (modulatory) projections. Pyramidal neurons in layers II, III, and V send apical dendrites into layer I while also sending out basal dendrites (Spruston, 2008). Work in brain slice has shown that apical and basal dendritic systems can act in concert as a coincidence detection mechanism resulting in gain control effects (Spruston, 2008). This represents one possible mechanism for the effects observed in chapter IV and would be an interesting avenue for further research. Regardless of the end mechanism gating is an important phenomenon that has been implicated in modes of attention (Crick, 1984; McAlonan et al., 2008). As reviewed in chapter

II, Sherman and Guillery have more recently de-emphasized modulatory processes such as gating in favor of tracing driving projections. Chapters IV and V suggest that both driver and modulators must be considered when modeling information flow in the brain.

The Pulvinar as Driver

In chapter VI we demonstrated that pulvinar projections to V2 layer IV have larger terminals then V1 projections to the same location. Further the pulvinar projections were shown to be Vglut2 positive whereas the V1 projections to V2 were not positive for Vglut2. These characteristics mean that of the two possible feedforward drivers of V2, pulvinar projections to V2 are more similar to the known driving connections from the LGN to V1. In chapter V we showed that the pulvinar projections to V2 have smaller boutons in layer I than in layer IV and that the layer I projections appear to be collaterals of the layer IV projections. These results lead to the conclusion that the pulvinar projections to layer IV of V2 are capable of driving cells while the layer I pulvinar projections modulate activity in V2. These conclusions represent the most straightforward reading of our data but several other interpretations are possible. I will explore two of these below.

As mentioned above, our findings indicate that pulvinar projections to V2 are most dense in layers III and IV but also send collaterals to layer I. Thalamo-cortical projections that primarily terminate in layer 3 and 4 but have collaterals in layer I have been previously reported for the pulvinar (Rockland 1999). It is unclear if every axon from the pulvinar necessarily sends a colateral to layer I. None the less the presence of layer I projections is interesting because layer I projections are lacking in V1 projections to V2 (Anderson and Martin, 2009; Marion et

al., 2013; Sincich and Horton, 2002). As mentioned above coincident excitation of apical and basal dendrites has been shown to have a strong excitatory effect on pyramidal cells (Spruston, 2008). The presence of layer 1 terminations in the pulvinar projections suggests that they may have a very strong excitatory effect on V2 pyramidal neurons in layers II/III. Further work will be needed to fully understand the direct effect of multi-layer synchronous input to V2.

There is little doubt that projections having the characteristics of class 1 projections (driver) tend to have greater synaptic efficacy than class 2 (modulatory) projections (see chapter II for review). This is especially true in the inputs to first order nuclei that serve as the models of these two classes of synapses (Sherman and Guillery, 1996; Sherman and Guillery, 1998). For example retinal projections to the LGN form very large terminals that show distinct paired pulse depression while V1 projections to the LGN have small terminals that show clear paired pulse facilitation (Sherman and Guillery, 2006; Sherman and Guillery, 2013). However in other systems these distinctions are not so clear. Consider that the 4 projections studied in chapter VI (LGN M to V1, LGN P to V1, pulvinar to V2 and V1 to V2) appeared to have 3 significantly different sizes. Is only the largest (M LGN) a driver? Is only the smallest (V1 to V2) a modulator? If these feedforward projections are grouped by the area that they target (projections to V1 in one group and projections to V2 in a second), it is clear that the feedforward projections appear to get smaller further up the classically defined hierarchy. This trend is mirrored in the thalamus where the terminals on the retina to LGN projections are larger than the terminals on the cortical projections to the lateral pulvinar that are in turn larger than the terminals on the cortical projections to the medial pulvinar (Rovo et al., 2012). It is noteworthy, that all of the projections listed in the latter example are considered drivers by Sherman and Guillery (Guillery and Sherman, 2002; Sherman and Guillery, 1998; Sherman and Guillery, 2002; Sherman and

Guillery, 2006; Sherman and Guillery, 2013). If these projections have the same function, why do they have different morphologies?

Sherman and Guillery's distinction between two classes of projections is, of course, not based on bouton size alone. They use multiple metrics to distinguish the 2 types of synapses, however, at least one other metric shows evidence of middle ground between class 1 and class 2 synapses. In the tree shrew Wei and colleagues (2011) described 3 sizes of terminals that form synapses in the pulvinar. They suggested that round small (RS) and round large (RL) terminals come from the cortex while round medium (RM) terminals come from the SC. The authors showed that RM terminals come in two varieties. One variety showed paired pulse depression which is typical of a class 1 synapse. A second variety showed no short term plasticity in response to paired pulse stimulation. In a class 2 projection paired pulse facilitation should, by definition, be observed (Sherman and Guillery, 2006; Sherman and Guillery, 2011). In other words Wei and colleague (2011) have found synapses displaying both the morphological and physiological characteristics somewhere between a typical class 1 and typical class 2. I suspect that these RM synapses are not unique and that there are many other projections that do not fit neatly into the categories of class 1 and class 2 synapses.

Why would synapses need to be stronger than an archetypical class 2 and yet weaker than an archetypical class 1? The number of feedforward inputs at different levels of the hierarchy provides a clue. In the retina to LGN connection the number of cells that provide feedforward information is small (1 or 2 in most cases as many as 6 in some cases; Cleland et al., 1971; Levick et al., 1972; Mastronarde, 1987; Mastronarde, 1992; Usrey et al., 1999) while one level higher in the LGN to V1 the number is substantially larger (calculated to be 15-125; Alonso et al., 2001). The number of feedforward inputs at higher cortical areas is unknown. However, it is

known that the number of spines on the basal dendrites of layer II/III pyramidal cells is greater in higher visual areas than in V1 (Elston et al., 2005). Bruno and Sakmann (2006) have shown that synchronous convergent input is needed for first order thalamic neurons (in the ventral posteromedial nucleus) to produce spikes in spiny stellate cells. Taken together these data point to a trend where progressively higher cortical areas have increasing numbers of feedforward synapses that are smaller than the preceding level. With many small low efficacy synapses, the cell is brought to threshold not by one single input but by many inputs firing synchronously. I would go so far as to predict cells where no single area's projections are capable of bringing the cell to threshold. Such cells would have no archetypical drivers but instead act as coincidence detectors. Inputs to these types of cells should lie somewhere in the middle ground between the archetypical class 1 and class 2 synapses as described originally for the LGN by Sherman and Guillery (1996; 1998; 2006). Given the evidence supporting the pulvinar's role in synchronizing cortical areas (see chapter II for review), I suspect that some pulvinar synapses will be neither full drivers nor full modulators.

The Pulvinar and the Visual Hierarchy

Where does the pulvinar belong in the visual hierarchy? As reviewed in chapter II and demonstrated in chapter III, the pulvinar is not a single entity, consisting instead of many subnuclei which may sit at different levels of the visual hierarchy. The retinotopically mapped region of the pulvinar has cells that are driven by V1 and appear to drive V2 (see chapter II for review and chapter VI), hence, at least part of the mapped region of the pulvinar sits at an intermediate level between V1 and V2 in the visual hierarchy. However, V2 also provides drive

to the retinotopically mapped areas of the pulvinar (see chapter II). Therein lies the problem faced by researches wishing to place the pulvinar within the visual hierarchy: it is likely that some subnuclei operate at multiple levels of the hierarchy. As reviewed in chapter II, Sherman and Guillery's work has shifted away from defining hierarchy by area to defining hierarchy at the level of the single neuron partly as a response to issues revolving around mixed cell populations like the one above. This approach may allow for different loops within the same area of the pulvinar to be classified at different levels of the hierarchy. Unfortunately, the approach defining hierarchy at the single cell level is fraught with problems. As discussed above, this method has a potential problem because not all synapses fall into clear classes. There is also a problem with this method in defining direction within the hierarchy. For example, recent work in both mouse and macaque has examined the connections between the primary visual area and the secondary visual area using a single cell or single synapse approach as is promoted by Sherman and Guillery. These data have suggested that while many projections from the primary visual area are capable of driving secondary visual neurons, projections from the secondary visual area are also capable of driving the primary visual area (Anderson and Martin, 2009; De Pasquale and Sherman, 2011). These data seem to indicate that, unlike in the retino-geniculate pathway, in the cortex drive is bidirectional. The possibility that visual drive might be looped from V1 to V2 and back to V1 is fascinating but also extremely detrimental to the concept of a visual hierarchy. It is ironic that Sherman and Guillery's attempt to include the pulvinar in the visual hierarchy may show that the visual hierarchy is not a very useful concept at the single cell level. That said, the ideas of Sherman and Guillery have inspired a great number of scientific works, including this thesis, and have re-invigorated thalamic research. Little more can be asked of a set of theories.

Hierarchy is a short hand, a condensation of ideas to allow for simple conceptualization. It is useful as an overview but is eventually confounding. The pulvinar with its difficult anatomy and underexplored physiology exposes these constraints. The pulvinar like other subcortical areas is challenging because it is difficult to know both the connections of a cell and the activity of a cell simultaneously. To make progress on the problem of the pulvinar's function, researchers must tackle the difficult task of knowing both a pulvinar cell's connections and its physiology. I think that it is unlikely that the pulvinar will ever be fully incorporated into a single niche in visual hierarchy; however, I predict that it will be part of many exciting discoveries to come.

Reference List

Adams MM, Hof PR, Gattass R, Webster MJ, Ungerleider LG. 2000. Visual cortical projections and chemoarchitecture of macaque monkey pulvinar. J Comp Neurol 419(3):377-393.

Alonso JM, Usrey WM, Reid RC. 2001. Rules of connectivity between geniculate cells and simple cells in cat primary visual cortex. J Neurosci 21(11):4002-4015.

Anderson JC, Martin KA. 2009. The synaptic connections between cortical areas V1 and V2 in macaque monkey. J Neurosci 29(36):11283-11293.

Bender DB. 1981. Retinotopic organization of macaque pulvinar. J Neurophysiol 46(3):672-693.

Bruno RM, Sakmann B. 2006. Cortex is driven by weak but synchronously active thalamocortical synapses. Science 312(5780):1622-1627.

Cleland BG, Dubin MW, Levick WR. 1971. Sustained and transient neurones in the cat's retina and lateral geniculate nucleus. J Physiol 217(2):473-496.

Crick F. 1984. Function of the thalamic reticular complex: the searchlight hypothesis. Proc Natl Acad Sci U S A 81(14):4586-4590.

De Pasquale R, Sherman SM. 2011. Synaptic properties of corticocortical connections between the primary and secondary visual cortical areas in the mouse. J Neurosci 31(46):16494-16506.

Elston GN, Elston A, Kaas JH, Casagrande V. 2005. Regional specialization in pyramidal cell structure in the visual cortex of the galago: an intracellular injection study of striate and extrastriate areas with comparative notes on new world and old world monkeys. Brain Behav Evol 66(1):10-21.

Guillery RW, Sherman SM. 2002. Thalamic relay functions and their role in corticocortical communication: generalizations from the visual system. Neuron 33(2):163-175.

Levick WR, Cleland BG, Dubin MW. 1972. Lateral geniculate neurons of cat: retinal inputs and physiology. Invest Ophthalmol 11(5):302-311.

Marion R, Li K, Purushothaman G, Jiang Y, Casagrande VA. 2013. Morphological and neurochemical comparisons between pulvinar and V1 projections to V2. J Comp Neurol 521(4):813-832 (PCMID 3513524).

Mastronarde DN. 1987. Two classes of single-input X-cells in cat lateral geniculate nucleus. II. Retinal inputs and the generation of receptive-field properties. J Neurophysiol 57(2):381-413.

Mastronarde DN. 1992. Nonlagged relay cells and interneurons in the cat lateral geniculate nucleus: receptive-field properties and retinal inputs. Vis Neurosci 8(5):407-441.

McAlonan K, Cavanaugh J, Wurtz RH. 2008. Guarding the gateway to cortex with attention in visual thalamus. Nature 456(7220):391-394.

Olszewski J. 1952. The Thalamus of the Macaca Mulatta: An Atlas for Use with the Stereotaxic Instrument. Basel: S. Karger.

Rovo Z, Ulbert I, Acsady L. 2012. Drivers of the primate thalamus. J Neurosci 32(49):17894-17908.

Sherman SM, Guillery RW. 1996. Functional organization of thalamocortical relays. J Neurophysiol 76(3):1367-1395.

Sherman SM, Guillery RW. 1998. On the actions that one nerve cell can have on another: distinguishing "drivers" from "modulators". Proc Natl Acad Sci U S A 95(12):7121-7126.

Sherman SM, Guillery RW. 2002. The role of the thalamus in the flow of information to the cortex. Philos Trans R Soc Lond B Biol Sci 357(1428):1695-1708.

Sherman SM, Guillery RW. 2006. Exploring The Thalamuc And Its Role In Cortical Function. Cambridge: The MIT Press. 484 p.

Sherman SM, Guillery RW. 2011. Distinct functions for direct and transthalamic corticocortical connections. J Neurophysiol 106(3):1068-1077.

Sherman SM, Guillery RW. 2013. Functional Connections of Cortical Areas. Cambridge, Massachusetts: MIT press.

Shipp S. 2001. Corticopulvinar connections of areas V5, V4, and V3 in the macaque monkey: a dual model of retinal and cortical topographies. J Comp Neurol 439(4):469-490.

Sincich LC, Horton JC. 2002. Pale cytochrome oxidase stripes in V2 receive the richest projection from macaque striate cortex. J Comp Neurol 447(1):18-33.

Spruston N. 2008. Pyramidal neurons: dendritic structure and synaptic integration. Nat Rev Neurosci 9(3):206-221.

Usrey WM, Reppas JB, Reid RC. 1999. Specificity and strength of retinogeniculate connections. J Neurophysiol 82(6):3527-3540.

Wei H, Masterson SP, Petry HM, Bickford ME. 2011. Diffuse and specific tectopulvinar terminals in the tree shrew: synapses, synapsins, and synaptic potentials. PLoS One 6(8):e23781.

Wong P, Collins CE, Baldwin MK, Kaas JH. 2009. Cortical connections of the visual pulvinar complex in prosimian galagos (Otolemur garnetti). J Comp Neurol 517(4):493-511.